UC-37
LBL-20354 c.1

Lawrence Berkeley Laboratory
UNIVERSITY OF CALIFORNIA

Materials & Molecular Research Division

RECEIVED
LAWRENCE
BERKELEY LABORATORY

NOV 20 1985

LIBRARY AND
DOCUMENTS SECTION

FOURIER TRANSFORM ZERO FIELD NMR AND NQR

D.B. Zax
(Ph.D. Thesis)

For Reference

Not to be taken from this room

September 1984

LBL-20354 c.1

Prepared for the U.S. Department of Energy under Contract DE-AC03-76SF00098

DISCLAIMER

This document was prepared as an account of work sponsored by the United States Government. While this document is believed to contain correct information, neither the United States Government nor any agency thereof, nor the Regents of the University of California, nor any of their employees, makes any warranty, express or implied, or assumes any legal responsibility for the accuracy, completeness, or usefulness of any information, apparatus, product, or process disclosed, or represents that its use would not infringe privately owned rights. Reference herein to any specific commercial product, process, or service by its trade name, trademark, manufacturer, or otherwise, does not necessarily constitute or imply its endorsement, recommendation, or favoring by the United States Government or any agency thereof, or the Regents of the University of California. The views and opinions of authors expressed herein do not necessarily state or reflect those of the United States Government or any agency thereof or the Regents of the University of California.

LBL-20354

Fourier Transform Zero Field NMR and NQR

David B. Zax

Lawrence Berkeley Laboratory
University of California
Berkeley, California 94720

September 1984

The United States Department of Energy has the right to use this thesis for any purpose whatsoever including the right to reproduce all or any part thereof.

This work was supported by the Director, Office of Energy Research, Office of Basic Energy Sciences, Materials Sciences Division of the U.S. Department of Energy under Contract Number DE-AC03-76SF00098.

Fourier Transform Zero Field NMR and NQR

Copyright © 1985

David Bruce Zax

FOURIER TRANSFORM ZERO FIELD NMR AND NQR

David Bruce Zax

Abstract

The characterization of the structural and chemical properties of matter, particularly in disordered condensed phases, is a difficult process. Few analytical methods work effectively on polycrystalline or amorphous solids. In many systems the chemical shifts measured by traditional high resolution solid state NMR methods are insufficiently sensitive or the information contained in the dipole-dipole couplings is more important. In these cases Fourier transform zero field magnetic resonance may make an important contribution. Zero field NMR and NQR is the subject of this thesis.

Chapter I presents the quantum mechanical background and notational formalism for what follows. Chapter II gives a brief review of high resolution magnetic resonance methods, with particular emphasis on techniques applicable to dipole-dipole and quadrupolar couplings. Level-crossings between spin-1/2 and quadrupolar spins during demagnetization transfer polarization from to low γ nuclei. This is the basis of very high sensitivity zero field NQR measurements by field cycling.

Chapter III provides a formal presentation of the high resolution Fourier transform zero field NMR method. Theoretical signal functions are calculated for common spin systems, and examples of typical spectra are presented. Chapters IV and V review the experimental progress in zero field NMR of dipole-dipole coupled spin-1/2 nuclei and for

quadrupolar spin systems.

Variations of the simple experiment described in earlier chapters which use pulsed dc fields are presented in Chapter VI. Some advantages of these variant experiments are suggested. Theoretical predictions for the experimental spectra are given and compared to experimental results. High sensitivity experiments closely related to traditional level-crossing spectroscopy are discussed. Some two-dimensional zero field correlation experiments are proposed.

Chapter VII contains a description of the application of group theory to problems of coupled spins in the absence of applied fields. Normal point group theory and time reversal are both important.

Experimental details and a description of a zero field NMR spectrometer appear in Chapter VIII. Design criteria are presented, along with suggestions as to some variations and technological improvements.

ACKNOWLEDGMENTS

It has been my pleasure these last five years at Berkeley to be associated with the research group of Professor Alex Pines. Alex's group has been an exciting place to learn about modern magnetic resonance. His enthusiasm infects the group so that excellence and originality in research work is expected and, in fact, demanded. No project is allowed to rest for long repeating the routine. Alex has been not only an inspirational research director but has grown into a friend as well.

Part of the excitement of working with his group is the intellectual quality of the entire group. In these five years the group has shifted from being a small, sharply focused ensemble into a much larger melange with many largely independent projects and too many individuals to acknowledge individually. The intellectual debt I owe to many of those both more senior to me and to my contemporaries is at least partially acknowledged in the author's lists on many papers.

Amongst those that have appeared as coauthors one is particularly deserving of individual mention. Tony Bielecki has worked closely with me for nearly four years and I only hope I do not flatter myself in thinking that working together as a team we have accomplished far more than twice what either of us might have produced individually. His technical expertise has been central to all our experimental accomplishments. Even more important, his indefatigable good humor, scientific sense, and tolerance for my peculiarities have kept our scientific endeavors marching forward and our personal relationship warm.

The debt I owe to many older members of the group is harder to repay, as some of those who contributed most I barely knew. The legacy they left in the laboratory equipment I have worked would have been hard to reproduce, and to those who built the Pines' laboratory I can only issue a generalized thanks. Of those who overlapped with me in the group, Dr. Joel Garbow deserves credit for teaching much of what I have learned about spectrometers and, more generally, the field of NMR. He was always willing to sacrifice a few minutes to track down some baffling inconsistency or ponder some scientific point, no matter how trivial. He and his wife Debbie were also good friends.

Other students and postdocs associated with Alex's group in the past few years have contributed many happy hours arguing the fine points of my and their projects. It is the sort of vibrant intellectual environment I doubt could be recreated in many other locations.

Within the Department of Chemistry, the support staff is central to the excellence of the research efforts. The advice and instruction of Don Wilkinson of the Electronics Shop, and more recently, Dr. Yau-Man Chan, will be sorely missed.

Finally, I would like to acknowledge my friends, and particularly Andrea Thompson, who have never given up reminding me that a life exists beyond the cement walls of the sub-basement of Hildebrand Hall.

TABLE OF CONTENTS

I. Preliminaries....1

A. Microscopic and Quantum Mechanical Formalities....1

1. The Nuclear Spin....1

2. Rotations and Tensors....5

3. Hamiltonians: Tensor Notation....10

B. Nuclear Spin Hamiltonians....12

1. Laboratory Frame Interactions....12

a. Zeeman Hamiltonian....12

b. The Rf Hamiltonian: Rotations in Spin Space....13

2. Local or Molecular Frame Interactions....15

a. Chemical Shift....16

b. Dipole-Dipole Couplings....18

c. Quadrupole Couplings....21

d. J Couplings....23

C. Macroscopic Considerations....24

1. The Density Operator....24

a. Time Evolution....25

b. The Density Operator at Equilibrium....26

2. Magnetization, Polarization, and Other Order....27

3. Spin Temperature....29

4. Adiabatic Demagnetization: Strongly Coupled Spins....29

II. High Resolution High and Zero Field Nuclear Resonance....32

A. High Field NMR Methods....34

1. Coherent Averaging....34

2. Deconvolution Methods....35

B. Zero and Low Field NQR Methods.....37

1. Local Fields > 1 MHz and Isotopic Abundance High.....38

2. Local Fields ≤ 1 MHz or Isotopic Abundance Low.....38

a. Adiabatic Demagnetization.....40

1. Isolated Spins.....40

2. Coupled Spins.....50

3. Deuterium-Hydrogen Level Crossings.....58

b. Sudden Demagnetization.....61

C. Summary.....62

III. Fourier Transform Zero Field NMR and NQR.....65

A. A Practical Two-Step Field Cycle.....65

B. A Formal Calculation of the Signal.....68

C. Coupled Spin-1/2 Systems.....75

1. Two Identical Dipole-Dipole Coupled Nuclei.....75

2. Two Distinguishable Dipole-Dipole Coupled Nuclei.....78

3. Heteronuclear J Spectroscopy in Liquids.....89

D. Quadrupolar Spin Systems.....93

1. Integer Spins: I = 1.....94

a. The Signal Function.....94

b. Explicit Calculation of ρ.....95

2. Half-Integer Spins: I = 3/2, 5/2.....98

IV. Experimental Results: Dipolar Coupled Systems.....104

A. Two and Three Coupled Spin-1/2 Nuclei.....105

1. Contributions to the Linewidth.....106

a. Residual Fields.....106

b. Other Dipole-Dipole Couplings.....106

c. Dilution Studies.....111

d. Double Frequency Lines and More Water.....114

2. Beyond Water: the Methyl Group.....119

B. Heteronuclear Spin Systems.....127

C. More Complicated Spin Systems.....133

1. Structure Determination: N = 4.....137

2. Comparison of Zero and High Field NMR in Model Systems148

3. Zero Field NMR for N → Avogadro's Number.....152

V. Experimental Results: Quadrupolar Spin Systems.....162

A. Comparison of Chemical Shifts and Quadrupolar Couplings...162

B. High Field NMR of Deuterium.....167

C. Zero Field NQR of Deuterium.....173

VI. Variant Experiments.....196

A. Other Initial Conditions.....196

1. Initial Conditions Prepared in High Field.....196

2. Demagnetization to Zero Field.....202

B. Zero Field NMR with Pulsed dc Fields.....206

1. Transformation and Evolution of Quadrupolar Order.....212

2. Transformation and Evolution of Eta Order.....214

3. Calculation of Signals.....216

a. Sudden Switching of B.....216

b. Two-Pulse Experiments.....221

4. Summary.....234

C. Indirect Detection.....239

D. Zero Field-Zero Field Correlation Experiments.....246

1. Correlation between Zero Field Lines.....247

2. Cross-Correlation Through Dipole-Dipole Couplings.....251

VII. Considerations of Symmetry.....255

A. Formal Aspects....259
1. Symmetry Operations....259
2. Operations in Spin Space....259
a. Rotations about a Fixed Axis....260
b. Reflections Through a Plane....262
c. Inversion....263
d. Improper Rotation Axis....263
3. Operations in Time....263
B. Examples....267
1. Two Coupled Spin-1/2 Nuclei....267
a. Homonuclear Pair....267
b. Heteronuclear Pair....268
2. Four Spin Systems....269
a. The Square....269
b. The Rectangle....272
c. General Four-Spin Systems....275
3. Three Spins 1/2....276
4. Heteronuclear Spins....279
C. Conclusions....281
VIII. Experimental Details....282
A. Zero Field Region....282
1. Timing Considerations....283
2. Field Cycling....283
3. Area of Zero Field....287
4. Details of the Field Cycle....288
5. Zero Field Homogeneity....291
B. High Field NMR Spectrometer....291

I. Preliminaries

The work described in this thesis is primarily concerned with the extraction of chemical and structural information from disordered solid state systems. The technique to be described is nuclear magnetic resonance (NMR). In NMR, the nuclear moments which occur naturally in a large number of nuclei are used as spies to relay to the experimentalist microscopic details about the local environment often inaccessible by any other technique. The interactions of nuclei with their environment help elucidate chemical and/or structural properties of matter and, less directly, dynamical behavior. This information appears in its richest form in solid state materials. Yet it is also in solids that it is most difficult to reveal. This thesis describes a new technique for the extraction of such information with both high sensitivity and high resolution and from disordered systems. The method to be described is zero field NMR. The goal of this first chapter will be to present the required fundamentals.

A. Microscopic and Quantum Mechanical Formalities

1. The Nuclear Spin

Due to considerations of nuclear bonding whose origins remain mysterious but much appreciated by chemists, most atoms contain nuclei with a degree of freedom known as spin. The spin degree of freedom corresponds classically to a dipolar (or higher order) nuclear magnetic moment. The energy of an atom or molecule containing a nucleus with a magnetic moment depends on the state of the nucleus. Formally the

nuclear moment is treated as an angular momentum operator, which I will label with the generic symbol I. (Occasionally, when two different spins types with significantly different properties simultaneously comprise our spin system, the second will be labeled S.) This angular momentum satisfies all the traditional properties of angular momenta. In units where h=1

$$I^2|\psi(I,m)\rangle = I(I+1)|\psi(I,m)\rangle \tag{1.1}$$

and

$$I_z|\psi(I,m)\rangle = m|\psi(I,m)\rangle, \quad m=-I,-I+1,\ldots,I \tag{1.2}$$

I_z is conventionally chosen to be the diagonal component of the angular momentum and m is the projection of the angular momentum along the (arbitrarily chosen) z-axis. I may be either integral or half-integral and each nuclear spin I has 2I+1 magnetic sublevels. For I=1/2 the eigenstates are often represented by the short hand notation,

$$|\alpha\rangle \equiv |\psi(\tfrac{1}{2}, \tfrac{1}{2})\rangle \qquad |\beta\rangle \equiv |\psi(\tfrac{1}{2}, -\tfrac{1}{2})\rangle \tag{1.3}$$

There are two additional components of the angular momentum which are off-diagonal in the conventional basis set. In terms of raising and lowering operators,

$$I_+ |\psi(I,m)\rangle = [(I-m)(I+m+1)]^{1/2}|\psi(I,m+1)\rangle \tag{1.4}$$

and

$$I_- |\psi(I,m)\rangle = [(I+m)(I-m+1)]^{1/2}|\psi(I,m-1)\rangle \tag{1.5}$$

or, as angular momenta

$$I_x = \frac{1}{2} (I_+ + I_-) \tag{1.6}$$

and

$$I_y = \frac{1}{2i} (I_+ - I_-) \tag{1.7}$$

For spin-1/2 particles, these operators are proportional to the Pauli spin matrices, and

$$I_j = \frac{1}{2} s_j \tag{1.8}$$

where

$$s_j^2 = E \tag{1.9}$$

for E the identity operator. The Pauli matrices s_j satisfy

$$\begin{aligned} s_j s_k s_j &= - s_k \qquad \text{if } j \neq k \\ &= s_k \qquad \text{if } j = k \end{aligned} \tag{1.10}$$

The different components of the angular momentum operators satisfy the commutation relations

$$[I_{jp}, I_{kq}] = I_{jp} I_{kq} - I_{kq} I_{jp} = i\epsilon_{jkl} \delta_{pq} I_l \tag{1.11}$$

where j,k, and l are any cyclic permutation of x, y, and z, and p and q identify a specific nucleus.

We will ignore the possibility that excited nuclear states might make any contribution to observables in whatever follows, as the energy differences between the ground and excited states is exceedingly large and requires exotic instrumentation.[1]

The magnetic moment of the nucleus interacts with any and all surrounding electromagnetic fields. The strength of that interaction

is governed by two parameters. The first is some physical constant characteristic of the structure of all similar nuclei (and presumably measured many years ago when magnetic resonance experiments were carried out in physics laboratories with the goal of measuring these nuclear properties). The second and more important parameter is some local environmental variables which differ from molecule to molecule and site-to-site and are characteristic of structural or chemical properties at those sites. The measurement and interpretation of these

Table 1.1: Nuclear Spin Hamiltonians

Interaction	Form of the Hamiltonian
Chemical Shift	$H_{cs} = -\gamma I \cdot \tilde{\sigma} \cdot B_0$
Dipole-Dipole	$H_D = -I_j \cdot \tilde{D} \cdot I_k$ where $j \neq k$ and
	$D_{\alpha\beta} = \gamma_j \gamma_k \hbar\, r_{jk}^{-3} (\delta_{\alpha\beta} - 3e_\alpha e_\beta)$ and
	$\alpha, \beta = x, y, z$ and e_α is a direction cosine
J coupling	$H_J = -I_j \cdot \tilde{J} \cdot I_k$ where $j \neq k$
Quadrupole	$H_Q = -\frac{eQ}{4I(2I-1)\hbar} I \cdot \tilde{V} \cdot I$ where
	$\tilde{V} = \{V_{\alpha\beta}\};\ \alpha, \beta = x, y, z$

latter parameters is the goal of this work and all modern NMR. These chemically sensitive terms include the chemical shift, the direct dipole-dipole coupling, the quadrupolar coupling, and the J coupling. The Hamiltonians corresponding to these interactions are summarized in Table 1.1.[2] More useful expanded forms will be derived below. To arrive at these other forms will require a brief development of tensor notation.

2. Rotations and Tensors

The Hamiltonians of Table 1.1 are expressed as products of spin (I) and spatial (e.g. $\tilde{D}$ and $\tilde{V}$) terms. Each is a tensor. It will prove necessary to delve rather deeply and often into the problem of the operations of angular momenta and their higher order relatives, with specific reference to their transformation properties under rotations. Traditionally rotations between axis systems are parameterized in terms of the Euler angles (α,β,γ) and a rotation operator $R(\alpha,\beta,\gamma)$.[3,4] These three angles relate a three-dimensional coordinate system to any other via three rotations: a rotation of γ radians about the original z-axis, β radians about the new y-axis, and α radians about the newest z-axis, with α and $\gamma \leq 2\pi$ and $\beta \leq \pi$. It is awkward to work with this set of rotations about a set of continually varying axes, and it is customary to derive the form of the rotation operator referenced to a fixed set of axes. In this fixed set of axes, the rotation operator R can be formally written

$$R(\alpha,\beta,\gamma) = R(0,0,\gamma)R(0,\beta,0)R(\alpha,0,0) \tag{1.12}$$

that is, a rotation about the fixed z axis by α radians, the fixed y axis by β, and the fixed z axis by γ. As an example, consider the form of a general operator ξ expressed in the basis set of the coordinate system (x,y,z) when viewed instead from a new reference frame (x',y',z'). The operator has not changed, and no observables associated with the operator ξ can be affected by simply reexpressing it in a new basis set. Only the description of that operator differs. This is made more formal if we note that, for any operator P

$$P^{-1}P = PP^{-1} = E \tag{1.13}$$

where E is the identity operator. By definition, multiplication by the identity operator leaves all operators unchanged; that is,

$$\begin{aligned} \langle x,y,z|\xi|x,y,z\rangle &= \langle x,y,z|P^{-1}P\xi P^{-1}P|x,y,z\rangle \\ &= \langle x',y',z'|P\xi P^{-1}|x',y',z'\rangle \end{aligned} \tag{1.14}$$

and

$$P|x,y,z\rangle = |x',y',z'\rangle \tag{1.15}$$

For $P = R(\alpha,\beta,\gamma)$ this establishes a simple relationship between the form of the operator in the old frame of reference and the new. For vectors in three space, the transformation R can be derived from geometric considerations. Its most general form is

$$R(\alpha,\beta,\gamma) = \begin{bmatrix} \cos\gamma & \sin\gamma & 0 \\ -\sin\gamma & \cos\gamma & 0 \\ 0 & 0 & 1 \end{bmatrix} \begin{bmatrix} \cos\beta & 0 & -\sin\beta \\ 0 & 1 & 0 \\ \sin\beta & 0 & \cos\beta \end{bmatrix} \begin{bmatrix} \cos\alpha & \sin\alpha & 0 \\ -\sin\alpha & \cos\alpha & 0 \\ 0 & 0 & 1 \end{bmatrix} \tag{1.16}$$

This sort of transformation functions merely as a bookkeeping operation and can have no fundamental effect on any observables. It may, however, serve as a notational aid by taking observables from one reference frame to a second. Presumably, the interesting behavior of these observables is more succinctly expressed or observed in the new reference frame.

The description of rotations on operators which are not readily expressed as vectors in three-space is more difficult, and is the motivation for the development of techniques for the study of the algebras of angular momenta.[5] Angular momentum and higher order spherical tensor operators serve as a convenient basis set for the

description of many problems in NMR. The general form of the spherical tensors is presented here and provides the groundwork for subsequent chapters. We will take as fundamental Racah's definition of the spherical tensors;[6] that is, an operator T_q^k is a spherical tensor operator of rank k and order q if

$$[I_{\pm 1}, T_q^k] = T_{q\pm 1}^k ((k\mp q)(k\pm q+1))^{1/2} \tag{1.17}$$

and

$$[I_0, T_q^k] = qT_q^k \tag{1.18}$$

where

$$I_{\pm 1} \equiv \pm(2)^{-1/2} (I_x \pm iI_y) \tag{1.19}$$

and

$$I_0 \equiv I_z \tag{1.20}$$

The commutation relations can be used to derive the transformation properties of the spherical tensors (and/or angular momenta) under rotations. The angular momentum operators are the generators of finite rotations. Following Edmonds,[3]

$$R(\alpha,\beta,\gamma) = \exp(i\gamma I_z)\exp(i\beta I_y)\exp(i\alpha I_z) \tag{1.21}$$

Writing down an expanded form for the exponential operators of Equation (1.21):

$$\exp(i\theta I_j) = 1 + i\theta I_j - \frac{1}{2}\theta^2 I_j^2 - \frac{i}{6}\theta^3 I_j^3 + \ldots \tag{1.22}$$

Because the nuclear spin basis vectors are chosen as eigenstates of I_z

rotations about the z-axis are particularly simply expressed and

$$\exp(i\theta I_z)|\psi(I,m)\rangle = (1 + i\theta m - \frac{1}{2}\theta^2 m^2 - \frac{i}{6}\theta^3 m^3 + \ldots)|\psi(I,m\rangle$$

$$= \exp(i\theta m)|\psi(I,m)\rangle \tag{1.23}$$

Rotations about the x- and y-axes are more difficult to derive from first principles. An explicit expression will be derived using the Pauli spin matrices and will therefore be a proof only for the case of a spin-1/2 nucleus. All higher dimensional systems follow by induction from this proof.

Consider a rotation through an angle $\theta \equiv 2\phi$ about the j axis. Using Equation (1.8) to reexpress the rotation in terms of the Pauli matrices;

$$R = \exp(i\theta I_j) = \exp(i\phi s_j) = 1 + i\phi s_j - \frac{1}{2}\phi^2 s_j^2 - \frac{i}{6}\phi^3 s_j^3 + \ldots$$

$$= \cos\phi + i\, s_j \sin\phi \tag{1.24}$$

For $s_j \neq s_k$ (otherwise, the rotation commutes with the operator),

$$\exp(i\phi s_j)(\frac{1}{2} s_k)\exp(-i\phi s_j) = \frac{1}{2}(\cos\phi + is_j\sin\phi)s_k(\cos\phi - is_j\sin\phi)$$

$$= \frac{1}{2}[\cos^2\phi\, s_k + \sin^2\phi\, s_j s_k s_j + i\sin\phi\cos\phi\,(s_j s_k - s_k s_j)]$$

$$= \frac{1}{2}((\cos^2\phi - \sin^2\phi)\, s_k - 2\sin\phi\cos\phi\, s_l)$$

$$= \cos 2\phi\, I_k - \sin 2\phi\, I_l$$

$$= \cos\theta\, I_k - \sin\theta\, I_l \tag{1.25}$$

Explicit matrix representations of the rotation operators are given by

the Wigner rotation matrices $D^j_{mm'}(\alpha,\beta,\gamma)$. Symmetry properties relate many of the elements of the D matrices,[7] and will often be exploited.

Summarizing, for any operator ξ

$$R\xi R^{-1} = D(\alpha,\beta,\gamma)\xi D^{-1}(\alpha,\beta,\gamma)$$

$$= D(\alpha,\beta,\gamma)\xi D(-\gamma,-\beta,-\alpha) \tag{1.26}$$

and

$$R = D(\alpha,\beta,\gamma) = \exp(im\gamma)\ d^j_{mm'}(\beta)\ \exp(im\alpha) \tag{1.27}$$

where the $d(\beta)$ matrices are the matrix representations of the operator which for j = y guarantee that Equation (1.27) holds. If ξ is a spherical tensor, a special relationship holds:

$$R\ T^k_q\ R^{-1} = \sum_{p=-q}^{q} D^k_{pq}(\alpha,\beta,\gamma)\ T^k_p \tag{1.28}$$

that is, tensors of rank k transform under rotations only into other tensors of the same rank. Generally, analytic forms for the transformation properties of the spherical tensors will only be required for k = 1 or 2 (as k = 0 is trivial and all others a bit too involved.) Zeroth rank tensors are invariant to all rotations; first rank tensors transform as vectors, and second rank tensors have the rotational properties of the d electronic orbitals. The important transformation properties of the spherical tensors are encapsulated in Equation (1.28).

As the spherical tensors are traditionally defined they exhibit particularly simple transformation properties with respect to rotations about the z-axis. More frequently in NMR applications rotations about the x-y plane are required. Table 1.2 gives the transformations of a

Table 1.2: Transformations of Operators

A. Definitions of Second Rank Tensors U_k:

$$U_0 \equiv 6^{-1/2}\,[3I_z^2 - I(I+1)]$$

$$U_{1+} \equiv 2^{-1/2}\,(I_yI_z + I_zI_y) \qquad U_{2+} \equiv 2^{-1/2}\,(I_x^2 - I_y^2)$$

$$U_{1-} \equiv 2^{-1/2}\,(I_xI_z + I_zI_x) \qquad U_{2-} \equiv 2^{-1/2}\,(I_xI_y + I_yI_x)$$

B. Transformation under Rotations $R_j(\theta)$:

$$R_x(\theta)\begin{bmatrix} U_0 \\ U_{1+} \\ U_{1-} \\ U_{2+} \\ U_{2-} \end{bmatrix} R_x(-\theta) = \begin{bmatrix} -\sqrt{3}\{\frac{1}{2}\sin^2\theta\, U_{2+} - \sin\theta\cos\theta\, U_{1+}\} + \frac{1}{2}(3\cos^2\theta - 1)U_0 \\ -\sin\theta\cos\theta\, U_{2+} + \cos 2\theta\, U_{1+} - \sqrt{3}\,\sin\theta\cos\theta\, U_0 \\ \sin\theta\, U_{2-} + \cos\theta\, U_{1-} \\ \frac{1}{2}(1+\cos^2\theta)\, U_{2+} + \sin\theta\cos\theta\, U_{1+} - \frac{\sqrt{3}}{2}\sin^2\theta\, U_0 \\ \cos\theta\, U_{2-} - \sin\theta\, U_{1-} \end{bmatrix}$$

$$R_y(\theta)\begin{bmatrix} U_0 \\ U_{1+} \\ U_{1-} \\ U_{2+} \\ U_{2-} \end{bmatrix} R_y(-\theta) = \begin{bmatrix} \sqrt{3}\,\{\frac{1}{2}\sin^2\theta\, U_{2+} - \sin\theta\cos\theta\, U_{1-}\} + \frac{1}{2}(3\cos^2\theta - 1)U_0 \\ -\sin\theta\, U_{2-} + \cos\theta\, U_{1+} \\ -\sin\theta\cos\theta\, U_{2+} + \cos 2\theta\, U_{1-} + \sqrt{3}\,\sin\theta\cos\theta\, U_0 \\ \frac{1}{2}(1+\cos^2\theta)\, U_{2+} + \sin\theta\cos\theta\, U_{1-} + \frac{\sqrt{3}}{2}\sin^2\theta\, U_0 \\ \cos\theta\, U_{2-} + \sin\theta\, U_{1+} \end{bmatrix}$$

$$R_z(\theta)\begin{bmatrix} U_0 \\ U_{1+} \\ U_{1-} \\ U_{2+} \\ U_{2-} \end{bmatrix} R_z(-\theta) = \begin{bmatrix} U_0 \\ \cos\theta\, U_{1+} + \sin\theta\, U_{1-} \\ -\sin\theta\, U_{1+} + \cos\theta\, U_{1-} \\ \cos 2\theta\, U_{2+} - \sin 2\theta\, U_{2-} \\ \sin 2\theta\, U_{2+} + \cos 2\theta\, U_{2-} \end{bmatrix}$$

set of linear combinations of the second rank spherical tensors which will frequently prove useful in the analysis of NMR experiments and in the zero field NMR and NQR experiments which follow.

3. Hamiltonians: Tensor Notation

The fundamental problem of NMR is the solution of the time-dependent Schroedinger equation. It is therefore necessary to find a convenient representation of the nuclear spin Hamiltonians which will simplify the task of the calculation and analysis of spectra. This presents a paradox. The Hamiltonian is a scalar operator and is presumably unaffected by rotations and/or translations in space. Yet it is a continuing theme in modern NMR experiments that an appreciation of the properties of tensors under rotations is essential to understanding modern NMR experiments.

The solution to this apparent paradox is that the nuclear spin Hamiltonians of Table 1.1 are the products of tensorial interactions. Just as the dot product takes two vectors and produces a number operator, the generalized dot product of two kth rank tensors is

$$H = (T \cdot C) = \sum_{q=-k}^{k} (-1)^q \, T_q^k \, C_{-q}^k \qquad (1.29)$$

Hamiltonians can always be expressed as just such a contraction of two tensor operators. One (C) operates on the spatial degrees of freedom and the other (T) on the spin degrees (which, however, are expressed in a basis set necessarily referenced to the laboratory frame fixed in space). While at intermediate stages of the calculation, either spin or spatial variables may take "center stage" separately or sequentially, actual calculation of Hamiltonians requires that ultimately the contraction of Equation (1.29) is performed. Rotations which operate

separately in only one or the other of the reference frames profoundly effect the observables. Bulk rotations of the entire system, which transform the two sets of spherical tensors identically from one reference frame to a second can have no effect on observables. An attempt will be made to clearly delineate between those rotations which are transformations between coordinates, and which effect only bookkeeping, (of which Equation (1.14) is an example) and a rotation of either the spin or spatial frames with respect to the other, whereby observables of the system are fundamentally altered.

B. Nuclear Spin Hamiltonians

The total nuclear spin Hamiltonian consists of a number of independent contributions. There are two broad classifications of interactions: laboratory frame interactions under the control of the experimentalist, and local or molecular frame interactions whose measurement is the goal of the experiment. As the laboratory frame interactions are the experimentalist's only tools, they will be detailed first.

1. Laboratory Frame Interactions

a. The Zeeman Hamiltonian

This Hamiltonian describes the direct coupling of the nuclear spin magnetic moment with an externally applied magnetic field. Its form is

$$H_Z = - \sum_j \gamma_j \hbar I_{zj} B_0 = \Sigma \omega_{0j} I_{zj} \tag{1.30}$$

where $\gamma_j \hbar$ is the nuclear moment of the jth spin and is characteristic of a particular nucleus and ω_{0j} is the Larmor frequency. Magnetogyric

ratios of many common nuclei are $\omega_0/2\pi \sim 1$ kHz/gauss in familiar units, or ~ 10 MHz/Tesla in more proper units. Nnumerical values are almost universally assigned not in angular frequency units of radians/sec (ω), but in the more common frequency units $\nu = \omega/2\pi$ where the standard unit is hertz. In common laboratory fields of a 1-10 Tesla (10-100 kgauss) the Larmor frequencies of most nuclei fall between 10-500 MHz.

b. <u>The Rf Hamiltonian: Rotations in Spin Space</u>

Oscillating magnetic fields are the experimentalist's primary tool for the manipulation of nuclear spin systems. We will assume that the rf field is applied in the plane perpendicular to the static magnetic field, and

$$H_{rf} = 2\gamma_j \hbar B_1 \cos \omega t \, I_\phi = \omega_1 [\exp(i\omega t) + \exp(-i\omega t)] \, I_\phi \quad (1.31)$$

where ω is the frequency of the applied rf field, ω_1 its strength, and

$$I_\phi = \cos\phi \, I_x + \sin\phi \, I_y \quad (1.32)$$

All subsequent calculations are simplified if the rf Hamiltonian is transformed into an equivalent time-independent form. This is known as moving to an interaction picture, or entering the rotating frame. All other Hamiltonians will need to be modified to consistently fit this rotating frame picture of the rf Hamiltonian. Starting from the time-dependent Schroedinger equation (with energies expressed in angular frequency units so as to remove all factors of Planck's constant):

$$i \frac{\delta \Psi}{\delta t} = H \Psi \quad (1.33)$$

with

$$H = H_Z + H_{rf} + H_{loc} \tag{1.34}$$

where H_{loc} refers to all the local interactions to be described immediately below. Substituting

$$\Psi = U\Theta = \exp(i\omega I_z t)\ \Theta \tag{1.35}$$

and Θ represents the eigenstate in the rotating frame. Then the Schroedinger equation can be rewritten

$$i\ \frac{\delta(U\Theta)}{\delta t} = i\ (\frac{\delta U}{\delta t}\ \Theta + U\ \frac{\delta\Theta}{\delta t}) = HU\Theta \tag{1.36}$$

Rearranging,

$$i\ \frac{\delta\Theta}{\delta t} = (U^{-1}H\ U - iU^{-1}\ \frac{\delta U}{\delta t}\ )\ \Theta \tag{1.37}$$

But

$$\frac{\delta U}{\delta t} = i\omega\ I_z U \tag{1.38}$$

and

$$i\ \frac{\delta\Theta}{\delta t} = (U^{-1}H\ U + \omega I_z)\ \Theta \tag{1.39}$$

Using the rotation operators tabulated previously, the rotating frame Zeeman Hamiltonian is written

$$U^{-1}\ H_Z\ U \equiv \tilde{H}_Z = \sum_j (\omega - \omega_0)\ I_{jz} = \sum_j \Delta\omega\ I_{jz} \tag{1.40}$$

where the rotated Hamiltonian is indicated by the ~ and $\Delta\omega$ is the resonance offset. Similarly, in the rotating frame

$$U^{-1}\ H_{rf}U \equiv \tilde{H}_{rf} = \omega_1\ [1 + \exp(2i\omega t)]\ I_\phi \tag{1.41}$$

and the rf Hamiltonian in the rotating frame contains both a static

component and a rapidly rotating component. If $\omega_0 >> \omega_1$ then only components of $\tilde{H}$ whose time average over many Larmor periods $(\omega_0)^{-1}$ is nonzero contribute (to first order) to observable features. The rapidly rotating component of Equation (1.41) has zero time average and can be ignored, and the first order rf Hamiltonian is

$$H'_{rf} = \langle \tilde{H}_{rf} \rangle_t = \omega_1 I_\phi \tag{1.42}$$

For each of the H_{loc}, these same two steps (entering the rotating frame and averaging over the Larmor period) will need to be repeated. If $\omega = \gamma B_0$ (Equation (1.40)), then in the rotating frame the Zeeman Hamiltonian is zero. This is referred to as the on-resonance condition and the rf field is most effective in causing transitions between eigenstates. As long as $\omega_1 \sim \Delta\omega$ the rf field is near resonance and can interact with the spin system. Generally the on-resonance condition is assumed. If the rf Hamiltonian is strong ($H_{rf} >> H_{loc}$) and on resonance then the effect of the applied rf field may be well-approximated as a rotation in spin space about the ϕ axis in the x-y plane.

2. <u>Local or Molecular Frame Interactions</u>

Each of the molecular frame Hamiltonians is a second-rank tensor, and a principle axis system exists where its matrix representation can be given a diagonal form. As these Hamiltonians are not necessarily observed in the principle axis system but more generally in the laboratory frame of reference and in the rotating frame, each of the local Hamiltonians will have representations in their own principal axes, in the lab frame, and in the rotating frame. As the rotation operators have been defined in this chapter, there exists a rotation R,

defined with respect to the fixed laboratory frame of reference, such that $R(\gamma,\beta,\alpha)$ takes operators from the local or molecular frame of reference (subscripted M) into the laboratory frame (subscripted L). This coordinate transformation is shown in Figure 1.1. R^{-1} performs the inverse rotation;

$$R\xi_M R^{-1} = \xi_L \tag{1.43}$$

In the rotating frame at high field the orientation of the x and y axes is arbitrary and without loss of generality we can choose $\gamma = 0$ and

$$R = R(0,\beta,\alpha) \equiv R(\Omega) \tag{1.44}$$

If the internal Hamiltonians are observed in high field this transformation between the principal axis system and the laboratory frame is required in order to explain the observed spectra. Where two or more interactions are simultaneously present there will be a different R for each interaction.

a. Chemical Shift

The symbol $\tilde{\sigma}_j$ represents the chemical shift tensor of the jth nucleus (typically ~ ppm). The largest component of the Zeeman interaction is isotropic and chemically uninformative. The chemical shift $\tilde{\sigma}_j$ is a correction to the Zeeman Hamiltonian which arises from the shielding of the external magnetic field due to perturbations in the electron cloud at a given site. The chemical shift is an anisotropic second rank tensor and different for chemically distinguishable sites. The size of the anisotropy is comparable to the interaction itself. In its principal axis system,

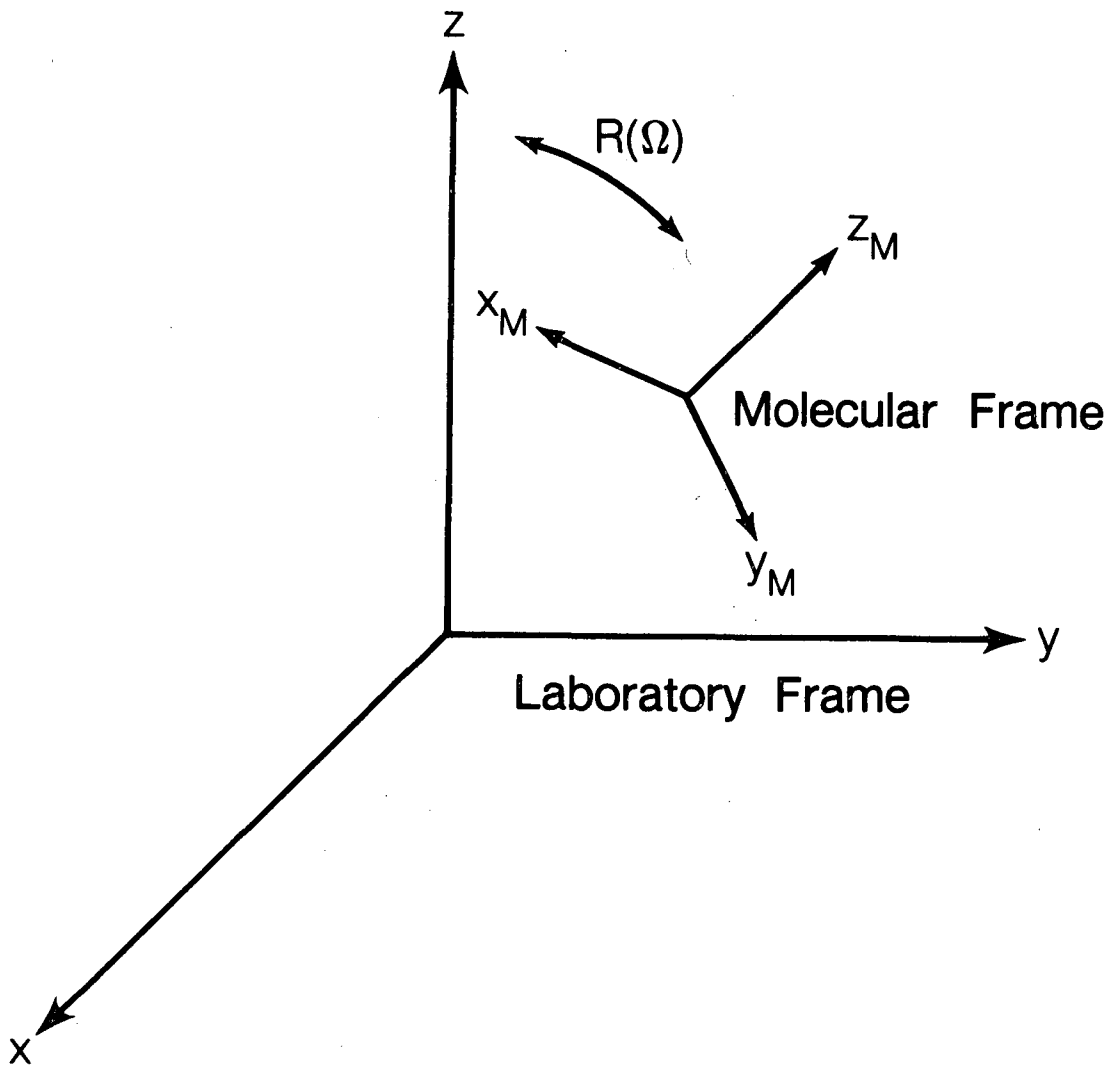

Figure 1.1. Relationship between the laboratory frame of reference (x,y,z) and the molecular frame (x_M,y_M,z_M). The laboratory frame is reached from the molecular frame by a rotation R(Ω) about the laboratory-fixed axis system. The most general rotation R(Ω) is described by rotations about the z, y, and z axes successively. In most NMR applications, only the latter two rotations are necessary.

XBL 855-8884

$$H_{cs} = - \sum_j \gamma_j \hbar B_0 \cdot \tilde{\sigma}_j \cdot I \tag{1.45}$$

Because its magnitude is proportional to the applied field B_0, in zero applied field $H_{cs} = 0$. In the rotating, laboratory frame related to the principal axis system by the transformation $R(0,\beta,\alpha)$

$$H'_{cs} = - \sum_j \gamma_j \hbar B_0 I_{zj} [\sigma_{iso} + \frac{1}{2} \sigma_{aniso} (3\cos^2\beta - 1 + \eta \sin^2\beta \cos 2\alpha)] \tag{1.46}$$

While most high resolution NMR techniques[2,8] emphasize the importance of measuring the isotropic component of the chemical shift and/or its anisotropic components, in the work to be described below the existence of a chemical shift will rarely prove relevant and in most cases it will be ignored.

b. <u>Dipole-Dipole Couplings</u>

In many spin-1/2 systems and in particular for ^1H nuclei, the dipole-dipole couplings dominate the spectral features in the solid state. The classical energy of one magnetic dipole in the field of a second is

$$H_D = - \frac{\mu_1 \mu_2}{r_{12}^3} \{I_1 \cdot I_2 - \frac{3}{r_{12}^2} (I_1 \cdot r_{12})(I_2 \cdot r_{12})\} \tag{1.47}$$

Substituting $\mu_i = \gamma_i \hbar$, the dipole coupling constant (again, in angular frequency units) is given by

$$\omega_D^{12} = \frac{\gamma_1 \gamma_2 h}{2\pi r_{12}^3} \tag{1.48}$$

For many coupled spins, the dipole-dipole Hamiltonian is given as a sum over all pairs, and

$$H_D = \sum_{j \neq k} H_{Djk} \tag{1.49}$$

Henceforth I focus on a single pair. In zero applied field, the two-spin dipole-dipole Hamiltonian (Equation (1.49)) has four eigenstates and three distinct energy levels. The eigenstates can be divided into the triplet manifold (T_+, T_0, and T_-) and a singlet (S), whose energies are

$$\begin{aligned} \langle T_+|H_D|T_+\rangle &= \langle T_-|H_D|T_-\rangle = -\frac{1}{2}\omega_D \\ \langle T_0|H_D|T_0\rangle &= \omega_D \quad \langle S|H_D|S\rangle = 0 \end{aligned} \tag{1.50}$$

The rotating frame form of Equation (1.49) is given by again expanding in a laboratory-based reference frame. As H_D and H_Q are formally identical (except that there is no asymmetry parameter η in the static dipolar tensor) the same treatment will apply to the quadrupolar coupling to be treated below, and[9]

$$H_D = -\omega_D (A + B + C + D + E + F) \tag{1.51}$$

with

$$\begin{aligned} A &= I_{1z}I_{2z}(1-3\cos^2\theta) \\ B &= \frac{1}{2}(1-3\cos^2\theta)(I_{1z}I_{2z} - I_1 \cdot I_2) \\ C &= -\frac{3}{2}\sin\theta\cos\theta\exp(i\phi)(I_{1z}I_{2+} + I_{1+}I_{2z}) \\ D &= C^* \\ E &= -\frac{3}{4}\sin^2\theta\exp(2i\phi)(I_{1+}I_{2+}) \\ F &= E^* \end{aligned} \tag{1.52}$$

(These forms differ slightly from those found in most standard

references[10,11] because I have defined the transformation between L and M frames with what amounts to opposite signs of the Euler angles from most authors.) When the dipolar Hamiltonian is observed in the presence of a large external magnetic field, it is further necessary to enter the rotating frame where the rf Hamiltonian is static and the dipole-dipole Hamiltonian observed in high field is

$$H_D' = \langle\tilde{H}_D(t)\rangle = -\frac{\omega_D}{\omega_0}\int\exp(-i\omega I_z t)(A+B+C+D+E+F)\exp(i\omega I_z t)dt$$

$$= -\omega_D(A + B) \qquad (1.53)$$

Because the A and B terms have an explicit dependence on R the energy levels of the truncated dipolar Hamiltonian do as well. In any reasonably large field, no higher order correction terms are necessary.

The truncated Hamiltonian described above may require further modification. The B term in Equation (1.53) contains spin operators which "flip" spin 1 while spin 2 "flops." These flip-flop terms are effective only if the total energy of the system is conserved. If the spin system contains spins with two different magnetogric ratios γ_I and γ_S then the spin reference frame is doubly accelerated with respect to each of the Larmor frequencies. The B terms of the dipolar Hamiltonian are then oscillatory at frequencies comparable to the difference in Larmor frequencies. For heteronuclear spins (say ^{13}C and ^{1}H) this large difference in Zeeman energies makes these flip-flop terms ineffective; their time average is zero. Even for a single spin species (meaning $\gamma_I = \gamma_S$) the flip-flop terms may be truncated by large chemical shift differences[12] or quadrupole coupling constants.[11]

c. Quadrupole Couplings

For spins $I \geq 1$, the largest of the internal Hamiltonians is most often the quadrupolar Hamiltonian. It arises from the electrostatic interaction of an asymmetric charge distribution in the nucleus with surrounding electric field gradients (created by an asymmetric electron cloud distribution). This interaction is present in ~70% of all the elements in the periodic table. In spherical tensor notation, the form of the quadrupolar Hamiltonian is

$$H_Q = -\sum_j \frac{eq_j}{4I(2I-1)\hbar} I_j \cdot \tilde{V}_j \cdot I_j \tag{1.54}$$

which emphasizes that it is characteristic of a single spin label and site. The nuclear quadrupole moment, eq, is a fixed nuclear parameter. Therefore, the nuclear quadrupole interaction in any particular compound is determined entirely by the size and direction of the electronic field gradient, $\tilde{V}$. H_Q is often more chemically sensitive than is the chemical shift. Quadrupole coupling constants are quite broad-ranged (~10 kHz - 1 GHz), and we will concentrate in this work on systems at the low end of this range.

In the principle axis system and using the conventional definitions,[13,14]

$$V_{zz} = eQ \tag{1.55}$$

$$\eta = \frac{V_{yy} - V_{xx}}{V_{zz}} \leq 1 \tag{1.56}$$

$$|V_{zz}| > |V_{yy}| > |V_{xx}| \tag{1.57}$$

and

$$V_{xx} + V_{yy} + V_{zz} = 0 \tag{1.58}$$

Further defining

$$A_{Qj}(I) = \frac{e^2 q Q_j}{4I(2I-1)\hbar} \tag{1.59}$$

the quadrupolar Hamiltonian for a single spin takes on the simple expanded form

$$H_Q = - A_Q(I) \; [3I_z^2 - I(I+1) + \eta \; (I_x^2 - I_y^2)] \tag{1.60}$$

For a spin 1 nucleus in zero field, there are three eigenstates (x,y, and z) with energies

$$\langle x|H_Q|x\rangle = -(1-\eta)A \qquad \langle y|H_Q|y\rangle = -(1+\eta)A \qquad \langle z|H_Q|z\rangle = 2A \tag{1.61}$$

For quadrupolar nuclei in high field, the same transformations performed on H_D must be applied to H_Q. Rotating into the laboratory frame and then into the rotating frame, the truncated first order quadrupolar Hamiltonian is

$$H'_{Qj} = - \frac{1}{2} A_{Qj}(I)(3I_z^2 - I(I+1)) \; [(1-3\cos^2\beta)+\eta\sin^2\beta\cos 2\alpha] \tag{1.62}$$

If

$$H_Z \gg A_{Qj}(I) \tag{1.63}$$

then the first order approximation may suffice. If the high field condition of Equation (1.63) does not hold, it may be necessary to go higher order in perturbation theory. The second order shift in energy due to the quadrupolar coupling is[15,16]

$$H''_{Qj} = -\frac{3A_{Qj}^2 \hbar I_z}{\omega_0} \{c_1(4I(I+1)-1-8I_z^2) + c_2(2I(2I+1)-1-2I_z^2)\} \quad (1.64)$$

where

$$c_1 = \left[\frac{\eta^2}{6}(\sin^2 2\alpha - \cos^2\beta\cos^2 2\alpha + \frac{3}{2}\cos^2\beta - \eta\cos^2\beta\cos 2\alpha\right] \sin^2\beta \quad (1.65)$$

$$c_2 = \frac{3}{8}\sin^4\beta + \frac{\eta^2}{6}\left[c_3^2\cos^2 2\alpha - \cos^2\beta\sin^2 2\alpha\right] + c_3\frac{\eta}{2}\sin^2\beta\cos 2\alpha \quad (1.66)$$

and

$$c_3 = 1 - \frac{1}{2}\sin^2\beta \quad (1.67)$$

d. <u>J Couplings</u>

The final significant interaction is the J coupling (also called the exchange coupling, electron mediated dipole coupling, or indirect dipole-dipole coupling). Its form is

$$H_J = -\sum_{j\neq k} I_j \cdot \tilde{J}_{jk} \cdot I_k \quad (1.68)$$

In general, the J couplings are anisotropic with an isotropic component. Only the latter is routinely measured. Anisotropic components of the J tensor have the same transformation properties as the dipolar couplings and are rarely separable from them. The isotropic J coupling takes the form

$$H_J = -\sum_{j\neq k} J(I_{zj}I_{zk} + \frac{1}{2}(I_{+j}I_{-k} + I_{-j}I_{+k})) \quad (1.69)$$

In zero field, two J coupled spins can be classified in the same sets of eigenstates as the dipolar coupled pair (i.e. the triplet and the singlet). All the triplet energy levels are degenerate, and

$$\langle T|H_J|T\rangle = -\frac{1}{4}J \qquad \langle S|H_J|S\rangle = \frac{3}{4}J \tag{1.70}$$

The isotropic J coupling is independent of orientation even in high field. If, however, the jth and kth spin Larmor frequencies differ by much more than the size of the J coupling, then the flip-flop terms are truncated and in the weak coupling limit

$$H_J = \sum_{j \neq k} J\, I_{zj} I_{zk} \tag{1.71}$$

C. Macroscopic Considerations

1. The Density Operator

The density operator is a convenient bookkeeping formalism for the description of macroscopic phenomena.[17] It serves as a shorthand method for summarizing all available information about macroscopic ensembles of quantum systems. Due to the small size of the quantum of nuclear spin energy (for example, $h\omega_0 \sim 100$ MHz corresponds to a thermal energy $kT \sim 5$ mK) no NMR detector is capable of observing individual events of absorption or emission. Only the average behavior weighted over a large number of similar systems is detected. The density operator serves as a convenient formalism for the calculation of the parameters of such macroscopic systems, to the extent that the experimentalist has any knowledge or control over such parameters. Formally, we can define the matrix representation of ρ as

$$\rho_{ab} = \overline{c_a^* c_b} \tag{1.72}$$

where the coefficients c_a and c_b are the probability factors that the

system is in eigenstate a or b, and the bar over the product indicates ensemble averaging over some large number of otherwise identical systems. The diagonal elements ρ_{aa} are the populations of the energy levels. Off-diagonal elements are termed coherences.

Expectation values for operators are given by

$$\langle\xi\rangle = \mathrm{Tr}\,[\xi\rho] = \mathrm{Tr}\,[\rho\xi] \tag{1.73}$$

a. Time Evolution

More importantly, time evolution under a Hamiltonian operator H is readily treated using this formalism. The Von-Neumann equation for the evolution of ρ is

$$\frac{\delta\rho}{\delta t} = i[\rho,H] = i(\rho H - H\rho) \tag{1.74}$$

For H time-independent, a formal solution to the differential equation is

$$\rho(t) = \exp(-iHt)\rho(0)\exp(iHt) \tag{1.75}$$

The abth element of ρ can be evaluated

$$\begin{aligned}\rho_{ab}(t) &= \exp(-iE_a t)\rho(0)\exp(iE_b t)\\ &= \rho_{ab}(0)\exp(i(E_b - E_a)t)\\ &= \rho_{ab}(0)\exp(i\omega_{ba}t) = \rho_{ab}(0)\exp(-i\omega_{ab}t)\end{aligned} \tag{1.76}$$

If H is not time-independent, we will assume it can be subdivided into n time-independent pieces. Then the Von-Neumann equation can be integrated stepwise over each time-interval and in each step Equation (1.75) holds. Over n such time intervals,

$$\rho(t) = \exp(-iH_n t_n)\ldots\exp(-iH_1 t_1)\rho(0)\exp(iH_1 t_1)\ldots\exp(iH_n t_n) \tag{1.77}$$

is a formal solution and $\exp(-iH_m t_m)$ is termed a propagator. Fourier

transformation with respect to any one of the t_m results in a one-dimensional spectrum with all the other time variables as parameters; Fourier transformation with respect to two different time variables results in a two-dimensional spectrum[18] where the one-dimensional spectra are the projections onto the ω_1 and ω_2 axes, and the crosspeaks correspond to correlations between the two time-variables.

b. The Density Operator at Equilibrium

For a spin system in equilibrium with the lattice at a finite temperature T_L, the populations of the system satisfy the Boltzmann distribution law,

$$\frac{n_a}{n_b} = e^{-\Delta E/kT} \tag{1.78}$$

where

$$\Delta E = E_a - E_b = \omega_{ab} \tag{1.79}$$

At equilibrium ρ is necessarily time-independent and no coherences may exist. The equilibrium density operator is completely characterized by the population ratios of Equation (1.78). As nuclear spin energies in attainable laboratory fields are considerably smaller than thermal energies, the exponentials of energy differences in the distribution law can be expanded in a power series and truncated after the first term, and

$$\frac{n_a}{n_b} \simeq 1 - \frac{\Delta E}{kT} \tag{1.80}$$

This is the high field, high temperature approximation. We will never be concerned with the density operator as such but instead its close relative, the reduced density operator defined by

$$\rho_o = \rho - bE \tag{1.81}$$

where E is the unit matrix and b is a normalization constant chosen such that

$$Tr[\rho] = 1 \tag{1.82}$$

The dynamical evolution of the reduced density operator, ρ_0, and the density operator, ρ, are identical as the identity operator E commutes with all unitary operations. All subsequent references to the density operator will refer to the reduced density operator and the subscript will be dropped.

The equilibrium density operator in the high temperature limit is proportional to its energy. In high field, the Zeeman Hamiltonian is much larger than the local Hamiltonians, and in operator form

$$\rho = b_I I_z = \sum_j b_I I_{zj} \tag{1.83}$$

with

$$b_I = - \frac{\gamma_I B}{ZkT} \tag{1.84}$$

and Z is the partition function. Where only a single spin species is involved, then all of the b_I's are identical and without loss of generality it can be omitted (as it serves only to scale the absolute size of all observables). When more than a single type of magnetic nucleus exists in the sample, it will generally prove important to retain at least the ratio between the normalization constants.

2. <u>Magnetization, Polarization, and Other Order</u>

The nuclear ordering which appears as a sample in high field reaches equilibrium with the lattice gives rise to a longitudinal

magnetization, whose value is given by

$$M = \gamma\hbar \, \mathrm{Tr}\, [\rho I_z] \tag{1.85}$$

At equilibrium in high field for all other operators ξ

$$\mathrm{Tr}\, [\rho\xi] = 0 \text{ if } \mathrm{Tr}\, [I_z\xi] = 0 \tag{1.86}$$

This is a restatement of the Curie law

$$M = \chi_0 B_0 = \frac{N\gamma^2\hbar^2 I(I+1)}{3kT} B_0 \tag{1.87}$$

Equally spaced energy levels are characterized by equal population differences. Transverse magnetization is longitudinal magnetization which has been rotated into the x-y plane and therefore $\mathrm{tr}(I_x\rho)$ or $\mathrm{tr}(I_y\rho)$ is nonzero. Transverse magnetization is normally the only observable. The magnitude of the signal observed in an rf coil is given by the Faraday law of induction, and

$$\epsilon \sim \frac{d\phi}{dt} \sim \omega_0 M_x \tag{1.88}$$

where ϕ is the flux in the coil. Polarization will be used rather loosely to describe the more general case of any long-lived steady state; i.e.

$$[\rho, H] = 0 \tag{1.89}$$

and at least one operator ξ exists, such that $\mathrm{Tr}\, [\rho\xi] \neq 0$. Last, coherence refers to any off-diagonal elements of the density operator (transverse magnetization or otherwise).

It will occasionally be necessary to talk about the "size" of an operator, e.g. when by some technique order is transferred from one spin to a second. Arguments about the "size" of an operator can be

made more exact by referring to a function called the norm. If P is a matrix, $||P||$ represents its norm. The norm is roughly analogous to the length of a vector. Formally, the norm is a function such that:[19]

1. $||P|| > 0$ unless $P_{ij} = 0$ for all i,j. Then $||P|| = 0$.
2. For all constants a, $||aP|| = a||P||$.
3. $||P_1 + P_2|| \leq ||P_1|| + ||P_2||$.

A definition of the norm of an (nxn) matrix is

$$||P|| = \sqrt{\mathrm{Tr}\ [PP^{\dagger}]/n} \tag{1.90}$$

The norm is equivalent to the rms eigenvalue of P. As the eigenvalues of ρ are just its population differences, as the norm decreases there is less nuclear spin polarization.

3. Spin Temperature

If in high fields a longitudinal magnetization exists in the sense of Equation (1.83) yet its magnitude is incommensurate with the Curie law for $T = T_L$ where T_L is the lattice temperature, then we will define a spin temperature T_s such that the Curie law holds. For times short compared to the spin-lattice relaxation time T_L, spin and lattice temperatures need not be correlated.

4. Adiabatic Demagnetization: Strongly Coupled Spins

The concept of spin temperature is intimately connected to the process known as adiabatic demagnetization in either the laboratory frame (ADLF)[20] or rotating frame (ADRF),[21-23] although I will be primarily concerned with the former. If a sample of polarized strongly coupled nuclei is removed slowly from the polarizing field, as long as $\gamma B_f \gg H_{loc}$ the density operator ρ remains unchanged and

$$T_s = \frac{B_f}{B_0} T_L \tag{1.91}$$

where B_0 is the initial value of the field and B_f its final value. If the demagnetization is allowed to proceed to $B_f = 0$, then Equation (1.91) cannot hold because it implies that the spin temperature vanishes. This difficulty is eliminated if the effects of the dipolar fields are included. The spin temperature hypothesis[24,25] assumes that the density operator remains describable by a spin temperature at all values of the field and therefore ρ is always proportional to the instantaneous Hamiltonian. If the spin temperature hypothesis holds, then the demagnetization can be followed through all values of the external field B_0, and Equation (1.91) is only an approximation to the complete description of T_s,

$$T_s = \left[\frac{B_f^2 + B_{loc}^2}{B_0^2 + B_{loc}^2}\right]^{1/2} T_L \tag{1.92}$$

for $B_{loc} = H_{loc}/\gamma$. For $B_0 = 0$, the final density matrix is (as usual, to within a proportionality constant)

$$\rho = H_{loc} \tag{1.93}$$

Because H_{loc} contains only bilinear terms the density operator of Equation (1.93) corresponds not to a magnetization but instead to some other form of nuclear spin polarization. If the spin system is not strongly coupled then the spin temperature hypothesis is not expected to hold and the results of an slow demagnetization are more difficult to predict. Some discussion of this more complex and interesting case is given in Chapter II and again in Chapter VI.

In the presence of extensive networks of dipole-dipole couplings, it may become difficult to define what in fact constitutes the system being studied. I will define a spin system as being any set of coupled spins where the B terms in the dipolar Hamiltonian are effective in establishing a common spin temperature. Therefore, I-S (e.g. ^{1}H-^{13}C) systems in high field will be treated as two independent systems. Furthermore, for S a quadrupolar ($I \geq 1$) nucleus in an ordered phase, two S spins with different quadrupole couplings also constitute two independent spin systems. In zero field, all spin-1/2 nuclei constitute a spin system which may be treated as isolated spins only to the extent that some of the dipole-dipole couplings are significantly larger than all others. In these systems the spin temperature hypothesis is not expected to hold. Quadrupolar spins in environments of lower than cubic symmetry are always isolated except perhaps at some accidental value of both the externally applied magnetic field and orientation of two neighboring spins where spin diffusion is rapid.

II. High Resolution High and Zero Field Nuclear Resonance

One of the greatest of impediments to the use of NMR as a technique for the routine analysis of solids is the problem of "powder broadening."[26] In the solid state all of the largest terms and most interesting constituents of the local frame Hamiltonians (chemical shift, dipole-dipole coupling, and quadrupole coupling) are anisotropic. When observed as a perturbation on the high field Zeeman Hamiltonian, their magnitude depends on the precise relationship between the orientations of the local principal axes and the externally applied field (as described in Section I.B).

Often only powders or similarly disordered systems are available. Then the absorption lineshape $f(\omega)$ consists of one or more absorption lines and essentially a different spectrum for each local system orientation present in the sample. The bandwidth of absorption is as large as the magnitude of the local Hamiltonians. Where the interaction of interest is a single-body interaction (i.e. a chemical shift or quadrupolar coupling) powder lineshapes may be sufficiently structured so that some information may be extracted.[26,27] But where the spectrum arises from large numbers of strongly interacting spins ($\geq$3 coupled spin-1/2 nuclei) resolved structure in high field powder patterns is unusual,[28-30] and the high field powder spectrum generally resembles a broad and featureless band like the spectrum of Figure 2.1. Even for the single-body interactions, the presence of overlapping lines from chemically or crystallographically inequivalent sites may render these spectra uninterpretable. In this chapter, I briefly review the most common approaches to high resolution NMR in solids and,

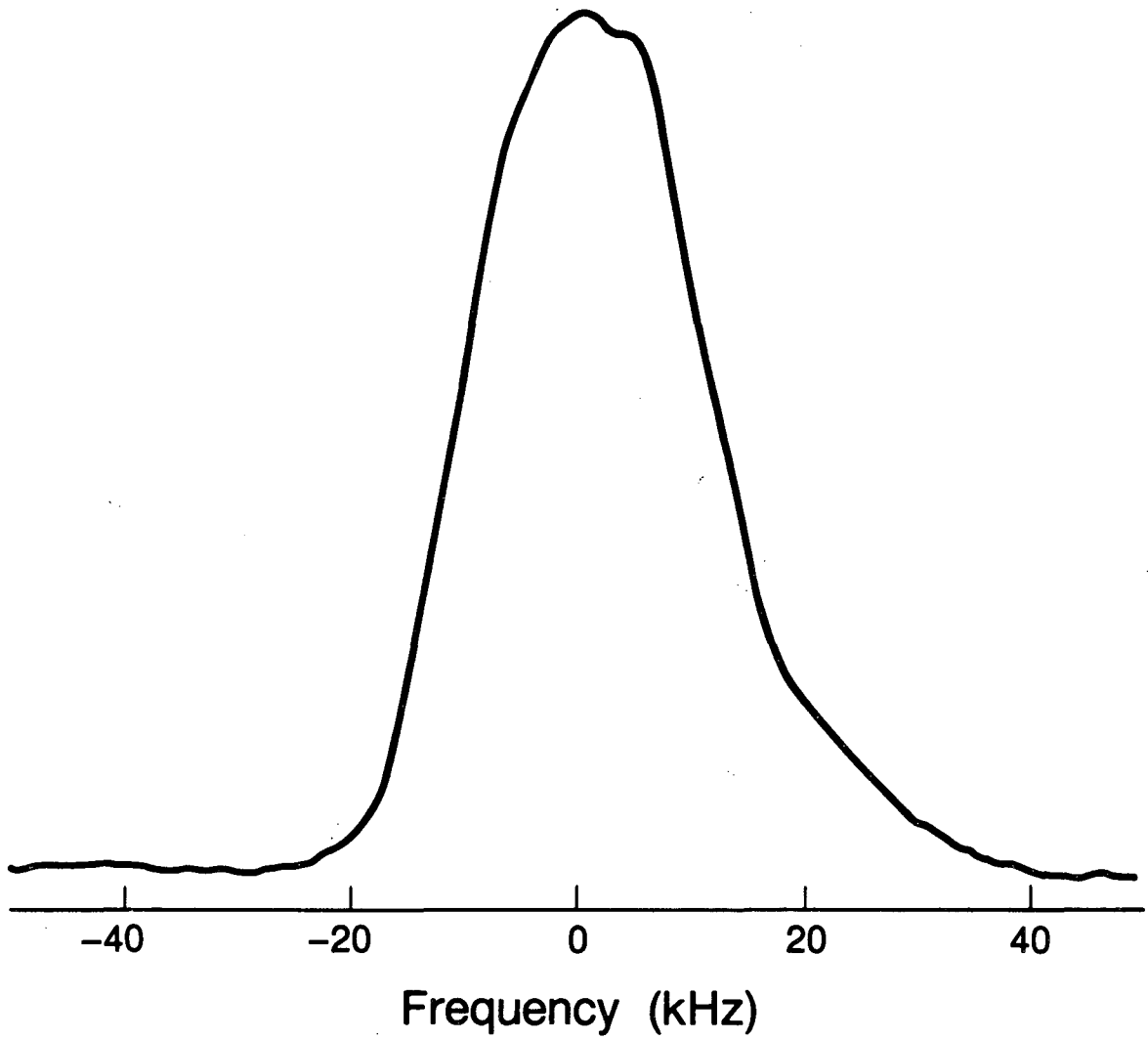

XBL 854-9808

Figure 2.1. High field spectrum of 1,2,3,4-tetrachloronapthalene bis(hexachlorocyclopentadiene) adduct. Like most dipolar powder patterns, little structure is resolved even though only a small number of spins (4) are strongly coupled one to another.

in somewhat more detail, to high sensitivity pure NQR.

A. High Field NMR Methods

1. Coherent Averaging

As the presence of high resolution NMR facilities at virtually every chemistry department testifies, the routine measurement of chemical shifts in solution by NMR is central to the identification and characterization of chemical compounds. In analogy to liquid state spectroscopy, by far the largest number of high resolution solid state NMR studies[2,8] emphasize the primacy of chemical shifts, due both to its chemical sensitivity and its ease of interpretation. Because the chemical shift is often no larger than (and generally much smaller than) the other local fields, these other terms must be suppressed before the solid state chemical shifts can be observed. In liquids, nature averages all the anisotropic interactions to zero via rapid, isotropic motion. In solids, the experimentalist attempts to mimic the process of stochastic averaging used in nature with some form of coherent averaging. As such, experimental work has emphasized:

1. Isolation of individual spins. Resonant rf fields can be used to decouple abundant spins (typically ^{1}H) from rare (^{13}C, ^{15}N, ^{31}P) so that the latter might be observed free of the heteronuclear couplings.[31] Alternatively, multiple pulse sequences (WAHUHA,[32] MREV-8,[33] BR-24[34]) which decouple the abundant spins from one another allow for observation of spectra dominated by only their chemical shifts.

2. Averaging out of the chemical shielding anisotropy (CSA). As

the solid state chemical shift contains an anisotropic component (Equation (1.46)), chemical shift spectra of powders are broad and may be poorly resolved. Chemical shift powder patterns can be transformed to narrow line spectra by:

a) Choosing to work with single crystals; or, more generally, by

b) Magic angle sample spinning (abbreviated MASS, occasionally MAS or MAR).[35] Slow spinning breaks the CSA powder pattern into a finite (preferably small) number of sharp lines.[36] Rapid spinning produces liquid-like spectra.

3. Combinations of (1) and (2).

In polycrystalline or disordered samples what is ideally accomplished is the obliteration of all anisotropic components of the local Hamiltonians. The traceless interactions (quadrupolar, dipolar, and heteronuclear J couplings) are averaged to zero and become irrelevant while the isotropic terms (homonuclear J couplings or isotropic chemical shifts) survive and are measured. Rarely, multiple-pulse NMR is used to isolate small numbers of interacting spins (typically an I_nS system). In favorable cases dipole-dipole couplings can be extracted from the resulting powder spectra[37-39]. Combinations of MAS and multiple pulse techniques result in high-resolution two-dimensional chemical shift-dipole-dipole correlation spectra.[40]

High resolution NMR in solids is reviewed in significantly greater detail in texts devoted to the subject.[2,8]

2. <u>Deconvolution Methods</u>

As the quadrupolar coupling constant A(I) often is large neither

the high field nor strong rf assumptions need hold. Because to first order the $|-1/2\rangle \rightarrow |1/2\rangle$ transition is unshifted by the quadrupolar Hamiltonian, the spectrum observed in NMR experiments on half-integral quadrupolar nuclei in asymmetric environments may be due exclusively to coherence between these two energy levels. Residual spectral broadening is often dominated by the second order quadrupolar frequency shift (Equation (1.64)). Correction terms from higher-order perturbation theory depend on angular factors which differ from the $P_2(\cos\theta)$ dependence of either the first order shifts or the chemical shift anisotropy, and there is no laboratory axis about which rapid spinning simultaneously eliminates both the second-order quadrupolar broadening and the CSA. Even with MASS, all that is observed is an averaged powder pattern which results from a convolution of the partially averaged second order quadrupolar and chemical shift anisotropy powder patterns.[41]

Even where only a portion of the quadrupolar spectrum can be observed it is possible to accurately measure quadrupolar couplings in half-integer spin systems using two-dimensional NMR techniques. The central transition spectrum can be observed as a function of the flip angle $\theta = \omega_1\tau_p$, where τ_p is the length of the applied rf pulse. Fourier transformation with respect to the rate of nutation of the observable in the rf field results in characteristic patterns which are matched to the fundamental parameters, A(I) and η.[42] Where many such patterns overlap, the analysis becomes more difficult.

In the important case of the spin-1 nucleus (^{14}N or ^{2}D) a third possibility exists. Bloom and coworkers use an algorithmic method they call "de-Paking" to extract quadrupolar tensors from experimentally

observed high field powder patterns.[43] If a specific form for the powder lineshape distribution function is assumed, high field spectra can be processed so as to separate out the quadrupolar couplings (which serve as a scaling constant determining the overall spectral width) from the assumed lineshape function. If the assumed lineshape (generally, η=0) is a good approximation to the real form the deconvolution results in a sharp line for each distinct quadrupolar coupling constant in the sample.[44,45] Where the actual lineshape function differs from the assumed form, the de-Paked spectra are distorted.

De-Paking is most successfully applied to ^{2}D NMR, where the quadrupolar tensor is often axially symmetric and the quadrupole moment not so large as to make the spectroscopy prohibitively difficult. This is not the case for ^{14}N. As its quadrupole moment is large and its magnetogyric ratio is small, solid-state ^{14}N NMR spectra are rarely observed.[46] Because high quality high field ^{14}N spectra are so difficult to measure, neither de-Paking nor any other high field technique is generally useable.

B. Zero and Low Field NQR Methods

The motivation for zero- and low-field solid state magnetic resonance experiments is clear; in zero field, the local frame Hamiltonians are observed directly and at their untruncated values. The high field powder methods described above achieve high resolution by averaging away the anisotropic terms in the Hamiltonian. Zero field methods aim instead to render the anisotropy irrelevant by removing the

laboratory-based reference axis.

Experiments in zero field NMR date from the earliest years of magnetic resonance.[47] Both theoretical and experimental work on the behavior of strongly coupled spin systems in low fields ($H_z \sim H_{loc}$), particularly in connection to the spin temperature hypothesis, is extensive.[11,24,25] Nonetheless, zero field NQR experiments are far more common.[14] For pure NQR, there are two experimentally very different cases which need be treated separately:

1. Local Fields > 1 MHz and Isotopic Abundance High

At high frequencies and nuclear densities, direct observation of the pure NQR spectrum is possible using straightforward techniques. For ^{35}Cl, the zero field resonance frequency is often ~30 MHz, and as this isotope appears at relatively high natural abundance (~75%) the expected signal amplitudes are comparable to many high field NMR experiments done at similar frequencies. In analogy to NMR experiments rf pulses applied at resonance to an NQR line result in a free induction signal whose transform is the spectrum of that transition[48] or a continuous wave (CW) sweep may reveal the spectrum more directly. Experimental complications arise because the NQR lines may appear at widely separated frequencies; or, for spin-3/2 nuclei, a small Zeeman field is required to lift some degeneracies and provide complete information about the quadrupolar tensor. These techniques are well-known and relatively unrelated to the work described in the rest of this thesis. Standard reference works provide a deeper treatment.[13,14]

2. Local Fields ≤ 1 MHz or Isotopic Abundance Low

Where the local fields are small and/or the interesting magnetic nuclei appear at low density, direct detection of pure NQR is difficult

due to the low frequencies and/or small numbers of nuclei which contribute to the signal. In most direct detection schemes the signal available for detection is $\sim O(\omega^2)$. In extraordinary circumstances (low T, high density of spins, and/or large sample volumes)[49] or with non-Faraday law SQUID detectors,[50] zero field signals can be detected at these low frequencies but such opportune circumstances are rare. Often the low sensitivity of pure NQR necessitates more elaborate experiments with higher sensitivity.

Most high-sensitivity methods use field cycling techniques of the sort introduced by Ramsey and Pound[51] to probe the zero field frequencies indirectly. Preparation of polarization and observation of the signal take place in as large an applied field as is available so as to maximize the detected signal. In between these two phases of the experiment, the spin system is brought to low or zero field and its behavior monitored as a function of the evolution in these low fields. Because nuclear spin-lattice relaxation times (T_1) in solids may be rather long (anywhere from 100 ms to 100 hours depending on the temperature, nuclear spin species, and the specific compound) the field cycle need not be executed particularly rapidly. Unless otherwise specified, the nuclear spin T_1's will be assumed much longer than any other time interval in the experimental scheme (an assumption which may often imply lowered temperatures and inconveniently long polarization periods!) and will not be a limiting factor in performing the experiments.

The field cycling and level-crossing experiments of Ramsey and Pound, Andersen,[52] Redfield,[53] Hahn,[54] and others[55-58] are closely related to the Fourier transform zero field experiments[59-63] which are

the main subject of this thesis, and will be described in some detail. Their high sensitivity is inextricably linked to the behavior of spin systems under demagnetization. In the presence of large quadrupolar splittings, quadrupolar nuclei are not strongly-coupled to one another and the demagnetization is not characterized by a spin temperature. Therefore, the rest of this chapter will be devoted to some predictions about the form of a system of spins after demagnetization from a large applied field.

a. Adiabatic Demagnetization

1. Isolated Spins

The simplest case that can be treated is that of an isolated spin (for concreteness, $S = 1$) initially polarized in a large external field, B_0. For simplicity, H_Z in the polarizing field is assumed much larger than H_Q. Then the initial density operator ρ^S corresponds to a magnetization proportional to S_Z (Equation (1.83)). The applied field is slowly reduced from its initial value B_0 to zero. At the end of the demagnetization ρ has some new form which we wish to make explicit.

In principle, the time development of ρ can be solved numerically by direct integration of the Von-Neumann time development Equation (1.73) through all values of the external field and times. This is, however, a tedious operation which results in little physical insight. In the limiting case of an adiabatic field sweep a more appealing, approximate presentation is possible.[64]

In an adiabatic process and where the Hamiltonian contains no degenerate eigenstates for any value of the time-dependent parameter, the populations which characterize the final density operator are those which characterize the initial density operator. Whatever populations

are prepared in high field are taken over smoothly into the zero field eigenstates which correlate to the high field eigenstates. The problem, then, is reduced to ascertaining the correlations between high and zero field eigenstates with particular attention to values of the field where eigenstates may become degenerate. At most values of the field, the correlations are obvious. Certainly as long as $H_Z \gg H_Q$, the eigenstates are always approximately equal to the eigenstates of the high field Hamiltonian H_Z. Similarly, at low values of the applied field (where $H_Z \ll H_Q$) the true eigenstates are nearly the eigenstates of the zero field Hamiltonian H_Q. Only for values of the external field where $H_Z \sim H_Q$ and where eigenstates of the full Hamiltonian become degenerate or nearly degenerate are the correlations between eigenstates problematic.

This situation is shown in Figure 2.2. The exact problem is to identify the correlations between eigenstates before and after a level-crossing of the sort illustrated in the figure. Near the level crossing field two possibilities exist: first, that the eigenstates follow the "trajectories" described by the solid lines in the boxed region. For some value of the external field the energies of the two eigenstates go through an "accidental degeneracy" where the eigenstates are degenerate. At any arbitrarily small distance on either side of the crossing the eigenstates are well-defined and correlations can be established. But within the framework of the adiabatic approximation, no conclusions can be drawn about the transfer of populations. For an energy splitting rigorously equal to zero, no finite rate of demagnetization can satisfy the conditions of the adiabatic approximation. If level crossings are frequent, then only a very

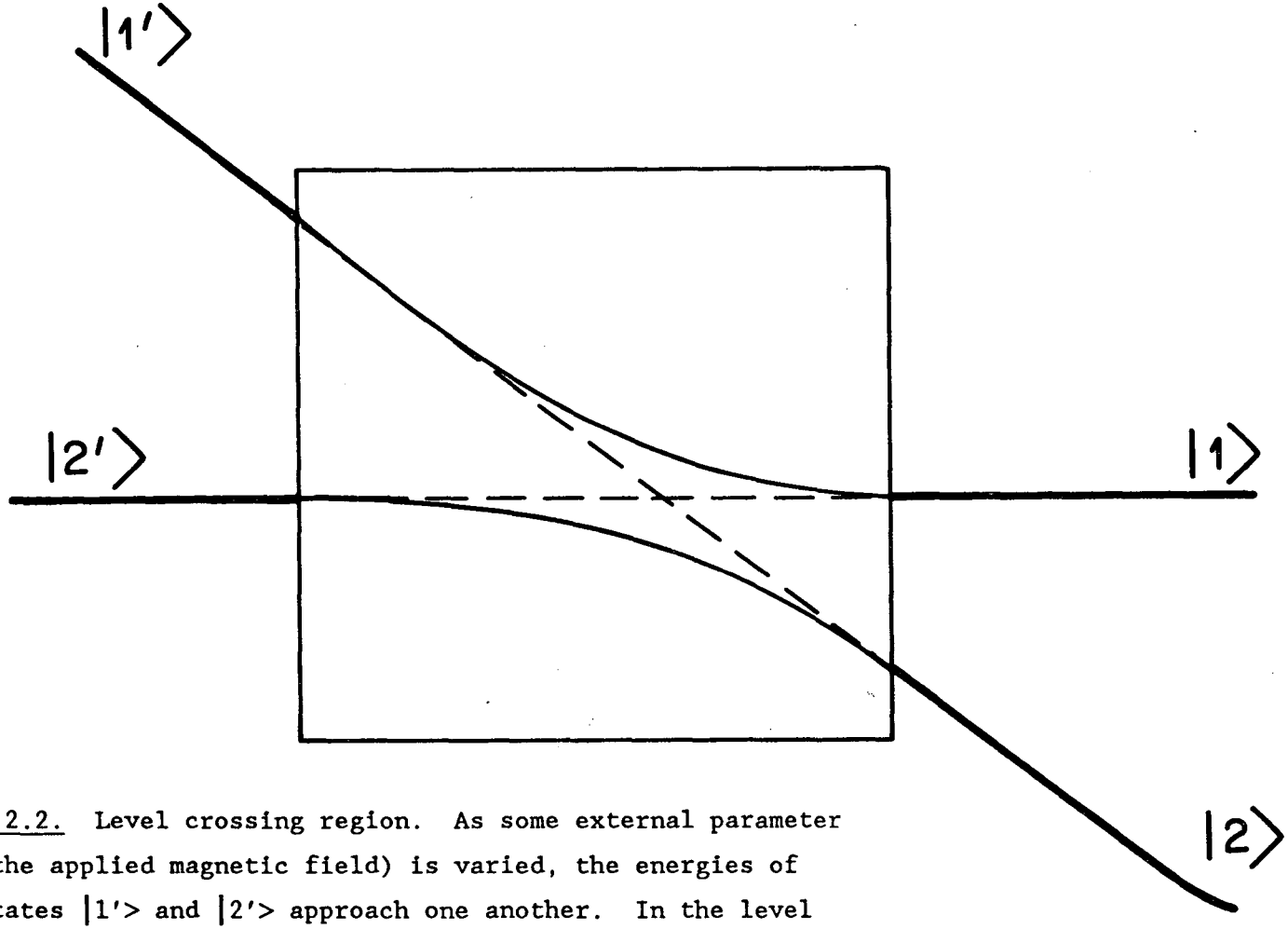

Figure 2.2. Level crossing region. As some external parameter (e.g. the applied magnetic field) is varied, the energies of eigenstates |1'> and |2'> approach one another. In the level crossing region (boxed area) the eigenstates may either cross (dotted lines) or avoid one another (solid lines).

XBL 858-3219

different approach will afford any insight into the nature of the demagnetized operator ρ.

The second possibility, of course, is that there is no level crossing. This case is shown in the correlation trajectory described by the dotted lines in Figure 2.2 and corresponds to an anti-level crossing or an avoided crossing. In an avoided crossing and within the framework of the adiabatic approximation, the populations are maintained in the same energy-ordered sequence before and after the avoided crossing. If there are only avoided crossings, then the demagnetized operator ρ is simple to predict. All populations are conserved in precisely the same energy level ordering scheme in high and low fields.

Yet again the question appears merely to have been reformulated, and in a form that appears no more tractable. Now the task is to identify whether allowed or avoided crossings are more likely, and whether the level-crossing behavior depends on the details of the spin system or not. The solution is surprisingly simple. Pairs of eigenstates which far from the level crossing region are uncoupled by off-diagonal matrix elements may cross. As no coupling term exists, two such energy levels cannot know that there is any crossing to be avoided. If, however, the Hamiltonian contains coupling terms which are off-diagonal and make no first order contribution to the energies far from the level crossing region all crossings are avoided. As the difference in energies of the two eigenstates becomes arbitrarily close to zero, what was formerly merely a perturbation can no longer be treated by perturbation theory, and the effect of the "perturbation" is to cause the eigenstates of the system to repel one another.

This difference will be made explicit using the specific example of a spin-1 nucleus. (Explicit expressions for the eigenstates and energies of spin-1 and spin-3/2 nuclei as a function of field are available[65] but will not be used because they provide little qualitative insight.) The full Hamiltonian consists of a term proportional to the Zeeman frequency in the applied field and a quadrupolar term,

$$H = H_Q + H_Z \tag{2.1}$$

The Zeeman Hamiltonian is generally represented in the laboratory frame of reference as described in Section I.B. As the high field approximation need not hold (because the applied field takes on all values and the crossing field occurs where $H_Z \sim H_Q$), it is preferable to represent both H_Q and H_Z in a single consistently defined frame and in practice I will use the molecular frame, where the total Hamiltonian is

$$H = H_Q + a_1 S_x + a_2 S_y + a_3 S_z \tag{2.2}$$

The a_j are proportional both to the direction cosines and sines derived from $R(\Omega)$ which relate the molecular axis system to the laboratory direction along which the external field is applied, and to the strength of the applied field. Only the latter changes during the demagnetizations. Therefore the eigenstates of H depend both on the strength and direction of the applied field. In either of the two extreme limits ($H_Z \gg H_Q$ or $H_Z = 0$) these eigenstates are readily identified as either the high field ($|1'\rangle$, $|2'\rangle$, and $|3'\rangle$) or zero field ($|1\rangle$, $|2\rangle$, and $|3\rangle$) eigenstates, numbered in order of descending energies. At intermediate values of the field, the eigenstates will be

represented as $|p\rangle$, $|q\rangle$, and $|r\rangle$ which correspond in the zero field limit to $|1\rangle$, $|2\rangle$, and $|3\rangle$.

Table 2.1

A. Eigenstates and Eigenvalues of Spin-1 in Zero Field:

$$|2\rangle \equiv |x\rangle = -i\,(2)^{-1/2}\,[\,|+1\rangle - |-1\rangle]; \qquad \langle 2|H_Q|2\rangle = -A(1-\eta)$$

$$|1\rangle \equiv |y\rangle = (2)^{-1/2}\,[\,|+1\rangle + |-1\rangle]; \qquad \langle 1|H_Q|1\rangle = -A(1+\eta)$$

$$|3\rangle \equiv |z\rangle = |0\rangle \quad ; \qquad \langle 3|H_Q|3\rangle = 2A$$

$|+1\rangle$, $|-1\rangle$, and $|0\rangle$ are the projections of I_z on the molecular z-axis

B. Matrix Representations of I_x, I_y, I_z

$$\sqrt{2}\,I_x = \begin{array}{c} \\ \langle x| \\ \langle y| \\ \langle z| \end{array}\!\!\begin{array}{c} \begin{array}{ccc} |x\rangle & |y\rangle & |z\rangle \end{array} \\ \begin{bmatrix} 0 & 0 & 0 \\ 0 & 0 & 1 \\ 0 & 1 & 0 \end{bmatrix} \end{array} \quad \sqrt{2}\,I_y = \begin{array}{c} \\ \langle x| \\ \langle y| \\ \langle z| \end{array}\!\!\begin{array}{c} \begin{array}{ccc} |x\rangle & |y\rangle & |z\rangle \end{array} \\ \begin{bmatrix} 0 & 0 & 1 \\ 0 & 0 & 0 \\ 1 & 0 & 0 \end{bmatrix} \end{array} \quad \sqrt{2}\,I_z = \begin{array}{c} \\ \langle x| \\ \langle y| \\ \langle z| \end{array}\!\!\begin{array}{c} \begin{array}{ccc} |x\rangle & |y\rangle & |z\rangle \end{array} \\ \begin{bmatrix} 0 & i & 0 \\ -i & 0 & 0 \\ 0 & 0 & 0 \end{bmatrix} \end{array}$$

In the conventional basis set of zero field NQR[66] given, along with a number of operator representations, in Table 2.1, each angular momentum operators couples pairs of eigenstates only, and in matrix form the Hamiltonian is

$$H = \begin{array}{c} \\ \langle 2| \\ \langle 1| \\ \langle 3| \end{array}\!\!\begin{array}{c} \begin{array}{ccc} |2\rangle & |1\rangle & |3\rangle \end{array} \\ \begin{bmatrix} -A(1-\eta) & ia_3 & a_2 \\ -ia_3 & -A(1+\eta) & a_1 \\ a_2 & a_1 & 2A \end{bmatrix} \end{array} \tag{2.3}$$

If any two of the a_j's are zero then the external field mixes only pairs of the zero field basis vectors. This problem can be diagonalized exactly and the eigenstates and energies written down as a function of the Zeeman energy. Choosing only $a_2 \neq 0$ (i.e. the field applied along the molecular y axis)

$$H = H_Q + a_2 S_y \tag{2.4}$$

The energy of state $|p\rangle$ is independent of the field and $|1\rangle$ is an eigenstate for all values of the a_2. $|1\rangle$, $|p\rangle$, and $|2'\rangle$ are identical. The other two ($|q\rangle$ and $|r\rangle$) are mixed states. The eigenvalue equation for this pair is

$$(-\lambda-(1-\eta)A)(-\lambda+2A) - a_2^2 = \lambda^2 - \lambda A(1+\eta) - (2A^2(1-\eta) + a_2^2) = 0 \tag{2.5}$$

with eigenvalues

$$\lambda = \frac{A(1+\eta)\pm\sqrt{A^2(1+\eta)^2 + 8A^2(1-\eta) + 4a_2^2}}{2} \tag{2.6}$$

$$= \frac{1}{2} A(1+\eta) \pm \frac{1}{2}\sqrt{A^2(3-\eta)^2 + 4a_2^2} \tag{2.7}$$

In the limit $a_2 \to 0$, the eigenvalues are (as might be expected)

$$\lambda_\pm = 2A, \ -A(1-\eta) \tag{2.8}$$

while in the high field limit $a_2 \gg A$ the eigenvalues are

$$\lambda_\pm = \pm a_2 + \frac{1}{2}(1-\eta)A \tag{2.9}$$

The details of the correlation diagram depend on the absolute sign of A (and the convention used in defining H_Q; NQR and NMR conventions generally differ.[65] Consistency with equation (1.54) is intended if not maintained). For A positive, $|1'\rangle$ correlates with $|1\rangle$; for A negative, to $|3\rangle$. In either case, $|3'\rangle$ correlates with $|2\rangle$. Also in either case, there is one level crossing in the correlation diagram for demagnetization along the molecular y-axis. The level crossing behavior expected for demagnetization precisely along the x, y, and z-

axes respectively is shown in Figure 2.3 for A assumed positive. For demagnetization along these axes, level crossings are allowed and the adiabatic approximation can not be applied.

If, however, at least two of the three coefficients a_j are nonzero, then all level crossings become avoided crossings. Thus as any pair of energy levels approach one another they repel and $|1\rangle$ always correlates with $|1'\rangle$, $|2\rangle$ with $|2'\rangle$, etc. As long as the adiabatic condition is satisfied, populations remain ordered as they were in high field.

Consider the Hamiltonian of Equation (2.3) with A positive, $a_2 \gg a_1$ and $a_3 = 0$. This corresponds to applying the external field not precisely along the molecular y-axis but instead tipped slightly into the y-z plane. It is reasonable to treat the component of the field along the molecular z-axis (whose magnitude is represented by a_1) as a perturbation and to ignore its effects on the mixing of states $|2\rangle$ and $|3\rangle$. It will have important consequences only in the range of values of the external field where the level crossing occurs for $a_1 = 0$ and where $|q\rangle$ and $|r\rangle$ are nearly degenerate. This corresponds to the range of values of fields where the energy of $|q\rangle$ in the absence of a_1 differs by no more than 2δ from $E = -A(1+\eta)$. Then the $|p\rangle$, $|q\rangle$ subblock of H is

$$H^{pq} = \begin{array}{c} \\ \langle p| \\ \langle q| \end{array} \begin{array}{c} \begin{array}{cc} |p\rangle & |q\rangle \end{array} \\ \begin{bmatrix} E + 2\delta & \epsilon \\ \epsilon & E \end{bmatrix} \end{array} \tag{2.10}$$

where ϵ is proportional to a_1. The associated eigenvalue equation is

$$(E + 2\delta - \lambda)(E - \lambda) - \epsilon^2 = E^2 + 2\delta E - \epsilon^2 - 2\lambda(E+\delta) - \lambda^2 = 0 \tag{2.11}$$

whose solutions are

Figure 2.3. Allowed level crossings for demagnetized spin-1 nucleus. The externally applied field is oriented along the principle axes of the quadrupolar tensor, and A is assumed positive. a). x axis; no level crossings occur. b). y axis; $|r\rangle$ and $|q\rangle$ cross. c). z axis; $|q\rangle$ and $|p\rangle$ cross.

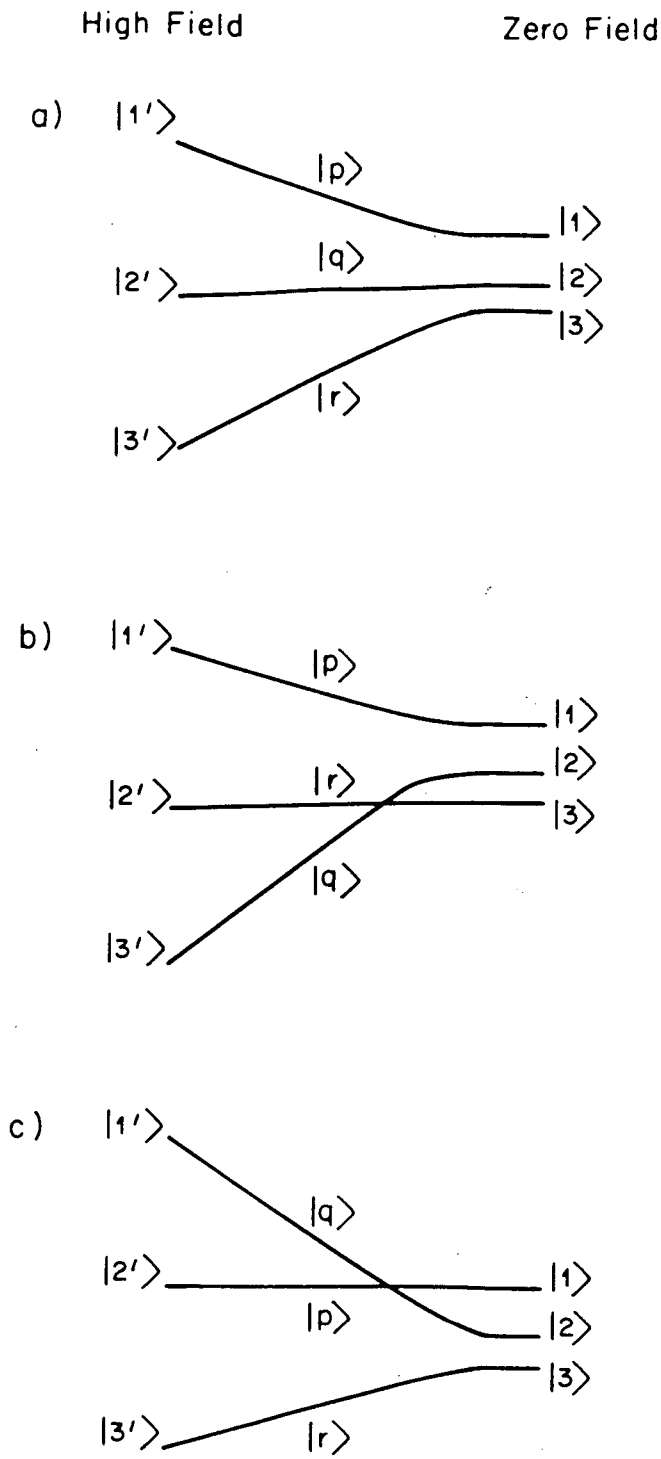

XBL 858-3320

$$\lambda_{\pm} = (E+\delta) \pm \sqrt{\delta^2 + \epsilon^2} \tag{2.12}$$

If $\epsilon \neq 0$, there is no value of δ where $\lambda_+ = \lambda_-$ and therefore no level crossing. For arbitrarily small displacements of the direction of the applied field from any of the principle axes of the quadrupolar tensor and in the adiabatic limit, only the level-anticrossing behavior is exhibited. Therefore, to a very high degree of approximation the demagnetized state of an isolated quadrupolar spin (with S arbitrary) is uniform over the entire powder pattern. Only for demagnetizations precisely along each of the axes do eigenstates cross. This fact will be used extensively in Chapter VI, where the assumption of a uniformly prepared demagnetized density operator will be an important simplification. In the absence of spin-lattice relaxation and in the adiabatic limit the entire order prepared in high field is transported to zero field.

2. Coupled Spins

It is rare that isolated spins are found in nature. Occasionally crystals may be found which contain only a single type of magnetic nucleus (e.g. ^1H in gypsum) or magnetic spins of a chemical identity which occur only as a low percentage of the total number of similar atoms (e.g. ^{13}C, ~1% natural abundance). As discussed in the first part of this chapter, spins are isolated in high field if their magnetogyric ratios differ significantly, or if appropriate sequences of rf pulses are used to artificially isolate them. But in demagnetizing a sample from high field to low field it is experimentally rather more difficult to maintain good isolation of one spin type from all others. In zero applied field the Zeeman energies

of all nuclei are identical independent of γ. In the absence of strong quadrupolar couplings (i.e. only spin-1/2 nuclei or quadrupolar nuclei in cubic crystals) all spin types are strongly coupled.[50] Even if there are strong quadrupolar couplings so that I and S spins are not matched in zero field, there may be some other value of the field intermediate between B_0 and zero where spin diffusion between the two spin species is allowed and efficient.[67]

Often, for example, a spin system contains a quadrupolar (S) nucleus in addition to some spin-1/2 species (labeled I and most often ^1H). It is in precisely this sort of system that the indirect, zero field level-crossing techniques[52-57,68,69] work best and attain the highest sensitivity. This section provides a brief description of the basic procedure with particular emphasis on the mechanism by which polarization is transferred in the laboratory frame.

In moderately high laboratory fields as are commonly used in NMR spectrometers, the ^1H resonance frequency is $\geq$ 60 MHz. Apart from ^3T and some covalently bound halogen compounds, the resonance frequencies (Zeeman plus quadrupolar) of all other spin species lie at frequencies below that of the ^1H nuclei. In zero field, on the other hand, the ^1H pure dipolar frequencies generally fall in a rather broad band from zero to as much as 100 kHz. Quadrupolar S spins have zero field resonance frequencies which range from zero to several megahertz. Inevitably, at some value of field intermediate between the large laboratory field B_0 and zero field the splittings between pairs of S spin energy levels equal those between the I spins.

In some range of fields about the level crossing field, the quadrupolar spin sublevels are capable of communicating via spin flip-

flops with the network of strongly coupled I spins. If the S spin sublevels are less polarized than the I spins and if the rate of passage through the level-crossing field is slow compared to the inverse of the I-S dipole-dipole couplings, some I spin magnetization should appear as order in the S spin system after demagnetization. In this section, I will try to give a simple quantitative argument which will illustrate the process of I-S polarization transfer and which clarify the essential process which lies at the heart of all high sensitivity zero field methods. Most of this model is developed in greater detail by Blinc[68] and Edmonds[69] and the description which follows relies heavily on the latter presentation.[69a]

Assume for simplicity that S = 1, and that in high field the S spins are unpolarized (as their T_1's may greatly exceed those of the I spins). The I spins consist of a set of equally spaced Zeeman levels. All level-crossings are assumed to take place in "large" fields $H_Z \gg H_D$ for the I spins but in "small" fields $H_Z \ll H_Q$ for the S spins. A rough energy level diagram is given in Figure 2.4. The total number of S spins is N′ (each assumed uncoupled from all others) and the initial density operator describing the S spins is

$$\rho^S_{jk} = 0 \tag{2.13}$$

Because the S spins are uncoupled ρ^S is of dimensionality 2S+1. The number of I spins is N (each assumed coupled to all other I spins in a system characterized at all times by a single spin temperature) such that

$$\rho^I_{jk} = 2b_I \, I_z \, \delta_{jk} \tag{2.14}$$

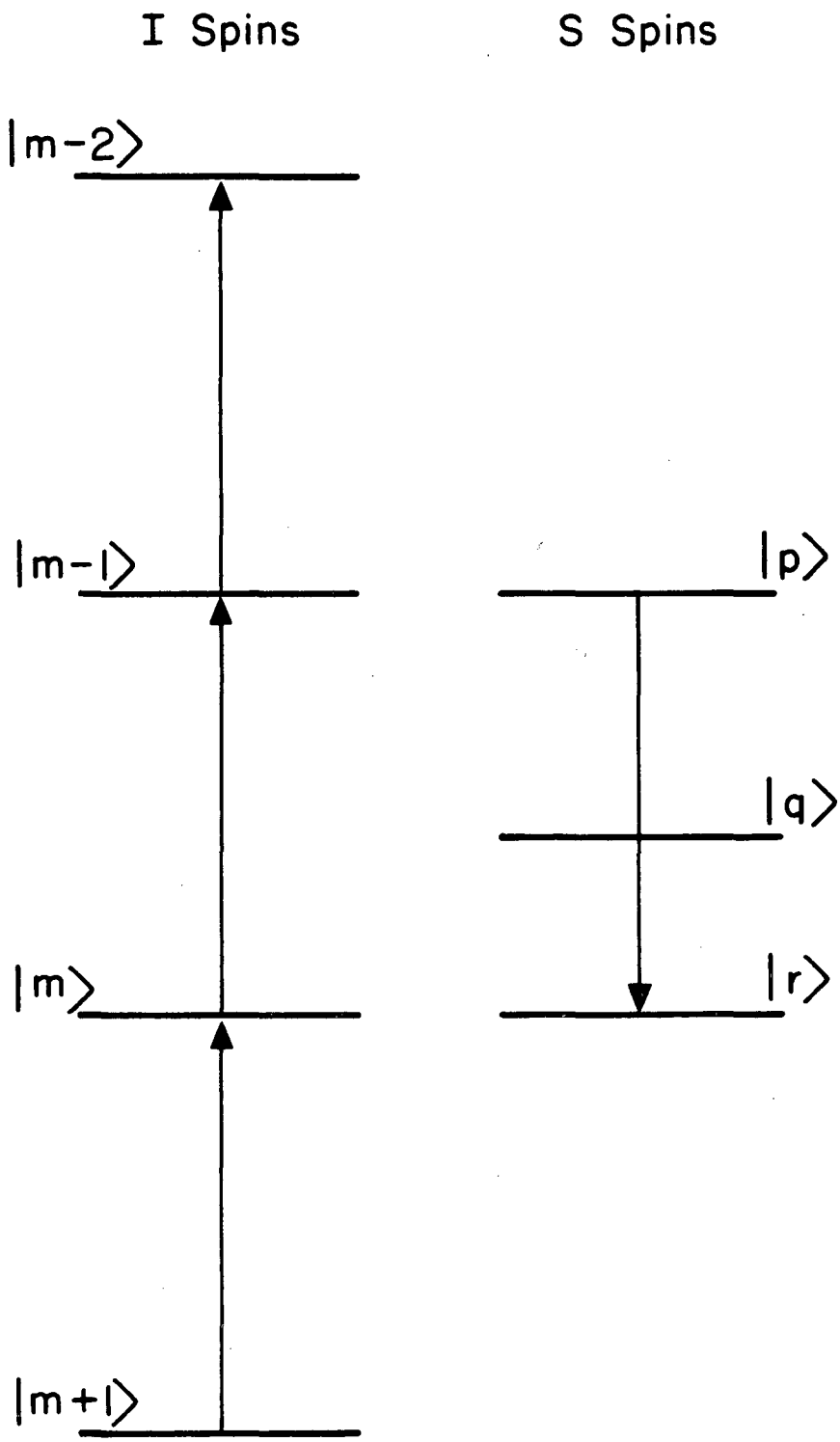

XBL 858-3543

Figure 2.4. Polarization transfer from I spins to S spins. I spins are in eigenstates of H_Z; S spins are in eigenstates of H_Q. As the external field is decreased to zero, energy splittings in the I spin bath successively match S spin quadrupolar splittings. I spins are warmed and S spins cooled until a common "spin temperature" is reached.

The dimensionality of ρ^I is $(2)^N$.

The S spins are in contact with the I spins only at fields where energy splittings of the S spin quadrupolar (plus Zeeman) Hamiltonian are equal to splittings in the I spin Zeeman (plus dipolar) Hamiltonian. For S = 1 the pairs of energy levels separated by the zero field ν_+, ν_-, and ν_0 lines become sequentially matched to the I spin splittings. At each level crossing, the population differences of the S spin levels reach a "spin temperature" associated with the pseudo-two level system which matches that of the I spin bath. Both the number of spins of either type and the energy of the system at a level crossing is fixed. These conservation laws are the basis of the rest of the analysis. At the first level crossing energy conservation requires that

$$2b_I'(N + N') = 2b_I N \tag{2.15}$$

where b_I' is the I spin population coefficient after the first level crossing. Rewriting in terms of the initial polarization and a number operator, X,

$$b_I' = \frac{N}{N+N'} b_I = X\, b_I \tag{2.16}$$

The I spins are now characterized by a new density operator

$$\rho^I_{jk} = 2X\, b_I I_z\, \delta_{jk} \tag{2.17}$$

and a new spin temperature. Some of the order originally stored in the I spins has "leaked out" into the S spin system. Because not all of the S spin levels participate in the polarization transfer at any one time ρ^S is not described by a spin temperature. Only diagonal elements

are nonzero, and they can be written compactly in terms of the eigenvalues of a population operator P where

$$\langle\psi_k|P|\psi_j\rangle = \rho^S_{kj}\delta_{kj} \tag{2.18}$$

At the end of the first level crossing the diagonal components of ρ^S are given by

$$\begin{aligned} P|p\rangle &= -Xb_I\ |p\rangle \\ P|q\rangle &= \quad\ |q\rangle \\ P|r\rangle &= Xb_I\ |r\rangle \end{aligned} \tag{2.19}$$

At the second level crossing, the ν_- line of the spin 1 comes in contact with the I spin reservoir and reaches equilibrium. The population difference between the $|q\rangle$ and $|r\rangle$ states equilibrates with the I spin bath (now somewhat warmer than before due to the transfer of polarization analyzed above). Subject to the same conservation laws and restrictions on numbers of particles, after the second level crossing the new populations of ρ^S are given by

$$\begin{aligned} P|p\rangle &= -Xb_I\ |p\rangle \\ P|q\rangle &= -\frac{1}{2}X^2b_I\ |q\rangle \\ P|r\rangle &= (X+\frac{1}{2}X^2)b_I|r\rangle \end{aligned} \tag{2.20}$$

Finally, the $|p\rangle$ and $|q\rangle$ eigenstates become energy matched and equilibrate with the I spin bath. After the final level crossing, the populations are

$$\begin{aligned} P|p\rangle &= -(\frac{3}{4}X^3+X)b_I\ |p\rangle \\ P|q\rangle &= (\frac{3}{4}X^3-\frac{1}{2}X^2)b_I|q\rangle \\ P|r\rangle &= (X+\frac{1}{2}X^2)b_I|r\rangle \end{aligned} \tag{2.21}$$

Similarly,

$$\rho^I = \frac{1}{4}[3\ X^3 - X^2 + 2\ X]\ b_I I_z\ \delta_{jk} \tag{2.22}$$

During the demagnetization, the norm of ρ^S is increased at the expense of ρ^I.

Reviewing the assumptions of the coupled spin model:

1. The I spins constitute a strongly coupled spin network characterized at all times and for all values of the field by a single spin temperature.
2. The S spins are isolated from one another and interact only with the I spins and then only at level crossing fields.
3. At the level crossing fields only pairs of S spin quadrupolar energy levels are matched to the I spin Zeeman energy.
4. All level crossings occur in fields large compared to the I spin dipolar fields.

If all these conditions hold then the model provides a reasonable description of the demagnetization. If the sample is merely returned to high field the level crossings described above occur again and in reverse order. Even if there is no relaxation and no additional fields are applied, the final populations returned to high field are not equal to the initial populations of ρ^I and ρ^S.[11,24] No matter how slow the field cycle, the polarization transfer process is not reversible.

In the commonly used frequency sweep methods the zero field spectrum is probed by low-frequency irradiation after demagnetization. If the irradiation is on-resonance with an S spin NQR transition that line is saturated and the populations of two S spin eigenstates are equalized. After the irradiation phase, the sample is returned to high

field and through the level crossing region where the S spin history is communicated to the I spins. The final spin temperature of the I spins depends on whether an S spin resonance was found, the populations of the S spins after irradiation, which specific line(s) was (were) saturated, all the relaxation times which characterized the system, and whether the level crossing sequence was repeated many times or only once. Detailed predictions as to the observed signal and sensitivity for many of these cases and for S>1 are given elsewhere in more complete reviews of field cycling NQR methods.[68,69]

Over a broad range of frequencies and types of spin systems of interest, the sensitivity of the technique is relatively frequency-independent and, to some extent, independent of the actual number of S spins in the sample. Higher sensitivity variants exist as well.[69b,70] What is common to them all is the idea that the polarization induced in the abundant, high γ I spins in the polarization phase is exploited by arranging the experimental parameters such that the S spins share in that order.

3. Deuterium-Hydrogen Level Crossings

For systems where the zero field absorption frequencies appear at very low frequencies, the theory presented above requires extensive modification. Neither the level-crossing sequence nor the irradiation phase proceeds quite as simply as described above. This is particularly true for the specific case of deuterium, where the zero field splittings generally are less than 200 kHz. As ^{1}H pure dipolar absorption may extend out to nearly those frequencies, none of the assumptions of the coupled spin model need hold. Even when the ^{1}H dipolar bath frequencies are much lower than the ν_+ and ν_- lines, they

almost certainly are as large as the ν_0 line. In the first level crossing both ν_+ and ν_- lines are likely to be polarized to nearly the same extent consistent with the ^{1}H Zeeman temperature at the crossing field. The ν_0 line is in resonance with the dipolar bath with its own spin temperature. As the Zeeman splittings collapse into the dipolar linewidth levels separated by the ν_0 line approach the new spin temperature of the combined Zeeman-dipole-dipole Hamiltonian (warmed somewhat by the first stage of polarization transfer). Where level crossing to the S spins occurs at such low frequencies, the extent to which the lines separated by the ν_0 line are differentially populated will certainly depend on the frequency of the ν_0 line, and a new spin temperature no cooler than that which characterizes the order stored in the (ν_+, ν_-) pair is established. Where η is small the population differences between the $|1\rangle$ and $|2\rangle$ states may be negligible. In any case, the final populations reached via demagnetization of systems with small quadrupolar couplings will differ markedly from those described in the above model. Nonetheless, the basic principle (that the order stored in the S spins is comparable to that stored in the I spins) is still valid.

A further consequence of this dependence on the polarization transfer from and to I spins is that there is a precipitous drop in available signal powers at very low S spin frequencies. The very source of the high sensitivity (the bath of ^{1}H nuclei) short circuits the indirect process by direct absorption of radiation. If the zero field ^{1}H energy levels are saturated by direct absorption of rf, quadrupolar transitions found in the same range of frequencies are not observable. Because the irradiation phase is non-selective, level

crossing techniques which monitor only the disappearance of ^1H signal in high field are unable to distinguish between energy absorption by the quadrupolar nuclei and direct absorption by the bath.

(In principle, the vastly differing linewidths between, say, deuteron (^2D) and proton (^1H) resonances might result in observable changes in the signal even at the lowest frequencies. Should the proton resonance be saturated while a ^2D line remains unaffected, magnetization transfer back from the rare spins to the ^1H bath during remagnetization would marginally repolarize the ^1H bath. Therefore, slight decreases in the observed ^1H signal should be observed for irradiation simultaneously near a ^2D resonance and at a bath frequency. To my knowledge, such effects have not previously been reported--which may be an indication of the small amount of order actually stored in the quadrupolar system in a single crossing, or the breakdown of the assumption that the two types of nuclei are non-interacting at the residual fields. In any case, the effect is probably too small to be routinely noticed.)

At the very lowest frequencies, frequency sweep methods suffer from another important disadvantage. The rate at which spin transitions occur under rf irradiation is proportional to the frequency at low frequencies.[51,71] The absorption of energy under irradiation decreases asymptotically towards zero at the very lowest frequencies. Spectral features near zero frequency become increasingly difficult to observe, particularly if accurate lineshapes are required. This may be the greatest advantage of the Fourier transform methods to be described in subsequent chapters; in principle, they are equally sensitive at all zero field frequencies (although as a practical matter they perform

best at frequencies somewhat lower than 500 kHz). Moreover, the lineshapes observed in the absence of all applied fields are reliable. This will prove important in any analysis of strongly coupled spins.

Further comments on level-crossing experiments and possible applications of level-crossings in Fourier transform zero field experiments with isotopic selectivity will appear in Chapter VI.

b. Sudden Demagnetization

In the opposite limit of sudden[64] or (ideally) instantaneous switching off of B_0 there is a different and simpler solution to the form of the demagnetized density operator ρ. No assumptions need be made about the spin system. Beginning from a spin system with a Hamiltonian

$$H = H_Z + H_{loc} \tag{2.23}$$

and a density operator ρ. At a time τ, the external polarizing field responsible for H_Z is instantaneously turned off. The spin system is unable to follow the change in the applied field, and the state of the system (and of ρ) is unchanged;

$$\rho(\tau_+) = \rho(\tau) \tag{2.24}$$

(Note that this is not equivalent to the final state reached by adiabatic demagnetization of an isolated spin system, where all populations are unchanged and in the new eigenstates.) Though the density operator is unchanged, the Hamiltonian and thus the eigenstates are different. Even if ρ expressed in the eigenbasis of the Hamiltonian including the Zeeman term is diagonal, it need not be in the zero field eigenbasis. If ρ contains off-diagonal elements, it begins to evolve at the frequencies characteristic of H_{loc} (cf Equation

1.75).

In principle, the evolution of ρ might be detected in zero field, just as the absorption of energy might be monitored directly in the field cycling methods described previously. Experiments based on this idea have been performed on liquid samples.[72,73] In solids, and where the natural frequencies of H_{loc} are so low that field cycling methods are required, high field detection is likely to prove much more sensitive. At a time t_1, the external field is instantaneously reapplied. The time-evolved operator $\rho(\tau+t_1)$ can subsequently be probed indirectly by measuring the high field free induction decay. Such an experiment is shown schematically in Figure 2.5.

Because the technical requirements for sudden demagnetization are experimentally more difficult to fulfill than for adiabatic demagnetization, the former approach is more rarely attempted.[53a,74] It is, however, the essential component of Fourier transform zero field NMR experiments. The basic zero field experiment is described more fully in Chapter III.

C. Summary

To sum up; if a measurement of the chemical shift tensor proves sufficiently informative, high field techniques are capable of providing such information. If, however, the chemical, structural, or dynamical information required is found most directly in the traceless, anisotropic interactions such as the dipolar or quadrupolar tensors, high field techniques generally observe only powder pattern lineshapes. Such spectra are simply interpretable only under restrictive

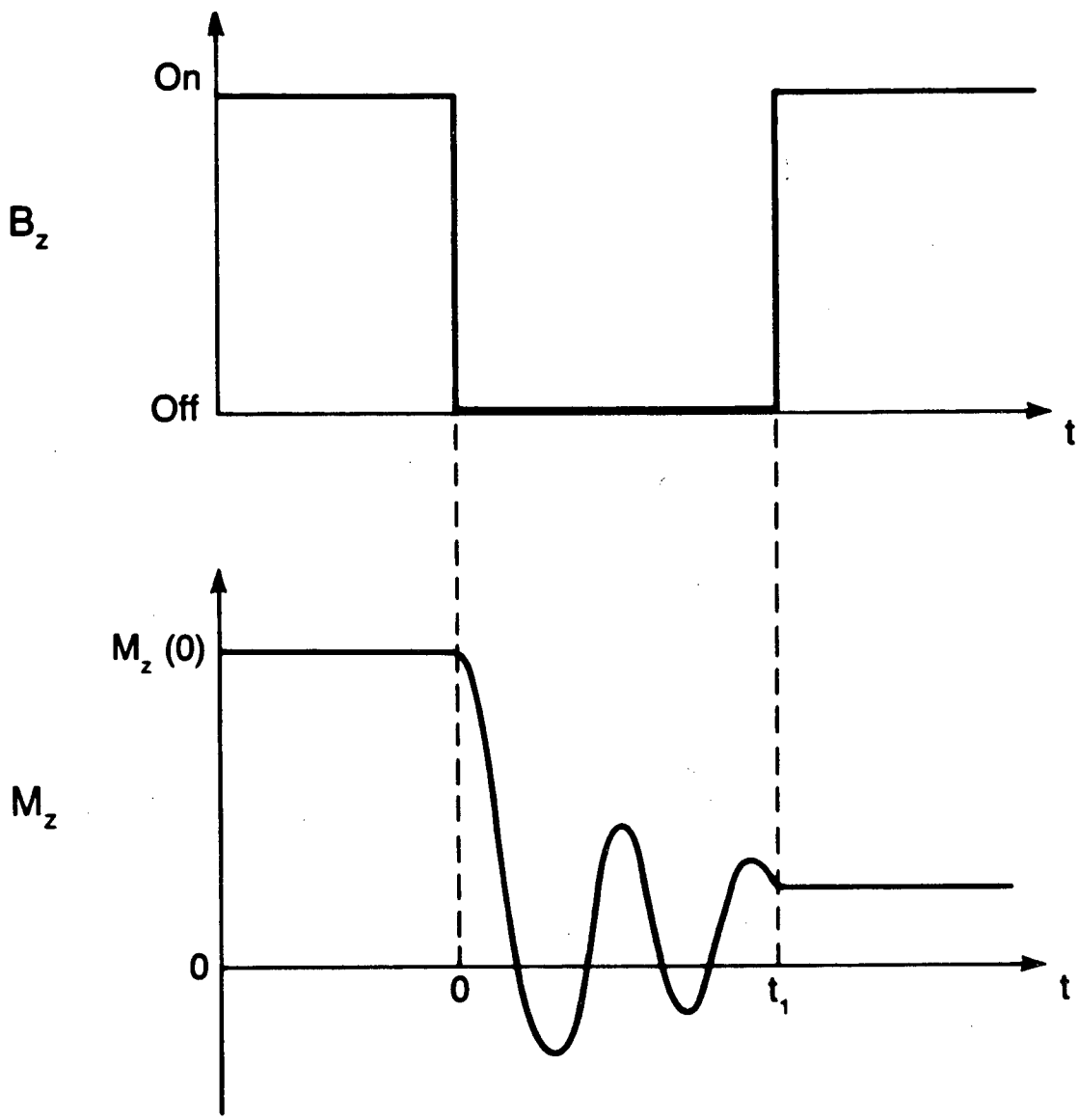

Figure 2.5. Response of a spin system to a sudden change in the strength of the applied field. At top: Strength of the applied field vs. time. Bottom: Magnetization vs. time. If the field is switched off rapidly, the magnetization oscillates and decays in a zero field. When the field is reapplied, magnetization is stored.

assumptions about the numbers of interacting spins and the form of the interaction. In the presence of larger numbers of interacting spins, or where the response from several different systems overlap, all information about these interactions is generally sacrificed in order to measure the isotropic interactions with greater precision.

Where the measurement and interpretation of these anisotropic interactions is desired, zero field methods are more promising. For systems with large quadrupolar couplings, pure NQR may be employed. At lower frequencies, lower concentrations, and at somewhat sacrificed resolution, field-cycling techniques utilizing level-crossings become essential. And at the lowest frequencies or where maximum resolution is required, or where indirect techniques fail due to the absence of a suitable bath of spin-1/2 nuclei, Fourier transform zero field techniques may be essential. Furthermore, working in the time-domain makes possible the extention of these experiments to include applications of two-dimensional correlation spectroscopy.[18] Some extensions using two-dimensional spectroscopy will be covered in Chapters VI and VIII.

III. Fourier Transform Zero Field NMR and NQR

Faraday's law (Equation (1.88)) gives the voltage induced in an rf coil by an oscillating magnetization. This signal is proportional to both the size of the initial magnetization and the frequency at which it oscillates (i.e. the resonance frequency). In high fields, both terms are field-dependent. The equilibrium magnetization given by the Curie Law (Equation (1.87)) is proportional to the applied field. In the high field limit the frequency of oscillation is essentially the Larmor precession frequency. The observed signal's strong field dependence is the continuing motivation for the purchase of higher field (and more expensive) superconducting magnets. Direct detection of low frequency magnetic resonance requires large sample volumes and extensive signal averaging. The alternative field-cycling methods outlined in Chapter II combine the resolution advantage of zero field experiments with the sensitivity of high field NMR. I will concentrate only on experiments where both polarization and detection phases take place in a large static magnetic field (in practice, nearly all of our experiments are performed in a persistent superconducting magnet of nominal field strength 4.2 Tesla (42 kgauss) where the ^{1}H Larmor frequency 185.032 MHz). Practical experimental details, and some thoughts on alternative instrumentation, are given in Chapter VIII.[75]

A. A Practical Two-Step Field Cycle

Since it is impractical and expensive to repeatedly energize and deenergize the high inductance magnets routinely used in modern NMR

spectrometers, in the field cycling experiments described in this thesis the field cycle presented in an idealized fashion in Figure 2.5 is always executed in two distinct steps as illustrated in Figure 3.1. In the first step, the sample is removed from the region of concentrated flux within the bore of the superconducting magnet and mechanically transported through space. This step takes the spin system at equilibrium in high field to an intermediate field B_{int}. This intermediate field arises from some combination of the fringe fields of the main solenoid, electromagnets, the earth's field, and other stray magnetic fields, and is are sufficiently reduced in size so as to be readily matched by electromagnets which can be rapidly switched in times ~1 μs. Practical values of the intermediate field are $\leq$ 500 gauss. Detailed descriptions of the apparatus are available elsewhere.[75] For simplicity I assume that the intermediate field is sufficiently large that the high field condition $H_Z \gg H_{loc}$ applies in the intermediate field. The eigenstates at high field and at the intermediate field are identical. In the absence of significant spin-lattice relaxation, the total magnetization prepared in high field is conserved in B_{int} and the density operator ρ which describes the spin system is unchanged independent of the rate of demagnetization. (Formally, however, ρ is characterized by a much reduced spin temperature;

$$T_s = \frac{B_{int}}{B_0} T_L \tag{3.1}$$

where T_L is the lattice temperature.)

At the intermediate field ρ corresponds to a bulk magnetization

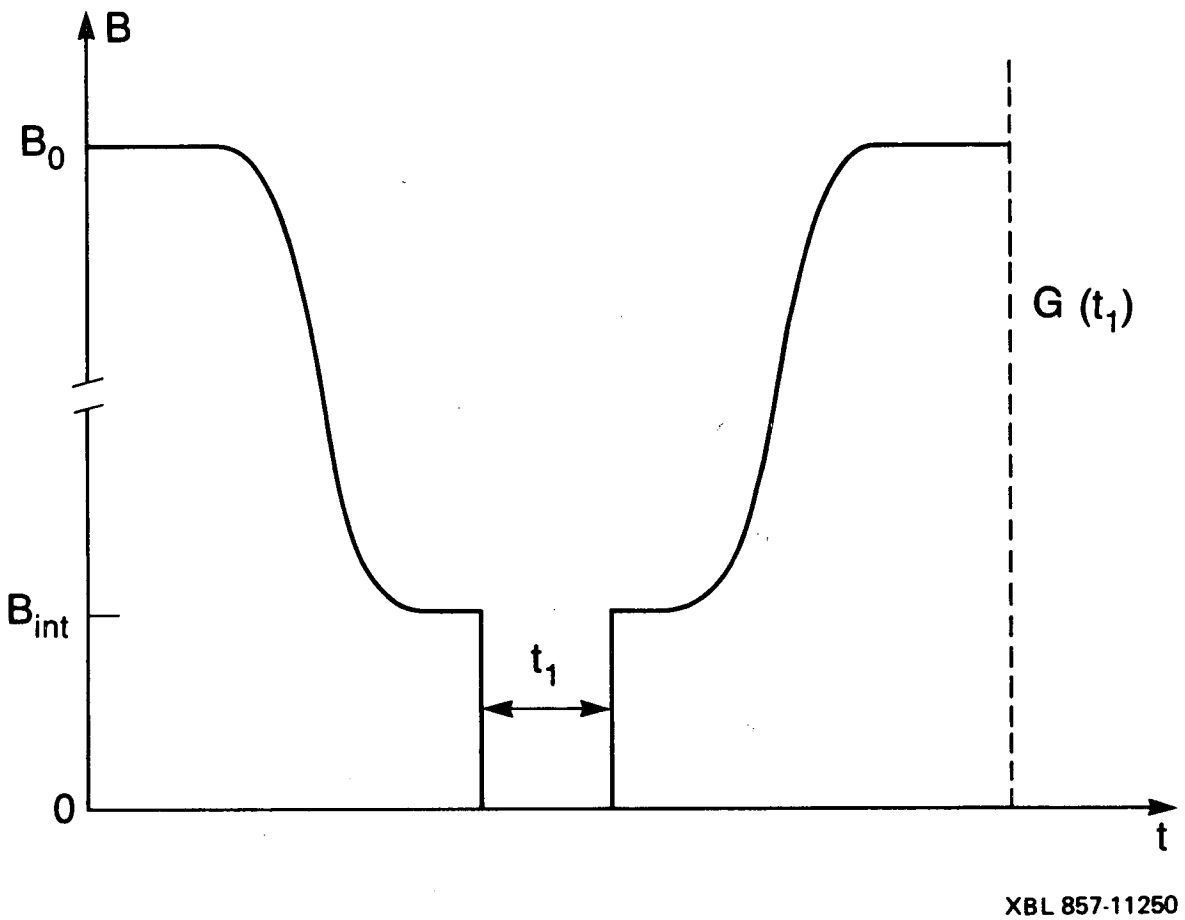

Figure 3.1. Magnetic field vs. time in two-step experimental field cycling diagram. In the first step the sample is removed from the polarizing field by mechanical means and the field slowly falls from B_0 to B_{int}. B_{int} is rapidly turned off. A time t_1 later, B_{int} is turned back on and the sample mechanically returned to B_0.

parallel to B_{int}. For simplicity I assume that B_{int} and B_0 are coaxial. At a time $t = 0$, B_{int} is suddenly switched off. The density operator ρ is unable to follow the rapid change in the field, becomes time-independent, and evolves in zero field. At $t = t_1$, B_{int} is suddenly reapplied and the sample transported back to B_0 for detection of the evolved operator $\rho(t_1)$. The two-step cycle of Figure 3.1 is equivalent to the hypothetical cycle of Figure 2.5 if B_{int} is large enough. This condition is assumed, and from here on I focus on the evolution of the magnetization transported to low field.

B. A Formal Calculation of the Signal

The central question is the prediction of the signal expected for the sequence in Figure 3.1, and its solution will occupy the rest of this chapter. Two coordinate systems (the high field frame with z-axis parallel to the applied field and some consistently chosen local or molecular frame), and the relationship between them, are required. The local frame is chosen so that otherwise identical but arbitrarily oriented systems have the same expanded form of the Hamiltonians (Equations (1.47), (1.54), and (1.68)). For simple systems (e.g. isolated quadrupolar spins or a pair of dipolar coupled spin-1/2 nuclei) it will prove convenient to choose the principal axis system of the main interactions, but this is neither necessary nor generally possible. Where some convenient choice of zero field axis system exists which will make subsequent calculations simpler or more informative, it will be useful to exploit that option.

As was described in Chapter I, transformations between axis

systems are conventionally described in terms of Euler angles, and in most NMR applications only two are required. The transformation which takes the laboratory (L) frame into the local or molecular (M) frame is $R^{-1}(\Omega)$;

$$\langle loc|\xi_M|loc\rangle = \langle lab|RR^{-1}\xi_L RR^{-1}|lab\rangle \tag{3.2}$$

The relationship between the laboratory and molecular frames is illustrated in Figure 1.1. In a disordered system, where many orientations of the local frame are allowed, R will differ for each of those orientations and the form of the operator ξ_M of Equation (3.2) will differ for each orientation because R does.

Following the logic of the sudden approximation described at the end of chapter II, at a time t = 0 the intermediate field B_{int} which guarantees the high field condition is instantaneously switched off. Before the switching of the field, the spin system was in eigenstates of the high field Hamiltonian (made up of a Zeeman term and a set of truncated local fields H'_{loc})

$$H = H_Z + H'_{loc} \tag{3.3}$$

with

$$[\rho, H] = [\rho, H_Z] = [\rho, H'_{loc}] = 0 \tag{3.4}$$

Except for special cases, in the untruncated fields H_{loc}

$$[\rho, H_{loc}] \neq 0 \tag{3.5}$$

and therefore

$$\frac{\delta\rho}{\delta t} \neq 0 \tag{3.6}$$

that is, there is time evolution under H_{loc}. At a time t

$$\rho(t) = \exp(-iH_{loc}t)\rho(0)\exp(iH_{loc}t) \tag{3.7}$$

At a time t_1, the evolution implied in Equation (3.7) is interrupted by reapplication of B_{int}. After a time $\sim T_2$ (which in solids may be as short as ~10 μs), coherence in a solid is assumed to disappear and

$$[\rho(t_1), I_{zL}] = 0 \tag{3.8}$$

Evolution of the density operator (Equation (3.7)) is most conveniently described in the molecular frame where the Hamiltonian is identical for all orientations and reached by a tranformation of variables as given in Equation (3.2). Because all measurements are made in the laboratory frame of reference, the calculation of observables must include the reexpression of ρ in that frame. This is followed by an integration over the known or assumed distribution of orientations, $R(\Omega)$. Starting from ρ expressed in the laboratory (L) frame of reference, the sequence of transformations resulting in the evolved density operator is

$$\rho_L(t_1) = \langle R^{-1}\exp(-iH_{loc}t_1)R\rho_L(0)R^{-1}\exp(iH_{loc}t_1)R\rangle \tag{3.9}$$

where the subscript L identifies ρ as being expressed in the laboratory frame of reference and the angle brackets $\langle\rangle$ imply an averaging over all $R(\Omega) \equiv R(0,\beta,\alpha)$. If the initial density operator prepared in the high field polarization interval is

$$\rho_L(0) = I_{zL} = \sum_j I_{jzL} \tag{3.10}$$

then ρ reexpressed in the molecular frame is

$$\rho_M(0) = R^{-1}(\Omega)\rho_L(0)R(\Omega)$$

$$= \exp(-i\alpha I_z)\exp(-i\beta I_y)I_{zL}\exp(i\beta I_y)\exp(i\alpha I_z)$$

$$= I_{zM}\cos\beta - I_{xM}\sin\beta\cos\alpha + I_{yM}\sin\beta\sin\alpha \qquad (3.11)$$

Ignoring the details of the zero field Hamiltonian H_{loc}, a general time-evolved zero field operator $\xi(t)$ can be defined by

$$\xi(t) \equiv \exp(-iH_{loc}t)\xi\exp(iH_{loc}t) \qquad (3.12)$$

and

$$\rho_M(t_1) = I_{zM}(t_1)\cos\beta - I_{xM}(t_1)\sin\beta\cos\alpha + I_{yM}(t_1)\sin\beta\sin\alpha \qquad (3.13)$$

Following the logic of Equation (3.9) the lab frame operator $\rho_L(t_1)$ is calculated by rotating the time-evolved form (Equation (3.13)) back to the laboratory frame. This is precisely the strategy adopted at the end of this chapter. Here, a different approach is used which simplifies subsequent algebraic manipulations. What is measured is never the density operator itself, but only the expectation value of some observable (Equation (1.73)). The theory is simplified if the observable is assumed to be I_{zL} (although in practice an rf pulse is required to transform longitudinal magnetization like I_{zL} into the observable transverse magnetizations I_{xL} and I_{yL}), and the actual quantity to be calculated is the signal function

$$G(t_1) = \mathrm{Tr}\,[\rho_L(t_1)I_{zL}] \qquad (3.14)$$

Using the general rule that

$$\mathrm{Tr}\ [ABC] = \mathrm{Tr}\ [CAB] = \mathrm{Tr}\ [BCA] \tag{3.15}$$

and, substituting for ρ_L from Equation (3.9),

$$G(t_1) = \mathrm{Tr}\ [\langle R\rho_M(t_1)R^{-1}I_{zL}\rangle] = \mathrm{Tr}\ [\langle\rho_M(t_1)R^{-1}I_{zL}R\rangle] \tag{3.16}$$

This is equivalent to calculating the signal function with the observable defined in the molecular frame rather than in the laboratory frame. The required transformation of I_{zL} is given in Equation (3.10). The signal $G(t_1, \Omega)$ for a given orientation, R, is

$$\begin{aligned} G(t_1, \Omega) = \mathrm{Tr}[&(I_{zM}\cos\beta - I_{xM}\sin\beta\cos\alpha + I_{yM}\sin\beta\sin\alpha) \\ &(I_{zM}(t_1)\cos\beta - I_{xM}(t_1)\sin\beta\cos\alpha + I_{yM}(t_1)\sin\beta\sin\alpha)] \end{aligned} \tag{3.17}$$

Integrating the signal function $G(t_1,\Omega)$ over the known or assumed distribution of local frame orientations, $P(\Omega)$, the observable $G(t_1)$ is

$$G(t_1) = \int G(t_1, \Omega)\ P(\Omega)\ d\Omega \tag{3.18}$$

In high field, the distribution of orientations $P(\Omega)$ is convoluted with orientation-dependent absorption frequencies to produce high field powder patterns.[26] In zero field, the distribution of orientations $P(\Omega)$ is convoluted instead with an orientation dependent intensity distribution. Where in high field $R(\Omega)$ is revealed by the shifts in frequency as a function of orientation, in zero field it is the intensities of the various absorption lines which change. This comparison is shown in Figure 3.2. For the common case where the probability distribution is uniform (e.g. a powder distribution where all orientations are equally probable)

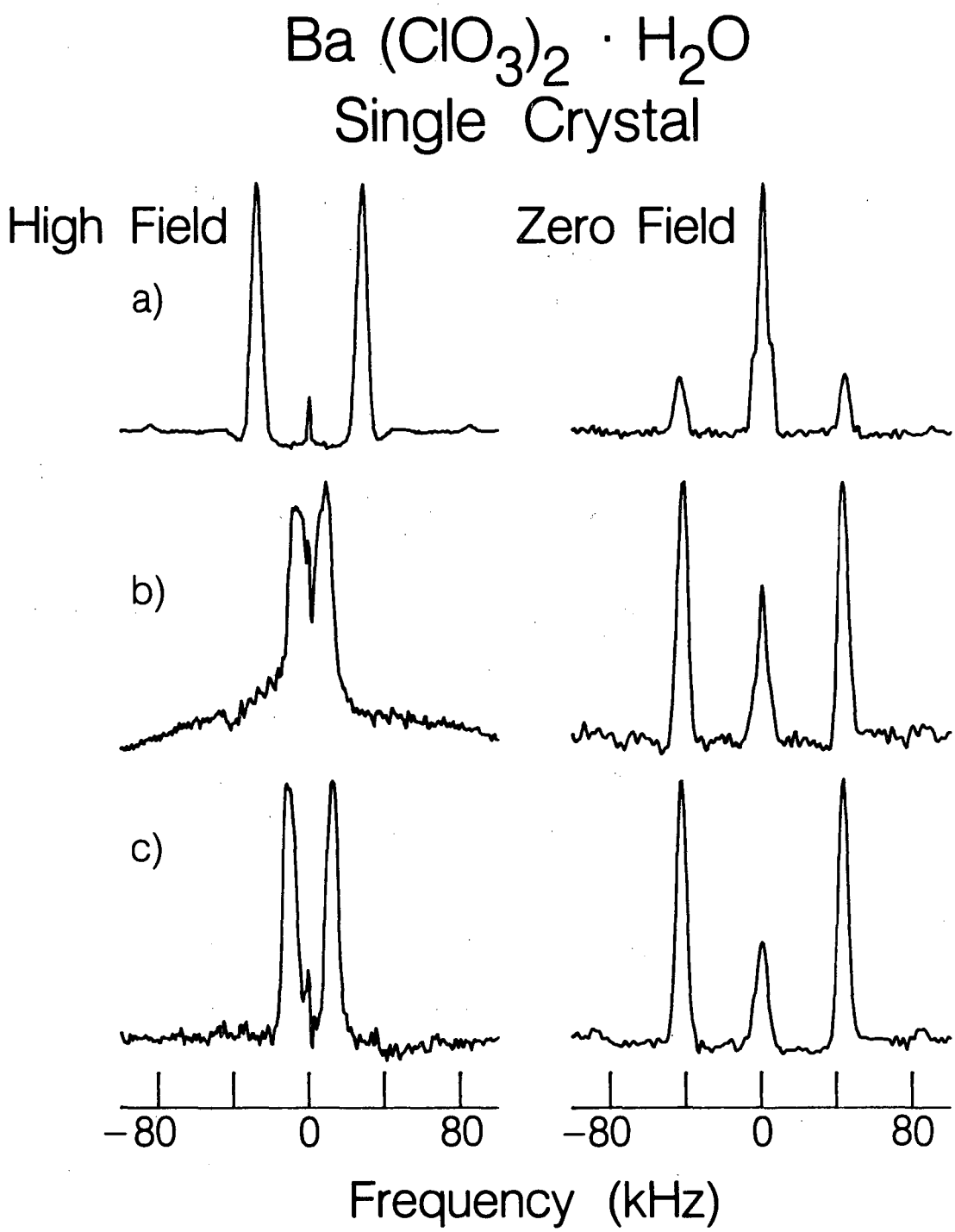

Figure 3.2. High and zero field ^1H NMR spectra of single crystals of $Ba(ClO_3)_2 \cdot H_2O$. Three orientations of the crystal are shown. As the crystal's orientation with respect to B_0 is rotated, the splitting of the high field doublet moves. In zero field, only amplitude variations are observed.

$$P(\Omega)d\Omega = -\frac{1}{4\pi}\, d(\cos\beta)d\alpha \tag{3.19}$$

Over the entire sphere, the orthogonality of the rotation matrices[7] restricts the signal function to only auto-correlations of the angular momenta. The orientation dependence of the zero field signal is easily integrated over Ω and yields

$$G(t_1) = \frac{1}{3}\,\mathrm{Tr}\,[(I_{zM}(t_1)I_{zM} + I_{xM}(t_1)I_{xM} + I_{yM}(t_1)I_{yM})] \tag{3.20}$$

$$= \frac{1}{3}\sum_{j,k}\ \sum_{p=x,y,z} \left|\langle j|I_{pM}|k\rangle\right|^2 \cos\omega_{kj}t_1 \tag{3.21}$$

Equation (3.21) provides a general prescription for the calculation of zero field spectra acquired by the sequence of Figure 3.1. It is also the heart of the program DBZINT.FOR which we commonly use for the simulation of zero field spectra of dipolar coupled spin-1/2 nuclei. From an assumed geometry the molecular frame Hamiltonian H_{loc} is calculated and diagonalized. The operators I_{xM}, I_{yM}, and I_{zM} are expressed in the eigenbasis of the zero field Hamiltonian. The zero field frequencies correspond to the difference in energy between pairs of eigenstates connected by nonzero elements of these operators, and the line intensities are the squares of the individual matrix elements.

For simple systems (i.e. quadrupolar nuclei with η=0 or some special cases of dipolar coupled systems where a molecular axis of quantization exists) simple selection rules may exist and components of the molecular frame operators may be diagonal, i.e. non-evolving. In more general systems, no choice of basis set results in particularly simple evolution operators and non-zero matrix elements exist between

any pair of eigenstates.

In the remainder of this chapter, I present solutions to Equation (3.21) for a number of examples of spin systems where the Liouville space of eigenstates is sufficiently small (and/or enough selection rules exist) so that the operations suggested in this section are conveniently made explicit.

C. Coupled Spin-1/2 Systems

1. Two Identical Dipole-Dipole Coupled Nuclei

A natural choice for the molecular frame z-axis is along the internuclear vector $\mathbf{r}_{12}$ connecting spins 1 and 2. Expressed in this frame of reference, Equation (1.47) becomes

$$H_D = -\omega_D (I_1 \cdot I_2 - 3I_{z1}I_{z2}) \tag{3.22}$$

where, as before,

$$\omega_D \equiv \frac{\gamma_1\gamma_2 h}{2\pi r_{12}^3} \tag{3.23}$$

The initial condition is assumed to be magnetization, i.e.

$$\rho(0) = I_z = I_{z1} + I_{z2} \tag{3.24}$$

As described in Subsection I.B.2.b, the eigenstates of this Hamiltonian are traditionally given as the triplet (symmetric with respect to interchange of the two spin labels) and the singlet (antisymmetric with respect to exchange). Table 3.1 provides explicit forms for the eigenstates and eigenvalues of Equation (3.22). The matrix representations of the angular momentum operators I_{xM}, I_{yM}, and I_{zM} are

identical to those given in Table 2.1 Table 3.1 adds matrix representations for the second rank tensors U_{kM}. No matrix elements of these operators couple the singlet state to the triplet manifold and

Table 3.1

A. Eigenstates of Two Coupled Spin-1/2 Nuclei in Zero Field

$$|T_-\rangle = -i\,(2)^{1/2}\,[\,|\alpha\alpha\rangle - |\beta\beta\rangle] \qquad |T_+\rangle = (2)^{1/2}\,[\,|\alpha\alpha\rangle + |\beta\beta\rangle]$$

$$|T_0\rangle = (2)^{1/2}\,[\,|\alpha\beta\rangle + |\beta\alpha\rangle] \qquad |S\rangle = (2)^{1/2}\,[\,|\alpha\beta\rangle - |\beta\alpha\rangle]$$

where α and β correspond to $\langle I_z\rangle = 1/2$ or $-1/2$, respectively

B. Matrix Representations of U_k

Matrix elements between S and T states are zero; within the T manifold

$$\sqrt{6}\,U_0 = \begin{array}{c|c} & |-\rangle\ |+\rangle\ |0\rangle \\ \begin{array}{c}\langle -\\ \langle +\\ \langle 0\end{array} & \begin{bmatrix} 1 & 0 & 0 \\ 0 & 1 & 0 \\ 0 & 0 & -2 \end{bmatrix} \end{array}$$

$$\sqrt{2}\,U_{1-} = \begin{array}{c|c} & |-\rangle\ |+\rangle\ |0\rangle \\ \begin{array}{c}\langle -\\ \langle +\\ \langle 0\end{array} & \begin{bmatrix} 0 & 0 & i \\ 0 & 0 & 0 \\ -i & 0 & 0 \end{bmatrix} \end{array} \qquad \sqrt{2}\,U_{1+} = \begin{array}{c|c} & |-\rangle\ |+\rangle\ |0\rangle \\ \begin{array}{c}\langle -\\ \langle +\\ \langle 0\end{array} & \begin{bmatrix} 0 & 0 & 0 \\ 0 & 0 & -i \\ 0 & i & 0 \end{bmatrix} \end{array}$$

$$\sqrt{2}\,U_{2-} = \begin{array}{c|c} & |-\rangle\ |+\rangle\ |0\rangle \\ \begin{array}{c}\langle -\\ \langle +\\ \langle 0\end{array} & \begin{bmatrix} 0 & 1 & 0 \\ 1 & 0 & 0 \\ 0 & 0 & 0 \end{bmatrix} \end{array} \qquad \sqrt{2}\,U_{2+} = \begin{array}{c|c} & |-\rangle\ |+\rangle\ |0\rangle \\ \begin{array}{c}\langle -\\ \langle +\\ \langle 0\end{array} & \begin{bmatrix} -1 & 0 & 0 \\ 0 & 1 & 0 \\ 0 & 0 & 0 \end{bmatrix} \end{array}$$

For $|-\rangle = |x\rangle$, $|+\rangle = |y\rangle$, and $|0\rangle = |z\rangle$ this same set of operators describes an isolated spin-1 system.

the singlet has no effect on the spectrum. The singlet is not included in any of the matrix representations of Table 3.1. Time evolution under the Hamiltonian can be described using Equation (1.75), and

$$I_j(t_1) = I_j \cos\omega_{1k}t_1 + (I_kI_1 + I_1I_k)\sin\omega_{1k}t_1 \tag{3.25}$$

and

$$(I_kI_1 + I_1I_k)(t_1) = (I_kI_1 + I_1I_k)\cos\omega_{1k}t_1 - I_j\sin\omega_{1k}t_1 \tag{3.26}$$

This describes time evolution for six of the eight operators first and second rank tensors necessary to describe the evolution of the three level system. The remaining two operators (proportional to U_0 and U_{2+}) are diagonal in the zero field basis set and undergo no evolution. The trace of Equation (3.20) is easily performed once a few general rules are described;

$$\mathrm{Tr}\ [I_jI_k] = \delta_{jk} \tag{3.27}$$

and

$$\mathrm{Tr}\ [I_jI_kI_l] = 0 \quad \text{for all } j,k,l \tag{3.28}$$

Therefore,

$$\frac{1}{3}\,\mathrm{Tr}[\sum_{j=x,y,z} I_{jM}(t_1)I_{jM}] = \frac{1}{3}\,(\cos\omega_{21}t_1 + \cos\omega_{32}t_1 + \cos\omega_{13}t_1) \tag{3.29}$$

For two coupled spin-1/2 nuclei, and in the basis set of Table 3.1

$$-\omega_{23} = \omega_{31} = \frac{3}{2}\,\omega_D \tag{3.30}$$

and

$$\omega_{12} = 0 \tag{3.31}$$

Normalizing to unity at zero time, the zero field free induction decay from two identical spin-1/2 nuclei is

$$G(t_1) = \frac{1}{3}[1 + 2\cos(\frac{3}{2}\omega_D t_1)] \tag{3.32}$$

An experimental example of this prediction is shown in Figure 3.3, where the zero field NMR spectrum of the ^1H nuclei in $Ba(ClO_3)_2 \cdot H_2O$ is presented. Crystalline water molecules are well isolated one from another, and the spectrum corresponds closely to the case of two coupled identical spin-1/2 nuclei. In the absence of molecular motion which may average the observed couplings, the observed line splitting (42.4 kHz) corresponds to a ^1H-^1H distance of 1.62±.02Å. Single crystal spectra of this same compound have already appeared in Figure 3.2. As this two-spin system is convenient for experiments, theoretical modeling and easy interpretation of results I will return to this compound and spectrum repeatedly in subsequent sections.

2. <u>Two Distinguishable Dipole-Dipole Coupled Nuclei</u>

The singular difference between the heteronuclear (I-S) spin pair (e.g. ^{13}C-^1H) and the homonuclear (I-I) spin pair described above is that for two spin species the high field density operator can no longer be written as I_{zL} alone. Rather,

$$\rho_L(0) = b_I I_{zL} + b_S S_{zL} \tag{3.33}$$

where the coefficients b_I and b_S differ in general because the magnetogyric ratios of the two spin species do. The density operator of Equation (3.33) corresponds to an unequal division of the initial magnetizations between the two spins in high field. Even though the zero field Hamiltonian for the two spin systems is independent (to within a scaling constant) of the chemical identity of the two spins,

Figure 3.3. ^{1}H NMR spectra of $Ba(ClO_3)_2 \cdot H_2O$. At top: High field single crystal spectrum. Middle: High field powder spectrum. Bottom: Zero field powder spectrum. The splitting in the zero field spectrum corresponds, in the absence of motion, to r = 1.62±.02 Å.

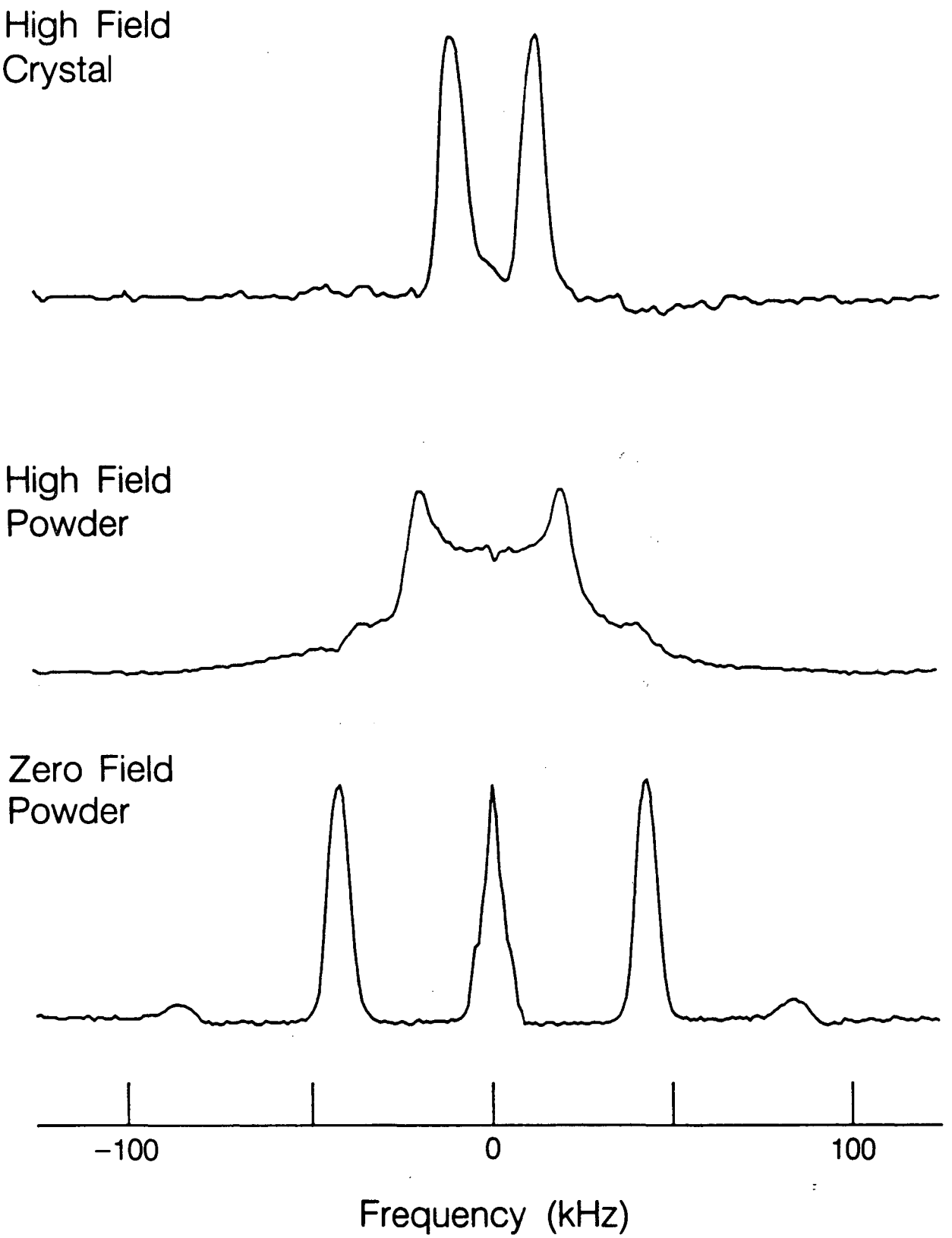

XBL 855-8886A

the high field preparation sequence can discriminate between the two spin species. Rewriting Equation (3.33) in a form which emphasizes the difference between it and the density operator of Equation (3.24)

$$\rho_L(0) = b_+ (I_{zL} + S_{zL}) + b_-(I_{zL} - S_{zL}) \tag{3.34}$$

with

$$b_+ = \frac{b_I+b_S}{2} \tag{3.35}$$

and

$$b_- = \frac{b_I-b_S}{2} \tag{3.36}$$

In this form I emphasize the existence of two distinct high field components of the initial density operator ρ with very differing symmetries. The first term corresponds to the average magnetization shared between the two spins, is symmetric with respect to interchange of the spin labels, and has the same characteristics as the magnetization in Equation (3.24). The second term in Equation (3.34) corresponds to the difference between the initial magnetizations at the two spins, is antisymmetric with respect to exchange of the two spin labels, and has no counterpart in the homonuclear problem. It couples the singlet state of the zero field Hamiltonian to the triplet manifold. It is responsible for new transition frequencies not allowed in the homonuclear case.

Both types of operators are first rank tensors. The symmetric combination behaves precisely as does the operator I_{zL} for two identical spin-1/2 nuclei as described immediately above. Under the influence of H_D, these operators evolve into second rank tensor

operators. The antisymmetric combination transforms under the rotation operator $R^{-1}(\Omega)$ into first rank antisymmetric molecular-frame operators proportional to $(I_{xM}-S_{xM})$, $(I_{yM}-S_{yM})$, and $(I_{zM}-S_{zM})$. The only nonzero matrix elements of these operators are $\langle -|I_{xM}-S_{xM}|S\rangle$, $\langle +|I_{yM}-S_{yM}|S\rangle$, and $\langle 0|I_{zM}-S_{zM}|S\rangle$. These operators evolve into a new set of first rank tensor operators (of the general form $(I_jS_k-I_kS_j)$) at frequencies characteristic of transitions between the singlet and triplet manifolds. Because of the differing symmetry characteristics of the two types of operators, no cross terms between these two sets can ever contribute to the trace of Equation (3.20). In the laboratory frame, ρ_L always consists of two orthogonal pieces, and

$$\rho_L(t_1) = b_+(t_1)(I_{zL} + S_{zL}) + b_-(t_1)(I_{zL} - S_{zL}) \tag{3.37}$$

where

$$b_+(t_1) = \frac{b_+(0)}{3}[1 + 2\cos(\tfrac{3}{2}\omega_D t_1)] \tag{3.38}$$

$$b_-(t_1) = \frac{b_-(0)}{3}[\cos(\omega_D t_1) + 2\cos(\tfrac{1}{2}\omega_D t_1)] \tag{3.39}$$

The zero field signal $G(t_1)$ depends on which nuclear spin reservoir is observed in high field. If the S spin system is observed,

$$G(t_1) = \mathrm{Tr}\,[S_{zL}\,\rho_L(t_1)] \tag{3.40}$$

$$= b_+(t_1) - b_-(t_1) \tag{3.41}$$

or, if the I spins are observed,

$$G(t_1) = \mathrm{Tr}\,[I_{zL}\rho_L(t_1)] \tag{3.42}$$

$$= b_+(t_1) + b_-(t_1) \tag{3.43}$$

Because the high field resonance frequencies ω_I and ω_S differ, it is possible to selectively irradiate either spin species in high field and alter the initial condition. In particular, if either b_+ or b_- is made equal to zero by an appropriate preparation sequence the observed spectrum is simplified by the disappearance of one set of lines. These predictions are confirmed by the zero field NMR spectra of the ^{13}C-^{1}H pair in β-$Ca(H^{13}COO)_2$ shown in Figure 3.4. The observed spectra precisely follow the predictions of Equations (3.41) and (3.43). Assuming no motion, the observed dipole-dipole coupling corresponds to a ^{13}C-^{1}H distance of 1.11Å. Figure 3.5 is a comparison of the high and zero field NMR spectra observed for I-I and I-S two-spin systems.

The signal function $G(t_1)$ corresponds to the magnetization stored in the I or S spins after a zero field evolution period t_1. Most frequently, it is the frequency-domain spectrum (the Fourier transform of $G(t_1)$) which is of interest. Where it is difficult to attain useful polarization levels in high field (either because the equilibrium S spin magnetization is small or where the S spin T_1 is inconveniently long), zero field evolution could conceivably be of use as a method of polarization transfer between spin species. As b_+ and b_- evolve differently in time, there exist values of t_1 which maximize the evolved S spin magnetization. The maximum in $S_{zL}(t_1)$ occurs when

Figure 3.4. ^{1}H detected zero field NMR spectra of ^{1}H-^{13}C pair in β-$Ca(H^{13}COO)_2$. ^{13}C spins are polarized by field-cycling preparation sequence. The sample is depolarized in zero field, then returned to high field for ~10 s (approximately T_{1H}). A complete field cycle is executed with fixed time $t_1 = 32\ \mu s$. This strongly magnetizes the ^{13}C nuclei to 160% of their equilibrium value. T_{1C} is several minutes. In high field the ^{1}H nuclei are repolarized. Prior to executing the field cycle with variable time t_1, a resonant rf pulse is applied to the ^{1}H spins of length, from top: 0°, 66°, 90°, 114°, and 180°. This generates the zero field initial conditions indicated in the plot. The spectra closely follow the predictions of the text. The observed ω_D corresponds to $\langle r^{-3}\rangle^{1/3} = 1.11$ Å.

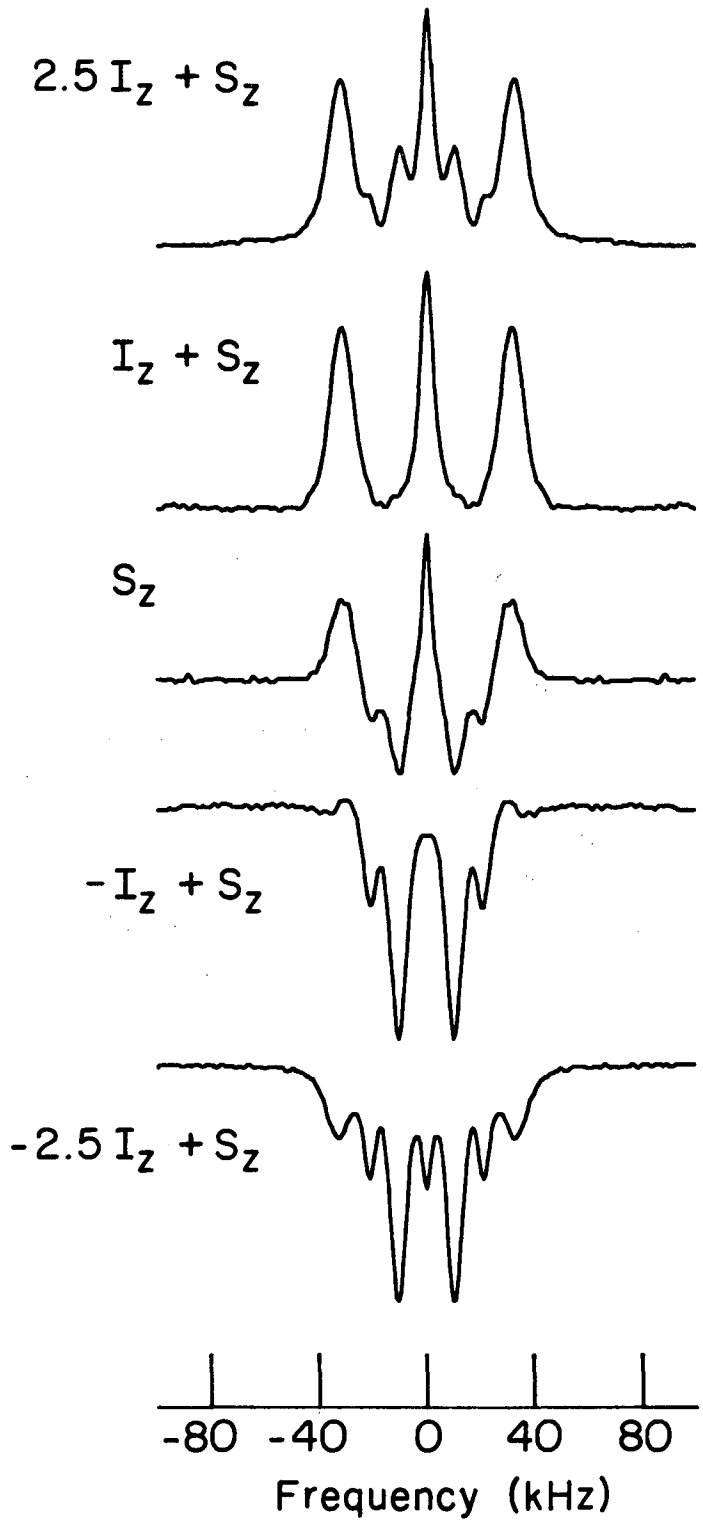

XBL 8312-4680

Figure 3.5. Summary of the high field and zero field Hamiltonians, eigenstates, and spectra for homonuclear (I-I) and heteronuclear (I-S) dipole coupled spin pairs. Transitions are indicated by the arrows. In high field the transition energies are orientation dependent and the spectrum is continuous absorption band. The zero field energy levels are orientation independent, and the zero field spectrum consists of a finite number of absorption lines. In I-I systems, only transitions within the triplet manifold are allowed.

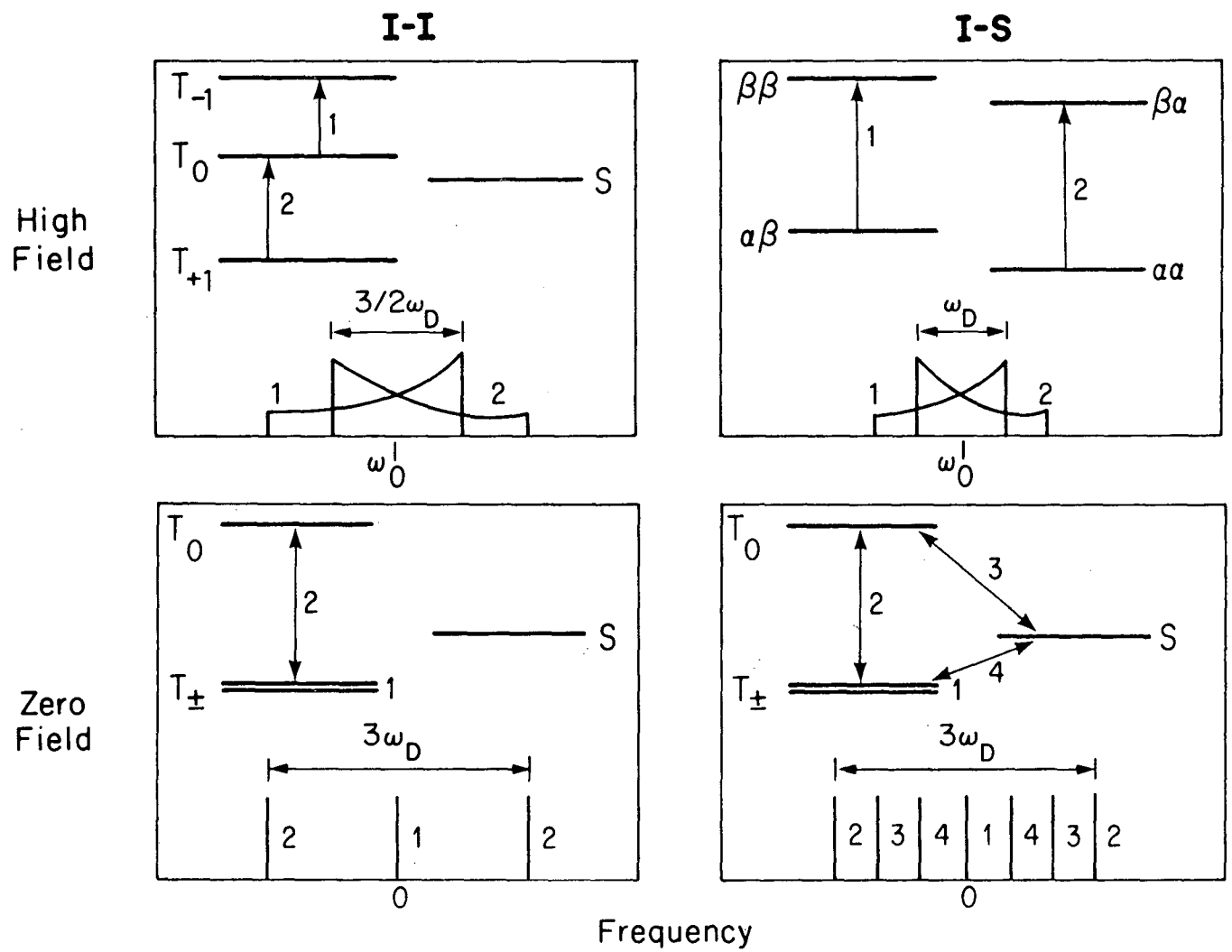
I-I
I-S
High Field
Zero Field
T_{-1}
T_0
T_{+1}
S
1
2
$3/2\omega_D$
ω_0^I
$\beta\beta$
$\beta\alpha$
$\alpha\beta$
$\alpha\alpha$
ω_D
$T_\pm$
3
4
$3\omega_D$
0
Frequency

XBL 855-2423

$$\frac{\delta S_{zL}}{\delta t_1} = \frac{\delta b_+}{\delta t_1} - \frac{\delta b_-}{\delta t_1} = 0 \tag{3.44}$$

or, defining $x = (\omega_D t_1/2)$,

$$[3\sin 3x\ b_+ - (\sin 2x + \sin x) b_-] = 0 \tag{3.45}$$

Solutions to Equation (3.44) include $\omega_D t_1 = 0, 2\pi, 4\pi, \ldots$, where $\mathrm{Tr}\ [\rho S_{zL}] = 0$. A second set of solutions is given by

$$\cos x = \frac{2b_- \pm (4b_-^2 + 144b_+^2 + 48b_+b_-)^{1/2}}{24b_+} \tag{3.46}$$

$$= \frac{b_- + 3b_+}{6b_+}\ ,\ -\frac{1}{2} \tag{3.47}$$

In the limit $b_S = 0$, then $b_+ = b_- = b_I$ and

$$\cos x = \frac{2 \pm 14}{24} = -\frac{1}{2}\ ,\ \frac{2}{3} \tag{3.48}$$

Choosing $\cos x = -(1/2)$,

$$\mathrm{Tr}(S_{zL}\rho) = \frac{1}{4}(3b_I + b_S) \tag{3.49}$$

which corresponds to a very significant transfer of polarization from the I to the S spin. In this two spin system, and for an initially depolarized S spin, 75% of the total order in the sample can be transferred from I to S. A derivation of the actual value of S_{zL} is more complicated for the last root of Equation (3.43) and only the results are given here;

$$\mathrm{Tr}(S_{zL}\rho) = \frac{1}{162b_+^3}\left[\frac{b_-^3 b_+}{2} - 9b_-^2 b_+^2 + \frac{27}{2} b_- b_+^3 - 54b_+^4\right] \tag{3.50}$$

In the limit $b_+ = b_-$ (i.e. no initial polarization on the S spins), Equation (3.49) simplifies to give

$$\mathrm{Tr}(S_{zL}\rho) = -\frac{49}{162} \quad b_+ \tag{3.51}$$

In the limit $b_- = 0$ (i.e. a homonuclear spin system) then this solution corresponds to a minimum at -1/3 of the originally prepared magnetization, precisely as is found in the homonuclear zero field free induction decay of Equation (3.32).

3. <u>Heteronuclear J Spectroscopy in Liquids</u>

The antisymmetric operators which allow transitions between the singlet and triplet manifold to take place provide a mechanism for the observation of pure J spectra in the zero field NMR of heteronuclear liquids. Ordinarily, one does not expect to observe oscillating magnetization from J couplings between pairs of nuclei in a liquid because the J coupling is isotropic in space. No spatial truncation occurs when a magnetic field is applied to a liquid. Thus, the removal of the field results in no discernable change in the density operator. In a residual field perpendicular to the polarizing field, oscillations corresponding to the Larmor frequency in the residual field may be observed. This is the basis of the Varian magnetometer experiment for the measurement of the earth's magnetic field.[72,73] In heteronuclear systems, the application of a magnetic field truncates the J coupling in the spin variables rather than the spatial variables. In a large field, the flip-flop terms in the J coupling tensor are rejected

because of the difference in Larmor frequencies (Equation (1.71)). The initial spin polarizations are also different (consistent with the magnetogyric ratios γ_I and γ_S).

The transitions within the triplet manifold of the two spin-1/2 system all appear at zero frequency because the J coupling shifts all energy levels within the triplet by the same amount in the same direction (Equation (1.70)). It is only the transition between the triplet and the singlet which carries any information and it appears at a frequency equal to the J coupling itself. Skipping the intermediate steps (which are similar to those in dipolar coupled systems as discussed above), and noting that without loss of generality $R(\Omega) = 1$, the zero field free induction decay from a heteronuclear J coupled pair of spin-1/2 nuclei is

$$M_z(t_1) = \frac{1}{2}(b_+ \pm b_- \cos Jt_1) \tag{3.52}$$

Rapid molecular reorientation in a liquid limits the interactions to those within a molecule and T_2's in liquids are usually long. In zero field the linewidths in the heteronuclear liquid are dominated by field inhomogeneities. Therefore, these systems provide a sensitive test for the effects of residual fields on the width of zero field resonance lines. Figure 3.6a shows the ^{31}P-detected zero field spectrum of diethyl phosphite ($(C_2H_5O)_2PH$). The directly bound ^1H-^{31}P coupling is very much larger than any of the couplings to methylene ^1H nuclei several bonds away and it is a good approximation to treat this systems as a two spin-1/2 system. The triplet of lines predicted by Equation (3.52) is observed and the spacing corresponds reasonably well with previously reported values of the J coupling.[76] Now consider the

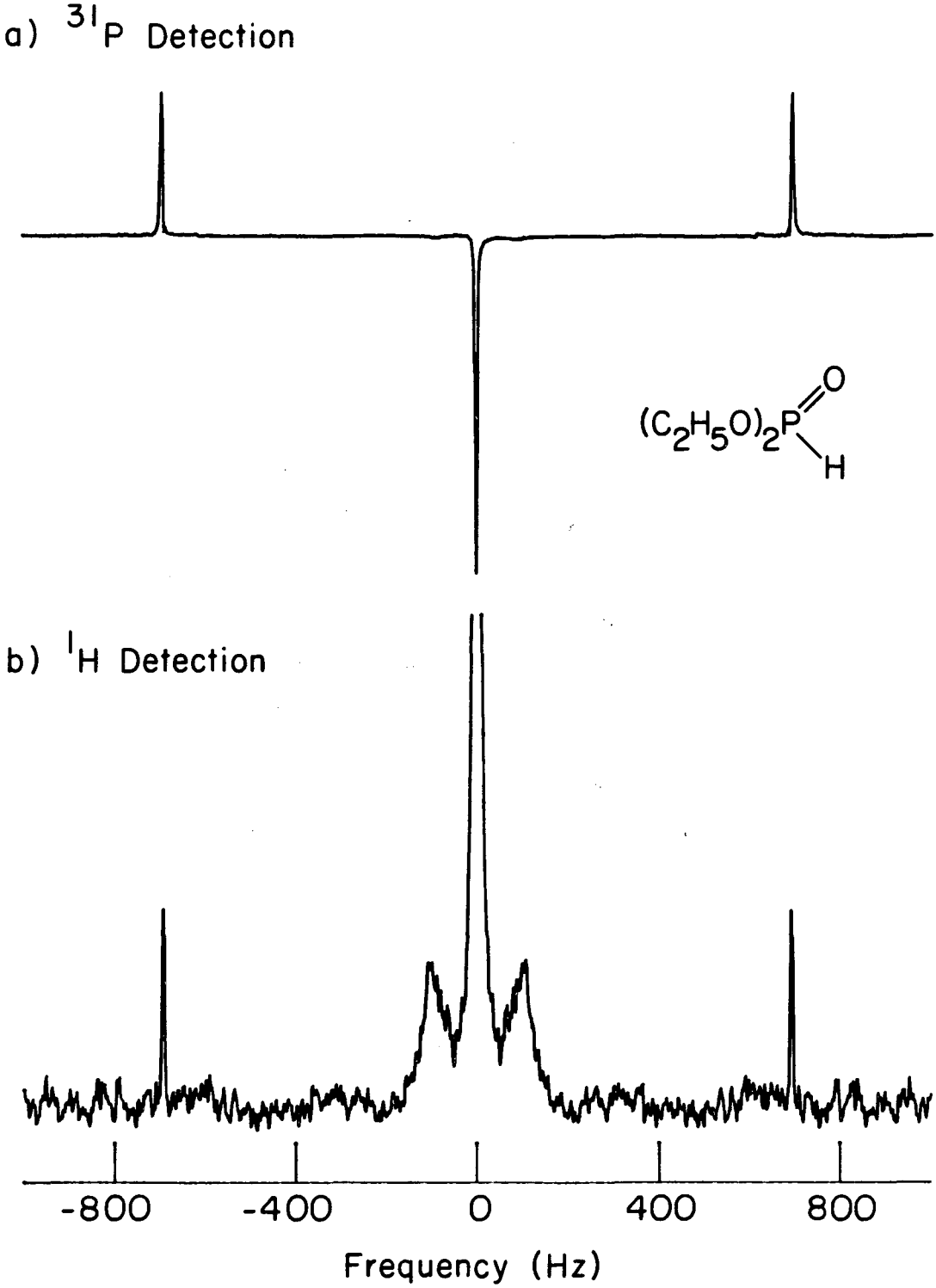
a) 31P Detection
(C2H5O)2P
O
H
b) 1H Detection
-800
-400
0
400
800
Frequency (Hz)

XBL 858-3509

Figure 3.6. Zero field J spectra of diethylphosphite ($(C_2H_5O)_2PHO$). Both spin systems equlibrate in high field. Immediately prior to the field cycle, a 180° pulse is applied to the ^1H spins. This enhances the amplitude of the peaks at $\pm J$. The coupling between ^{31}P and the directly bound ^1H contributes the sharp line at $\pm$ 692 Hz. a). ^{31}P detected spectrum. Only signal from the directly bound pair is observed. The spectrum is artificially broadened for purposes of display. The true linewidth is ~ 1 Hz. b). ^1H detected spectrum. The same line at $\pm$ 692 Hz is observed. In addition, broad peaks corresponding to the ethyl group ^1H's are observed at $\pm$ 100 Hz. This most likely corresponds to their Zeeman frequency and a residual field ~.02 gauss.

effect on the spectrum of a small applied field;

$$H = (\gamma_I I_j + \gamma_S S_j)B_{res} + J\,\tilde{I}\cdot\tilde{S} \tag{3.53}$$

with $J \gg \gamma_I B_{res}$. The eigenvalues of H are changed from their zero field values only to second order in the field, and the Zeeman Hamiltonian is truncated by the much larger J coupling. The absence of Zeeman-broadened lines in the spectrum of Figure 3.6a indicates the quality of the zero field region. (Just how bad the zero field region can afford to be is shown in Figure 3.6b. Here, the same experiment is performed with ^{1}H detection of the high field signal. The same narrow three-line spectrum is observed for the P-H pair. In addition, all the other ^{1}H nuclei appear at approximately their Larmor frequency of ~100 Hz, with a spread of ±20 Hz. At this level of residual field the J-coupled line is still less than 1 Hz wide.) Where broad lines are observed in zero field, the source will rarely be imperfections in the applied fields which can routinely be adjusted to within several hundredths of a gauss of zero. Broad lines are more often the result of a distribution in local Hamiltonians.

D. Quadrupolar Spin Systems

NQR spectra of integer and half-integer spins differ greatly from one another. A general and more detailed presentation of pure NQR is given in the standard reference works.[13,14] Here I dwell only on those aspects which are essential to the remainder of this work.

As the quadrupolar Hamiltonian H_Q is generally much larger than H_D, in this section I will deal with only those aspects of Fourier

transform NQR which apply to isolated quadrupolar nuclei. Experimental data on coupled spin-1 nuclei, and a discussion of the possible use of dipole-dipole couplings in structure determination, appear in Chapters V and VI.

1. Integer Spins: I = 1

Of the integer spins, only I = 1 (^{2}D and ^{14}N) systems are commonly observed. This will be the only case I will discuss. In the case of the spin 1 nucleus, operator techniques prove extremely powerful and the majority of my discussion will rely heavily on the operator set presented in Tables 2.1 and 3.1.[66,77] The spin-1 quadrupolar Hamiltonian (Equation 1.68) consists of two commuting terms, one proportional to the spin operator U_0 and a second proportional to the spin operator U_{2+}; it and its three eigenstates (with η=0) are formally identical to the triplet manifold of two spins-1/2, and therefore the problem of the homonuclear pair. For nonzero η, the term in H_Q proportional to η breaks the degeneracy of the two states ($|x\rangle, |y\rangle$) and requires that the eigenstates be chosen proportional to what otherwise would appear to be the rather awkward linear combination of the tables.

a. The Signal Function

All of the algebraic machinery established in the calculation of $G(t_1)$ for the homonuclear pair is directly applicable to the problem of the spin-1 nucleus in zero field. As there are three distinct energy levels there are also three distinct transition frequencies. In direct analogy to Equation (3.32), the zero field free induction decay from a polycrystalline sample for I = 1 is

$$G(t_1) = \frac{1}{3}(\cos \omega_{23}t_1 + \cos \omega_{31}t_1 + \cos \omega_{21}t_1) \tag{3.54}$$

with

$$\omega_{12} = 2\eta A \qquad \omega_{23} = -(3+\eta)A \qquad \omega_{31} = (3-n)A \tag{3.55}$$

In keeping with the convention long established in zero field NQR, only positive frequencies will be displayed and therefore three lines will be observed (where the same signal function $G(t_1)$ would result in three pairs of lines as we have chosen to display the spin-1/2 spectra). A number of illustrative examples of typical spin-1 zero field NMR spectra appear in Chapter V. Figure 3.7 shows a comparison between the zero field spectra of I-I and I-S dipole-dipole coupled spin systems and of a spin-1 quadrupolar nucleus.

b. Explicit Calculation of ρ

In this section, I take a somewhat different approach to the calculation of the signal function of Equation (3.54). Rather than calculating $G(t_1)$ as in Section B, I obtain an explicit expression for the lab frame representation of the density operator for a specific orientation, $\rho_L^{\Omega}(t_1)$. This corresponds to following the evolution of the lab frame magnetization at each orientation of the powder for all times t_1.

While it is always possible to represent ρ as a matrix of numbers, somewhat greater insight is gained if instead ρ is represented in an operator basis set. This approach has gained popularity in the use of fictitious spin-1/2 operator bases in the analysis of multiple-quantum NMR[77-80] but its use in NQR is older.[81] Generally, a traceless NXN Hermitian matrix is represented by N^2-1 independent traceless

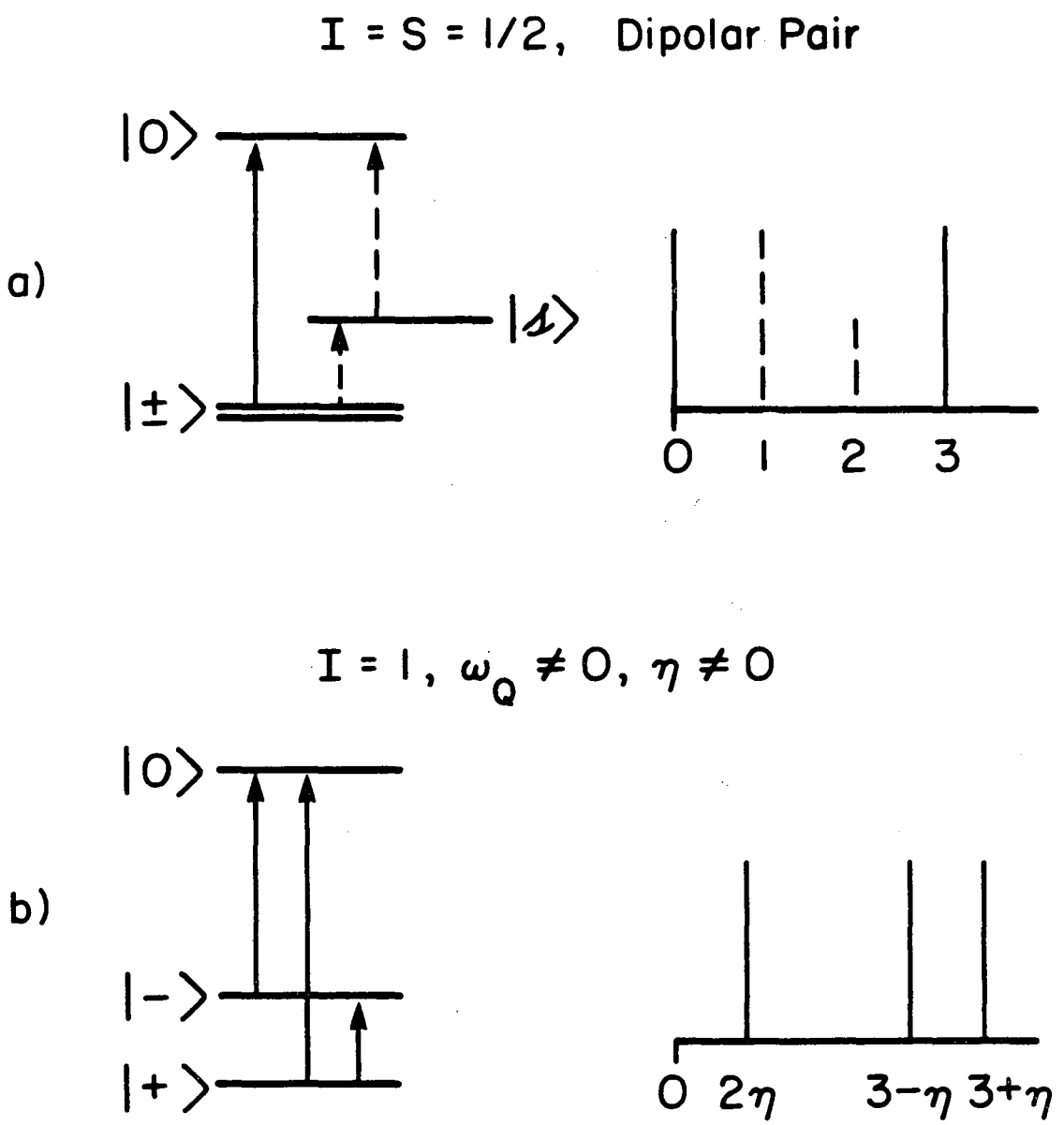

Figure 3.7. Comparison of spectra and Hamiltonians for two dipole-coupled spin-1/2 nuclei, and for a spin-1 quadrupolar nucleus. a). Summary of zero field eigenstates and transition frequencies of dipole-coupled pair. Transition frequencies allowed in both I-I and I-S systems are shown in bold lines; allowed only in I-S, dashed. For comparison to quadrupolar spins, only positive frequencies are shown. b). Eigenstates and energy levels of spin-1 system in the notation of Table 3.1. A non-zero value of η splits the |+> and |-> eigenstates. For $\eta = 0$, the spectrum is identical to that of the I-I pair.

operators. The operators in Tables 2.1 and 3.1 provide a convenient basis set for the discussion of spin-1 nuclei in zero field. The transformations of the first rank tensors under rotations are given by Equation (1.25); the second rank tensors U_k, in Table 1.2. Time evolution is summarized in Equations (3.25) and (3.26).

Until Equation (3.13) the treatment of Section III.B is adequate. At a time t_1 the density operator $\rho^{\Omega}(t_1)$ is

$$\begin{aligned}\rho_M^{\Omega}(t_1) = \; & \cos\beta(I_{zM}\cos\omega_{12}t_1 + (I_{xM}I_{yM}+I_{yM}I_{xM})\sin\omega_{12}t_1) \\ & -\sin\beta\cos\alpha(I_{xM}\cos\omega_{23}t_1 + (I_{yM}I_{zM}+I_{zM}I_{yM})\sin\omega_{23}t_1) \\ & +\sin\beta\sin\alpha(I_{yM}\cos\omega_{31}t_1 + (I_{xM}I_{zM}+I_{zM}I_{xM})\sin\omega_{31}t_1) \qquad (3.56)\end{aligned}$$

or, in slightly more compact notation,

$$\begin{aligned}\rho_M^{\Omega}(t_1) = \; & \cos\beta(I_{zM}\cos\omega_{12}t_1 + U_{2+M}\sin\omega_{12}t_1) - \sin\beta\cos\alpha(I_{xM}\cos\omega_{23}t_1 + \\ & U_{1+M}\sin\omega_{23}t_1) + \sin\beta\sin\alpha(I_{yM}\cos\omega_{31}t_1 + U_{1-M}\sin\omega_{31}t_1) \qquad (3.57)\end{aligned}$$

Finally, ρ_M^{Ω} must be rexpressed in the laboratory frame $\rho_L^{\Omega} = R^{-1}\rho_M^{\Omega}R$, and

$$\begin{aligned}\rho_L^{\Omega}(t_1) = \; & a_1(t_1)I_{xL} + a_2(t_1)I_{yL} + a_3(t_1)I_{zL} + a_4(t_1)U_{0L} + a_5(t_1)U_{1+L} \\ & + a_6(t_1)U_{1-L} + a_7(t_1)U_{2+L} + a_8(t_1)U_{2-L} \qquad (3.58)\end{aligned}$$

where

$$a_1(t_1) = \sin\beta\cos\beta[\cos\omega_{12}t_1 - (\cos^2\alpha\cos\omega_{23}t_1 + \sin^2\alpha\cos\omega_{31}t_1)]$$

$$a_2(t_1) = \sin\beta\sin\alpha\cos\alpha(\cos\omega_{31}t_1 - \cos\omega_{23}t_1)$$

$$a_3(t_1) = \cos^2\beta\cos\omega_{12}t_1 + \sin^2\beta(\cos^2\alpha\cos\omega_{23}t_1 + \sin^2\alpha\cos\omega_{31}t_1)$$

$$a_4(t_1) = -\frac{\sqrt{3}}{2}\cos\beta\sin^2\beta\sin2\alpha\ (\sin\omega_{23}t_1 + \sin\omega_{31}t_1 + \sin\omega_{12}t_1) \qquad (3.59)$$

$$a_5(t_1) = \cos\beta\sin\beta(\sin^2\alpha\sin\omega_{31}t_1 - \cos^2\alpha\sin\omega_{23}t_1 - \cos2\alpha\sin\omega_{12}t_1)$$

$$a_6(t_1) = \sin\alpha\cos\alpha\sin\beta[2\cos^2\beta\sin\omega_{12}t_1+\cos2\beta(\sin\omega_{23}t_1+ \sin\omega_{31}t_1)]$$

$$a_7(t_1) = \sin^2\beta(\sin^2\alpha\sin\omega_{31}t_1- \cos^2\alpha\sin\omega_{23}t_1) + \cos2\alpha\cos^2\beta\sin\omega_{12}t_1$$

$$a_8(t_1) = -\frac{1}{2}\sin2\alpha\cos\beta[(1+\cos^2\beta)\sin\omega_{12}t_1- \sin^2\beta(\sin\omega_{23}t_1+\sin\omega_{31}t_1)$$

Normally when the external field is reapplied only I_{zL} and U_0 are stored as diagonal elements of ρ_L, but suitable detection sequences can be designed to transform any of these lab-based tensor operators into an observable transverse magnetization. In the most general ordered system all of these coefficients may be non-zero. Magnetization initially aligned in the laboratory frame may appear as any other type of operator. If $\eta = 0$, a_2, a_5, a_7, and a_8 vanish and the magnetization is limited to excursions in the plane defined by the laboratory and molecular z-axes. Where the sample contains a distribution of orientations $P(\Omega)$, the a_k coefficients must be integrated over that distribution function. In powders where $P(\Omega)$ is a constant, only a_3 has non-zero integral over all space, and is responsible for the free induction signal of Equation (3.54). In powders there are no observables orthogonal to the initially prepared operator. I return to this point in Chapter VI.

2. <u>Half-Integer Spins: I = 3/2, 5/2</u>

Kramer's theorem (which will be introduced and explained more

rigorously in Chapter VII) states that each energy level of a zero field Hamiltonian with half-integral spin must be at least doubly degenerate. An isolated spin $\bar{I}$ nucleus has 2I+1 eigenstates but because of this degeneracy there are no more than (2I+1)/2 distinct energy levels. If each energy level were coupled to all others, the number of lines which would be expected to be observed (ignoring the inevitable line at zero frequency which corresponds to coupling between degenerate pairs of eigenstates) would be $(2I+1)(2I-1)/8 = (4I^2-1)/8$. Generally far fewer lines are observed. In contrast to the integer spin, the Hamiltonian of a half-integer spin nucleus consists of two non-commuting pieces. The asymmetry parameter η couples only eigenstates with vastly differing quadrupolar energies and perturbs their energies only to second order in perturbation theory. In the basis set where I_{zM} is a good quantum number, corrections to the zeroth order eigenstates are small. Particularly for small values of η, but even for larger values, the eigenstates of the quadrupolar Hamiltonian can be identified as being almost eigenstates of $|I_{zM}|$. Were I_{zM} a rigorously good quantum number, then in the molecular frame the dipole selection rule

$$\Delta m_M = \pm 1 \tag{3.60}$$

would hold and only I-1/2 distinct non-zero frequency lines can be observed by the experimental scheme developed in this chapter. Even where the asymmetry parameter η breaks this selection rule, the amplitudes of the "forbidden" lines are small and they are rarely observed.[82]

The spectrum observed in high field is generally not the entire

powder pattern but instead only that portion which is unshifted to first order by the quadrupole coupling (for spin systems where the second order quadrupolar broadening in not too severe. For other systems, no high field technique is well suited and only zero field methods with direction detection in low field, or with indirect detection via level crossings are applicable.) As long as some portion of the high field powder pattern is uniformly observed, it can be shown (see Appendix A) that the intensities of the zero field spectra are uniformly scaled by the detection sequence. Calculation of the spectrum in this chapter will therefore be based on the assumption of uniform and, implicitly, complete detection.

The simplest case is for I = 3/2. By either of the counting schemes outlined above, only a single non-zero line can be observed and the two components of the electric field gradient tensor cannot be individually determined. On the other hand, each unique line must correspond to a unique site. Performing the calculation indicated in Section III.B, the zero field free induction decay is

$$G(t_1) = \frac{1}{5}(3 + 2\cos\omega_Q t_1) \tag{3.61}$$

with

$$\omega_Q = \frac{e^2qQ}{2\hbar}\sqrt{1 + \frac{1}{3}\eta^2} \tag{3.62}$$

The existence of only a single nonzero frequency line is from the counting arguments discussed above. It is less obvious that the relative intensities of the nonevolving and evolving components should also be independent of e^2qQ and η. It can be shown, independent of the size of η, that this is generally true.

An illustration of the zero field NQR spectrum of a system of spin-3/2 nuclei is shown in Figure 3.8, in the ^7Li spectrum of $Li_2SO_4 \cdot H_2O$. Diffraction studies reveal two sites, and they are clearly resolved in the zero field spectrum at frequencies consistent with the values of e^2qQ and η derived from high field single crystal studies of the same compound.[83] The broad lines are presumably due to dipolar couplings to ^1H nuclei in nearby H_2O molecules and should be considerably narrowed by replacement of the ^1H atoms with ^2D.[84]

For I = 5/2 no closed form solution to the eigenvalue equation can be given. For any given value of η, the eigenvalue equation can be reduced to a pair of identical cubic equations which can be solved analytically. Tables of the eigenvalues for spin-5/2 nuclei in zero field have been given;[82] most often, the eigenvalue equation is given as an expansion in η. For $\eta = 0$ and where I_{zM} is a good quantum number, the form of the zero field signal is

$$G(t_1) = \frac{1}{105}(53 + 32\cos\omega_Q t_1 + 20\cos 2\omega_Q t_1) \qquad (3.63)$$

for

$$\omega_Q = \frac{3e^2qQ}{10\hbar} \qquad (3.64)$$

Slightly more than half of the magnetization fails to evolve (either because it originally corresponds to I_{zM} or because it corresponds to matrix elements of I_{xM} or I_{yM} which couple degenerate eigenstates). Of the rest, nearly twice as much evolves in the coherence associated with the transitions $|1/2\rangle \rightarrow |3/2\rangle$ than at transitions of the form $|3/2\rangle \rightarrow |5/2\rangle$. Unlike the spin 3/2 case, and in common with all larger half-integer spin systems, as η grows both the spacing between lines

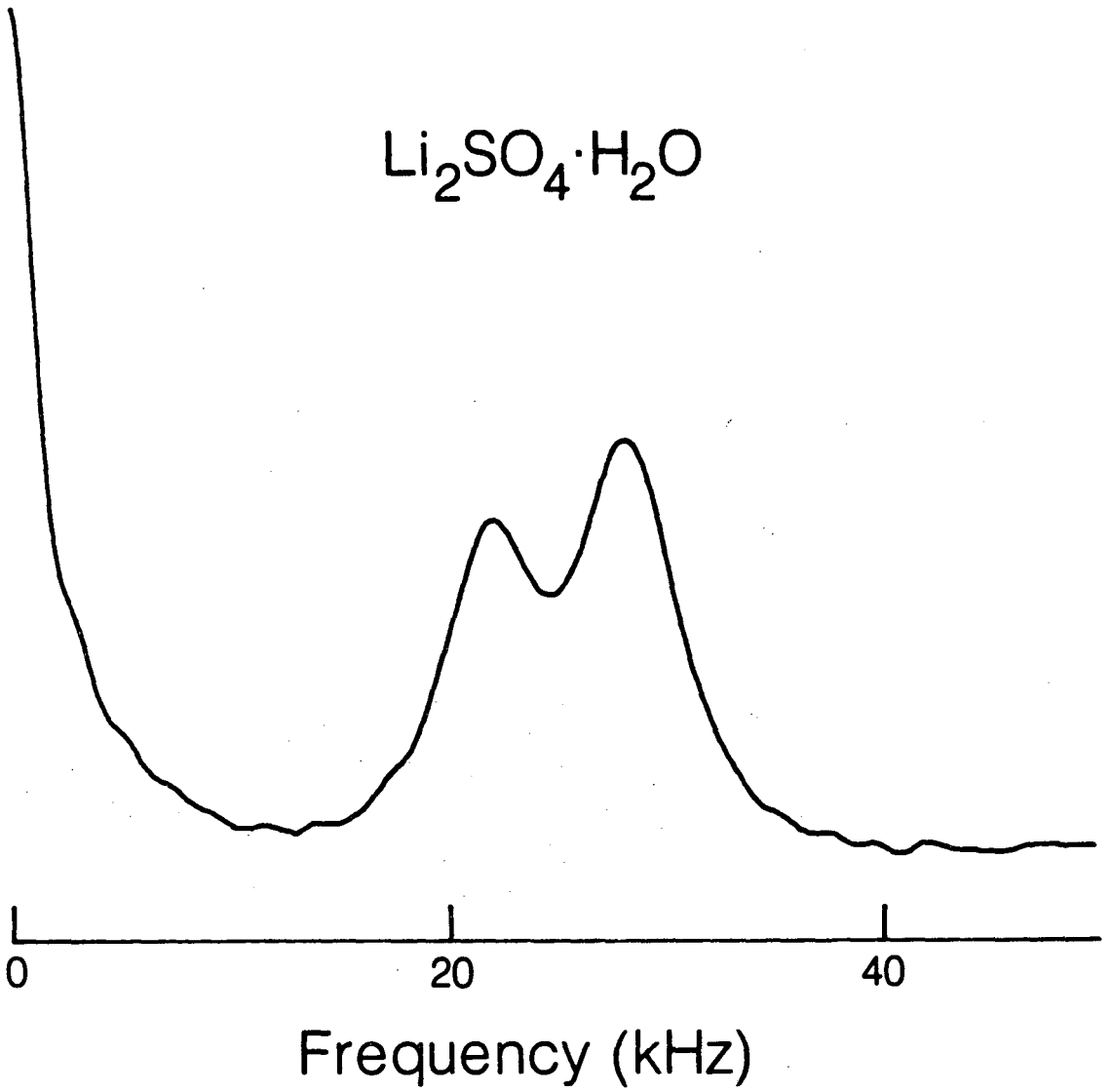

XBL 8310-12108

Figure 3.8. Zero field ^{7}Li NQR spectrum of polycrystalline $Li_2SO_4 \cdot H_2O$. The lithium zero field evolution was sampled at 10 μs intervals for a total of 630 μs. One line (in addition to non-evolving signal which appears at zero frequency in the spectrum) is expected for each site and two such sites are resolved. The zero frequency line is partially truncated.

and their relative intensities will vary in a regular fashion. For $I = 5/2$ and larger values of η, a third line may appear at the sum of the two "allowed" lines but even for $\eta = 1$ its amplitude is less than 7% of that of either of the two other lines. Tables of dipole-allowed intensities and normalized frequencies as a function of η are given for $I = 5/2$, 7/2, and 9/2 elsewhere.[82] For $I = 5/2$ and to order η^2, the transition frequencies are[11]

$$\omega^{3/2,5/2} = A\left(12 - \frac{22\eta^2}{9}\right) \tag{3.65}$$

for the line between the states which for $\eta = 0$ can be associated with $|I_{zM}| = 3/2$ and 5/2, and

$$\omega^{1/2,3/2} = A\left(6 + \frac{59\eta^2}{9}\right) \tag{3.66}$$

for the line between the 1/2 and 3/2 eigenstates. Where it is observed, the transition frequency between the 1/2 and 5/2 eigenstates appears at the sum of these two frequencies.

Figure 3.9 shows an example of a typical zero field NQR spectrum for $I = 5/2$. It shows the ^{27}Al spectrum of polycrystalline potassium alum ($KAl(SO_4)_2 \cdot 12H_2O$). Using Equations (3.65) and (3.66), the quadrupolar tensor elements $e^2qQ/h = 391 \pm 2$ kHz and $\eta = .17 \pm .05$ can be derived. Presumably, the abundant ^1H nuclei in the lattice are responsible for the breadth of the observed spectral lines.

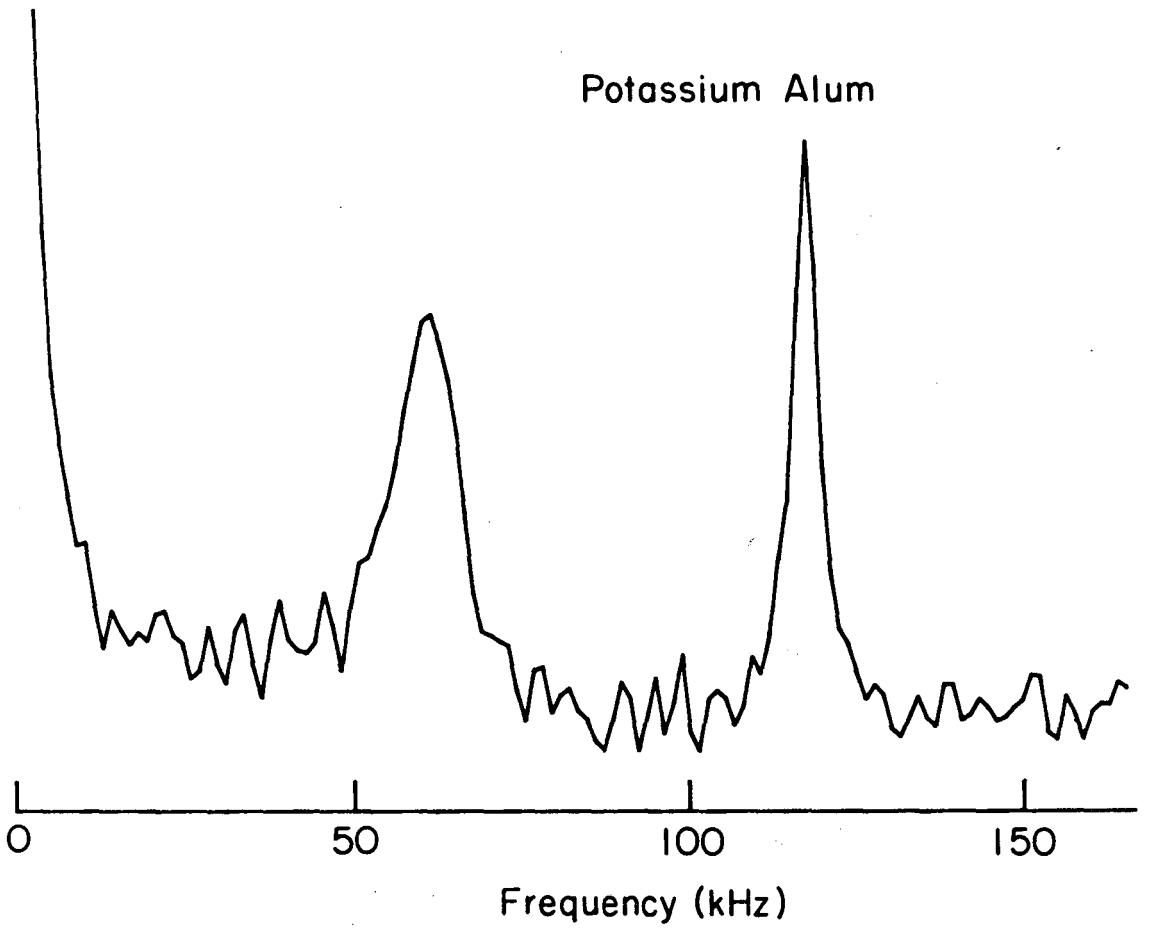

XBL 847-3141

Figure 3.9. Zero field ^{27}Al NQR spectrum of polycrystalline $KAl(SO_4)_2 \cdot 12H_2O$. Each distinct spin-5/2 nucleus has two zero field frequencies in addition to some non-evolving magnetization. Only one site is observed.

IV. Experimental Results: Dipolar Coupled Systems

Both high and zero field NMR are sensitive to structure and geometry in disordered solids. The spectrum of the local nuclear spin Hamiltonians detailed in Section I.B reflect the crystalline or molecular characteristics which are the source of these Hamiltonians. In the presence of motion, NMR spectra are averaged in a fashion characteristic of the dynamic processes and an analysis of the spectrum may reveal these processes. High field magnetic resonance yields information whose fundamental content is identical to that of zero field spectra but whose analysis is considerably more difficult because of the superposition of orientational broadening on top of the useful structural information in the spectrum. Because the evolution of the nuclear spin systems is observed (ideally) in the absence of all perturbing fields (dc or rf) the only limitation on the observed linewidths is that imposed by the nature of the spin system itself, rather than by orientational broadening, field inhomogeneity, or saturation. The spectral linewidths correspond to the minimum allowed for that system (sample and T) and consistent with the Hamiltonians being observed. Multiple pulse sequences have the potential to modify the information content of zero field spectra,[85-87] but no applications to zero field dipolar spectra have appeared. In this chapter and the next, what is intended is a critical review of the current experimental situation.

Since an understanding of many of the results of this and subsequent chapters requires an appreciation of the effects of motion on nuclear spin interactions a brief review is given in Appendix B.

More complete treatments using more sophisticated models are available throughout the literature of modern NMR.[88] The focus in this work has been not on a deep understanding of the dynamics themselves but rather on the interpretation of the spectra. Motional averaging will be discussed on an ad hoc basis and only where necessary.

All spectra which appear in this thesis are of polycrystalline samples at room temperature.

A. Two and Three Coupled Spin-1/2 Nuclei

In Chapter III the simple case of two coupled spin-1/2 nuclei was discussed. Still, a number of minor but interesting points remain undiscussed. The gross features of Figure 3.2 (three lines of equal intensity) are explained by the exact treatment of the two-spin system. In this section, I confront some of the finer details which arise, for the most part, from the breakdown of the static two-spin model. In this chapter I hope to explore some of the current capabilities and limitations of the technique of zero field NMR.

Two details in Figure 3.2 merit further discussion: contributions to the zero field linewidth (as the "high resolution" zero field NMR lines are still ~4 kHz full width at half maximum and are significantly broader than would be acceptable in most other high resolution applications), and the low intensity absorption bands at roughly double the frequency of the main bands. (These latter are almost certainly <u>not</u> due to instrumental artifacts. While an obvious source for lines at multiples of some fundamental frequency is non-linearity in the receiver section of the spectrometer, the relative

amplitudes of these lines show little or no dependence on the strength of the input signal.)

1. Contributions to the Linewidth

a. Residual Fields

One possible source for contributions to the linewidths observed in zero field NMR spectra is the effect of residual dc fields. In routine operation the zero field region is shimmed using a Hall effect gaussmeter and the residual dc field is certainly less than 100 milligauss. For isolated ^1H nuclei, 100 mgauss corresponds to a Larmor frequency of ~400 Hz. Dipole-dipole couplings in a solid truncate the Zeeman interaction just as the J coupling truncates the effects of residual fields in diethylphosphite (Figure 3.6). The anisotropy of the dipole-dipole coupling introduces a directional dependence; additionally, the zero field spectrum must depend on whether the residual field is primarily parallel or perpendicular to the prepared magnetization. (In the limit of exceedingly large longitudinal fields $H_Z \gg H_{loc}$, there is no signal in a "zero field" experiment as the polarizing field is never turned off!) In Figure 4.1 the powder pattern lineshape is simulated for a pair of coupled spin-1/2 nuclei in the presence of small residual dc fields. The resulting Zeeman-perturbed dipolar spectra bear no close resemblance to the experimental results of Figure 3.2 even for applied fields much larger than might actually be expected to be present.

b. Other Dipole-dipole Couplings

In any real solid, small numbers of spins are isolated only to the extent that the dipole-dipole couplings between clusters have not had sufficient time to act; roughly, for a time τ such that

Figure 4.1. Simulations of low field NMR spectra. The sample is assumed composed of two-spin ^{1}H systems with r = 1.60 Å. Spectra are calculated for transverse (a,c,e) and longitudinal (b,d,f) residual fields of:

a, b). 0.35 gauss (1.5 kHz).

c, d). 1.17 gauss (5.0 kHz).

e. f). 2.34 gauss (10.0 kHz).

The spectra are seen to broaden and acquire structure but none of these simulations closely reproduces the observed features. The residual fields are almost certainly smaller than 0.35 gauss.

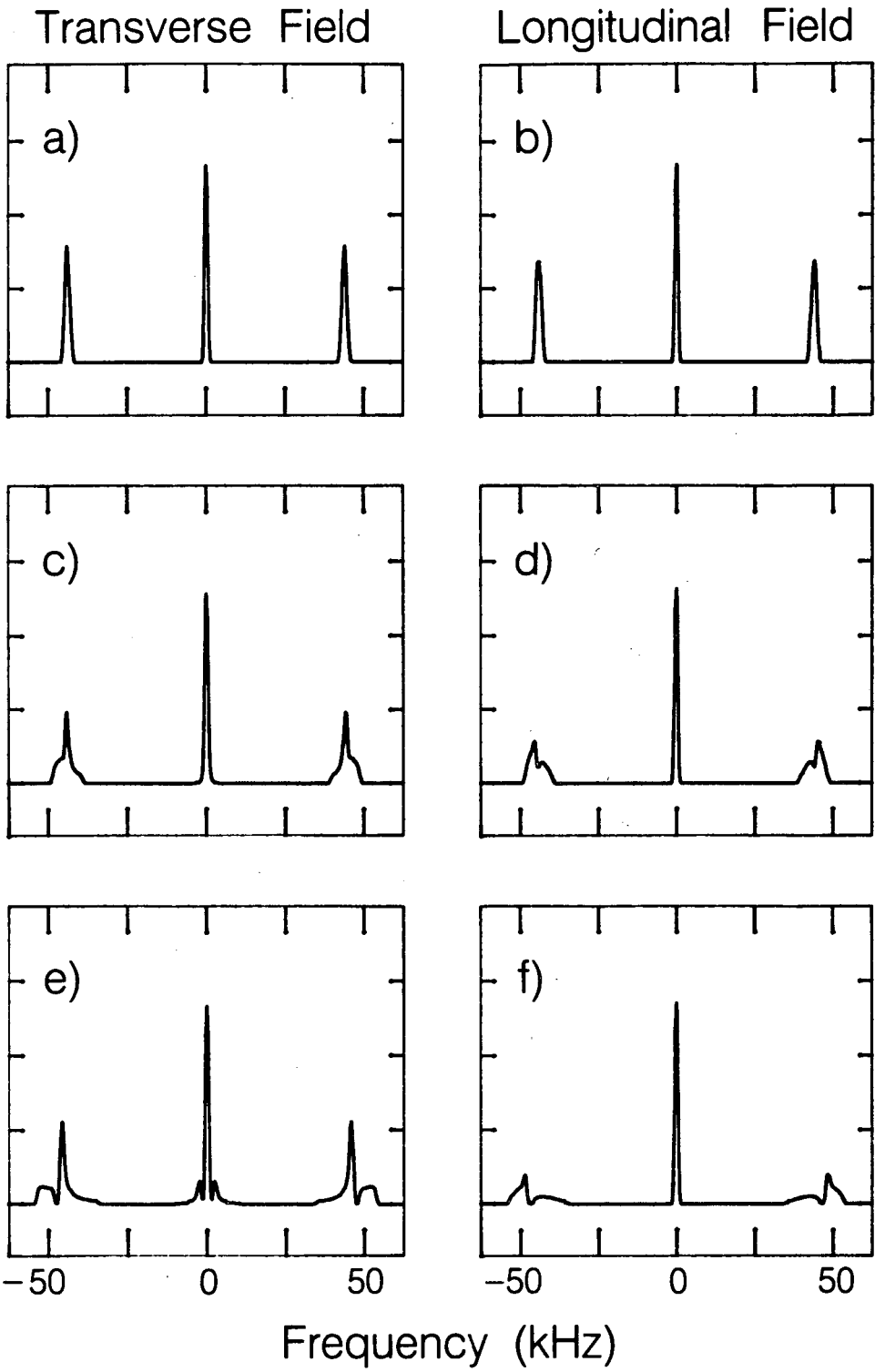
Transverse Field
Longitudinal Field
a)
b)
c)
d)
e)
f)
−50
0
50
−50
0
50
Frequency (kHz)

XBL 857-8935

$||H_{Dcc}||\tau < 1$ where $||H_{Dcc}||$ is a "mean" dipole-dipole coupling constant characteristic of the distance between clusters. Dipole-dipole couplings are zero only for two magnetic nuclei infinitely far apart. In most high field solid state techniques high resolution is achieved by causing the time-average of the dipole couplings to become vanishingly small and observing only those components of the total spin-Hamiltonian which survive the averaging process.[2,8] The approach in this work is instead to emphasize these couplings and at their full values. Where these multi-spin couplings are emphasized and no active effort is made to discriminate between large and small couplings,[40] "clusters" and thus well-resolved zero field dipole-dipole spectra may be observed only in carefully chosen real-world systems.

Traditionally, linewidths in solids are expressed (and calculated) in terms of moments of the lineshape, where the nth moment of the lineshape is given by

$$\langle\Delta\omega^n\rangle = \int_0^\infty(\omega - \langle\omega\rangle)^n f(\omega)d\omega \Big/ \int_0^\infty f(\omega)\, d\omega \qquad (4.1)$$

and $f(\omega)$ is the lineshape of the specific line or band of interest. The moments can be calculated from first principles and without reference to exact dynamical calculations or numerical diagonalization of multi-spin Hamiltonians.[9,11] (Note that in this section I refer not to the more usual second moment of an entire high field spectrum referenced to its center at $\omega = \omega_0$, the Larmor frequency, but rather to the second moment of an isolated line referenced to its center of gravity.) Several authors have treated the moments of the lineshapes for pure NQR lines.[66,84,89] Two coupled spin-1/2 nuclei closely resemble a spin-1 nucleus, and few modifications to the theories for

NQR linewidths are necessary to accomodate pairs of ^1H nuclei. In an attempt to explain the observed zero field linewidth, the experimental moment of the spectral line at ~42 kHz was calculated from the spectrum for comparison to theoretical results. The experimentally observed second moment is

$$M_2 = \langle\Delta\omega^2\rangle = (2.82 \pm .05 \text{ kHz})^2 \tag{4.2}$$

The ^1H-^1H dipole-dipole tensor trivially substitutes for the spin-1 quadrupolar tensor. The only necessary modification to the theory for spin-1 nuclei is that only the contribution from 3/4 of the total number of crystalline H_2O molecules is included. Two coupled spin-1/2 nuclei comprise a four-level system. The triplet mainfold (3/4 of the total number of pairs) mimics a spin-1 three level system while the singlet (the other 1/4) corresponds to a nonmagnetic spin-0 particle. In the theoretical calculation of $\langle\Delta\omega^2\rangle$ the numerical constants tabulated by Vega were used.[66] Based on the neutron diffraction data,[90] all ^1H-^1H vectors in the unit cell are parallel. Using the single-crystal neutron diffraction coordinates, the theoretical second moment is

$$\langle\Delta\omega^2\rangle = (1.95 \pm .01 \text{ kHz})^2 \tag{4.3}$$

If the angle between the crystalline axis system and the internuclear vector is changed, the theoretical value takes on values as large as the observed but only for severe and improbable deviations from those of the diffraction study. Therefore other dipole-dipole couplings appear unlikely to explain the entire linewidth. More complicated calculations which might include not only the dipole-dipole couplings

but also small residual fields might be attempted but were not.

c. Dilution Studies

In order to observe at higher resolution the line at 42 kHz, samples of $Ba(ClO_3)_2 \cdot H_2O$ were recrystallized from D_2O solution. In the recrystallization, most of the crystalline ^1H atoms were replaced by ^2D atoms. This greatly reduces the dipole-dipole couplings between sites as the ^2D quadrupolar tensor is known to have a large motionally-induced asymmetry parameter at room temperature[91] and couplings between integer spins with large η and half-integer spins are quenched in zero field[66,84]. Simultaneously, the number of ^1H-^1H pairs decreases as the square of the percentage of residual ^1H nuclei in the lattice. ^1H-^1H pairs within a single water molecule should still have nearly unchanged resonance frequencies. ^1H nuclei which share an oxygen atom with a ^2D nucleus are coupled only much more weakly to far distant ^1H's and appear near zero frequency. Pairs of ^2D nuclei are not expected to be observed in the ^1H spectrum.

The second moment calculation suggests a significant percentage of the linewidth is due to unresolved couplings to other molecules in the lattice. This contribution to the linewidth decreases approximately linearly with the decrease in ^1H concentration. Figure 4.2 shows zero field NMR spectra observed as a function of the ^1H concentration. Removing ^1H from the lattice decreases the width of the lines in the spectrum of the residual pairs. As these lines narrow it becomes apparent (Figure 4.2c,d) that two distinct resonance frequencies were hidden beneath the single peak observed in the completely protonated form. (Whatever is happening to the spectral features of the line at zero frequency is unfortunately masked by the spectra of all the

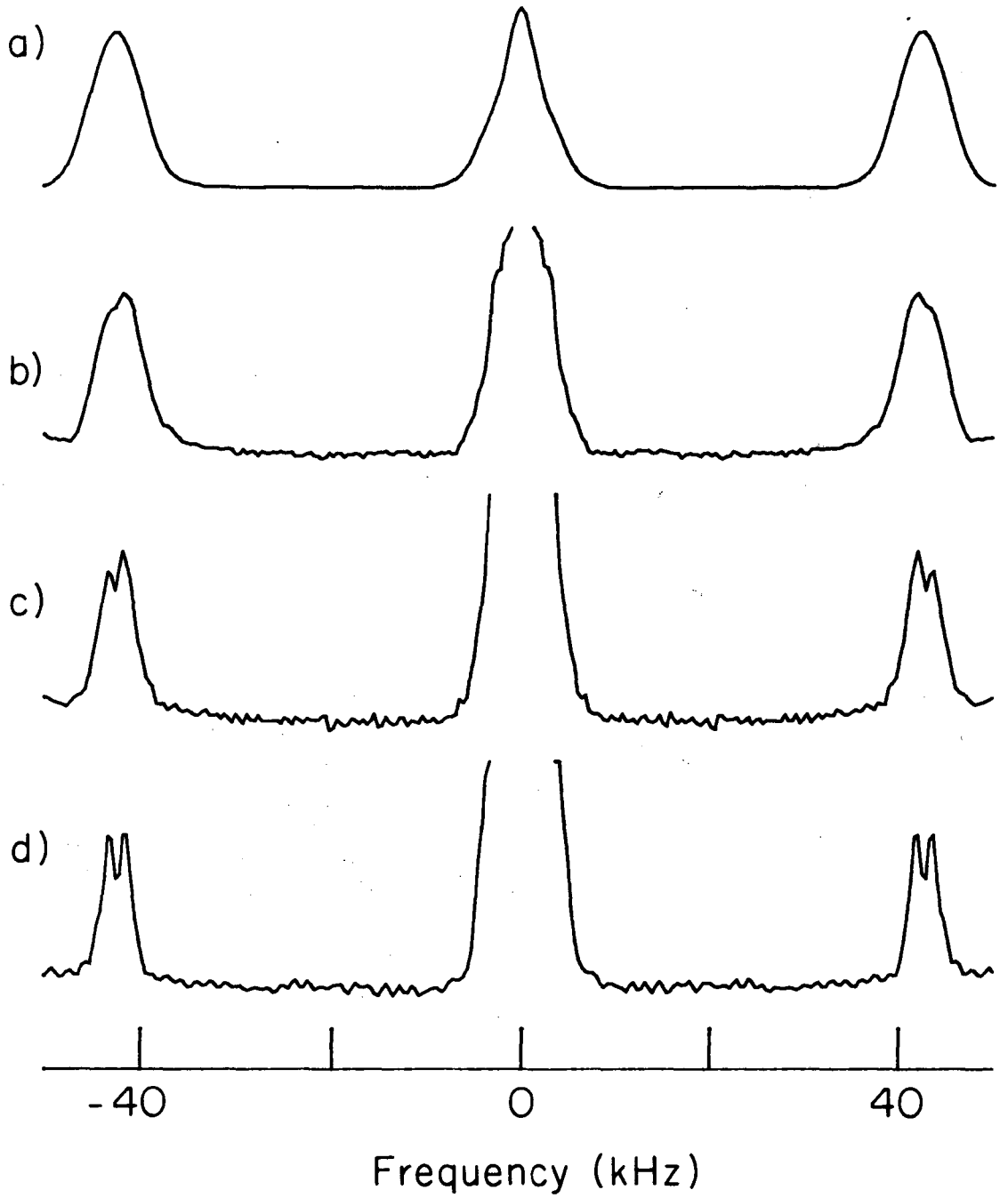

Figure 4.2. ^1H zero field NMR spectra of partially deuterated $Ba(ClO_3)_2 \cdot H_2O$.

a). 100% ^1H.

b). 60% ^1H.

c). 31% ^1H.

d). 10% ^1H.

unpaired sites, which is concentrated in a broad blob characteristic of the range of local fields in the crystal about zero frequency.) This splitting is similar to that expected for quadrupolar spin-1 nuclei with an asymmetric tensor $\tilde{V}$. Residual fields, which cause the entire absorption pattern to broaden and move to higher frequencies, cannot be the source of this splitting.

Motionally induced asymmetries in ^{13}C-^{1}H dipole-dipole couplings,[92] in carboxylic acids,[93] and in hydrate crystals[94] have previously been observed in high field. It is known from ^{2}D NMR studies[91] that the water molecules in this and many other hydrates execute jumps which interchange the two nuclear sites. If the flips occur rapidly, this sort of motion cannot be observed in pure NMR because the dipolar tensor is unaffected by the interchange of the two nuclear positions. The dipolar tensor is, however, modified if these flips are not precisely rotations by π but instead have a mean value of π. Small angle librations superposed on the flipping motion should be observable in the NMR spectrum. Section C of Appendix B treats the effect of small amplitude librations on quadrupolar tensors (relying on the presentation by Abragam[11] of the results of Bayer[95]). These results are equally relevant to the problem of two spins-1/2. Assuming the rather unphysical but eminently tractable picture that only rocking modes in the plane defined by the internuclear vector and normals to the bisector of the HOH bond are allowed, the motionally averaged zero field dipolar Hamiltonian $\langle\tilde{H}_D(t)\rangle$ is

$$\langle\tilde{H}_D(t)\rangle = \omega_D\ (1 - \eta)[3I_z^2 - I(I+1) + \eta(I_x^2 - I_y^2)] \qquad (4.4)$$

where

$$\eta \equiv \frac{3<\theta^2>}{2} \tag{4.5}$$

To first order in η, the high frequency transitions are shifted by $-\eta\omega_D$ and $-2\eta\omega_D$ from the static value of $3\omega_D/2$. Solving for η and ω_D,

$$\eta \approx .052 \tag{4.6}$$

and

$$\omega_D/2\pi \approx 29.87 \text{ kHz} \tag{4.7}$$

In terms of the molcular parameters,

$$<\theta^2(t)>^{1/2} = .19 = \sim 11^\circ \tag{4.8}$$

and, corrected for the libration,

$$r_{12} = 1.59 \pm .01 \text{ Å} \tag{4.9}$$

in closer agreement with neutron diffraction results.[90]

d. Double Frequency Lines and More Water

The high frequency lines at multiples of the fundamental dipolar frequency conclusive argue for the breakdown of either the zero field or two-spin approximations. Two coupled spins in zero field cannot support the observed energy splitting. It is well-known[51,71,96] that in low applied fields overtone lines at multiples of the fundamental absorption frequency are allowed. Figure 4.3 shows simulated low field spectra of $Ba(ClO_3)_2 \cdot H_2O$ as a function of the strength of the applied Zeeman field. At fields $H_Z \sim H_D$ a rather complicated pattern is observed and for applied fields $\sim 2H_D$ lines appear at roughly twice the Zeeman energy. For larger fields these lines grow progressively weaker. But no double-frequency lines are observed in the range of

Figure 4.3. Low field NMR simulations, showing the transition from zero field spectrum to high field spectrum as a function of the applied field in two-spin system. The assumed spin system is two ^1H nuclei 1.60 Å apart ($\omega_D/2\pi$ = 29.3 kHz). The magnetic field is assumed perpendicular to the magnetization so that precession occurs. a). 2.94 gauss (12.5 kHz). b). 5.87 gauss (25 kHz). c). 11.74 gauss (50 kHz).
d). 23.5 gauss (100 kHz). e). 47.0 gauss (200 kHz). f). 93.9 gauss (400 kHz). In (d-f) the horizontal scale is changing. These simulations show the source and decay of the allowed transitions at twice the Larmor frequency in addition to the transformation of the zero field spectrum into the high field Pake pattern.

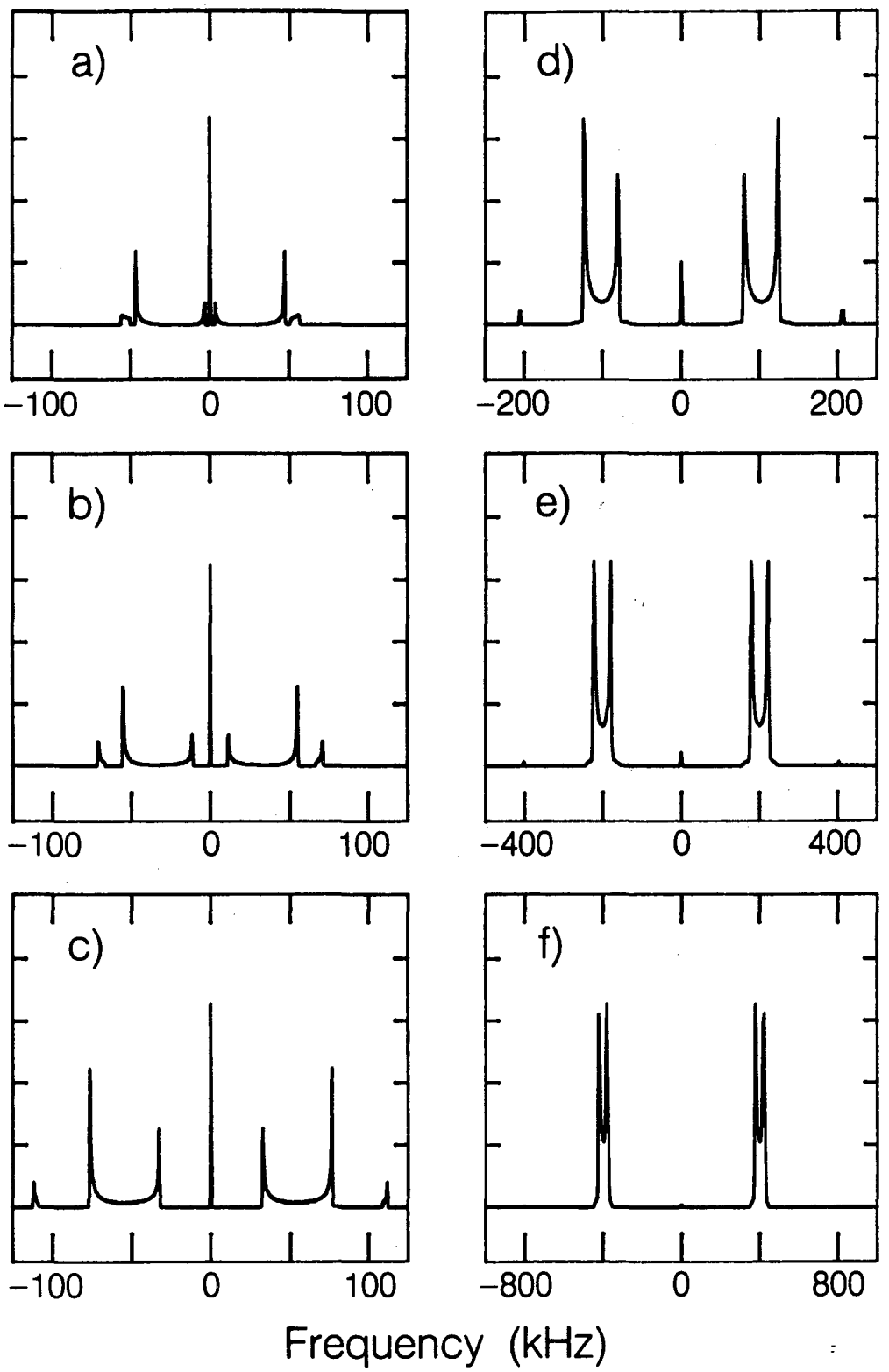
a)
d)
b)
e)
c)
f)
−100
0
100
−200
0
200
−100
0
100
−400
0
400
−100
0
100
−800
0
800
Frequency (kHz)

XBL 857-8934

fields where the dipolar spectrum is still sharp.

In dilution studies of $Ba(ClO_3)_2 \cdot H_2O$ the double frequency lines disappear, which suggest that near-neighbors are involved. Simulations of small numbers of interacting pairs (≤ 3) fail to reproduce these features. For many more than six interacting spin-1/2 nuclei, an exact calculation of the spectrum using the formalism of Section III.B is difficult.

Even allowing for an enlarged nuclear spin system the double frequency lines remain mysterious. For pairs of pairs, lines at this frequency appear at vanishingly small intensities if the prepared and detected operator is I_{zL}. The amplitudes of these lines vary with changes in an as-yet unidentified variable. Figure 4.4 shows two spectra of $Ba(ClO_3)_2 \cdot H_2O$ taken with all routinely set experimental parameters identical and separated in time by two days. In the first spectrum, the amplitude of the high frequency satellite lines is ~5% that of the main lines; in the second, nearly zero. Often, these high frequency lines appear badly phased with respect to the main lines in the spectrum.

All of these observations are consistent with the possible preparation and detection of interpair dipolar order created at some point in the field cycle and detected in high field. Dipolar order between two pairs has been observed in high field studies of gypsum, $CaSO_4 \cdot 2H_2O$.[97] The amount of such order prepared during the field cycle might depend on factors which are not routinely well-regulated, such as the precise rate of demagnetization. Were such a state prepared before the field B_{int} is quenched it would evolve at the observed frequencies. Transported back to high field, this type of dipolar order can be

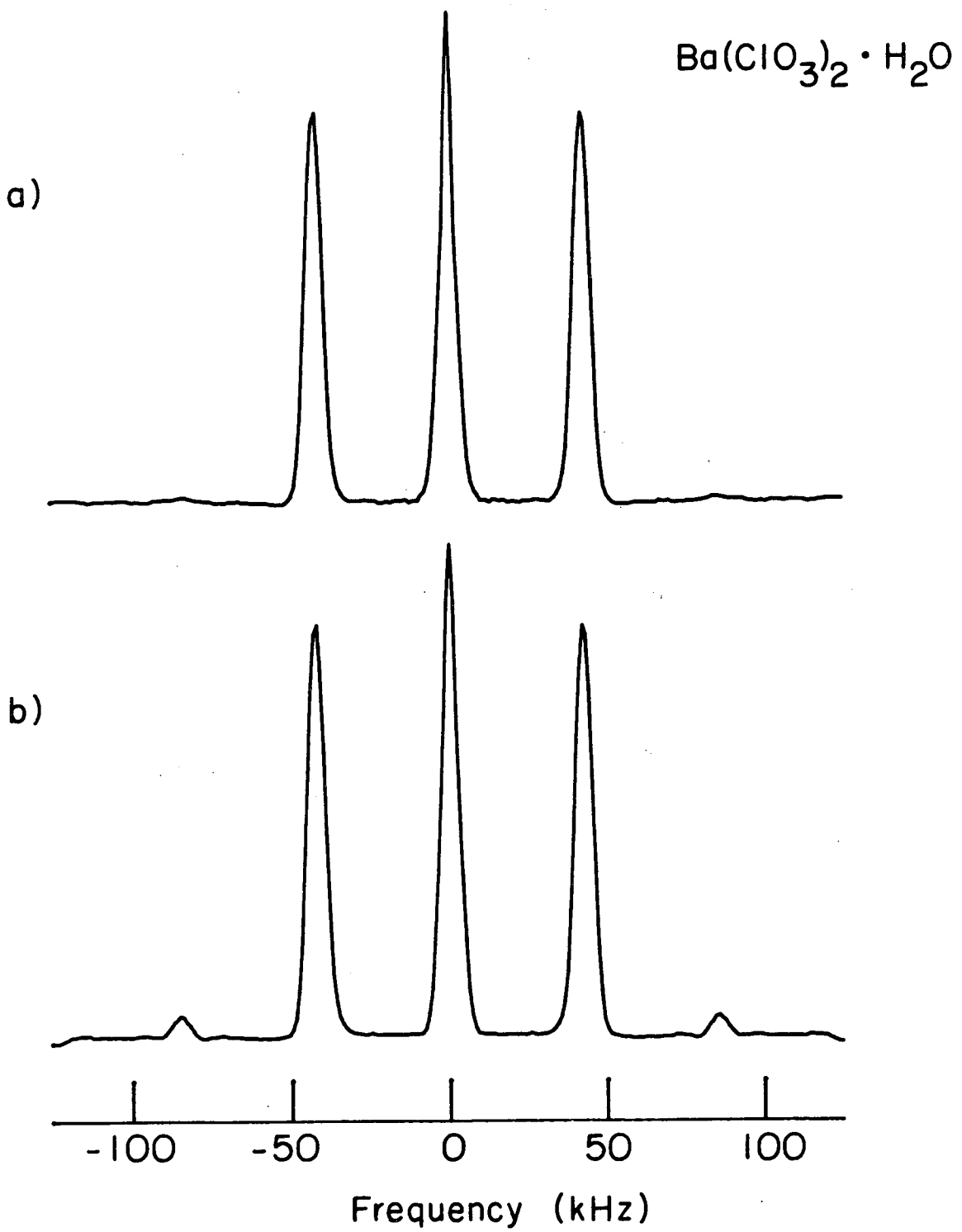

Figure 4.4. ^1H zero field NMR spectra of polycrystalline $Ba(ClO_3)_2 \cdot H_2O$. All experimental parameters which the experimentalist routinely sets were identical. In a) little evidence appears of the double frequency lines. In b), these lines are of relatively large amplitude.

converted into an observable by any pair of pulses and would appear in quadrature with the signals due to the evolution of Zeeman order. This may serve as a warning as to the complexity of the demagnetization process in systems of discrete energy levels and where the spin temperature hypothesis does not hold.

Other two spin systems exhibit spectra similar to that of $Ba(ClO_3)_2 \cdot H_2O$. Two spin systems differ from one another only to the extent that they really are two spin systems and therefore to the extent that the ideal three-line spectrum is broadened and ultimately split by dipolar couplings to other magnetic nuclei. In Figure 4.5, two zero field NMR spectra of other two spin systems are shown. The spectrum of the first ($K_2C_2O_4 \cdot H_2O$) is nearly indistinguishable from that of our model hydrate, $Ba(ClO_3)_2 \cdot H_2O$ and even reproduces the weak double frequency transitions. In other systems ($Li_2SO_4 \cdot H_2O$ and $CaCl_2 \cdot H_2O$, shown in Figure 4.6) the ideal triplet is significantly broadened. Couplings to other high γ nuclei (either the ^7Li or other water molecules in the lattice) contribute to the linewidths. Nonetheless, these weaker interactions are insufficient to produce any radically new features.

2. Beyond Water: the Methyl Group

In search of new and different zero field NMR spectra, Figure 4.7 shows a series of spectra of sodium acetate trihydrate. Each sample was recrystallized from D_2O and the only ^1H nuclei in the sample are found in the methyl groups of the acetate anion. Despite this dilution, the zero field NMR spectrum of the network of $-CH_3$ groups, whose spectrum is shown at the top of the figure, is basically unstructured. Couplings between methyl groups are strong and the

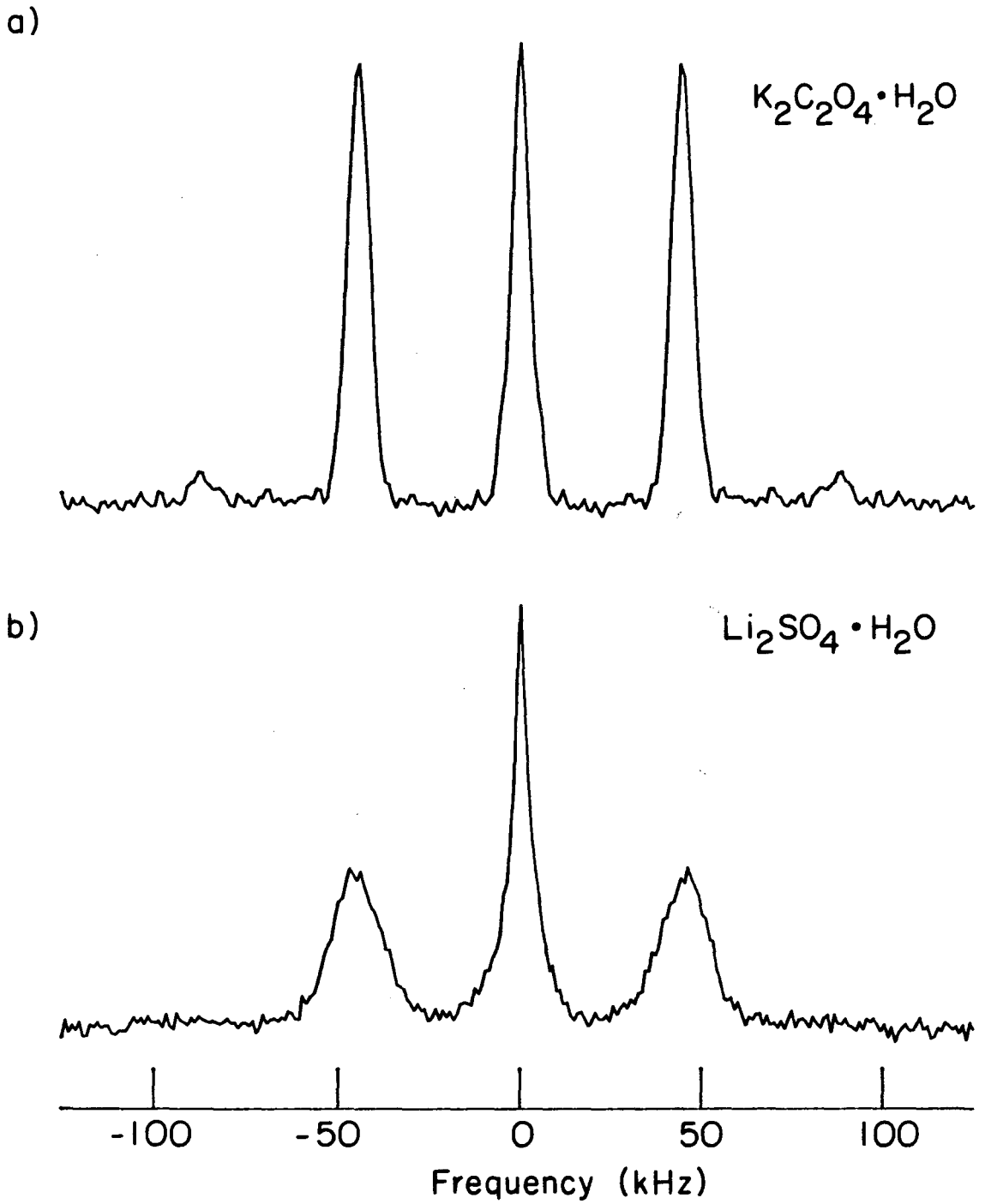

Figure 4.5. ^1H zero field NMR spectra of polycrystalline a). $K_2C_2O_4 \cdot H_2O$ and b). $Li_2SO_4 \cdot H_2O$. In both the three-line spectrum is observed. In a). the spectrum is stikingly similar to that of $Ba(ClO_3)_2 \cdot H_2O$; even the double frequency lines are reproduced. In b). the lines are significantly broadened by nearby H_2O sites and the ^7Li spectrum.

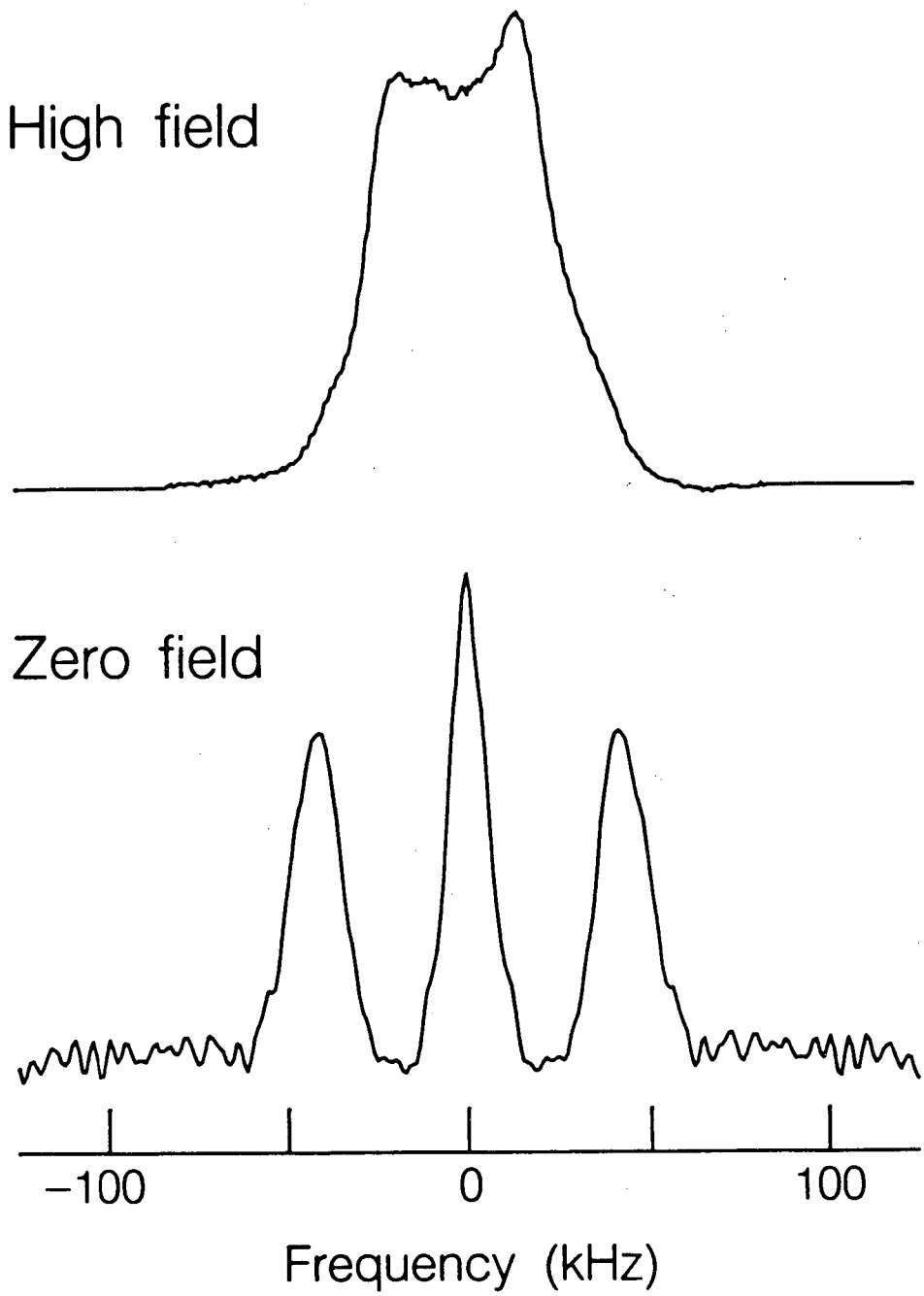

Figure 4.6. High field and zero field ^1H NMR spectra of polycrystalline $CaCl_2 \cdot 2H_2O$, acquired after a two-pulse solid echo sequence. The high field Pake pattern is significantly broadened and the singularities ill-defined. The zero field lines are broad yet well-resolved.

Figure 4.7. Zero field NMR spectra of polycrystalline $-CH_3$ group in sodium acetate ($NaOAc \cdot 3D_2O$) as a function of concentration of the $-CH_3$ groups. At top, the spectrum of the system with 100% $-CH_3$ groups. Middle and bottom, $-CH_3$ groups have been replaced by $-CD_3$ groups. At low concentrations the spectrum shows the features characteristic of isolated methyl groups. Assuming rapid rotation about the C_3 axis the splitting observed in the spectrum at bottom corresponds to $\langle r^3 \rangle^{-1/3} = 1.89$ Å.

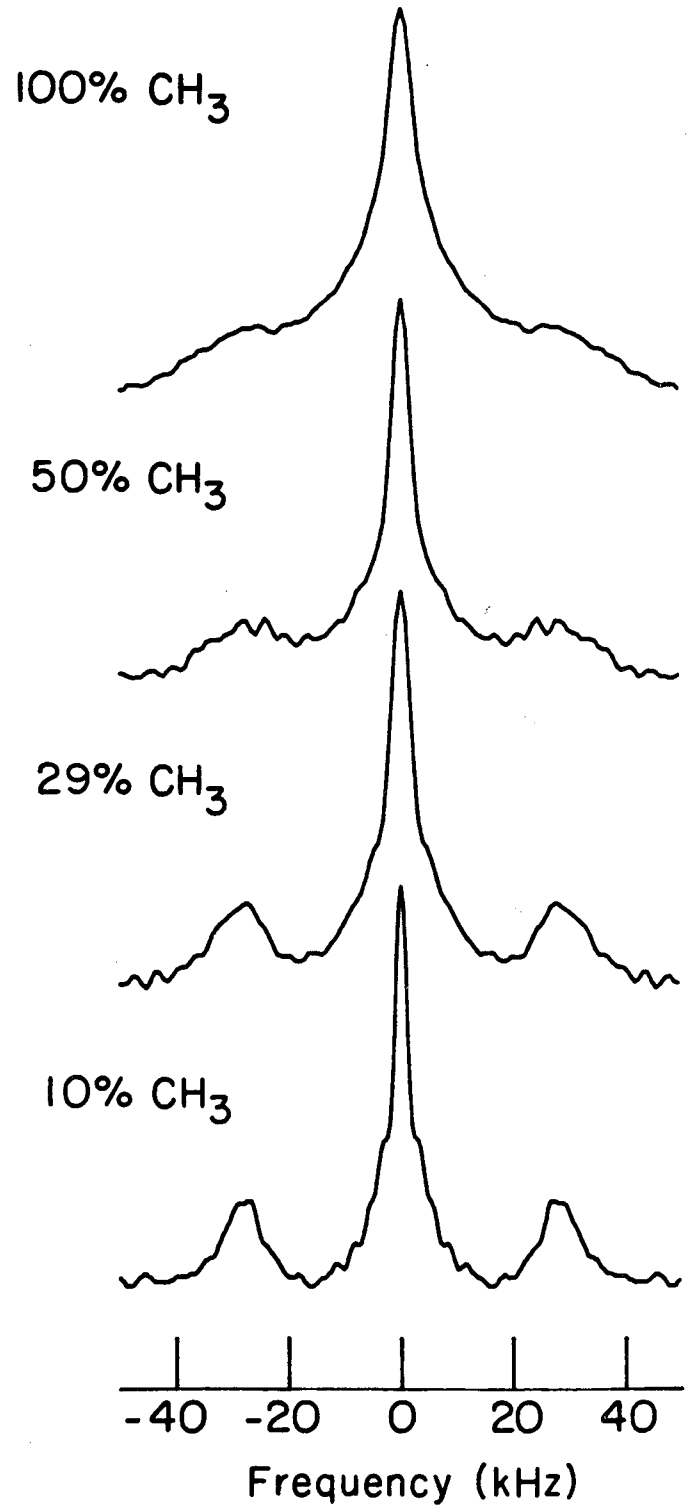

XBL 8312-4681

system closely resembles a dense lattice of coupled spins (discussed in more detail below) rather than a collection of isolated groupings of three spins. Replacing a large percentage of the remaining ^1H's with ^2D previously was shown to greatly increase the resolution in zero field NMR. To avoid complications which might arise from mixtures of isomers (and because of the extremely small number of three spin systems found in a statistical distribution at low concentrations), three samples were recrystallized from solution as mixtures of $NaOAc \cdot 3D_2O$ containing only perdeuterated $-CD_3$ and perprotonated $-CH_3$ groups. At low concentrations (~10% or less protons) the spectrum of the isolated methyl groups appears. It, like the spectrum of the dipolar coupled pair, consists of a triplet of lines. Unlike the two spin systems, most of the integrated intensity appears at zero frequency.

Using the formalism of Chapter III and the results of Appendix B it is simple to numerically calculate the spectrum of the isolated $-CH_3$ group. In this section, I attempt less formalism if no less rigor. The simulation of the spectrum in the fast motion limit consists of two nearly distinct problems: first, the calculation of the eigenstates and energies of the zero field Hamiltonian, and second, a calculation of the relative intensities of the observed lines. First, the Hamiltonian:

At high temperature the $-CH_3$ group undergoes rapid rotation about its C_3 axis and the zero field molecular frame will be referenced to this symmetry axis. (None of the conclusions which follow depend in any way on any assumptions about that motion except that it is rapid and that, over a time period comparable to the inverse of the dipolar

couplings, the methyl group rotational potential well is at least three-fold symmetric.) The Hamiltonian can be written

$$H_D = \omega_D \sum_{j \neq k} [I_j \cdot I_k - 3(I_j \cdot \hat{r}_{jk})(I_k \cdot \hat{r}_{jk})] \tag{4.10}$$

where all the r_{jk} are assumed equal in length. H_D can be expanded and ω_D defined as in Chapter I. Because of the assumption of rapid motion about the molecular z axis, the averaged Hamiltonian $\langle \tilde{H}_D(t) \rangle$ is most readily calculated in an interaction frame where the spatial variables are changing with time. This is in contrast to the more familiar high field picture where the spin variables are accelerated with respect to the spatial and laboratory frames. (A somewhat more formal treatment is given in Appendix B.) In this accelerated frame of reference, and as long as the methyl group motion is rapid, the Hamiltonian observed in an NMR experiment is Equation (4.10) averaged over many periods of the rotation. This corresponds to truncating all terms in the Hamiltonian which do not commute with rotations about the axis of rotation, and if the spin Hamiltonian is expanded with its z-axis chosen as above

$$\langle \tilde{H}_D \rangle_t = H_{eff} = \omega_D [I_{1z}I_{2z} + I_{2z}I_{3z} + I_{3z}I_{1z} - \frac{1}{4}(I_{1+}I_{2-} + I_{1-}I_{2+} + I_{2+}I_{3-} + I_{2-}I_{3+} + I_{3+}I_{1-} + I_{3-}I_{1+})] \tag{4.11}$$

The eigenstates of H_{eff} are

$$|\psi_1\rangle = |\alpha\alpha\alpha\rangle = \overline{|\psi_4\rangle} \qquad |\psi_2\rangle = \frac{1}{\sqrt{3}}[|\alpha\alpha\beta\rangle + |\alpha\beta\alpha\rangle + |\beta\alpha\alpha\rangle] = \overline{|\psi_3\rangle}$$

$$|\psi_5\rangle = \frac{1}{\sqrt{3}}[|\alpha\alpha\beta\rangle + \exp(i\pi/3)|\alpha\beta\alpha\rangle + \exp(2i\pi/3)|\beta\alpha\alpha\rangle] = \overline{|\psi_6\rangle} \tag{4.12}$$

and

$$|\psi_7\rangle = |\psi_5\rangle^* \qquad |\psi_8\rangle = |\psi_6\rangle^* \tag{4.13}$$

The bar over an eigenstate is a symbol I will occasionally use to indicate the inversion of all spin operators (i.e. $|\alpha\rangle$ is changed to $|\beta\rangle$ and vice versa). No particular significance can be attributed to any specific choice of eigenstates, as any linear combinations of degenerate levels are also eigenstates. Because of the rapid motion about the C_3 axis, molecular quantum numbers J (the total angular momentum) and $|M|$ (the projection of J on the quantization axis) can be defined and are good quantum numbers. Eigenstates $|\psi_1\rangle$-$|\psi_4\rangle$ comprise a quartet with J=3/2 which is functionally equivalent to a pseudospin-3/2 particle. Eigenstates $|\psi_5\rangle$-$|\psi_8\rangle$ correspond to a pair of J = 1/2 two-level systems and can be treated as two isolated pseudo spin-1/2 particles. Where $E_n \equiv \langle\psi_n|H_{eff}|\psi_n\rangle$,

$$E_1 = -E_2 = -E_3 = E_4 = \frac{3}{4}\omega_D \tag{4.14}$$

$$E_5 = E_6 = E_7 = E_8 = 0 \tag{4.15}$$

Formally, the normalized signal averaged over a powder distribution function is given by

$$G(t_1) = \frac{\sum_{j=x,y,z} Tr[I_j I_j(t_1)]}{\sum_{j=x,y,z} Tr[I_j I_j]} \tag{4.16}$$

The operators I_j are block-diagonal in the expectation values of J. The sums over the traces can be separated into traces over each of the pseudo-particles, and

$$G(t_1) = \frac{\sum_j \{2\mathrm{Tr}\,[I_{j1/2}I_{j1/2}] + \mathrm{Tr}\,[I_{j3/2}I_{j3/2}(t_1)]\}}{\sum_j \{2\mathrm{Tr}\,[I_{j1/2}I_{j1/2}] + \mathrm{Tr}\,[I_{j3/2}I_{j3/2}]\}} \tag{4.17}$$

The zero field Hamiltonians H_{loc} vanish for a spin-1/2 particle and magnetization associated with these two pseudo particles is nonevolving. Only $I_{x3/2}$ and $I_{y3/2}$ contain off-diagonal matrix elements between nondegenerate states. All other operators are non-evolving. For the spin-1/2 submatrices, $\mathrm{Tr}\,[I_{j1/2}I_{j1/2}] = 1/2$ and $\mathrm{Tr}\,[I_{z3/2}I_{z3/2}] = 5$. For each of $I_{x3/2}$ and $I_{y3/2}$,

$$\mathrm{Tr}\,[I_{j3/2}I_{j3/2}(t)] = 2 + 3\cos(\tfrac{3}{2}\,\omega_D t_1) \tag{4.18}$$

Substituting back into Equation (4.17),

$$G(t_1) = \frac{3 + 4 + 6\cos(\frac{3}{2}\,\omega_D t_1) + 5}{3 + 4 + 6 + 5}$$

$$= \frac{1}{3}\,[2 + \cos(\tfrac{3}{2}\,\omega_D t_1)] \tag{4.19}$$

In the frequency domain this produces a triplet of relative intensities 1:4:1 and is closely reproduced by the spectrum of the most dilute system shown at the bottom of Figure 4.7. The observed dipole-dipole coupling corresponds to a ^1H-^1H distance of 1.89Å.

B. Heteronuclear Spin Systems

The basic differences between hetero- and homonuclear spin systems have been covered in Chapter III. In this section, I present simulations of spectra for larger heteronuclear spin networks and

comment on the possible use of field-cycling NMR as a means for inducing polarization transfer from abundant, high γ spins to lower sensitivity spin-1/2 nuclei. Some aspects of this problem were covered in detail in Section C of Chapter III. These are really the same problem because the magnetization function, Tr $[S_z\rho(t_1)]$, and the spectrum, $f(\omega)$, are a Fourier-conjugate pair.

In Section III.C I showed that in an I-S pair t_1 might be chosen so that the final transfer of polarization from I to S spin is more efficient than by any other technique. The final value of the S spin magnetization is much larger than might be observed if the two spins were brought into equilibrium in high field via standard techniques like cross-polarization.[98,99] The complete undamped time evolution of the magnetization function for the I-S pair is shown in Figure 4.8a. This technique is not, unfortunately, of general utility. As the number of interacting spins becomes larger (Figures 4.8b,c,d), magnetization tends to wander rather more chaotically from site to site. Maxima in the function $S_{zL}(t_1)$ are not as well defined nor as dramatic as in larger spin systems. Where small numbers of spins are not well-isolated, couplings to other spins rapidly damp out the oscillations and the theoretical maxima may not be achieved. In the experiments illustrated in Figure 3.4 the maximum observed transfer of order to the ^{13}C nuclei in ^{13}C-calcium formate was ~40% of the initial ^{1}H order. This is only about half the maximum predicted in Figure 4.8a. Figures 4.9 and 4.10 illustrate the zero field spectra predicted for the other common spin groupings occurring in organic compounds, $^{13}CH_2$ and a rapidly spinning $^{13}CH_3$. The spectra observed for $S_z(0) = 0$ are in fact the Fourier transforms of the magnetization functions

Figure 4.8. Simulated polarization transfer functions $S_z(t_1)$ for I_nS spin systems for I = ^1H and S = ^{13}C. In each simulation, the S spins are assumed initially depolarized. The y-axis is in units of the equilibrium ^1H magnetization. a.)- c). Common groupings of spins in organic compounds. Realistic bond lengths (1.095 Å) and angles (109.5°) are used.

a). I-S dipole-dipole coupled pair. At its peak, S_z = .75. An equilibrium distribution would correspond to $I_z = S_z$ = .5.

b). $^{13}CH_2$ group. Peaks are well-defined but the maximum value (~.55) is somewhat less than equilibrium (.67).

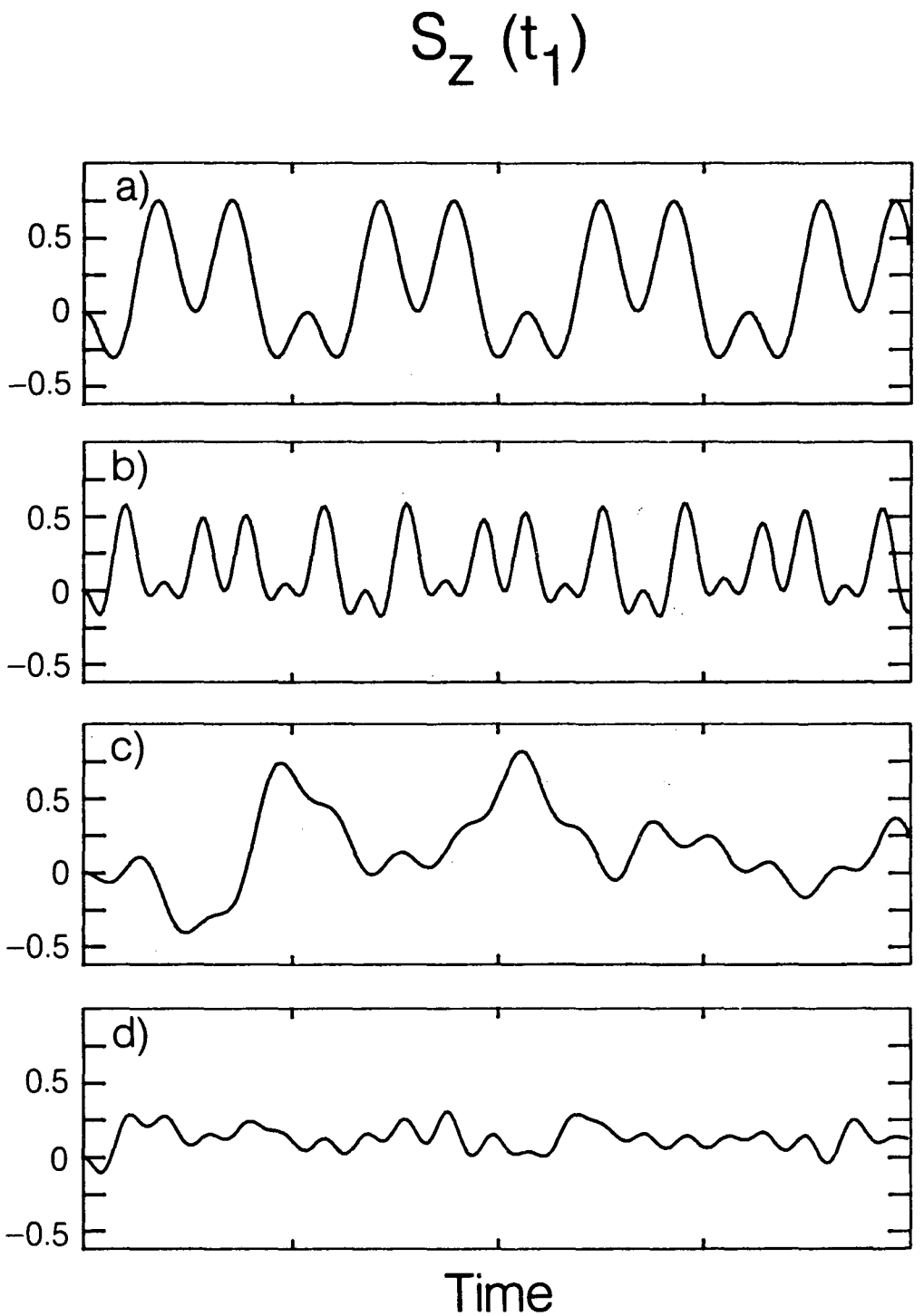

XBL 857-8929

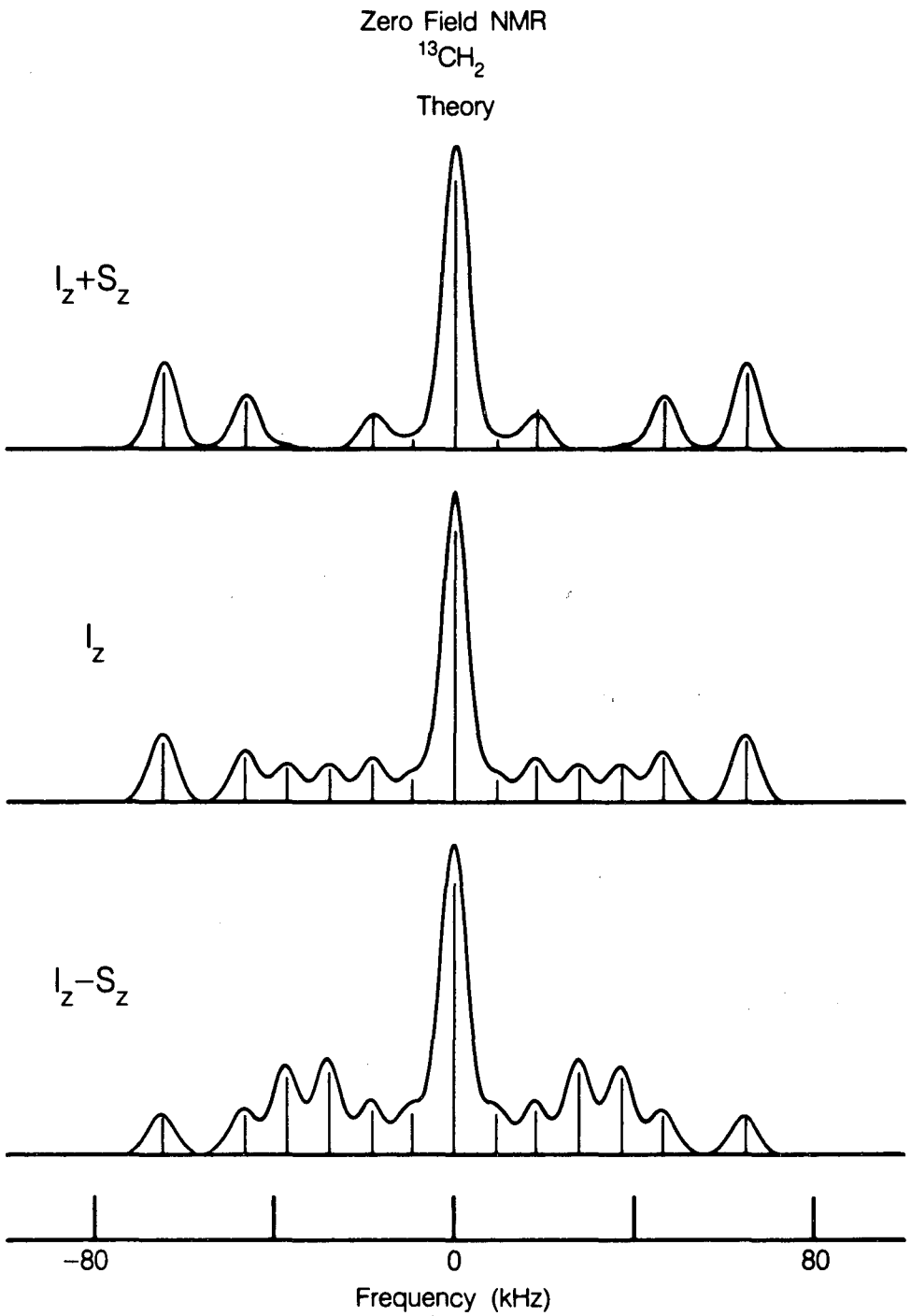

Figure 4.9. Simulated zero field spectra of $^{13}CH_2$ groups as a function of the high field initial condition. Tetrahedral bond angles and r_{C-H} = 1.095 Å assumed. The stick spectra are shown in the insets; superposed, spectrum convoluted with a 6 kHz Lorentzian line. For the initial condition where the magnetization is shared equally between sites, several of the allowed transitions have nearly vanishing intensity.

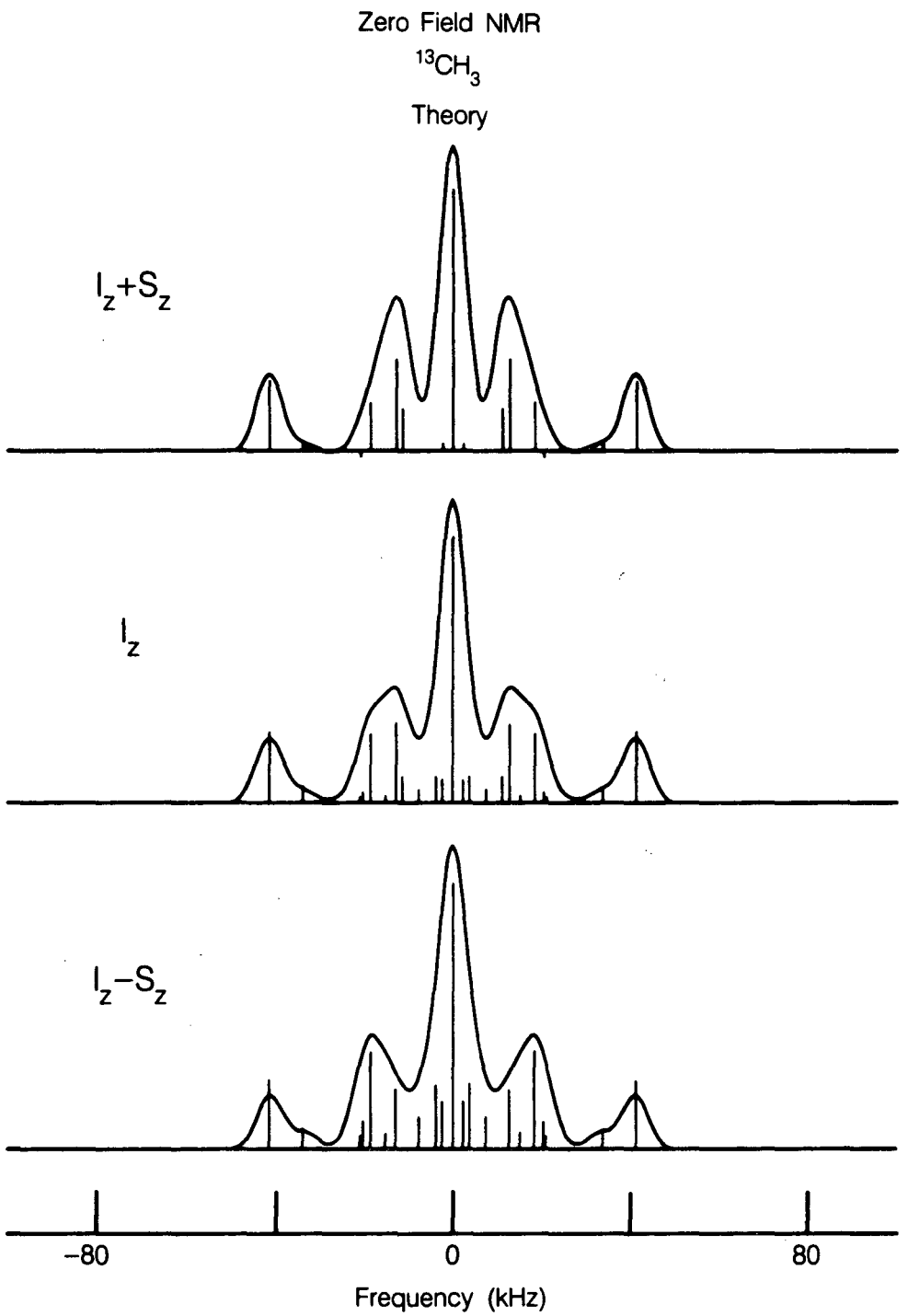

Figure 4.10. Simulated zero field spectra of rapidly spinning $^{13}CH_3$ group as a function of high field initial condition. Tetrahedral bond angles and r_{C-H} = 1.095 Å assumed. The stick spectra are shown in the insets; superposed, spectrum convoluted with a 6 kHz Lorentzian line.

plotted in Figure 4.8b and 4.8c and are calculated with the simulation program HETZF.FOR, which is similar to DBZINT.FOR but also accepts heteronuclear spins.

A more general approach to the problem of transferring order from one spin species to a second in low field is to use the level-crossings described in Chapter II; or, in systems of spin-1/2 nuclei, adiabatic demagnetization. In a coupled spin system demagnetized to zero field, polarization stored in the I nuclei is transferred to the S nuclei consistent with equilibrium in the the untruncated Hamiltonian H_D. As the remagnetization reestablishes Zeeman order, the magnetization stored in the S spins while in zero field remains there.[11,24]

C. More Complicated Spin Systems

As the number of strongly coupled spins increases, the number of discrete transition frequencies present in the spectrum multiplies rapidly. A treatment based on considerations of symmetry will be given in Chapter VII. For the present, these comments aim to establish a framework for the understanding of subsequent zero field NMR spectra presented in this chapter.

Depending upon which Hamiltonians dominate the spectrum, predictions about the numbers of lines expected from systems of coupled spin-1/2 nuclei vary greatly. In high field and if there are no couplings between spins, then N spins produce N transition frequencies, and each line is characteristic of the chemical shift σ at a specific site. This situation is common in high field, high resolution dilute spin spectroscopy (often ^{13}C). In the weak coupling limit ($\Delta\sigma \gg J$)

the energy levels of isolated spin-1/2 nuclei are split by the secular component of the J coupling (Equation (1.71)) and each chemical shift line breaks up into a number of lines roughly equal to the number of near neighbors. There are certainly no more than N such neighbors and often far fewer. This is commonly the situation for ^1H high resolution NMR in liquids. A gross overestimate of the number of allowed lines is N^2. More often, the number of spectral lines increases only linearly with N.

In strongly coupled spin systems, the eigenstates of the Hamiltonian can no longer be identified as belonging to a single spin but rather are characteristic of the system of N spins in concert. Excitation under an rf pulse corresponds to the flipping of a single spin and each eigenstate is excited simultaneously. In high field and the rotating frame where I_z is a good quantum number a single pulse can only excite coherences where $\Delta m = 1$. This dipole selection rule for Δm can be manipulated so that different values of $\Delta m = n$ are excited.[100,101] Fewer lines are observed in these higher order spectra and these lines are presumably more readily interpreted. In strongly coupled systems in high field,[102]

$$W = \frac{(2N)!}{(N+n)!(N-n)!} \qquad \text{for } n \neq 0 \qquad (4.20)$$

where W is an upper bound to the number of allowed lines per order.

As described in Section 4 of Chapter III, the zero field spectrum acquired by the sequence of Figure 3.1 is also the product of dipolar selection rules (although the alteration of these selection rules is one of the topics covered in Chapter VI). In the absence of uniaxial molecular motion (as in the CH_3 group above) where zero field molecular

frame selection rules exist, or other unusual circumstances, all energy levels are coupled to all others by the three angular momentum operators. The number of eigenstates in an N spin-1/2 system is 2^N; therefore, the maximum number of lines which might be expected to be observed is

$$W = 2^N (2^N - 1) \tag{4.21}$$

As was shown by explicit calculation for I = 1 and will be generalized in Chapter VI, in a powder sample the only observables are proportional to those operators which appear in the prepared density operator $\rho(0)$. For $\rho(0) = I_{zL}$, only a single oscillating component of the magnetization is detected and there is no distinction between positive and negative frequencies. To facilitate comparison to high field spectra, we have chosen in dipolar coupled spin systems to treat the real data set $G(t_1)$ as if it were a complex function and a Fourier transformation yields a symmetrized spectrum $f(\omega) = f(-\omega)$. Only half the lines enumerated in Equation (4.21) contain independent information.

There is one coupling constant for each pair of nuclei in the sum of Equation (1.49), and only N(N-1)/2 couplings provide all available structural information. Even for small spin systems, the geometrical problem is grossly overdetermined as there are far more lines than couplings. If individual lines are not well-resolved because too many lines appear in the spectrum, this may prove to be a crippling difficulty which renders any analysis difficult or impossible. The technique of multiple quantum NMR is designed specifically to overcome this difficulty.[103]

Equation (4.21) overcounts the actual number of lines which appear in the spectrum if there are symmetries in the Hamiltonian. A more detailed treatment is given in Chapter VII. One symmetry operation in particular plays a sufficiently important role to be mentioned here. Time reversal symmetry[104,105] has a profound effect on the spectra of systems where the total spin angular momentum is half-integral. Time reversal symmetry guarantees that for N odd, all eigenstates are at least doubly degenerate. W is really equal to the number of coupled pairs of energy levels (rather than eigenstates). For N odd Equation (4.21) overcounts the number of allowed lines by a factor of four. (An additional line appears at zero frequency; as in half-integer quadrupolar nuclei, this corresponds to magnetization shared between degenerate pairs of eigenstates.) For strongly coupled spin systems in zero applied field,

$$\begin{aligned} W &= 2^N(2^N - 1) && \text{N even} \\ W &= 2^{N-1}(2^{N-1} - 1) + 1 && \text{N odd} \end{aligned} \qquad (4.22)$$

In any case, for $N \geq 4$ the number of allowed transitions becomes large and lines corresponding to individual transitions are rare. Dipolar couplings to distant spins (for two ^1H nuclei 10Å apart the dipolar coupling constant is still ~ 100Hz) may fail to split lines but still contribute significantly to the linewidths. (The near-neighbors in $Ba(ClO_3)_2 \cdot H_2O$ are > 5 Å away). Given a large number of inherently broad lines it is rare that any will be well resolved. Geometric information in larger spins networks will rarely be derived by solving for observed line frequencies and extracting the dipole-dipole couplings. Instead, this information is most conveniently derived by

computer simulation.

1. Structure Determination: N = 4

In this section, two examples of spectra of isolated groupings of four coupled ^1H nuclei will be shown. Distances within a "spin system" are, for the most part, short compared to the distances between "spin systems." The evolution in zero field is determined primarily by the near-range couplings, and if there are few enough of these couplings sufficient structure might be observed in the spectrum to characterize the configuration and geometry of these isolated groups.

Figure 4.11 shows the zero field powder NMR spectrum of 1,2,3,4-tetrachloronaphthalene bis(hexachlorocyclopentadiene) adduct. The high field spectrum was shown in Figure 2.1. To our knowledge, no structure determination has been performed on this compound. The geometric question of interest is the configuration of the ^1H nuclei situated about the central ring. These course details are readily modeled. Figure 4.12 shows spectra predicted to arise from six possible conformations. Only one of the predicted zero field spectra bears a close resemblance to the observed spectrum.

A sketch of the molecular structure of di(μ-hydrido) decacarbonyl triosmium ($(\mu\text{-H})_2Os_3(CO)_{10}$) is shown in Figure 4.13a. $(\mu\text{-H})_2Os_3(CO)_{10}$ is a metal carbonyl cluster complex whose crystal structure has been studied both by single crystal neutron and x-ray diffraction.[106] Two molecules share one unit cell whose volume is ~800 $Å^3$. The carbonyl groups contain only a negligible number of magnetic nuclei; neither are the heavy metal nuclei likely to complicate the observed spectrum. In zero field the more abundant magnetic isotope, ^{189}Os (I = 3/2), evolves independently of the spin-1/2 nuclei due to its large quadrupole

Figure 4.11. Top: the molecule 1,2,3,4-tetrachloronaphthalene bis(hexachlorocyclopentadiene) adduct. The configuration of the four ^1H atoms about the central ring is unknown. All other ring positions are chlorinated. The high field spectrum of this compound is shown in Figure 2.1.
Bottom: Zero field NMR spectrum. The sharp peak at zero frequency is truncated for purposes of display. The evolved zero field magnetization is sampled at 5 μs intervals giving an effective zero field bandwidth of ±100 kHz. Only half that spectral width is shown. The magnetization is sampled once every minute. Twelve 256-point zero field FID's were summed and Fourier transformed to yield this spectrum.

Figure 4.12. Simulated zero field spectra for six possible configurations of the ^1H nuclei about the central ring in the molecule 1,2,3,4-tetrachloronaphthalene bis(hexachlorocyclopentadiene) adduct.For clarity, only the configuration of the central ring is shown, to the left of the associated spectrum. For each configuration, the zero field spectrum is calculated, broadened to match the experimentally observed linewidths, and plotted. The simulation at bottom right closely resembles the observed spectrum (Figure 4.11). A C_2 axis of symmetry which interconverts the two innermost (1 and 1') and two outermost (2 and 2') sites is assumed. Because of the assumed symmetry, only four distances characterize the simulation; $r_{11'}$ = 2.83 Å; r_{12} = 2.22 Å, $r_{12'}$ = 4.34 Å, and $r_{22'}$ = 5.01 Å.

1,2,3,4 Tetrachloronaphthalene-
bis (hexachlorocyclopentadiene) adduct

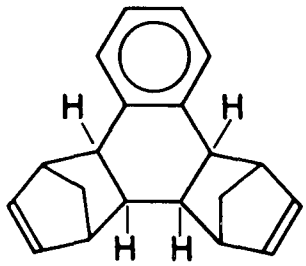

Zero Field NMR
Powder Spectrum

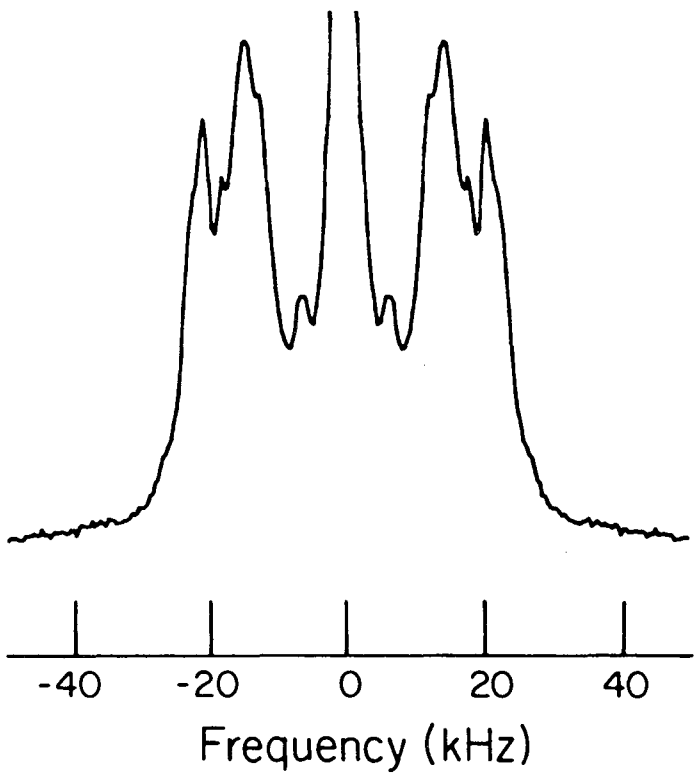

Figure 4.11

XBL 853-10397

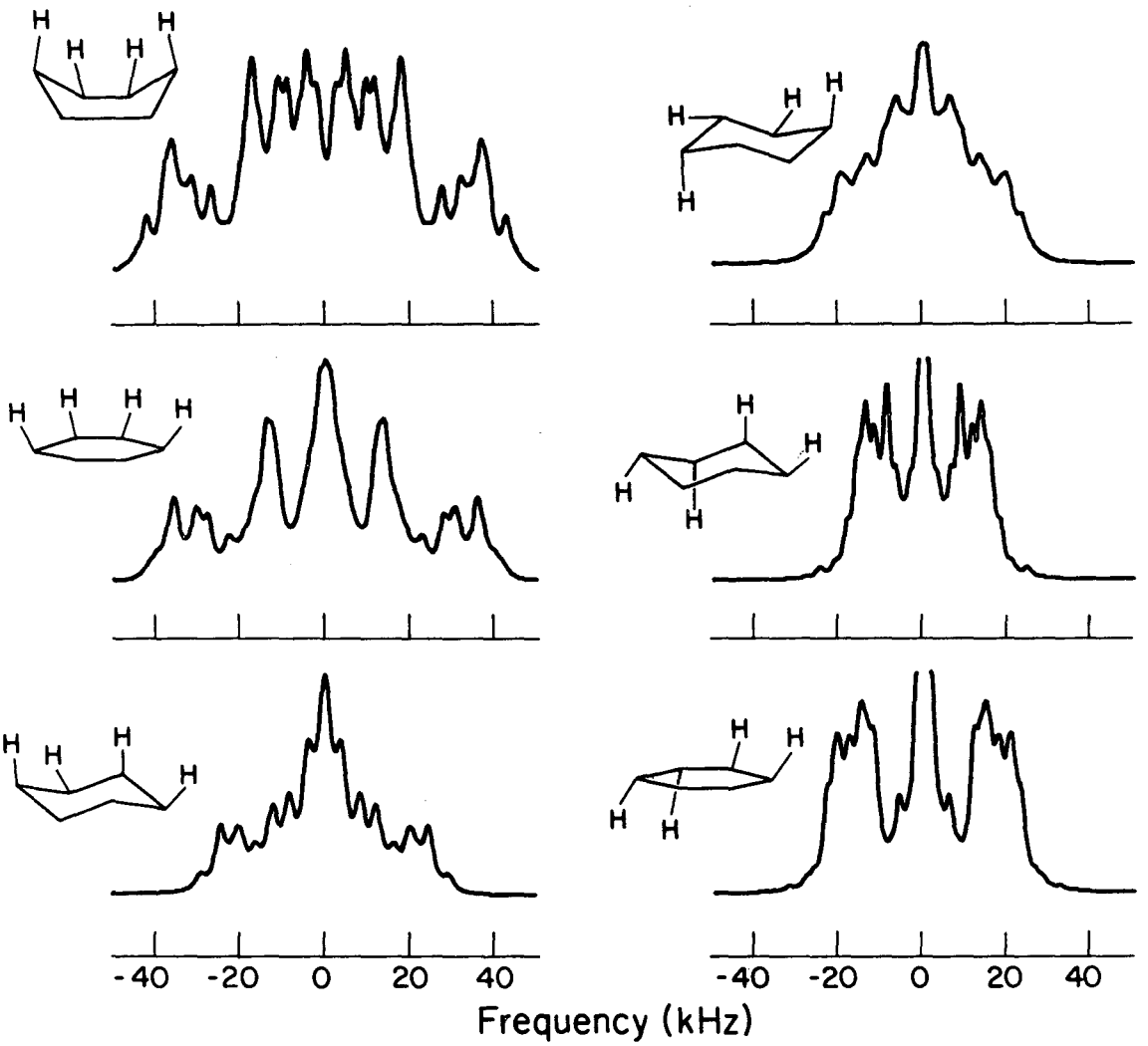

XBL 853-10396A

Figure 4.12

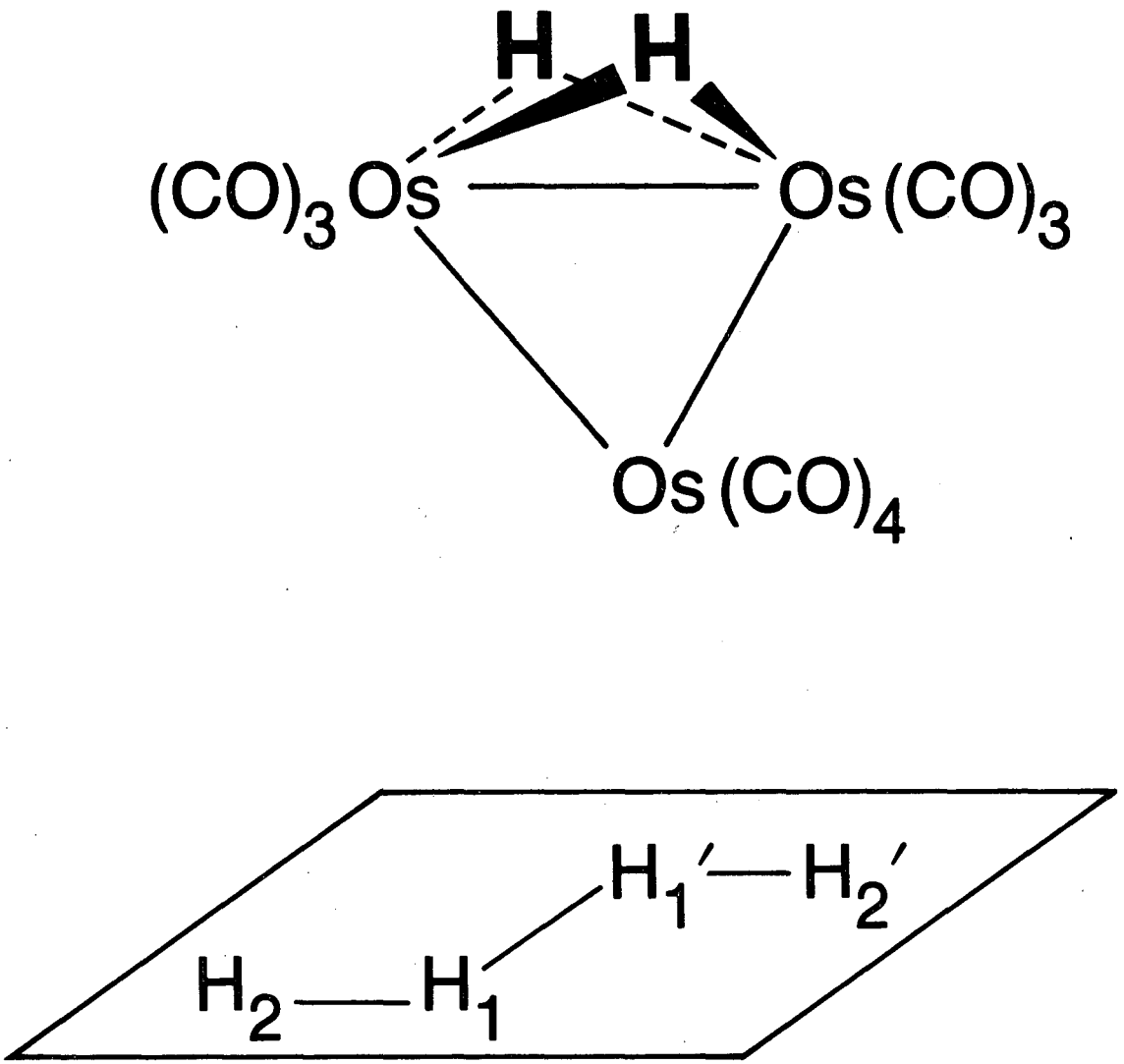

XBL 855-9832

Figure 4.13. Structure of $(\mu\text{-H})_2Os_3(CO)_{10}$ in the solid state. Top: Approximate molecular geometry. Bottom: Simplified representations showing only the arrangement of the ^1H atoms within a single unit cell. Positions 1 and 1′ and 2 and 2′ are related by an inversion center.

moment. The spin 1/2 isotope, ^{187}Os, has a low magnetogyric ratio and appears at low natural abundance.

The four ^{1}H nuclei in one unit cell are relatively isolated from all other magnetic spins. The approximate arrangement of the four ^{1}H nuclei is shown if Figure 4.13b. The spin lattice relaxation time T_1 for the ^{1}H nuclei is long (≈ 1 minute) and there appears to be little motion which might complicate the interpretation of the spectrum. An early powder NMR study of the high field spectrum of this compound (shown in Figure 4.14) which assumed only two protons interacted strongly was unable to reproduce the observed spectrum.[107] Thus $(\mu\text{-H})_2Os_3(CO)_{10}$ makes a good test case for the applicability of zero field NMR to the location of ^{1}H nuclei in moderately large spin systems.

Figure 4.15 (top) shows the experimentally obtained zero field NMR spectrum of $(\mu\text{-H})_2Os_3(CO)_{10}$. The zero field spectrum proves unequivocally that the two-spin interpretation is incorrect. In comparison with the H_2O spectra of section A, far too many features are resolved to allow for the possibility that the coupling between only two spins dominates the spectrum. To reasonably approximate the spectrum requires that the spin network be treated as (minimally) four interacting spins; i.e. considering both sets of ^{1}H pairs in the unit cell.

Figure 4.15 (bottom) shows a simulated zero field spectrum based on the neutron diffraction study done at low (110 K) temperature. While some similarities are evident, the match between the observed zero field NMR powder spectrum and that predicted by the coordinates of the diffraction study is not particularly good. Attempting to improve

Figure 4.14. High field NMR spectra of polycrystalline $(\mu\text{-H})_2Os_3(CO)_{10}$. Upper: Experimental spectrum obtained by solid echo sequence, with polarizing period between successive shots of 2 minutes. Center and below: computer simulations of the high field spectrum ignoring chemical shifts based on a "best fit" to the room temperature zero field NMR results ($r_{11'}$ = 2.81 Å, r_{12} = 2.38 Å, and $r_{12'}$ = 5.17 Å) and the low temperature neutron diffraction data ($r_{11'}$ = 2.94 Å, r_{12} = 2.38 Å, and $r_{12'}$ = 5.28 Å). The simulations are convoluted with a Gaussian lineshape function to account for the finite number of orientations sampled in the simulations.

Figure 4.15. Zero field NMR spectrum of polycrystalline $(\mu\text{-H})_2Os_3(CO)_{10}$. Upper: Experimental spectrum. Eleven zero field FID's 256 points long were summed and Fourier transformed. The zero field signal was sampled at 5 μs intervals; only half the full bandwidth is shown. Center and below: computer simulations of the zero field spectrum based on the distances given in Figure 4.14. The stick spectra of the simulations are broadened with a Lorentzian lineshape function of ~2.8 kHz to more closely match the observed features. A sharp line at zero frequency has been truncated.

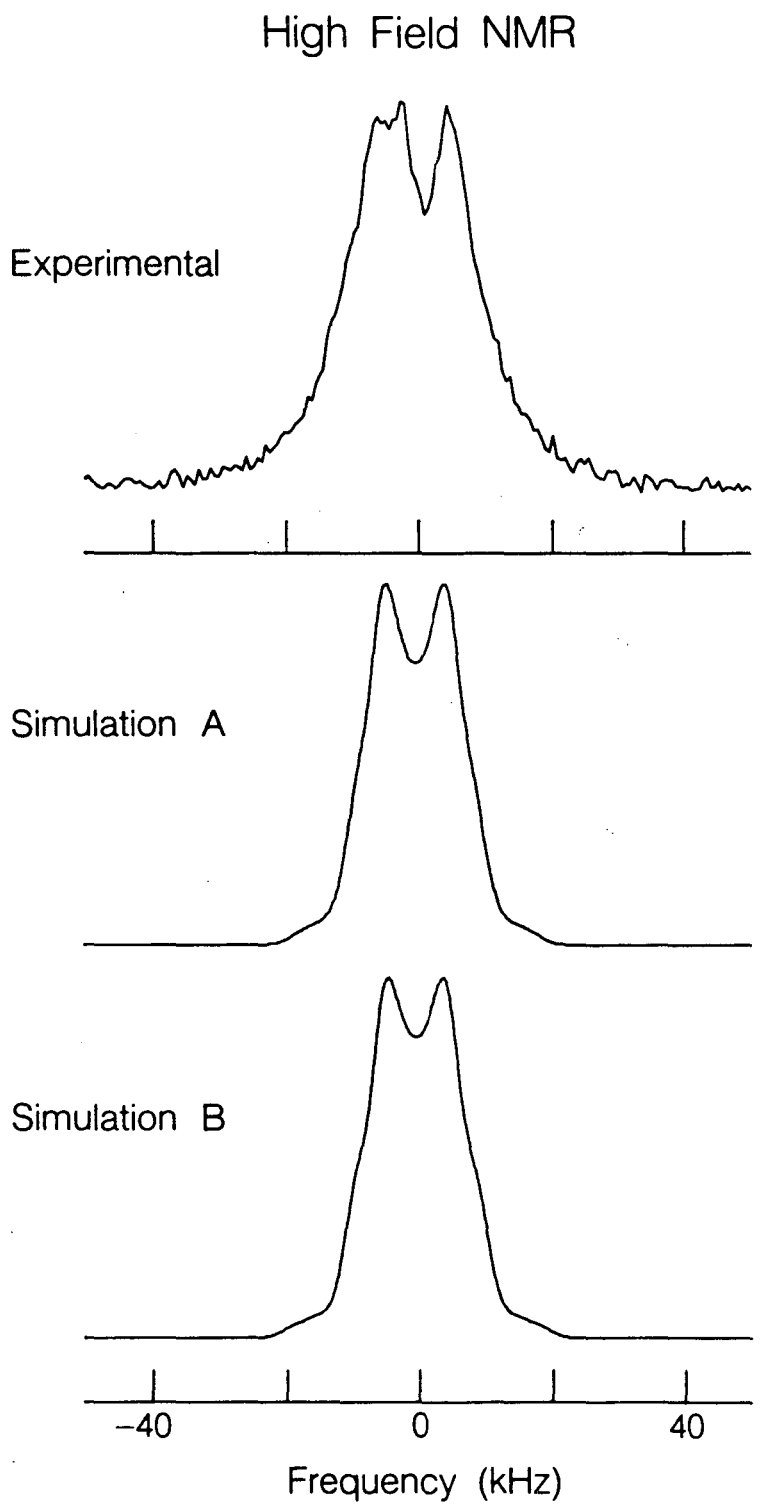

Figure 4.14 XBL 853-9787

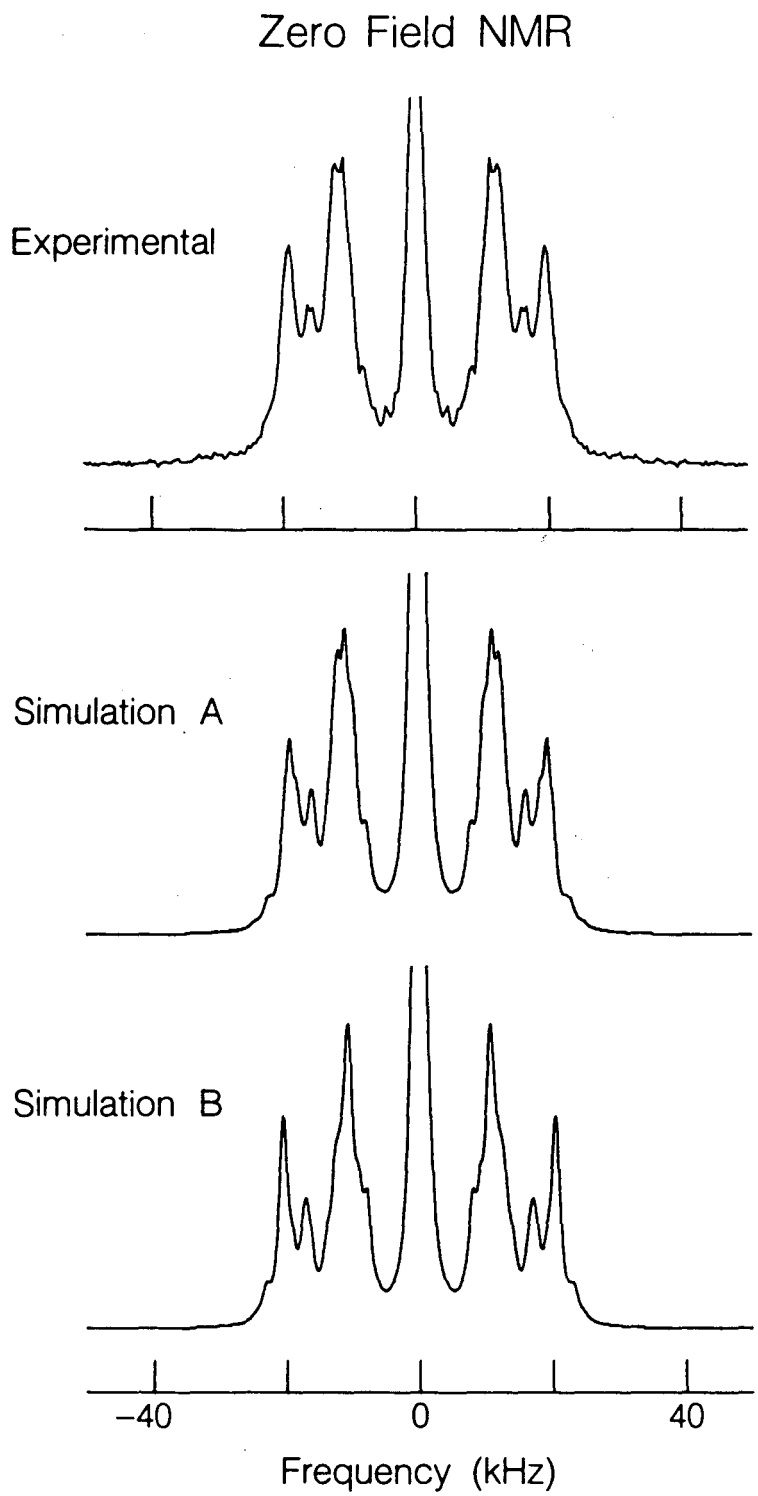

Figure 4.15 XBL 853-9788

the fit, an iterative brute force three step process (simulation, plot, and comparison to the experimental results by the graduate student eyeball) was developed. Assuming that the equilibrium positions of the ^1H nuclei are consistent with the known inversion symmetry of the unit cell, all four ^1H nuclei lie in one plane, and only three distinct distances ($r_{11'}$, $r_{12'}$, and r_{12} in the notation of Figure 4.13) are independent. One of these distances serves as a scaling constant which determines only the absolute width of the zero field spectrum. The other two parameters determine the spectral appearance and were exhaustingly varied until an acceptable fit was achieved. (In practice, it was simpler to choose r_{12} and the angle between r_{12} and $r_{11'}$ as the two parameters.) Finally, the spectrum was scaled so that the strongest bands appeared at identical frequencies in the experimental and simulated spectra. Small variations in the remaining parameters lead to noticeable changes in the shape of the spectral bands, as is shown in Figure 4.16. In favorable cases, distances derived from zero field NMR experiments appear reliable to ~.02Å, even in larger spin systems where individual lines may not be resolved.

Small deviations remain between the observed and calculated spectra even for the four-spin geometry which gives the "best fit" within the assumed constraints. One disturbing element is that there are comparatively short inter-^1H contacts between 2 and 2′ sites in different unit cells; in fact, shorter than the 2-2′ distance within a given cell. This may call into question the appropriateness of considering only a four-spin network rather than eight, twelve, or Avogadro's number. Practical constraints on computer memory make it infeasible to model larger (>8) spin networks. In cases such as this,

Figure 4.16. Simulations of the zero field NMR spectrum of polycrystalline $(\mu\text{-H})_2Os_3(CO)_{10}$. e) corresponds to Simulation A of Figure 4.15 with slightly less broadening (~2.6 kHz). By columns, r_{12} varies by -0.03, 0.00, and +0.03 Å from that of simulation e). By rows, the angle between $r_{11'}$ and r_{12} varies by -5°, 0°, $+5^{o}$ from that of simulation e).

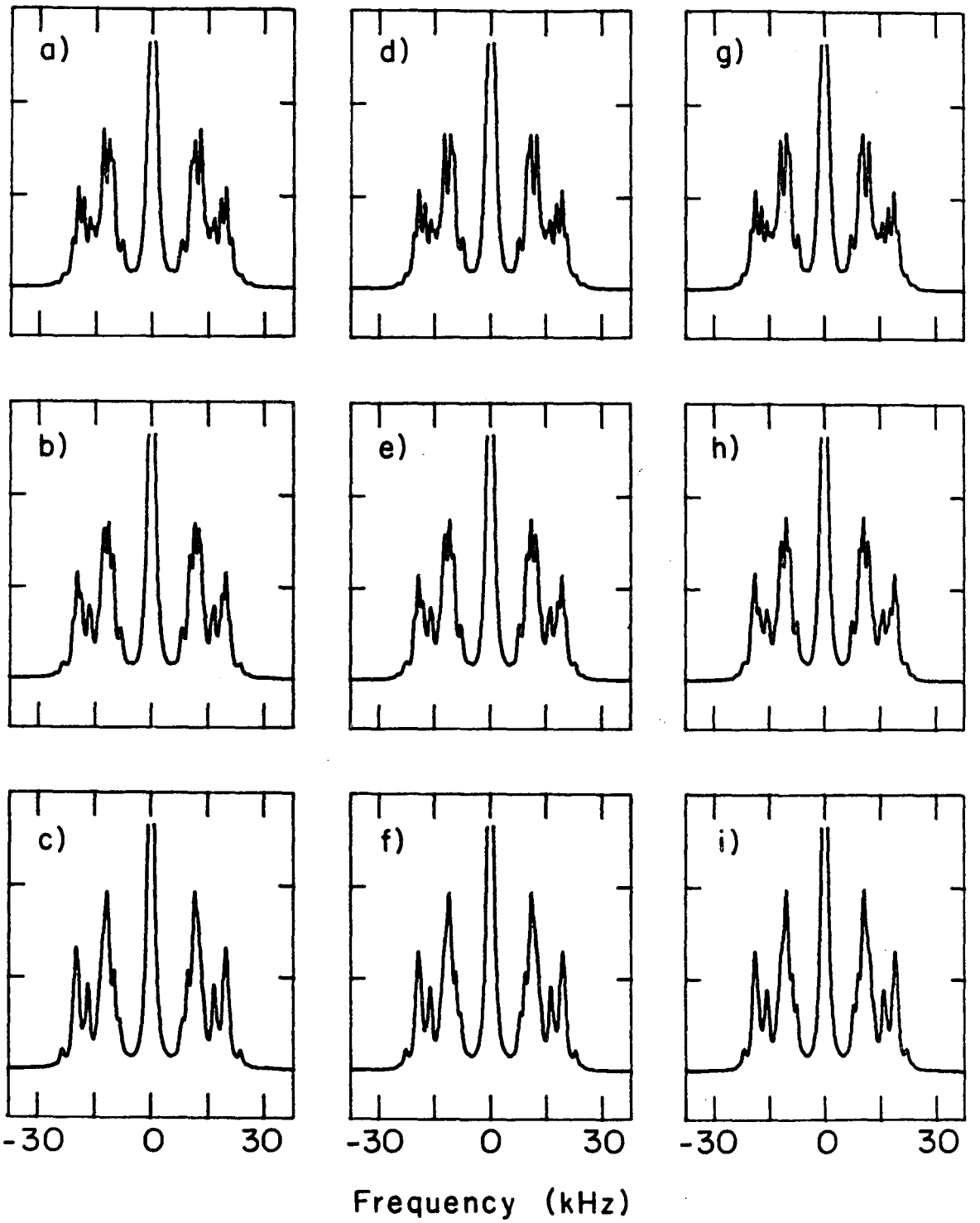

XBL 858-3625

it should also be unnecessary. The assumed Lorentzian linewidth of 2.8 kHz is much broader than whatever additional features might be introduced by a new coupling constant $\omega_D/2\pi$~700Hz. More importantly (and generally), the effect of an isolated spin at a distance **r** is very different from that of a cluster whose closest approach is **r**. In the former case, the main interaction of the isolated spin is with the nearby cluster. In the latter case, the main interaction is with its nearest neighbors, and the dipole-dipole coupling to nearby spins will partially truncate the interactions with more distant neighbors.

2. Comparison of Zero and High Field NMR in Model Systems

Figures 4.17 and 4.18 show the simulated zero and high field NMR spectra for ten model groupings of identical nuclear spins (all chemical shifts equal and chosen equal to zero). The zero field spectra are calculated using the program DBZINT.FOR (largely written by Dr. James B. Murdoch). The simulated powder patterns were calculated using the program PAT6.FOR. The powder patterns are calculated by formulating H_D as in DBZINT.FOR and performing a numerical truncation by adding on a large Zeeman interaction. In order to simulate the powder, the effective field is applied over a large number of directions relative to the arbitrarily chosen "molecular frame". The number of orientations depends primarily on the patience of the programmer and the expense of computer time, and ranged from ~14400 (for the 3 spin systems) to 400 (for the six spin systems). The spectrum for each orientation is summed with all others, and the resulting powder pattern convoluted with a Gaussian lineshape to account for "residual couplings" and all unsampled orientations. Although a Lorentzian more accurately reproduces observed zero field

Figures 4.17, 4.18. Calculated high field and zero field NMR spectra for systems of small numbers of static, equivalent coupled ^1H spins and for a variety of geometries as illustrated. Internuclear distances were chosen so that all the spectra appear to fit in the same frequency range. The base distance is that of the two-spin Pake pattern where r_{ij} = 1.60 Å. Each of the high field spectra is calculated by summing the simulated spectra over a large number of orientations of the spin system in an externally applied field (varying from as many as 14,400 orientations for the three-spin systems to as few as 400 for the six-spin systems. The resulting spectra (see insets) are then convoluted with a Gaussian lineshape to account for the finite sampling intervals and the effects of all other spins. The zero field spectra are calculated using the procedure indicated in Chapter III. The delta function simulations (the insets) are convoluted with the same Gaussian as the high field spectra for comparison, although a Lorentzian line seems to more accurately reproduce experimental results. In most of the odd-spin systems, a sharp zero frequency peak has been truncated in the unbroadened spectra; occasionally, in the broadened spectra as well.

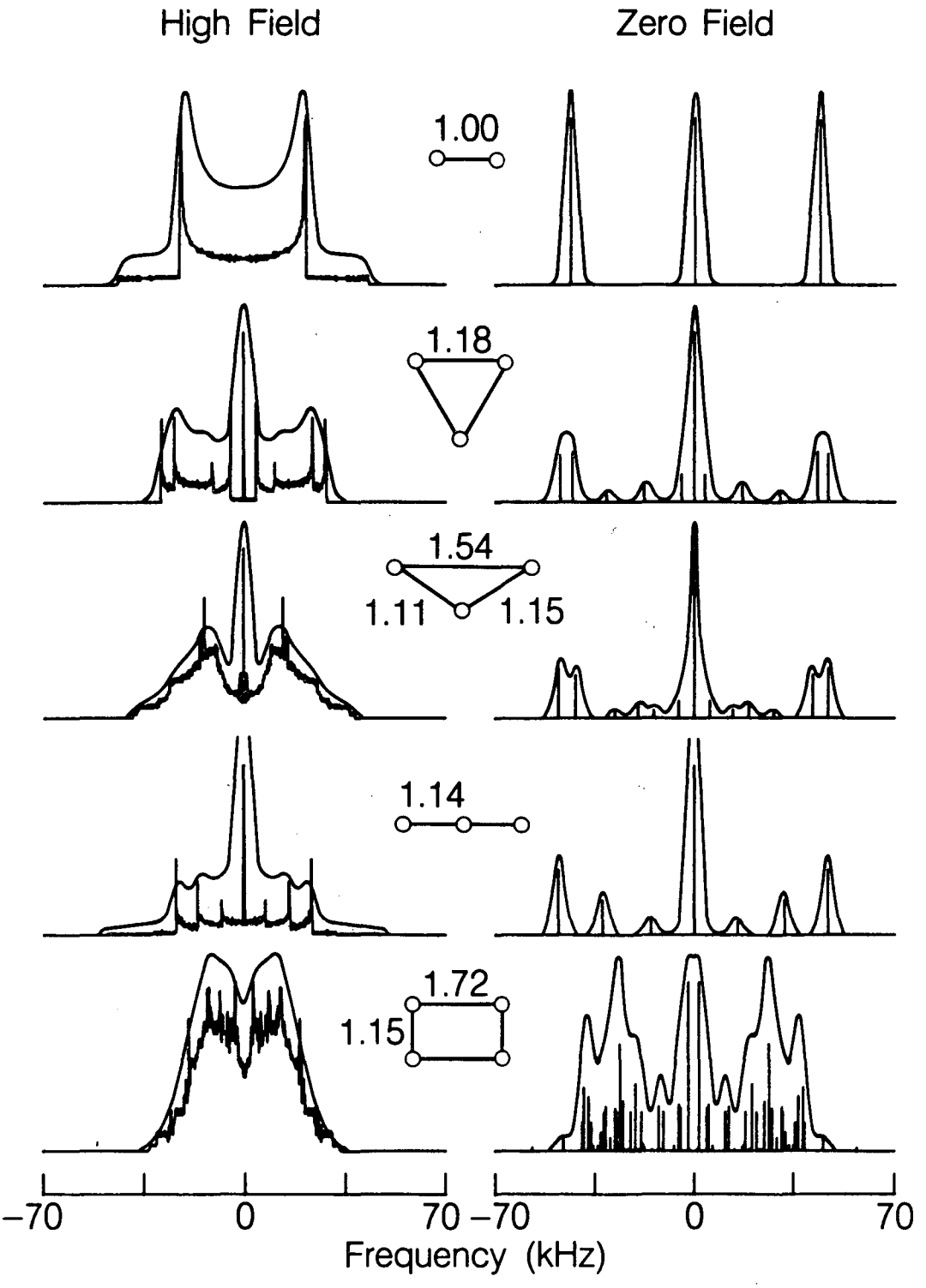

Figure 4.17

XBL 852-1109

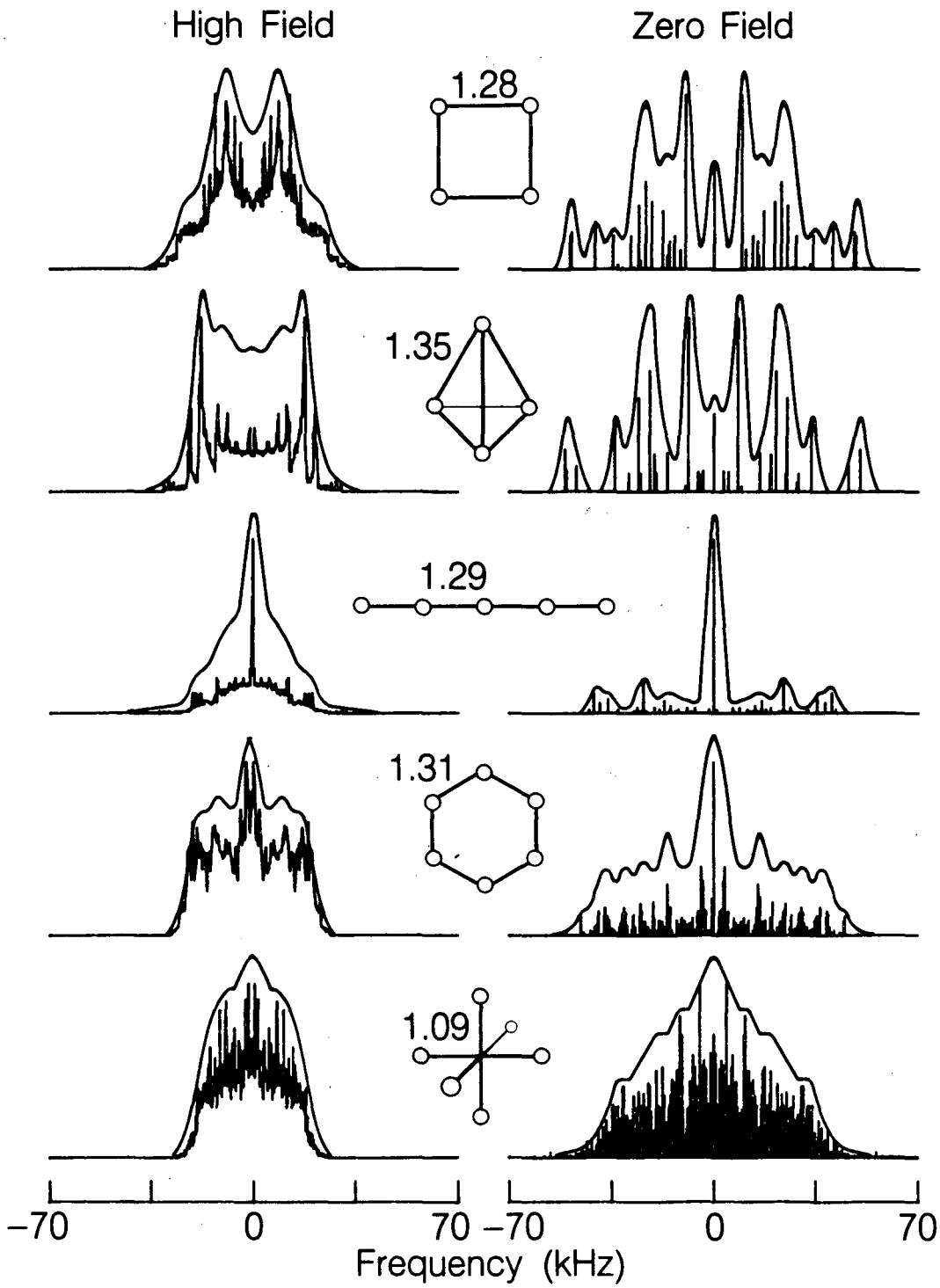

Figure 4.18

XBL 852-1110

lineshapes, the same Gaussian lineshape was used to broaden the zero field spectra so these figures are a worst-case estimate of the resolution advantage of zero field NMR for the observation of dipole-dipole couplings in solids. In all systems the zero field spectrum is more structured, but for large N neither spectrum need contain many resolved features.

3. Zero Field NMR for N → Avogadro's Number

As the number of coupled spins grows large, the zero field spectrum rapidly becomes too complex to be modeled exactly. Exact dynamical approaches require that a density matrix with $\sim 2^{2N}$ matrix elements, and corresponding angular momentum operators of equivalent size, be multiplied, diagonalized, and otherwise manipulated. Even for relatively large machines, for $N > 10$ it will be impossible for the program to remain core-resident and execution times will become intolerably long. Moreover, it is in precisely these cases that the result of an exact spectral simulation are least meaningful. For these large N systems, the spectrum merges slowly into a broad, continuous absorption band where individual dipole-dipole couplings are unmeasureable and only a statistical model of the lattice as a whole can be extracted.

The model for zero field NMR lineshapes in dense spin-1/2 systems is due to Kubo and Toyabe.[96] For dipolar fields which are stationary, Gaussian, and Markoffian a simple form can be derived for the decay of an initial polarization. In zero field, these assumptions lead to a polarization function

$$I_z(t_1) = \frac{1}{3} [1 + 2(1 - \Delta^2 t_1^2)(\exp(- \frac{1}{2}\Delta^2 t_1^2)] \quad (4.23)$$

where Δ^2 is one half of the second moment of the resonance line. This polarization decay function is identical to $\rho_L(t_1)$ if $\rho_L(0) = I_z$. The Fourier transform of this decay function is shown in Figure 4.19, along with the same decay function multiplied by a Lorentzian decay to account for finite T_1. This theory has found its primary application to the analysis of muon polarization decay.[108] Further modifications can be introduced account for motional effects[109] but these corrections are not large. The Kubo-Toyabe form provides a convenient model for comparison to experimental results in densely coupled lattices. Even in sparse spin systems, the prediction that 1/3 of the total magnetization fails to evolve corresponds closely to what is observed.

Figure 4.20 shows the zero field spectrum of squaric acid.[110] This system does not strictly satisfy the conditions of the Kubo-Toyabe model. The magnetic nuclei in squaric acid correspond more closely to a linear distribution than to the isotropic distribution assumed in the model. Nonetheless, the general shape of the spectrum is similar to that predicted in the statistical approach.

Figure 4.21 is the zero field NMR spectrum of lauric acid ($CH_3(CH_2)_{10}COOH$). The proton zero field spectrum at natural abundance (Figure 4.19a) is broad and virtually featureless, and characteristic of most "off-the-shelf" organic compounds. An attempt was made to increase the resolution by observation of the residual ^1H nuclei in a highly enriched randomly deuterated samples (>90% ^2D) of lauric acid (Figures 4.19b,c). While the spectrum is considerably narrowed little structure other than that predicted in Equation (4.23) is resolved.

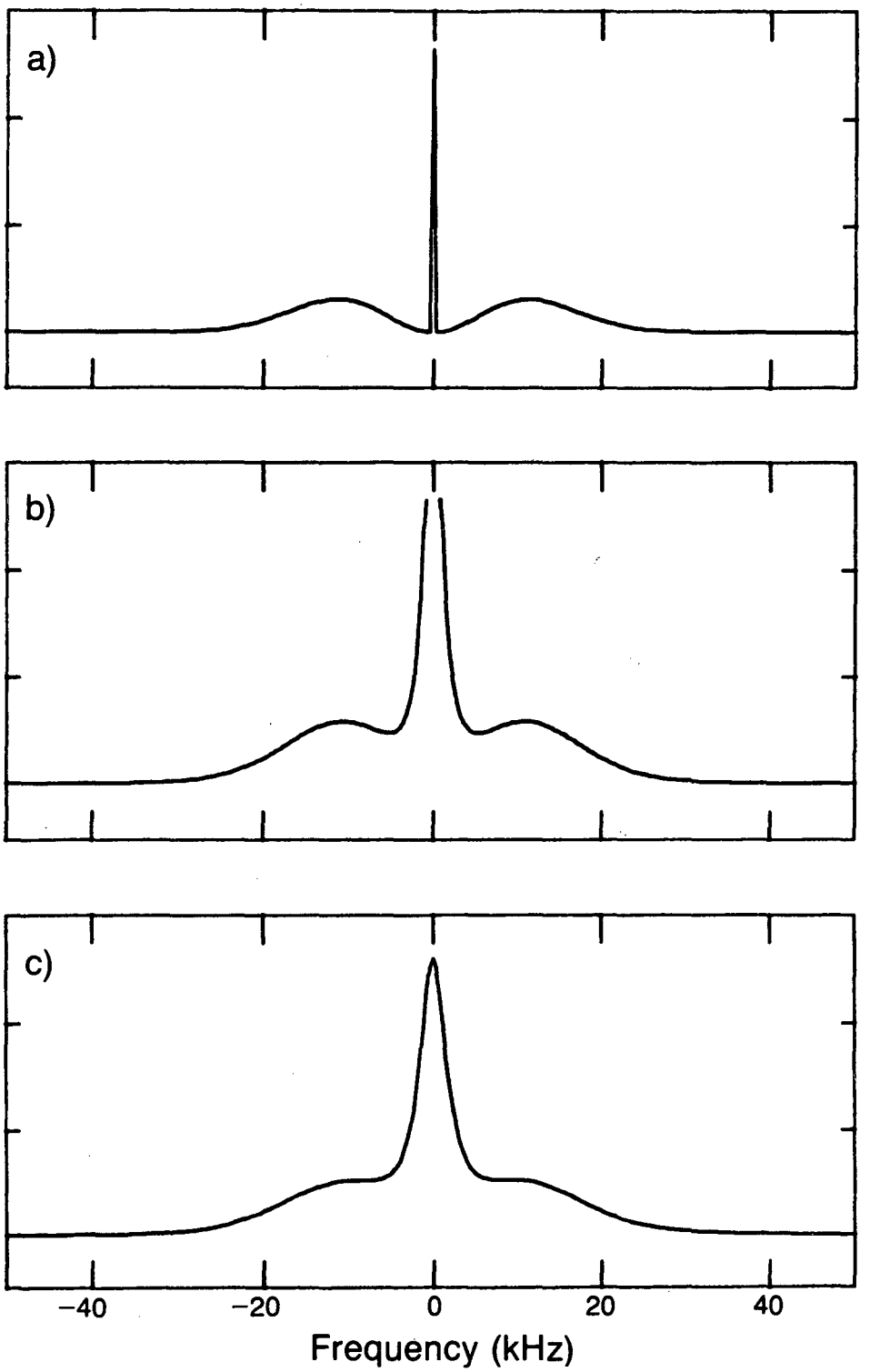

Figure 4.19. Fourier transform "spectrum" of the Kubo-Toyabe magnetization decay function (Equation (4.23)), with $\Delta^2 = 3900\ \mathrm{Hz}^2$. a). With no Lorentzian decay superposed; central line is truncated. b). With 2 kHz Lorentzian decay superposed; central line is truncated. c). With 4 kHz Lorentzian decay superposed.

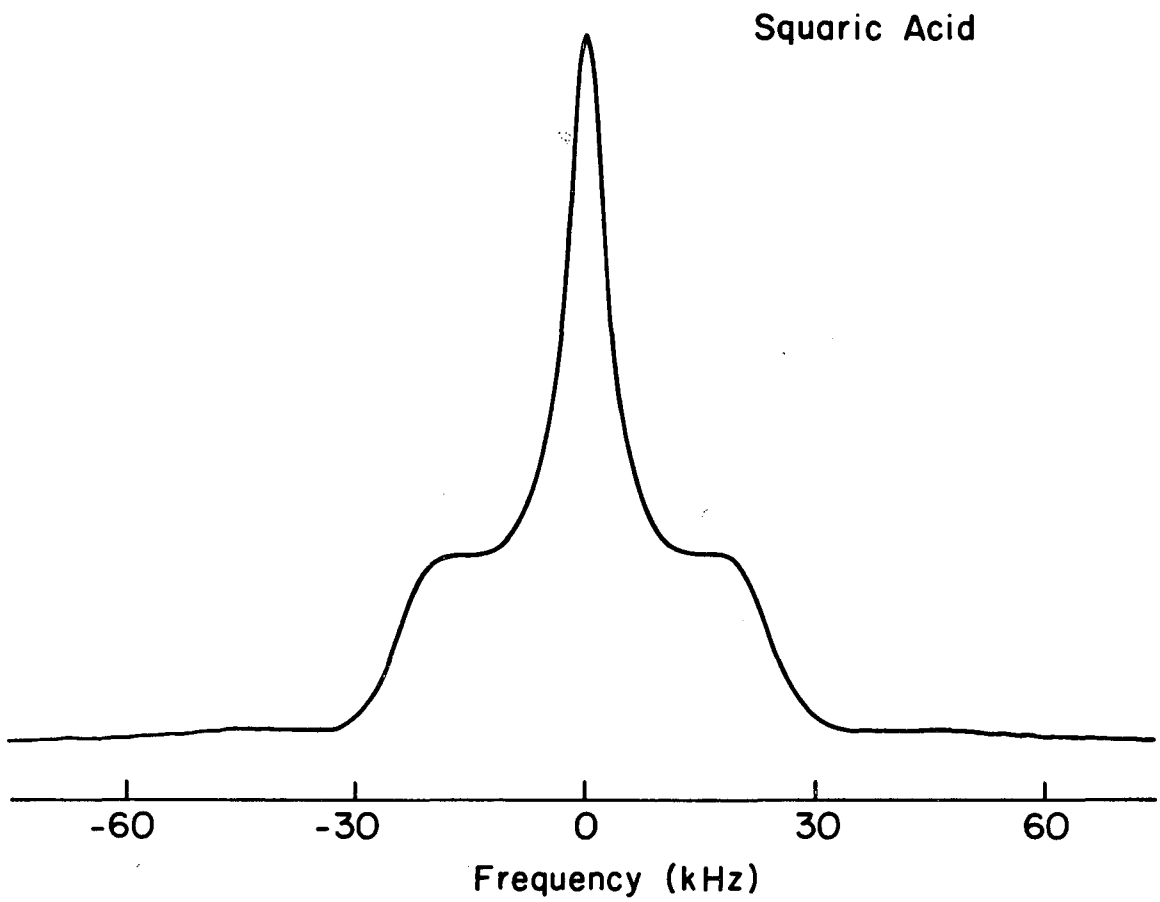

Figure 4.20. Zero field ^{1}H NMR spectrum of polycrystalline squaric acid. The flat wings and sharp central spike correspond closely to the spectrum of Figure 4.19c.

Figure 4.21. Zero field ^{1}H NMR spectra of polycrystalline lauric acid ($CH_3(CH_2)_{10}COOH$). a). Spectrum of completely protonated material. Sharp features centered at zero frequency are distorted due to truncation of the decay function. b). Spectrum of 93% randomly deuterated lauric acid. Relatively sharp peaks at ~±35 kHz may be due to residual pairs. Continuing to replace residual ^{1}H's by ^{2}D's results in c). Spectrum of > 96% deuterated randomly deuterated lauric acid and little improvement in resolution.

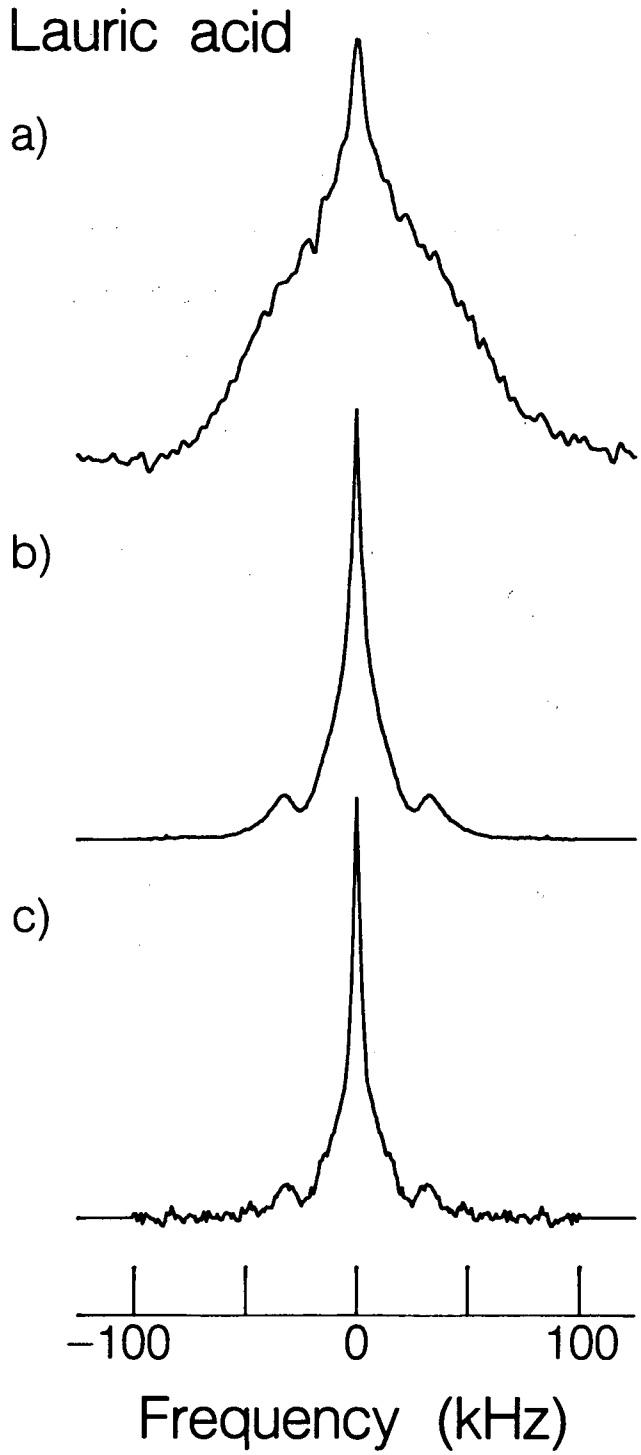

XBL 857-8930

Figures 4.22-4.24 show the zero field spectra of amorphous Si:H, >90% randomly deuterated palmitic acid, and 1,4-dimethoxybenzene ($CH_2DOC_6D_4OCH_2D$). In each sample, the magnetic spin-1/2 nuclei are reasonably dilute and reasonably uniformly distributed throughout the sample volume. Each resembles the spectrum of the Kubo-Toyabe theory, with a broad, occasionally structured central band. In addition, and at much lower intensity, absorption lines appear at relatively higher frequency which may be due to small numbers of strongly coupled pairs or triplets. At extremely high dilution (>99% ^2D) these sharper features might begin to dominate the spectrum (but at significantly lowered signal-to-noise).

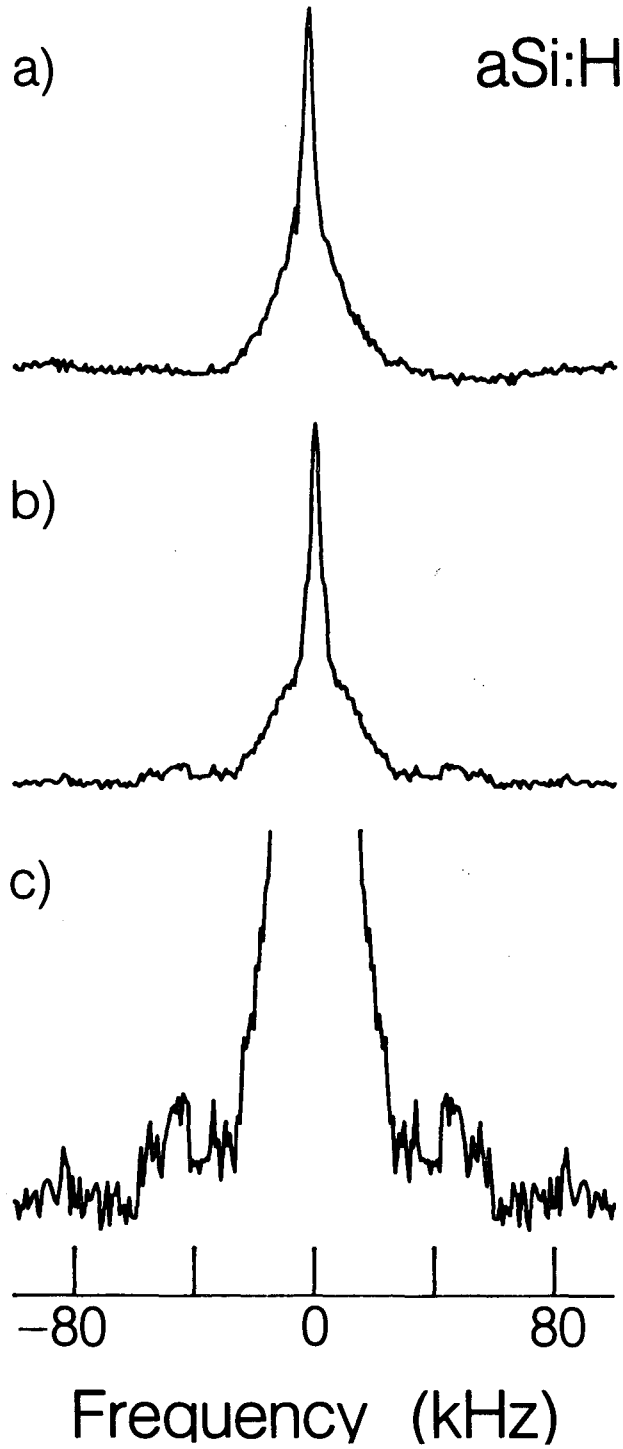

Figure 4.22. ^{1}H NMR spectra of materials-grade amorphous silicon hydride. a). High field spectrum after solid echo sequence.

b). Zero field spectrum. c). Zero field spectrum X 6. Broad, low intensity lines at ~45 kHz are presumably due to tightly bound species.

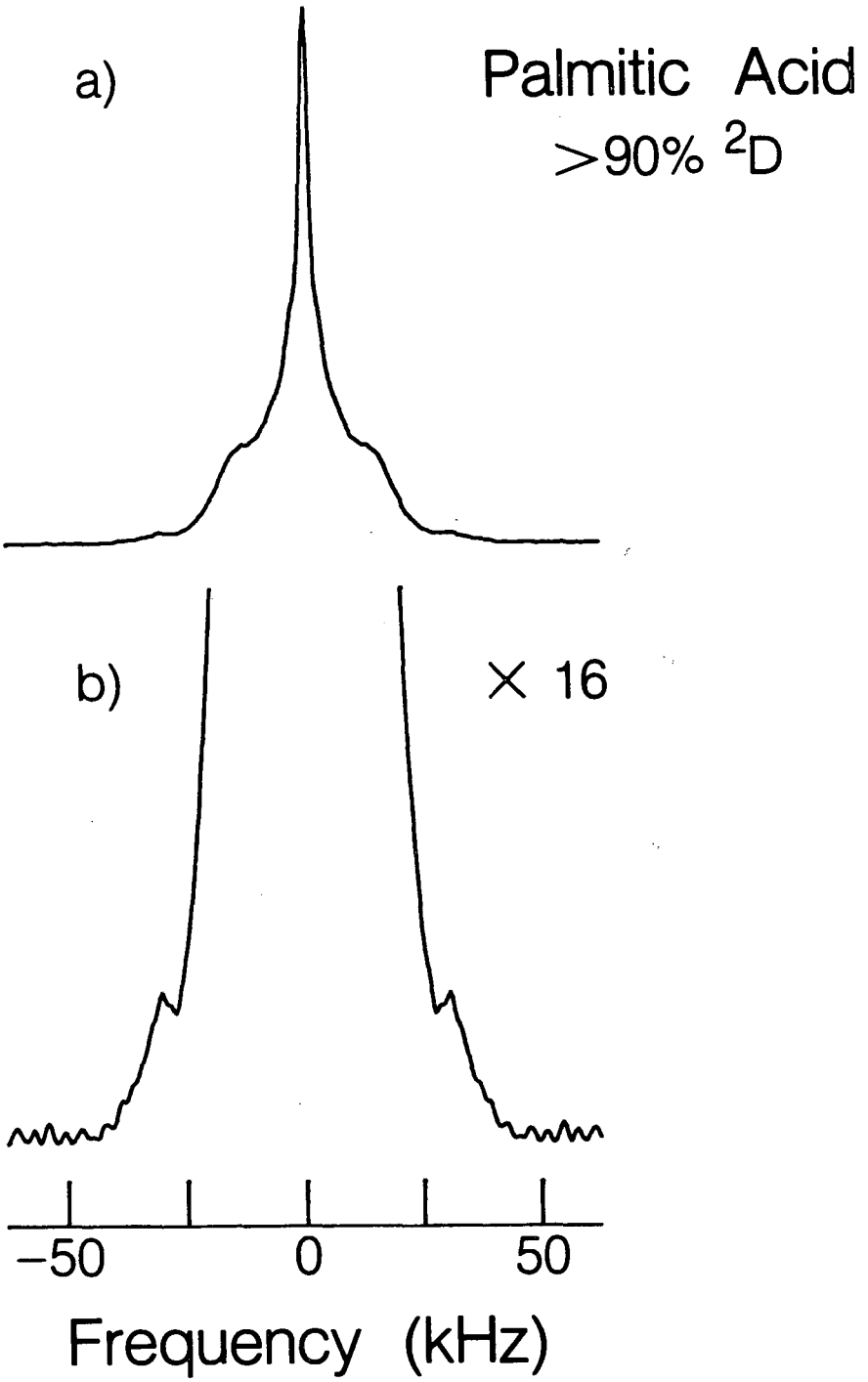

Figure 4.23. a). ^1H zero field NMR spectrum of >90% randomly deuterated palmitic acid ($CH_3(CH_2)_{14}COOH$), closely matching the Kubo-Toyabe form. b). The same spectrum X16. Small peaks at ~ 30 kHz may be due to isolated pairs.

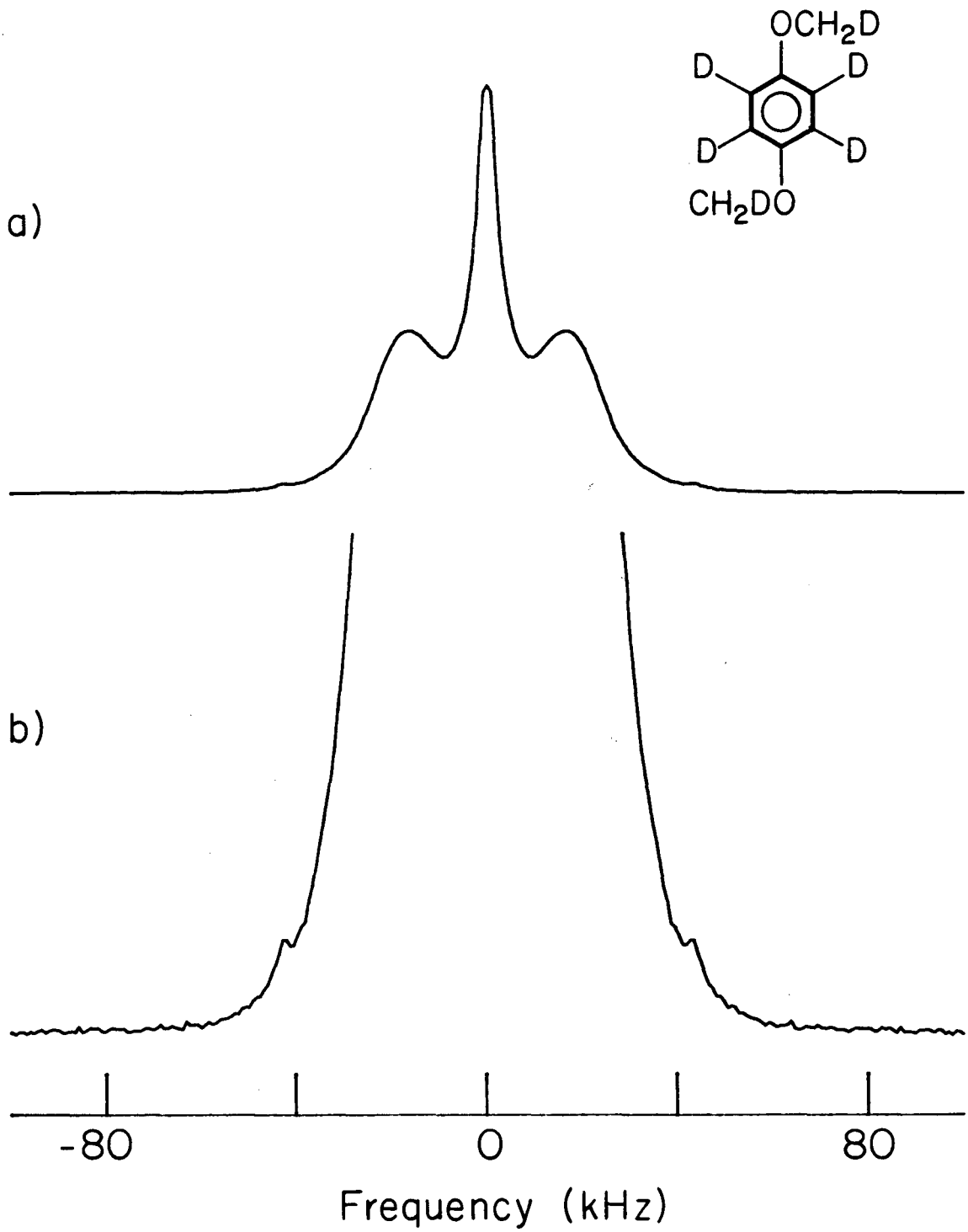

Figure 4.24. a). ^1H zero field NMR spectrum of d_6-dimethoxybenzene ($CH_2DOC_6H_4OCH_2D$). The spectrum appears much like the Kubo-Toyabe form, although the observed structure at ±15 kHz probably reflects the pair-wise dipole-diple couplings within the methyl group, instead.

V. Experimental Results: Quadrupolar Spin Systems

The interactions between the local electric field gradients and quadrupolar moments of nuclear spin systems with $I \geq 1$ often give a more detailed picture of the local electronic environment than do the chemical shifts observed in the same systems. Yet the chemical shifts are far more frequently measured. In no small part, this is because experimental techniques for the sensitive and accurate measurment of quadrupolar couplings are less well developed.

A. Comparison of Chemical Shifts and Quadrupolar Couplings

As a comparison of the chemical sensitivity of chemical shifts and quadrupolar couplings, Figures 5.1 and 5.2 show experimental ^{27}Al MASS and zero field NQR spectra of two inorganic aluminum salts, potassium and ammonium alum ($KAl(SO_4)_2 \cdot 12H_2O$ and $(NH_4)Al(SO_4)_2 \cdot 12H_2O$). The high field (7.05 Tesla) MASS spectra were graciously provided by Dr. Steven W. Sinton of the Exxon Corporation. The high resolution, high field spectra of these two compounds are essentially identical. Isotropic shifts in these two compounds are nearly the same and the chemical shift is insufficiently sensitive to distinguish between the two. In the MASS spectrum of a mixture of the two salts, only a single main line appears. This is a common limitation of high field studies of ^{27}Al. MASS studies of ^{27}Al reveal the isotropic chemical shifts only where the second order quadrupolar broadening (and thus the quadrupolar coupling itself) is small. Except in rare cases and at very high fields[110] the chemical shift differences between similarly

Figure 5.1. From top to bottom: ^{27}Al magic angle sample spinning (MASS) NMR spectra of potassium alum ($KAl(SO_4)_2 \cdot 12H_2O$), ammonium alum ($NH_4Al(SO_4)_2 \cdot 12H_2O$), and a 1.3:1 mole ratio mix of the two. Spectra are observed at 78.2 MHz with a spinning speed of 4 kHz. Chemical shifts are referenced to $Al(H_2O)_6^{3+}$.

Figure 5.2. From top to bottom: ^{27}Al zero field NQR spectra. Each site conributes two lines to the zero field spectrum. For potassium alum, $e^2qQ/h = 391 \pm 2$ kHz; for ammonium alum, $e^2qQ/h = 438 \pm 2$ kHz. In each compound $\eta = 0.17 \pm .05$. The pair of high frequency lines in the spectrum at bottom clearly indicates the presence of two distinct sites.

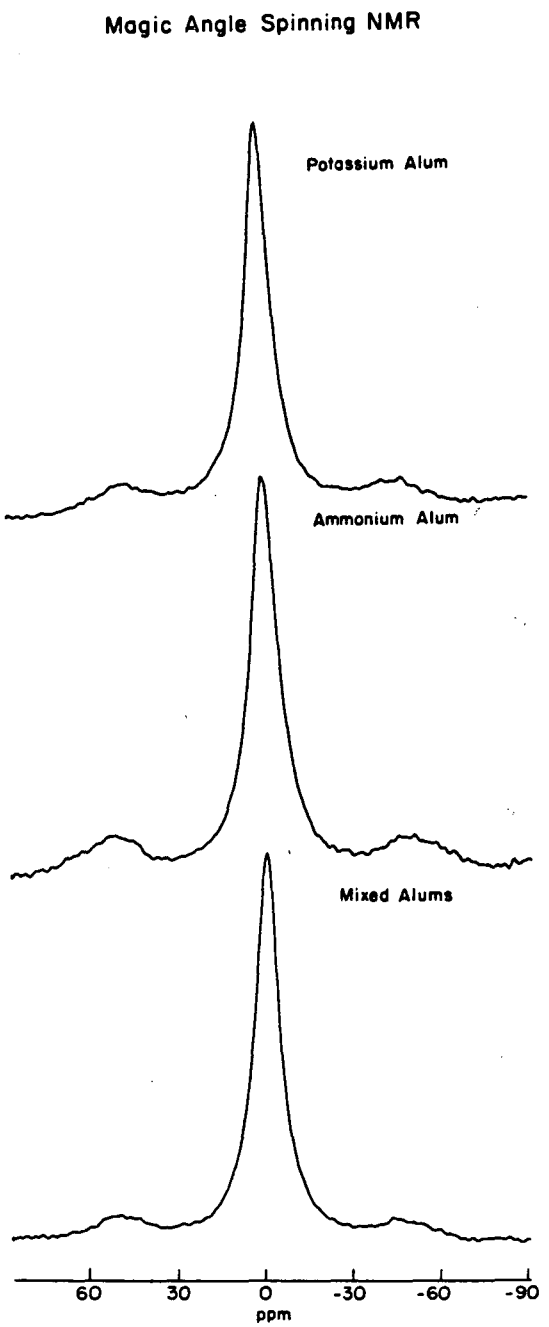

XBL 844-1461

Figure 5.1

Pulsed Field Cycling NQR

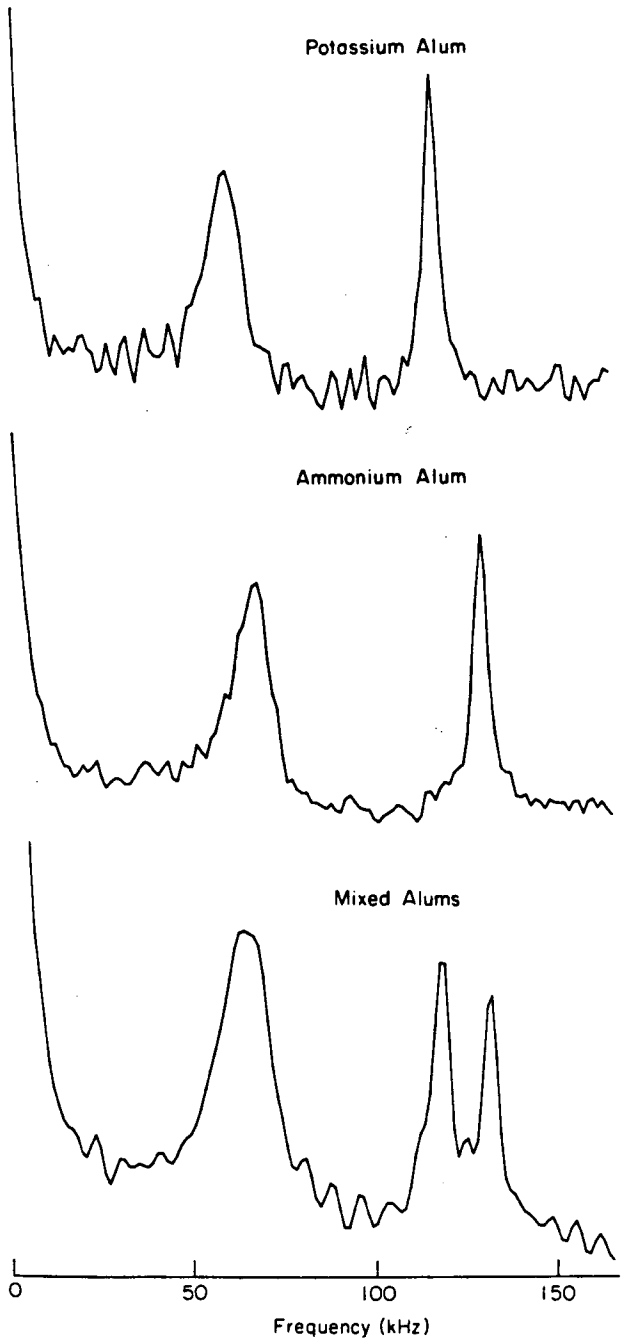

Figure 5.2 XBL 844-1460

coordinated aluminum sites are too small to be resolved. Only the difference between tetrahedral (at ~60 ppm from the chemical shift reference, $Al(H_2O)_6^{3+}$) and octahedral coordination (~0 ppm) is routinely resolved.[111]

Figure 5.2 shows the zero field spectra of these same two compounds obtained by the experimental technique described in Chapter III. In the pure NQR spectrum and for I = 5/2, two lines are predicted for each type of site, and the predicted pair is indeed observed for each pure compound. Even though the zero field resonance lines are broad, the mixture at bottom certainly contains at least two chemically distinct aluminum nuclei. The broader peaks at ~50 kHz merge into a single line in the spectrum of the mix, but the pair of lines at high frequency remain distinct and clearly indicate the presence of two identifiable components.

Because both the chemical shift and quadrupolar contributions to the nuclear spin Hamiltonian result from interactions of the nucleus with the surrounding electron cloud (rather than with other magnetic nuclei like the dipole-dipole coupling) spectra dominated by these single-spin interactions are more simply interpreted than those which primarily reflect the correlations between multiple spins. Spectral lines in quadrupolar systems are generally associated with specific crystalline or molecular sites. The assignment of lines is often automatic because sum rules relate the frequencies of the allowed transitions at a given site. This is in contrast to the dipole-dipole coupled systems presented in Chapter IV where modeling the interactions of more than two or three spins requires a computer modeling. The high

resolution achieved in ^{2}D Fourier transform NQR spectra, the observation of dipole-dipole couplings between sites is routine. As they appear only as a perturbation to the main Hamiltonian, the rate of increase in the number of lines is far slower than in systems where the dipole-dipole coupling dominates the spectrum.

The existence of small couplings between chemically distinguishable sites is analogous to the common "weak-coupling" limit in liquid state high resolution NMR, and suggests possible two-dimensional applications of time-domain NQR to the problems of structure determination and crystallography in disordered solids. Double-transition spectroscopy[69a,112] in ^{2}D NQR is a frequency domain approach. Some time-domain experiments with the same goal are described in Chapter VI.

The rest of this chapter will focus on studies of spin 1 systems--specifically, ^{2}D--where field cycling Fourier transform zero field NQR is most powerful and generally applicable. The local fields characteristic of quadrupolar spin systems are generally larger than is pure spin-1/2 networks and necessitate the use of switched fields larger than are required to satisfy the high field condition in systems of dipole-dipole coupled spins. All experiments in this chapter used switched fields of ~300 gauss (three times larger than was used in obtaining the spectra of dipolar coupled systems shown in Chapter IV).

B. High field NMR of Deuterium

High field quadrupole perturbed NMR studies of integer spin nuclei (realistically, ^{2}D and occasionally ^{14}N) are among the most

demanding of solid state experiments. The sensitivity of ^{2}D NMR to dynamical processes in molecules has accelerated the development of new techniques for efficient broadband excitation[113] and interpretation of the observed spectra.[114] Even in highly enriched samples high quality high field spectra are far from routine: its magnetogyric ratio is low, the quadrupole moment results in high field spectra often 250 kHz wide, and relaxation times may be inconveniently long. Magic angle spinning of integer spin nuclei requires extremely careful adjustment of the spinning axis[115] and the range of isotropic shifts is small. While cross polarization revolutionized high field NMR of low γ spin-1/2 nuclei it is not generally applicable to quadrupolar nuclei. Even with high power rf transmitters (~1 kwatt) experimentally observed spectra are distorted by incomplete excitation of the entire powder pattern.[116] This may be particularly serious if the derivation of important information depends on a comparison of the observed lineshape function $f(\omega)$ to that predicted by a particular model.

For comparison to the zero field spectra of the remainder of this chapter, Figures 5.3-5.5 show high field powder spectra of four of the perdeuterated compounds to be discussed in this and the next chapter. All spectra were acquired using the 5-pulse low power composite quadrupolar echo sequence introduced by Levitt[113] (~200 watts of rf power and 5.0 μs 90° pulses) and phase cycling. The spectrometer data acquisition system (see Chapter VIII) is incapable of sampling the FID at the required rate (> 300 kHz). The bandwidth of the spectrometer was artificially doubled by accumulating two transients in succession with their sampling periods offset by one-half of a sampling period. These two FID's were subsequently interwoven to provide a single data

set with an effective sampling rate twice that of either data set individually. Prior to Fourier transformation the out-of-phase component of the detected magnetization was zeroed to eliminate contributions from non-echoed signals[116] and to facilitate comparison to the zero field spectra where a similar procedure is routine.

Figure 5.3 shows high field spectra of perdeuterated 1,4-dimethoxybenzene (DMB) and 1,4-dimethylterephthalate (DMT). In both compounds, only high field signals from the $-CD_3$ groups are observed. T_1 relaxation times differ greatly between the methyl group and sites on the aromatic ring. Even when the spins are allowed to polarize for several minutes between successive shots, little additional signal is observed. The ratio of the integrated signals arising from the ring sites to that of the methyl groups is much less than the stoichiometric ratio of 3:2. Moreover, whatever ring site signal exists is spread over a frequency range more than three times as large.

Figure 5.4 shows high field spectra of perdeuterated 1,8-dimethylnapthalene. From top to bottom I illustrate the effect of the length of the high field polarization period on the observed spectrum. For very short polarization periods (~200 ms) only signal from the $-CD_3$ groups is observed. At longer times, signals from the aromatic ring sites begin to grow but at different rates. (There is also evidence for anisotropic relaxation within the $-CD_3$ group. For very short times the central singularities in the Pake pattern are less pronounced than at longer times.) Finally, for polarization periods as long as minutes little additional signal is observed.

The spectrum of perdeuterated lauric acid ($CD_3(CD_2)_{10}COOD$) in

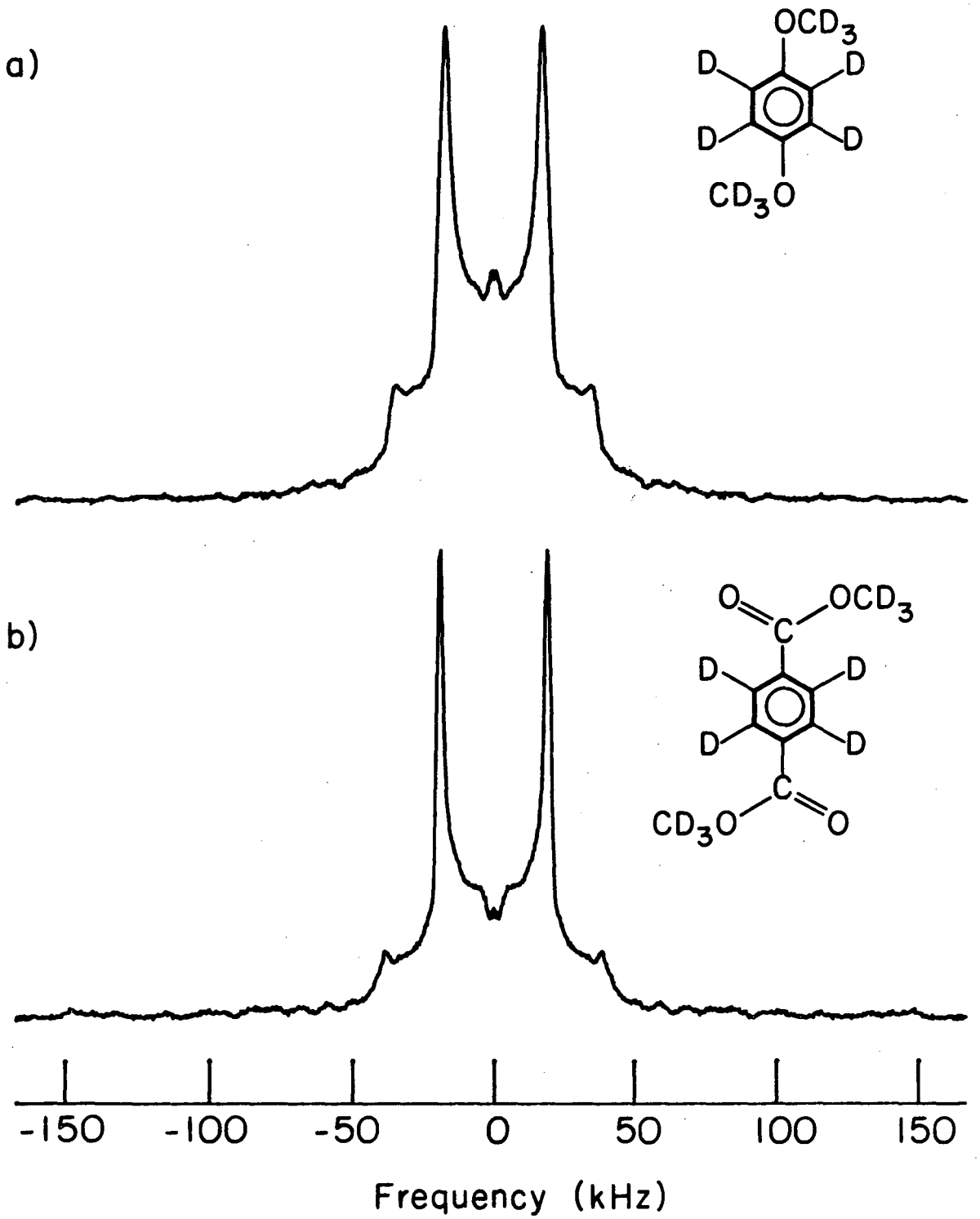
a)
OCD3
D
D
D
D
CD3O
b)
O
OCD3
C
D
D
D
D
C
CD3O
O
-150
-100
-50
0
50
100
150
Frequency (kHz)

XBL 858-3502

Figure 5.3. High field ^2D powder pattern spectra. The 5-pulse quadrupolar echo sequence $\{(\pi/2)_0(\pi)_\pi(\pi/2)_0(3\pi/4)_\pi(\pi/4)_0$ replaces each of the $\pi/2$ pulses of the normal quadrupolar echo sequence) is applied and the echo sampled until no signal can be observed. Rf pulse strength was $\omega_1/2\pi$ = 50 kHz and the dephasing period τ between sets of pulses was 30 μs. a). Spectrum of perdeuterated 1,4-dimethoxybenzene (DMB). Spectrum is result of 1034 scans with 30 s between scans. b). Spectrum of perdeuterated 1,4-dimethylterephthalate (DMT). Spectrum is the result of 800 scans with 10 s between scans. No additional signals were observed with recycle rates as long as 2 m.

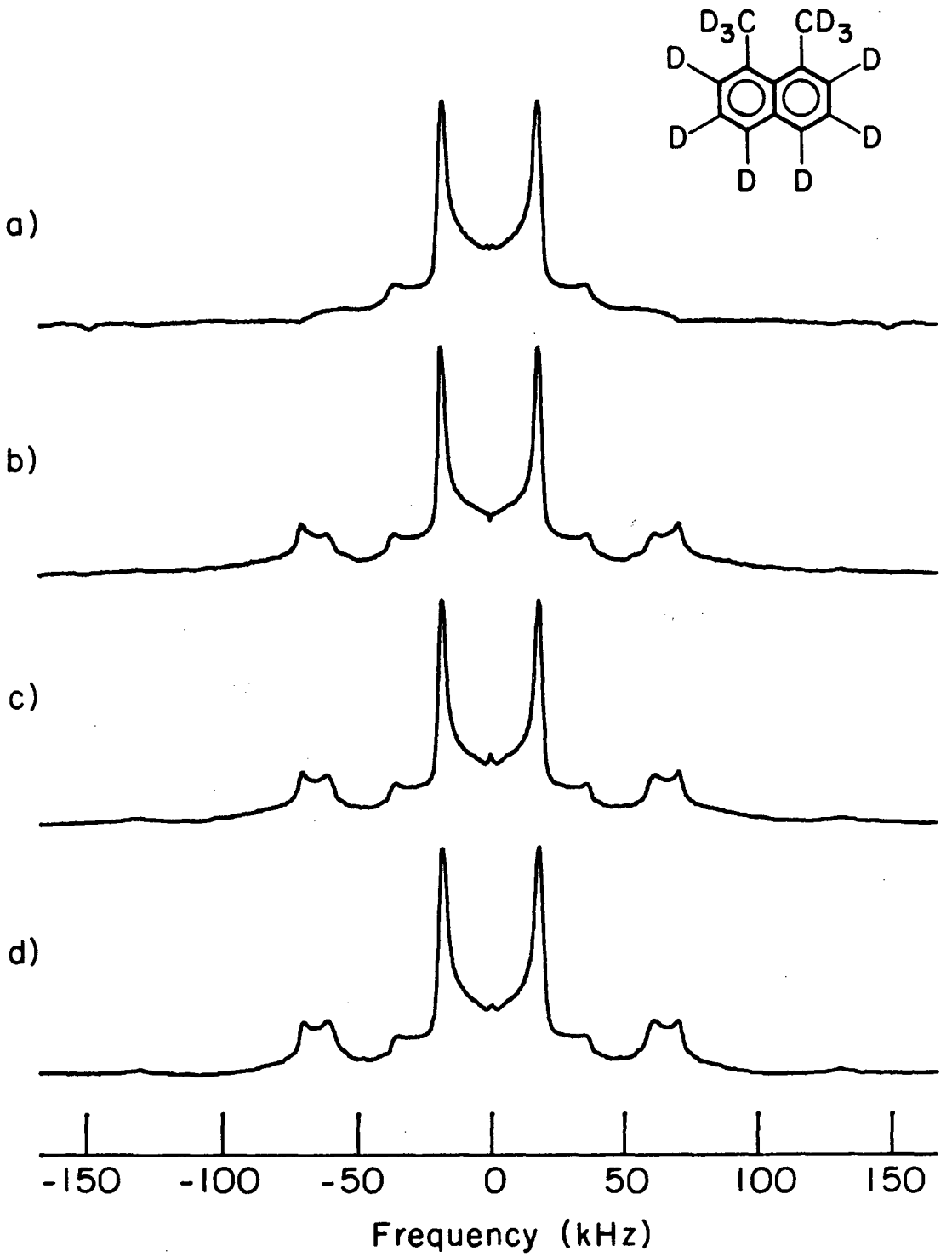

Figure 5.4. High field ^2D powder pattern spectra of perdeuterated 1,8-dimethylnaphthalene (DMN) acquired with the five-pulse quadrupolar echo sequence, as a function of the polarization period between scans.

a). 200 ms/shot, 1710 shots. b). 3 s/shot, 616 shots.

c). 6 s/shot, 2000 shots. d). 15 s/shot, 1436 shots.

Figure 5.5 shows a similar progression. For short times, only signal from the methyl groups is observed. At longer times, the deuterons on the alkane chain contribute more and more significantly to the overall intensity of the signal. These spectra illustrate some of the difficulties associated with high field NMR studies of ^2D. In none of the experimental spectra of these samples is the entire powder pattern corresponding to the static sites be observed.

C. Zero field NQR of Deuterium

These technical difficulties associated with high field NMR of ^2D make zero field NQR studies attractive. Instead of a powder pattern hundreds of kilohertz wide, all of the magnetization which evolves in zero field is concentrated in a small number of lines which can be individually as narrow as ~100 Hz. All the signal energy is concentrated in a comparatively small bandwidth. Because the signal-to-noise ratio is generally referenced to a unit bandwidth, this provides a significant signal-to-noise advantage in the zero field experiment which may more than compensate for the disadvantage of having to observe the evolving magnetization indirectly in a point-by-point manner. The high field spectra of Figures 5.3-5.5 and the zero field spectra which follow are acquired in comparable amounts of time.

Many of the most powerful applications of ^2D NMR spectroscopy are in systems which are motionally averaged and it is the dynamic process itself which is interesting.[117] In this chapter, only systems which are static or where the motion is rapid will appear and the results of Appendix B will generally be adequate for an interpretation of the

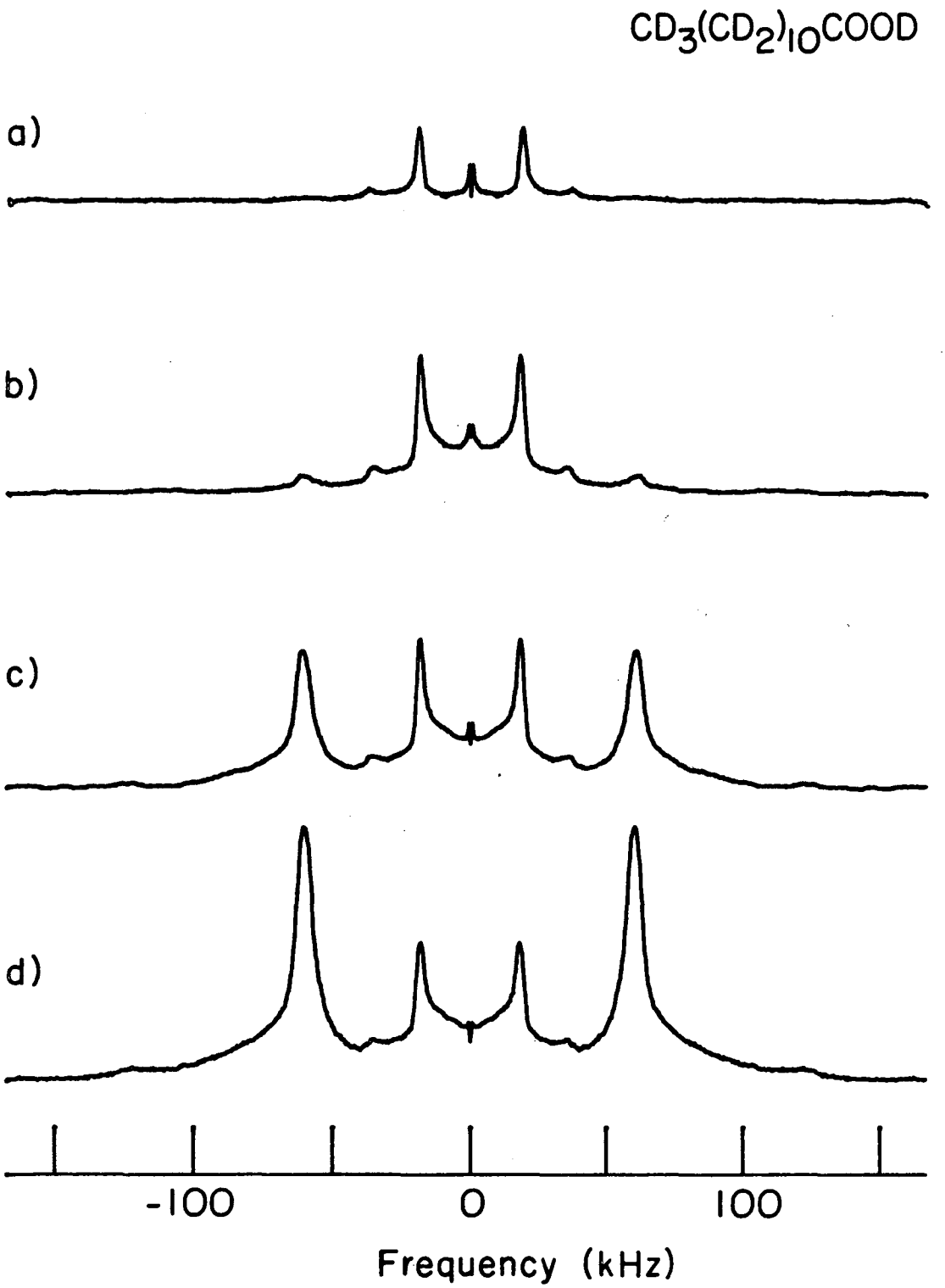

XBL 858-3505

Figure 5.5. High field ^2D powder pattern spectra of perdeuterated lauric acid ($CD_3(CD_2)_{10}COOD$) acquired with the five-pulse quadrupolar echo sequence, as a function of the polarization period between scans.

a). 200 ms/shot, 6454 shots.

b). 1 s/shot, 4324 shots.

c). 15 s/shot, 1146 shots.

d). 1 m/shot, 444 shots.

experimental results which follow.

In Section III.C the zero field free induction decay for an isolated spin-1 nucleus evolving under H_Q was shown to be (in slightly different form)

$$G(t_1) = \frac{1}{3}\,[\cos(2\eta At_1) + \cos(3-\eta)At_1 + \cos(3+\eta)At_1] \tag{5.1}$$

where for I = 1, $A = e^2qQ/4\hbar$. Each isolated deuteron contributes three lines of equal intensity to the zero field spectrum. The principle axis of the quadrupolar tensor $eQ = V_{zz}$ often lies along the bond axis and the electron cloud distribution in C-D bonds is nearly cylindrically symmetric about that axis.[57a] In the absence of motion, η is generally small. In deuterated systems, one line generally appears at a very low frequency and the other two at higher frequencies. For static C-D bonds, typical values are $A \leq 50$ kHz and $\eta \leq .1$. Two lines are predicted to appear near or below 150 kHz and the third at somewhat less than 10 kHz. (Following the convention established in other pure NQR studies, all zero field quadrupolar spectra are presented with positive frequencies only displayed.)

If at least two of the three lines can be assigned to a particular site, then the field gradient parameters A and η are determined. Observation of the third, low frequency lines becomes important when the sample contains multiple sites. Pairs of high frequency ν_-, ν_+ lines are identified if a third line can be found at the difference frequency

$$\nu_0 = \nu_+ - \nu_- \tag{5.2}$$

The ν_0 lines are rarely accessible in any ^{2}D level-crossing experiments

because they appear well within the band of direct ^1H dipolar absorption. When strong couplings ($\omega_D \approx \eta A$) exist between sites with similar values of their quadrupolar tensors, then the spectral pattern may require a detailed and presumably iterative simulation. Dipolar structure between spin-1 nuclei in zero field NQR spectra have previously been observed and explained in N_2, $-ND_2$, and D_2O groups.[69,118,119]

The ^2D spectrum of perdeuterated dimethylterephthalate (DMT) in Figure 5.6 illustrates many of the general features of zero field ^2D NQR. The intense band at ~38 kHz is assignable to the methyl groups. The treatment of rapid rotation given in Appendix B explains why the $-CD_3$ group appears at this relatively low frequency. Assuming the methyl group configuration is nearly tetrahedral, Equation (B.3) applies with θ the complement of the tetrahedral angle, or $\theta = 70.5^o$. The principle component of the quadrupolar tensor V_{zz} is averaged to the value

$$V_{ZZ} = \frac{1}{2}(3\cos^2\theta - 1)\, V_{zz} \approx -.33 \qquad (5.3)$$

where Z is the principal axis of the motionally averaged tensor $\langle\tilde{V}(t)\rangle$ and θ is the angle between the axis of rotation and the C-D bond. The experimentally observed quadrupolar frequency is very nearly 1/3 that which characterizes other chemically similar C-D bonds. No lines are observed near zero frequency and therefore $\eta \approx 0$. The high frequency region of Figure 5.6 shows four resolved lines and indicates two distinct aromatic ring sites exist. These presumably correspond to those sites "near to" and "far from" the methyl groups which are locked in the trans configuration in the solid state. Whatever ν_0 lines might

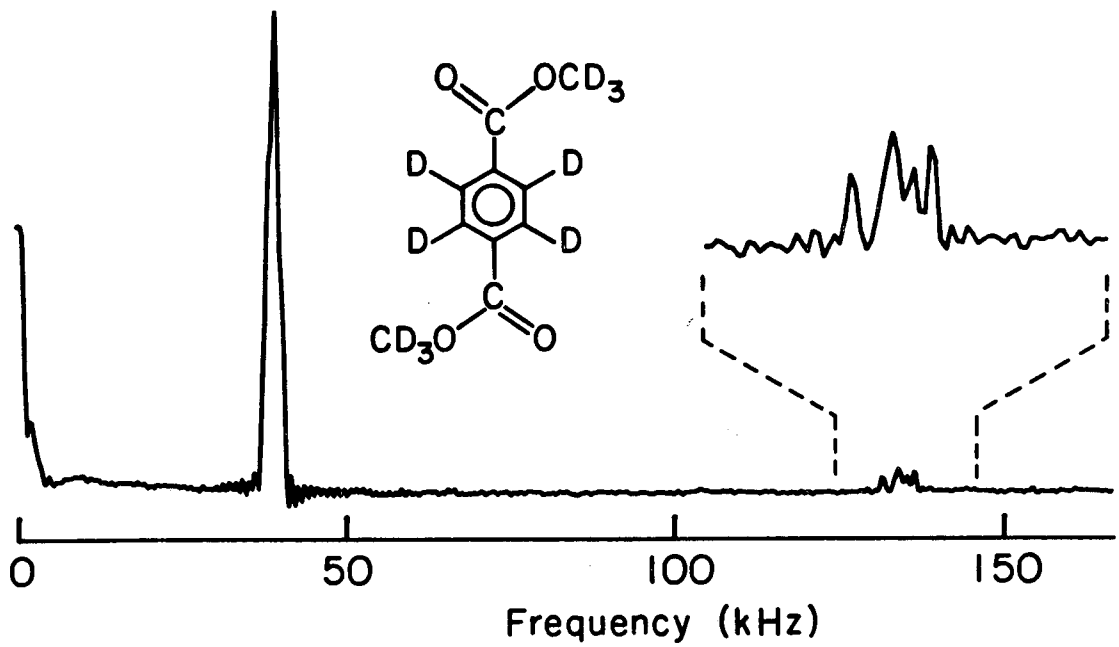

XBL 847-3143

Figure 5.6. Zero field ^{2}D NQR spectrum of DMT, with polarization period of 2 minutes/shot. Sampling increment was 3 μs. A total of 334 points were sampled, and two zero field free induction decays were added together. The methyl group signal is concentrated near 40 kHz. The ring sites appear at ~135 kHz. Four lines are observed which correspond to ν_+ and ν_- lines for ring sites "near to" and "far from" the methyl groups. Cf Figure 5.3b.

exist should appear at very low frequencies. Due to their low intensity and frequency, these lines are undoubtedly buried under the tail of the methyl group zero frequency line. In high field (Figure 5.3b) no trace of these sites is observed. Despite the fact that these sites never approach equilibrium during the high field polarization period, the signal intensity associated with these sites appears in such a narrow bandwidth that while the zero field signal is weak it is also clearly visible.

Figure 5.7 is an expanded view of the methyl group region of DMT (observed in a different experiment than that shown in Figure 5.6). Much additional structure is resolved. Dipole-dipole couplings between methyl deuterons are the source of these splittings. The motion of the methyl group rapidly interchanges the spatial locations of the three individual deuterons. They therefore have identical (and, in this case, axially symmetric) quadrupole coupling tensors. Where H_Q is highly degenerate small perturbations like the dipole-dipole couplings dramatically affect the spectrum. Similar spectra are observed for ordered $-CD_3$ groups in nematic phases of liquid crystals in high field.[120] The precise value of the dipolar coupling constant ω_D, and therefore the distance between deuteron nuclei, is found by computer simulation of both $\langle H_Q(t)\rangle$ and $\langle H_D(t)\rangle$.

A simulation of the spectrum produced for $\omega_D/2\pi = 540$ Hz is indicated in the stick spectrum inset in Figure 5.7. The ^2D-^2D internuclear distance (1.79 Å) agrees within experimental limits with the value previously observed for the distance between methyl group sites in the protonated form of this molecule as derived by zero field NMR.[58] It is a curious and as yet unexplained fact that an accurate

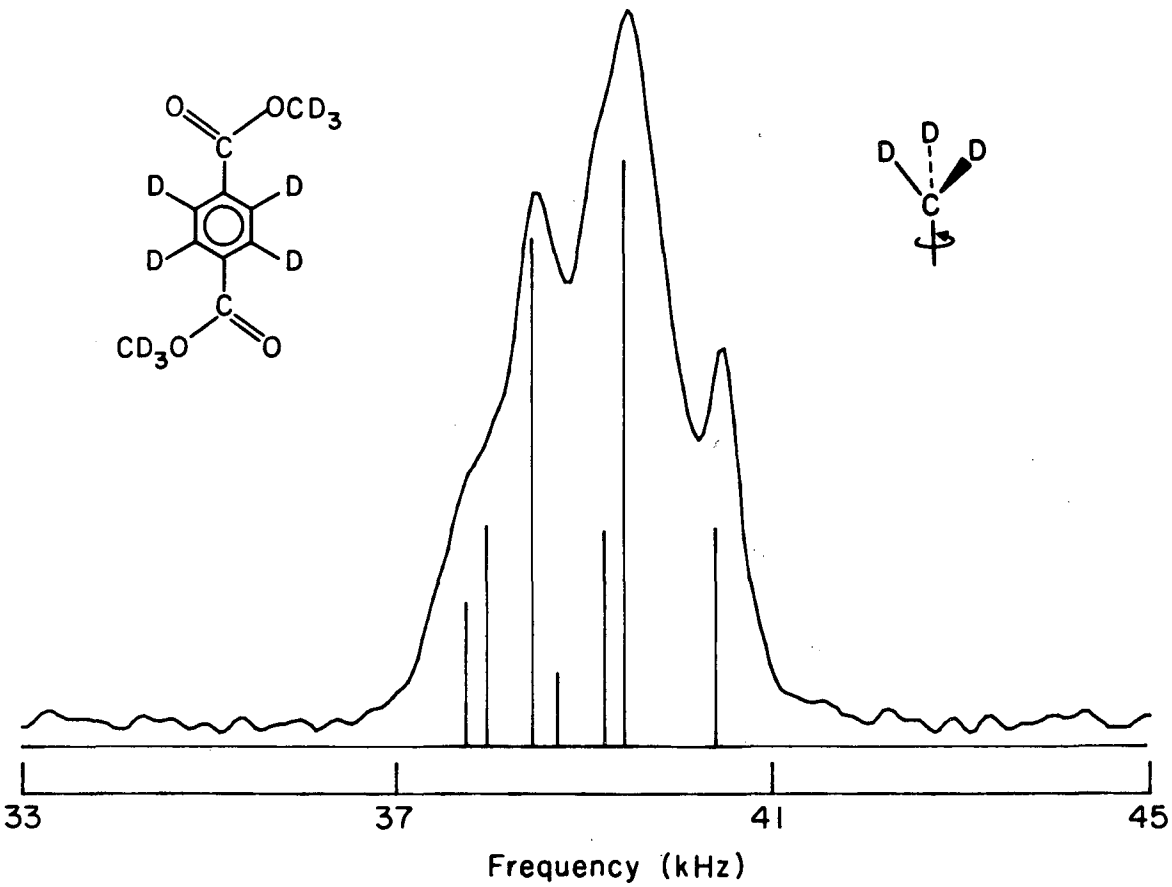

XBL 848-3324

Figure 5.7. Zero field ^{2}D NQR of the $-CD_3$ group of DMT. Cycle time: 10s; sampling increment: 3 μs; number of points: 1001. At this recycle rate no signal from the ring sites could be observed. Splittings within the methyl group line correspond to the dipole-dipole couplings between methyl group deuterons; the stick spectrum inset is a simulation of the motionally averaged system with $\omega_D/2\pi$ = 490 Hz, or $\langle r^3\rangle^{-1/3}$ = 1.79 ±.03 Å.

simulation of this spectrum (and all other similar solid state axially symmetric $-CD_3$ groups measured to date) requires that the dipolar and quadrupolar couplings have the same sign. This is in direct conflict with the conclusion drawn from all the liquid crystal studies, where the dipolar pattern of Figure 5.7 appears inverted about the center of the unperturbed quadrupolar line and the two couplings have opposite signs.

The spectrum of 1,4-dimethoxybenzene (DMB) in Figure 5.8 shows similar gross features. Four lines appear at frequencies characteristic of the ν_+ and ν_- lines of the aromatic ring sites. A complex absorption band centered at ~36 kHz is the spectrum of the spinning $-CD_3$ group. In addition, a large number of low frequency ν_0 lines are observed; a broad, structured band centered at ~2 kHz, and two other single lines at 4 and 6 kHz. These latter two lines appear at precisely the splittings between pairs of lines centered at ~135 kHz and satisfy the sum rule Equation 5.2. Even the lineshapes in the triplets of lines indicated by the letters "A" and "B" match and conclusively determine which sets of lines correspond to a single site. It is likely that the site nearest to the methyl group corresponds to the broader triplet of lines labeled "B". The inequivalence of the two ring sites has previously been observed in ^2D and ^{13}C chemical shifts.[121]

The $-CD_3$ methyl group spectrum, however, is significantly more complicated than either the ring sites or the $-CD_3$ group in DMT. The structured band at ~2 kHz indicates that the quadrupolar tensor in the CD_3 group is non-axially symmetric. The dipole-dipole couplings are superposed on this asymmetry. Even if the methyl group rotation lies

Figure 5.8. Zero field ^{2}D NQR spectrum of DMB. Top: Cycle time: 7 s; sampling increment: 3 μs; number of points; 1001. Signals from both methyl and ring sites are observed, in addition to ν_0 lines at frequencies less than 10 kHz. Bottom: Blow-ups of the three regions where peaks are observed. From 0-9 kHz, ν_0 lines for both methyl and ring sites. From 32-41 kHz, methyl group lines. From 130-139 kHz, ν_+ and ν_- lines of the ring sites. Lines "B_1" and "B_2" are split by exactly the frequency of the line "B_0"; similarly, A_0, A_1, and A_2. The "A" lines presumably correspond to the ring site far from the methyl group, and the "B" lines those near to the methyl group.

$$\left(\frac{e^2qQ}{h}\right)_A = 178.5 \text{ kHz} \qquad \left(\frac{e^2qQ}{h}\right)_B = 179.1 \text{ kHz}$$

$$\eta_A = .045 \qquad \eta_B = .067$$

Cf. the high field spectrum, Figure 5.3a.

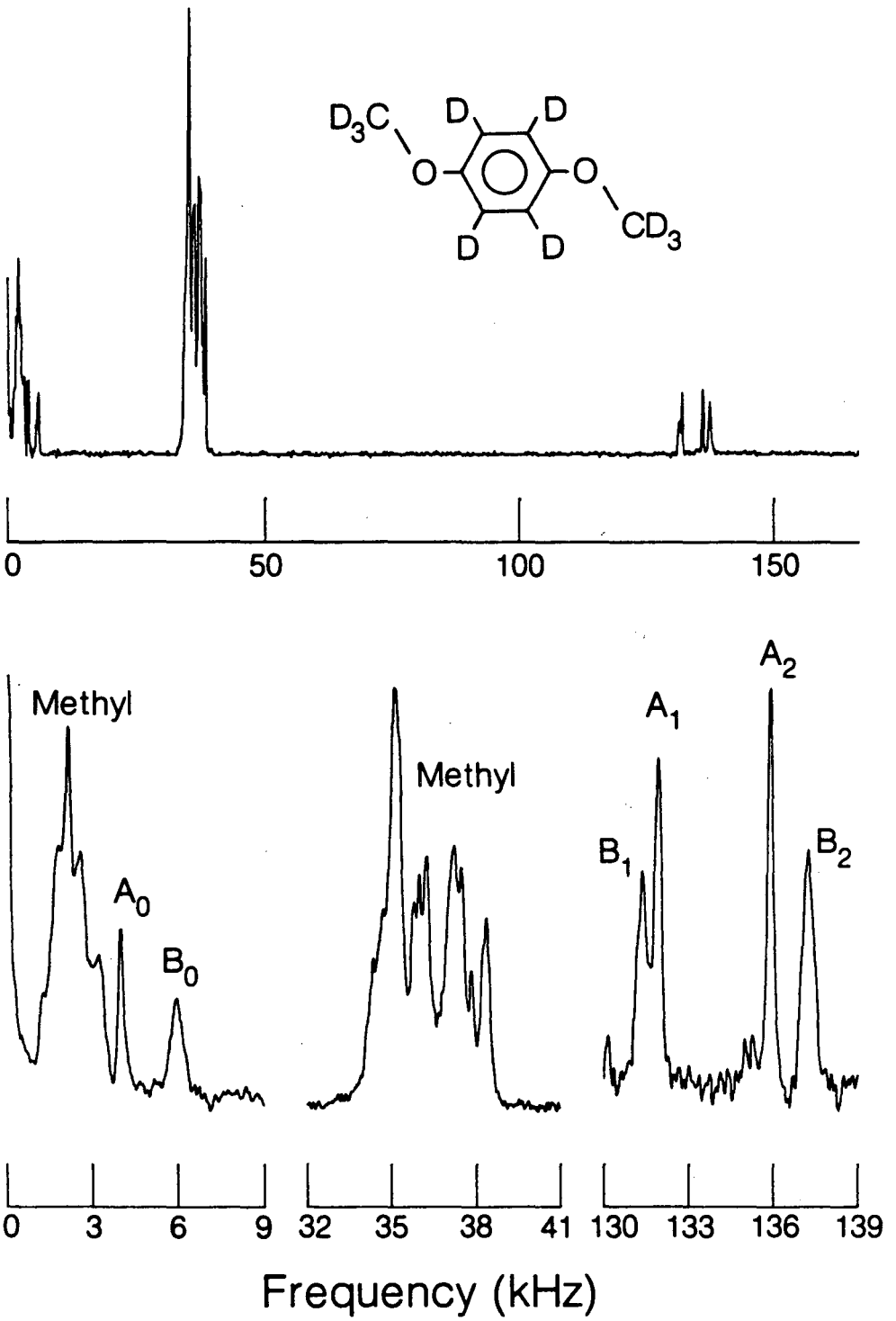

XBL 8310-12107

in a potential well of at least three-fold symmetry such that each methyl group deuteron has an identical quadrupolar tensor η need not be zero. One model for the introduction of an asymmetry into $\langle\tilde{V}(t)\rangle$ is to assume that the motion is in a three-fold well where in one orientation (site 1) the unaveraged tensor differs from the other two.[122] For simplicity, assume that each of the instantaneous values of $\tilde{V}$ is axially symmetric and that the methyl group motion corresponds to jumps through 120°. In the molecular frame XYZ rotating with the methyl group,

$$H_{Q1} = (A+3\Delta A)\{[3I_Z^2-I(I+1)]d_{00}^2 + \sqrt{6}\,[(I_X^2-I_Y^2)d_{02}^2 - (I_XI_Z+I_ZI_X)d_{01}^2]\} \quad (5.4)$$

$$H_{Q2} = P\left[A\,\{[3I_Z^2-I(I+1)]d_{00}^2 + \sqrt{6}\,[(I_X^2-I_Y^2)d_{02}^2 - (I_XI_Z+I_ZI_X)d_{01}^2]\}\right]P^{-1}$$

$$H_{Q3} = P^2\left[A\,\{[3I_Z^2-I(I+1)]d_{00}^2 + \sqrt{6}\,[(I_X^2-I_Y^2)d_{02}^2 - (I_XI_Z+I_ZI_X)d_{01}^2]\}\right]P^{-2}$$

where $3\Delta A$ is the difference between the coupling constant at site 1 and that at sites 2 and 3, and $P \equiv \exp(2i\pi I_Z/3)$. Averaging over the motion corresponds to summing the time-averaged contributions from each of the three sites, and

$$\langle H_Q(t)\rangle = (A + \Delta A)d_{00}^2[3I_Z^2-I(I+1)] + \sqrt{6}\,\Delta A\,[d_{02}^2(I_X^2 - I_Y^2) - d_{01}^2(I_XI_Z + I_ZI_X)]$$

$$= \frac{1}{2}(A + \Delta A)(3\cos^2\theta-1)[3I_Z^2-I(I+1)] - 3\Delta A\sin\theta\cos\theta(I_XI_Z + I_ZI_X)$$

$$+ \frac{3}{2}\Delta A\sin^2\theta(I_x^2 - I_y^2) \quad (5.5)$$

In this frame the Hamiltonian is no longer diagonal. The terms in $(I_XI_Z + I_ZI_X)$ contribute only to second order, however, and the effective asymmetry parameter is approximately

$$\eta_{eff} = \frac{3\ \Delta A \sin^2\theta}{(A + \Delta A)(3\cos^2\theta - 1)} \tag{5.6}$$

In a methyl group where $\theta \approx 70.5^{o}$

$$\eta_{eff} \approx \frac{4\ \Delta A}{A + \Delta A} \tag{5.7}$$

Motionally averaged methyl group field gradient tensors are axially symmetric if the instantaneous values of $\tilde{V}$ have at least three-fold symmetry over the rotational cycle. The methyl group in DMB lies very close to one hydrogen atom on the ring and there is no reason to expect such symmetry. The nearness of the methyl group to one of the ring sites is also reflected in the breadth (due to unresolved dipole-dipole couplings) of the set of ring site lines marked A, and it is on this basis that we suggest that the A sites are those near to the methyl group. Other types of motion superposed on the pure rotational modes of the $-CD_3$ group (e.g. "rocking" as it attempts to avoid the ring ^2D) further complicate the analysis.

Precisely because the resolution in this spectrum is exceedingly high these smaller features (dipole-dipole couplings ~500 Hz and small asymmetry parameters) which no other technique could detect appear and complicate the analysis. De-Paking[43] of the spectrum of Figure 5.3a would allow for the extraction of only the average value of the (assumed) axially symmetric quadrupolar tensor and perhaps a hint that $\tilde{V}$ was not quite axially symmetric. Values for the motionally averaged quadrupolar tensor alone can be extracted from the spectrum even in the absence of a complete simulation of the observed pattern. Vega has shown that dipolar couplings between spin-1 nuclei leave the first

moment of the resonance line unshifted.[66] As long as the zero field NQR intensities are undistorted by different T_1 relaxation rates during transit, the first moment can be measured by integrating over the band. From the measured centers of gravity of the (ν_+, ν_-) and ν_0 regions, the tensor components

$$\frac{e^2qQ}{h} = 47.9 \text{ kHz}$$
$$\eta = .096 \tag{5.8}$$

can be derived.

Figure 5.9 compares the spectrum of the methyl group region of monodeuteromethyl ($-CH_2D$) DMB to that of perdeuterated DMB. One might think that observation of the methyl group in the absence of dipole-dipole couplings (or, at least quenched to the order that they are quenched) would afford more accurate measurement of $\langle\tilde{V}(t)\rangle$. In the partially deuterated compound only a pair of lines are observed and it would be tempting to assign them as the ν_+ and ν_- lines associated with $\langle\tilde{V}(t)\rangle$. Unfortunately, the first moment of the absorption lines is shifted to much higher frequency in the $-CH_2D$ group. This is neither an indication of experimental error nor a counterproof of the effect of dipolar couplings on the first moment. Rather, it serves as a warning about attempts to extrapolate results from one system to other closely related systems. In replacing two of three methyl group deuteron nuclei with protons only half as massive, the moment of inertia of the methyl group is significantly perturbed. There is certainly reason to expect that the details of the motion are similarly perturbed. While the static value of $\tilde{V}$ may be no more than marginally changed by the isotope effect, this is almost certainly not the case for motionally

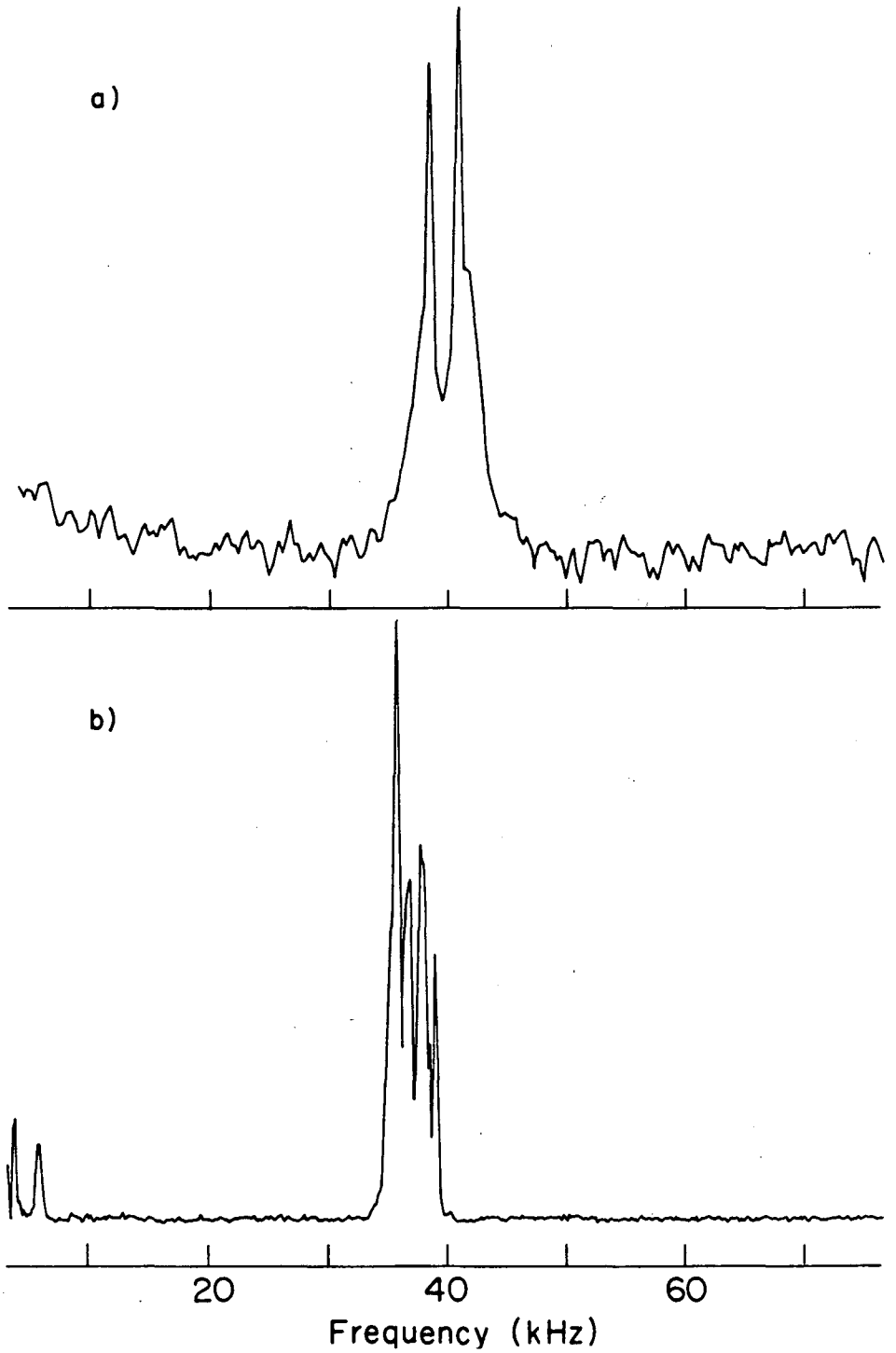

Figure 5.9. Comparison of ^2D zero field NQR spectra of methyl group regions in a). partially deuterated (CH_2D) DMB and b). perdeuterated DMB. While only a pair of lines appear in the former, they are shifted to much higher frequency and considerably broader than the lines in the latter.

averaged systems.[84]

The linewidths in the partially protonated methyl group of Figure 5.9 are broader than those in the perdeuterated molecule. With only small asymmetry parameters, the quenching of the dipole-dipole coupling between integer and half-integer spins may become ineffective. Unless $\eta A \gg \omega_D(^1H\text{-}^2D)$, the heteronuclear couplings may be more effective in broadening zero field NQR lines than homonuclear couplings between nuclei the same distance apart.

Figure 5.10 shows the zero field spectrum of perdeuterated 1,8-dimethylnaphthalene (DMN). As might by now be expected, absorption lines appear in the traditional three regions of the spectrum. The methyl group spectrum is surprisingly similar to those observed in DMT and show no asymmetry. As the two neighboring methyl groups are extremely close to one another, it might be expected that the field gradient for sites pointing nearly at the neighboring $-CD_3$ group should differ from that observed for sites pointing away. Dipole-dipole couplings between groups are not much smaller than those within a group and might be expected to contribute to the observed features. Nonetheless, except for a small frequency shift its spectrum appears nearly identical to that of the $-CD_3$ group in DMT.

Despite the high resolution and good signal-to-noise ratio in the spectrum of Figure 5.10 the complete set of ring site tensors cannot yet be assigned. Not all of the high frequency ν_+, ν_- lines can be assigned to mates in the ν_0 which satisfy the sum rule of Equation (5.2). The source of the intensity variations in the ring site region lines is also unclear. There is evidence for differing T_1's, which is an explanation for the small intensity of the ring site lines in DMT

Figure 5.10. Zero field ^2D NQR of DMN. Lines appear in ν_0 region, $-CD_3$ region, and at the ring sites. The methyl group shows the same structure observed in DMB. Cf. Figure 5.4.

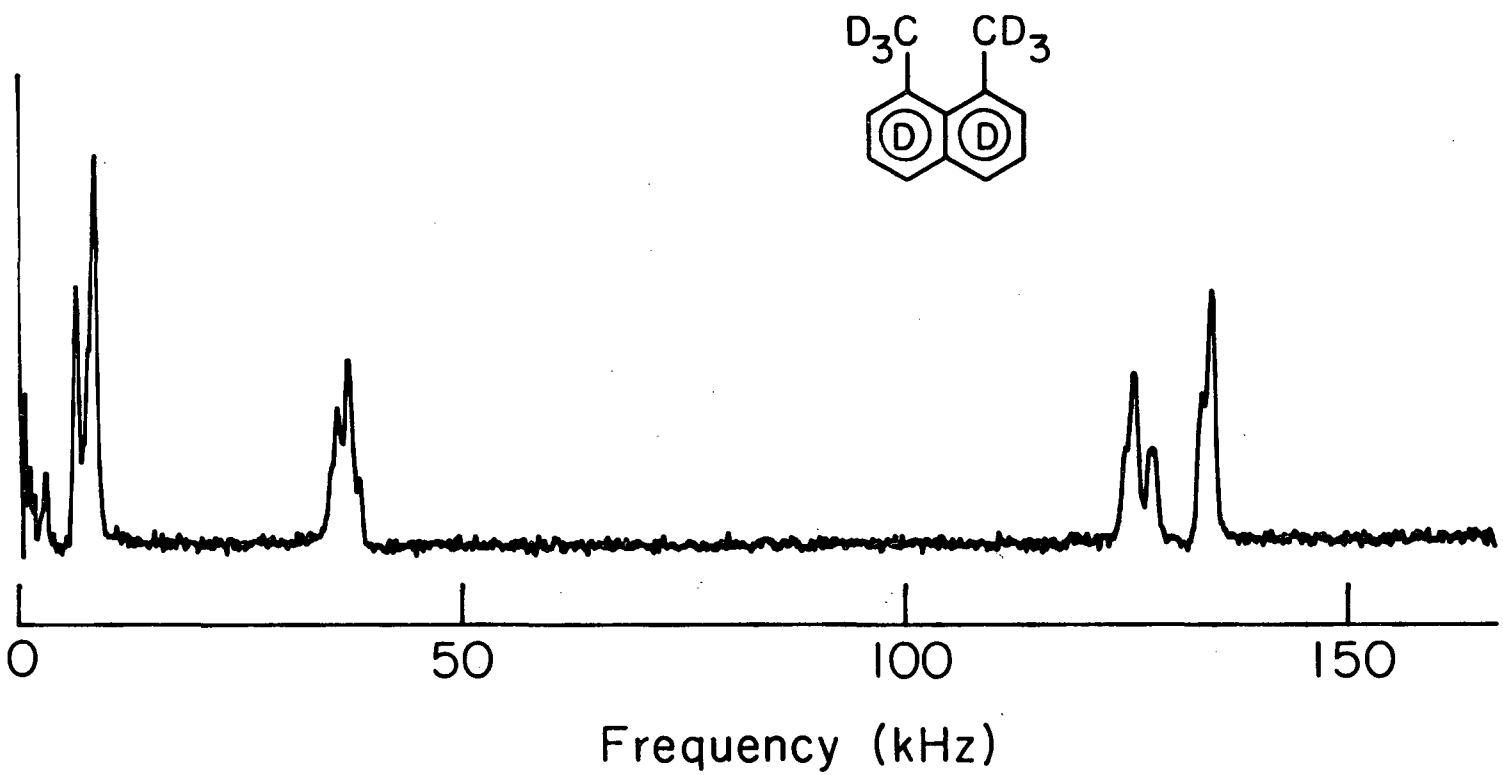

XBL 844-1458

and DMB, in the high field spectra of Figure 5.4. Some sets of lines might coincidentally overlap and dipole-dipole couplings between sites might split some lines. The coupling between the equivalent 4 and 5 sites, opposite to the methyl groups, should be ~200 Hz and may well spread signal from these two deuterons over a relatively broad range. Some of these possibilities might be experimentally resolved using some of the two-dimensional correlation experiments described in Chapter VI.

Not all ^{2}D NQR spectra are as simple and well-resolved as the rest of the examples given in this chapter. Figure 5.11 shows the zero field NQR spectrum of polycrystalline perdeuterated lauric acid, ($CD_3(CD_2)_{10}COOD$). Again the same three traditional regions of the spectrum appear. The methyl group region (~35 kHz) resembles no other methyl group yet observed. The region where the methylene groups appear is unusually broad and few resolved features appear anywhere in the spectrum. There are two reasonable explanations: first, unresolved dipole-dipole couplings between sites may broaden out the structural features. This possibility might explain the lack of resoved features but cannot account for the broad range of quadrupole couplings. Theoretical studies of ^{2}D quadrupolar couplings in simple alkanes predict that A should range from only ~42-45 kHz,[123] and thus that the high frequency band should appear at ~130 kHz. A more likely source of such a distribution of quadrupolar absorption frequencies is a distribution of motional modes. In zero field spectroscopy, spectral features are broadened primarily by terms inherent to the observed Hamiltonian. Instrumental or experimental contibutions to the linewidths are negligible. Broad zero field lines reflect the intrinsic breadth of the nuclear interactions.

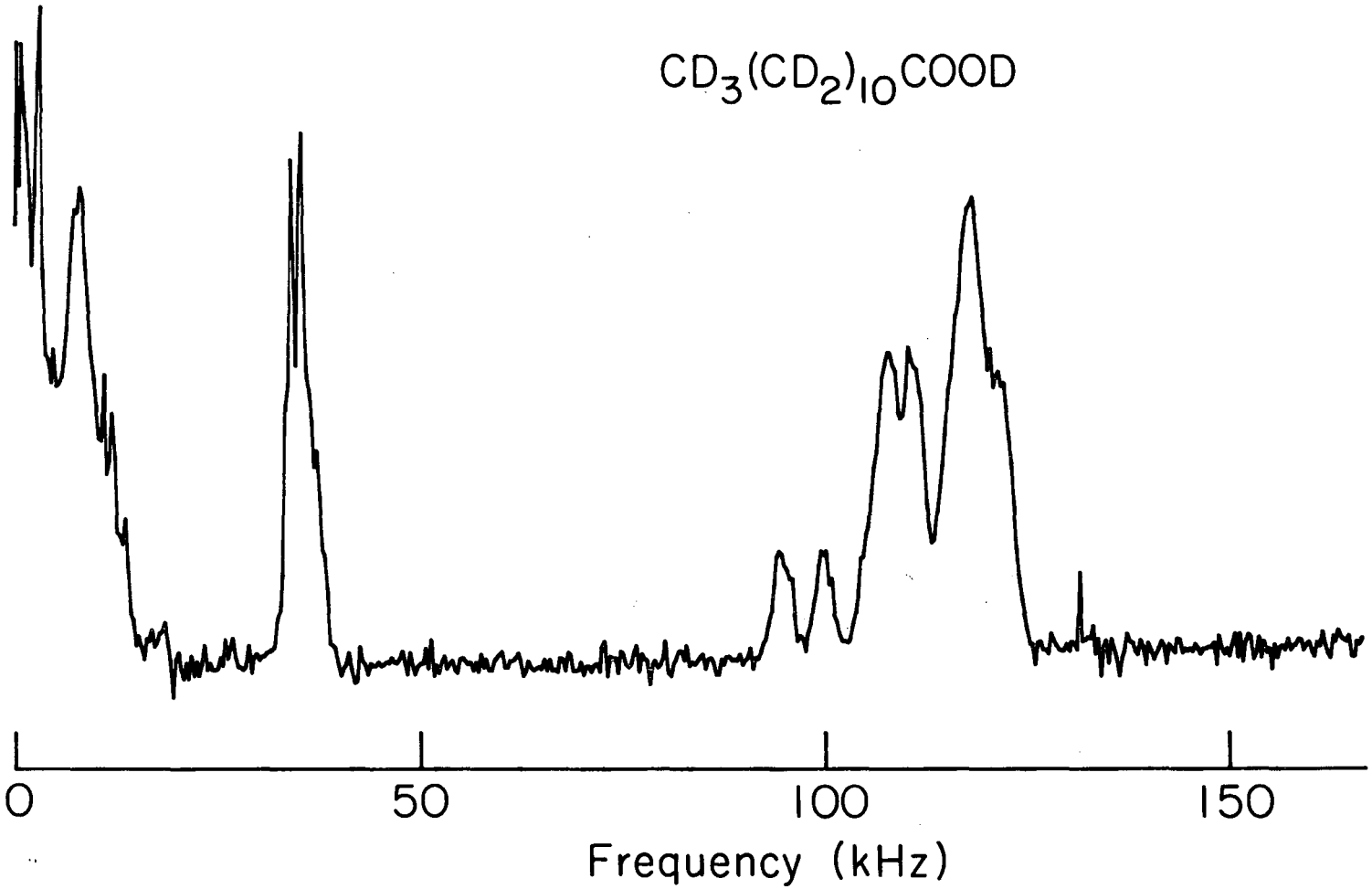

XBL 844-1459

Figure 5.11. Zero field ^2D NQR of lauric acid. Lines appear in ν_0 region, $-CD_3$ region, and at the alkane sites (>100 kHz). The methylene absorption region is unusually broad and probably reflects a range of librational modes in the sample. Cf. Figure 5.5.

The resolution advantage of zero field NMR can be used to assist in the study of high field parameters of nuclear spin systems. Figure 5.12 shows an experiment which affords an experimental method of differentiating between the high field T_1's of different types of deuterons. The experimental strategy is to obtain the zero field spectrum by whatever means possible. Normally it is advantageous to sample the evolved magnetization as quickly as possible after the return to the magnet to minimize its decay via spin-lattice relaxation. In the experiment of Figure 5.12 the sample is allowed to sit in high field a time T comparable to that of a spin-lattice relaxation time. If spin diffusion between all sites is allowed, then the amplitude of all lines in the zero field spectrum disappear with a uniform time constant T_1. If spin diffusion is allowed only between some subset of spins, then the lines in the spectrum disappear with different rates at the different sites.

Figure 5.13 shows the results of such an experiment on DMN. At the top, at the end of the zero field period t_1 the sample is returned to high field and the evolved magnetization is sampled as soon after the sample is safely lodged in the high field detection coil as was deemed possible (probably within ~35 ms of the actual return to the rf probehead). In the middle and below, the experiment was repeated with longer values of T. Over the space of ~500ms, the methyl group spectrum disappears into the noise while the spectra of the ring sites are virtually unaffected in either amplitude, phase, or any other readily observed experimental parameter. This suggests that the $-CD_3$ group high field T_1 is ~200 ms. As the cycle time of the zero field experiment is ~250 ms, it is also virtually field independent. (If T_1

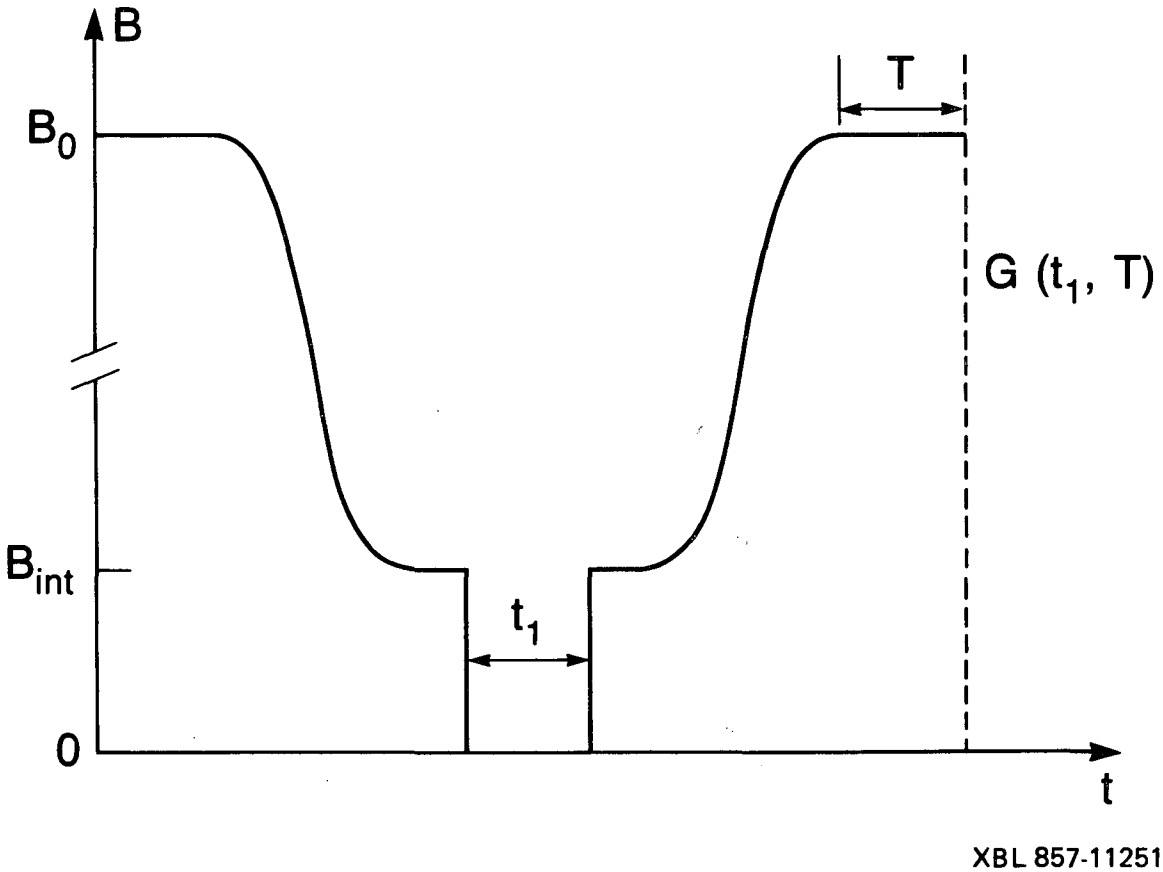

Figure 5.12. Zero field-high field relaxation rate correlation experiment. The zero field spectrum is observed as a function of T, where $T \sim T_1$. If different parts of the sample have very different relaxation times, the zero field spectrum will disappear nonuniformly with T.

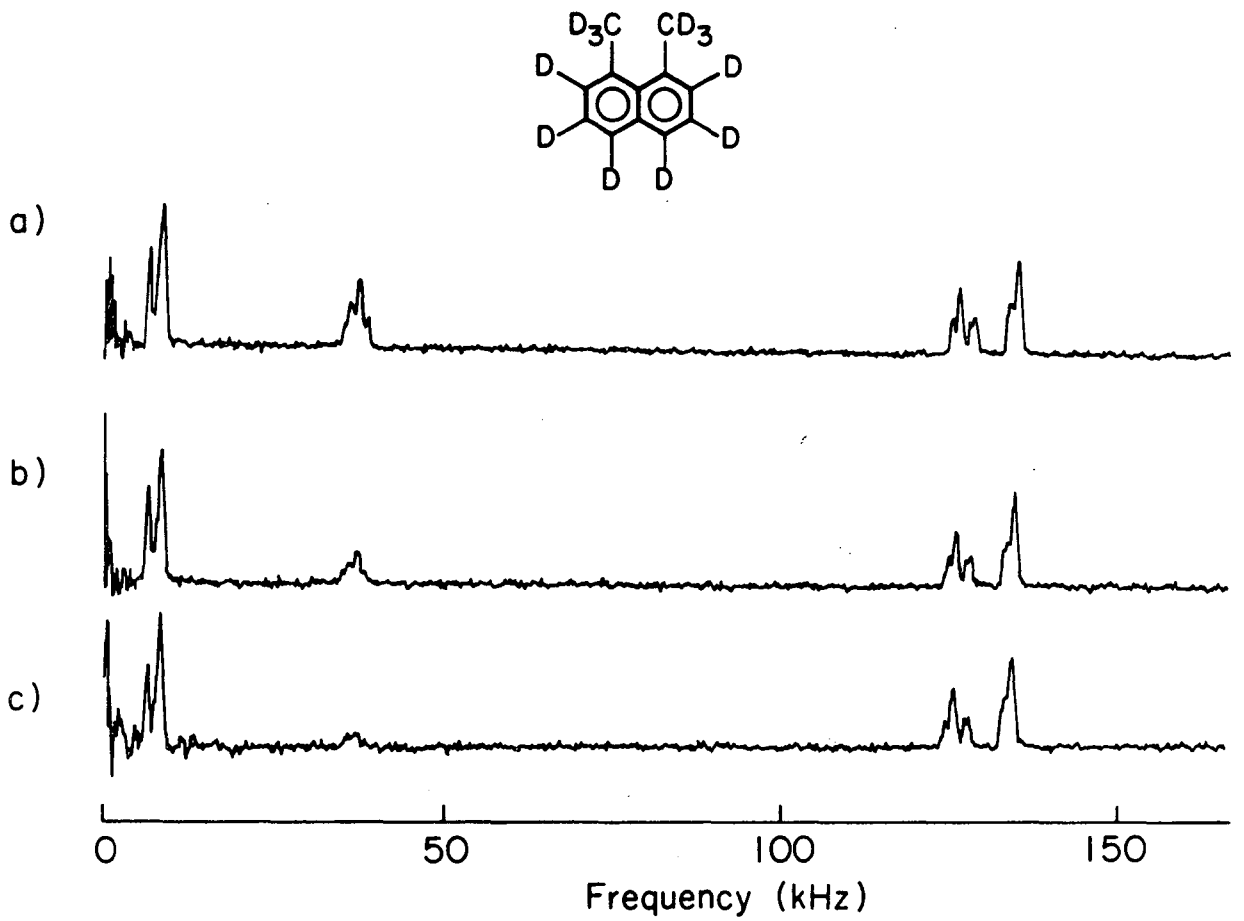

XBL 857-3134

Figure 5.13. Example of zero field-high field relaxation rate correlation experiment. The sample is DMN. a). T = T′ ~ 35 ms (i.e. the signal is measured as soon as possible after the sample is securely within the bore of the magnet. b). T = T′ + 115 ms; c). T = T′ + 315 ms. Over the space of 315 ms the methyl group signal largely disappears; no change is observed in the ring site signals.

is field dependent, it generally increases with increasing field. If at any field strength between B_0 and zero T_1 were significantly shorter than 200 ms, it would be surprising to observe any $-CD_3$ group signal after returning to high field. In Chapter VI I present some experiments which give an approximate upper bound to T_{1Q} in very low fields.) No decay in signal amplitude at the ring sites is observed over these short times. This is consistent with the interpretation of the T_1 data contained in Figure 5.4.

VI. Variant Experiments

In this chapter, I apply some of the principles of zero field NMR established in previous chapters to a variety of possible variant experiments whose merits (if they exist) will be described along with their interpretation. Section A covers the possibility of changing the selection rules which govern the zero field evolution period. In Section B several of the experiments suggested by the discussion of Section A are analyzed. Section C discusses an approach to high-sensitivity zero field NQR via level crossings. Finally, Section D presents some two-dimensional applications.

A. Other Initial Conditions

1. Initial Conditions Prepared in High Field

Among the simplest variants are experiments where different high field conditions are prepared or detected in combination with the experimental field cycle of Figure 3.1. Throughout this section, comments about the prepared operator apply equally to the detected operator, and should really read prepared and/or detected. Examples of possible operators include time dependent states (such as transverse magnetization, I_+ or I_-) or non-equilibrium longitudinal order (such as dipolar or quadrupolar order). To within a proportionality constant, a dipolar or quadrupolar ordered spin system is described by a density operator

$$\rho_L = [3I_{zL}^2 - I(I+1)] \tag{6.1}$$

which is time independent (at least for times short compared to T_1).

In this section I repeat the calculation of Section III.B. All experimental conditions are assumed unchanged except for the possibility of a more general initial condition. The initial density operator $\rho(0)$ is most generally a sum over operators of arbitrary tensor rank and order rather than just the first rank tensor operator corresponding to Zeeman order (Equation (3.10)). Steps in the analysis of the signal function include reexpressing ρ in the local frame, allowing evolution under H_{loc} for a time t_1, returning to high field, taking the trace of ρ with the detected operator and finally integrating over the orientational distribution function $P(\Omega)$ to give the signal function $G(t_1)$. Well-known properties of the rotation matrices[7] are used to simplify the calculations. Two of the more important relationships are

$$D^{j*}_{\mu m}(\alpha,\beta,\gamma) \quad = \quad (-1)^{\mu-m}\, D^{j}_{-\mu-m}(\alpha,\beta,\gamma) \tag{6.2}$$

and the orthogonality condition

$$\int D^{j*}_{\mu m}\,(\alpha,\beta,\gamma)\; D^{j'}_{\mu' m'}(\alpha,\beta,\gamma)\; d\Omega \;=\; \frac{8\pi^2}{2j+1}\;\delta_{jj'}\delta_{\mu\mu'}\delta_{mm'} \tag{6.3}$$

For simplicity I assume that the initial operator $\rho_L(0)$ and the detected operator (which I will call Λ) are each proportional to a single spherical tensor operator. The generalization to cases where ρ is a sum over such tensors is trivial. Assuming that

$$\rho_L(0) \quad = \quad T^{j}_{kL} \tag{6.4}$$

ρ reexpressed in terms of molecular frame operators is

$$\rho_M(0) = \sum_{\kappa=-j}^{j} D^j_{\kappa k}(-\alpha,-\beta,0)\ T^j_{\kappa M} \tag{6.5}$$

Time-evolution is appended formally, and

$$\rho_M(t) = \sum_{\kappa=-j}^{j} D^j_{\kappa k}\ (-\alpha,-\beta,0)\ T^j_{\kappa M}(t) \tag{6.6}$$

At a time t_1, the intermediate field B_{int} is reapplied and in a short time ρ commutes with the high field Zeeman Hamiltonian. As in Chapter III, the signal function is the trace of the detected operator with the evolved operator integrated over all orientations;

$$G(t_1) = \int G(t_1,\Omega)d\Omega = \int Tr\ [\rho(t_1)\Lambda]\ P(\Omega)\ d\Omega \tag{6.7}$$

The trace is invariant to unitary transformations and it will again prove convenient to transform the observed operator Λ to the molecular frame rather than reexpressing the evolved density operator $\rho(t_1)$ in the laboratory frame (cf Equations (3.15) and (3.16)). If Λ is proportional to another laboratory frame spherical tensor, T^λ_{mL}, then in the molecular frame

$$\Lambda_M = \sum_{\mu=-\lambda}^{\lambda} D^\lambda_{\mu m}(-\alpha,-\beta,0)\ T^\lambda_{\mu M} \tag{6.8}$$

and the signal function is

$$G(t_1) = \int Tr\ [\{\sum_{\mu=-\lambda}^{\lambda} D^\lambda_{\mu m}\ T^\lambda_{\mu M}\}\ \{\sum_{\kappa=-j}^{j} D^j_{\kappa k}\ T^j_{\kappa M}(t_1)\}]\ P(\Omega)\ d\Omega \tag{6.9}$$

Rearranging Equation (6.9) so as to separate the integration over Ω from the trace over the operators,

$$G(t_1) = \mathrm{Tr}\ [\{ \sum_{\mu=-\lambda}^{\lambda} T^{\lambda}_{\mu M} \sum_{\kappa=-j}^{j} T^{j}_{\kappa M}(t_1\} \int D^{j}_{\kappa k}\ D^{\lambda}_{\mu m}\ P(\Omega)\ d\Omega)] \qquad (6.10)$$

Substituting for $D^{\lambda}_{\mu m}$ from Equation (6.2),

$$G(t_1) = \mathrm{Tr}\ [\{ \sum_{\mu=-\lambda}^{\lambda} T^{\lambda}_{\mu M} \sum_{\kappa=-j}^{j} T^{j}_{\kappa M}(t_1)\}(-1)^{\kappa-k} \int D^{j*}_{-\kappa-k}\ D^{\lambda}_{\mu m}\ P(\Omega)\ d\Omega)] \qquad (6.11)$$

For $P(\Omega)$ uniform over the sphere the integration over Ω is given by Equation (6.3) and

$$G(t_1) = \left[\frac{(-1)^{\kappa-k}}{2j+1} \sum_{\kappa=-j}^{j} \mathrm{Tr}\ [T^{j}_{\kappa M}(t_1)\ T^{j}_{-\kappa M}]\ \delta_{mk}\right] \qquad (6.12)$$

Equation (6.12) states that in a powder sample for the field-cycle of Figure 3.1 and a uniformly prepared $\rho(0)$, $G(t_1) = 0$ if the initial and detected operators are orthogonal, and the signal is maximized if $\Lambda = \rho(0)$. As long as this latter condition is satisfied all Λ of a given tensor rank result in identical selection rules and identical spectra independent of order. For $\rho(0) = I_+$ or I_-, the signal function is identical to that for $\rho(0) = I_z$. Practically it will always be easier to work with populations operators such as I_z than with coherences of the same rank.

Initial conditions of higher rank (e.g. dipolar or quadrupolar order) result in spectra where the selection rules governing line frequencies and intensities are derived from these higher rank tensors (e.g. the five second rank tensors if the initial condition is quadrupolar order). Time development of the second rank tensor operators ($j = 2$) in a spin-1 system is given in Section III.C (Equations (3.25) and (3.26)). Two of the five second rank tensors

(U_{2+} and U_0) are time-independent. Each of the others evolves at one of the frequencies corresponding to the ν_0, ν_+, or ν_- lines. If quadrupolar order is uniformly prepared and detected with unit efficiency in high field the zero field spectrum is the same three-line spectrum observed starting from Zeeman order except that 40% of the total order stored in the initial density operator does not evolve.

Techniques which prepare high field dipolar[124] and higher order operators (such as multiple quantum[100,101]) are known. If a spin temperature can be defined, then adiabatic demagnetization in the rotating frame[21-23] (ADRF) creates a state corresponding to pure truncated dipolar order. But when a spin temperature exists and dipolar order can be uniformly prepared the zero field spectrum is virtually guaranteed to be unstructured. The spin temperature hypothesis holds only in the limit of a large number of tightly coupled spins. For these "infinite" spin systems the zero field spectrum acquires the characteristic Kubo-Toyabe form discussed in Section IV.C.3. For isolated quadrupolar systems or where small groups of coupled spins are isolated from all others, ρ can be calculated for arbitrary high field preparation sequences but this requires foreknowledge of precisely those coupling constants which presumably are the goal of the experiment. Perhaps more troubling, it is the orientation-dependent values of the truncated Hamiltonians which determine the initial condition.

In disordered systems, few techniques exist for the uniform preparation of any type of order[125] other than Zeeman order (which nature provides). If the density operator prepared in high field is orientation-dependent it depends on the Euler angles α and β and the

same transformation $R(\Omega)$ which takes the spin system between the molecular and laboratory frames. If the initial condition is orientation-dependent then

$$\rho_L(0) = \sum_{j,k} T^j_{kL}(\Omega) \tag{6.13}$$

and Equations ((6.10)-(6.12))) no longer follow because the integration over Ω must include the (often rather involved) dependence of ρ on α and β. There is no general analytic solution of the form of Equations (3.21) or (6.12) to the intensities of zero field lines. This is a serious (in fact, fatal) handicap in the analysis of all but the simplest dipolar-coupled spin systems. For more than three coupled spins, the zero field spectrum $f(\omega)$ is often a nearly continuous absorption band. Then the intensities as well as the frequencies must be modeled if useful information is to be derived from the spectrum.

In spectra of isolated quadrupolar spins this is less of an objection. Complete information about $\tilde{V}$ can often be derived from the frequencies alone. (It will, of course, make modeling of any small dipolar couplings superposed on the quadrupolar spectrum virtually impossible.) In many quadrupolar systems, the existence of new selection rules associated with higher rank tensor operators may prove essential to a complete assignment of the quadrupolar tensors. Under dipole selection rules not all possible transition frequencies can be observed in spectra of half-integer quadrupolar spins with $I \geq 5/2$ (as explained in Section III.C). These dipole selection rules are overcome when $\rho(0)$ corresponds to a higher rank tensor. When a sample contains several inequivalent sites, the observation of these new lines may prove as important as the observation of the ν_0 line is in NQR studies

of spin-1 nuclei.

Generation of high field initial conditions proportional to higher rank tensors will not generally prove worth the effort. In any disordered system pulsed methods for the transformation of Zeeman order into other forms of order are inefficient precisely because sequences which uniformly prepare any given initial condition are unknown. Only populations survive the time it takes to travel between high and low fields; oherences prepared in ρ dephase and are lost. Thus, the prepared density operator is "smaller" than after equilibration in B_0 and results in correspondingly smaller signals. Any non-adiabatic preparation sequence suffers from this same objection. In the next section, I describe techniques which achieve the same end (non-dipole selection rules) with greater efficiency, in that the norm of ρ is more nearly conserved during the preparation sequence.

2. Demagnetization to Zero Field

This process has been described in detail in Chapter II. In this section I aim not to repeat that discussion but rather to approach it from a slightly different perspective. If a polarized sample is removed from the polarizing field so that the rate of change in H is slow compared to all the frequency differences between eigenstates the demagnetization is said to be adiabatic.[64] In the absence of spin-lattice relaxation, the full order prepared in high field is conserved and transported as populations to zero field and the norm of ρ is conserved during demagnetization. Depending upon the details of the spin system and the demagnetization that order can be distributed in ρ in many different ways but for isolated spins populations remain ordered according to energy level.

In the thermodynamic limit of large numbers of coupled spins evolution of ρ under adiabatic demagnetization in the laboratory frame (ADLF) is treated by invoking the spin temperature hypothesis.[24,25] At all times the density operator is described by a single spin temperature and at all fields remains proportional to the instantaneous Hamiltonian. If a spin temperature exists, then for B = 0 the demagnetized density operator is (to within a proportionality constant)

$$\rho_M(0) = H_{loc} \tag{6.14}$$

Again, where the spin-temperature hypothesis holds the zero field spectrum tends to be uninteresting. It is in precisely those systems where the spin temperature hypothesis does not apply that the zero field spectrum contains resolved structure. In the general case there may be a different "spin temperature" associated with each degree of freedom in the zero field Hamiltonian. The most general statement about the density operator after slow demagnetization to zero field is

$$[\rho_M, H_{loc}] = 0 \tag{6.15}$$

and the slower the rate of demagnetization the larger the ratio between the norm of ρ in high and zero fields. Except for the isotropic component of the J coupling tensor, the zero field Hamiltonians are exclusively second rank tensor operators. I choose to expand ρ as a sum over operators ζ_j such that

$$[\zeta_j, H_{loc}] = 0 \tag{6.16}$$

where the ζ_j constitute an orthonormal basis set

$$\mathrm{Tr}(\zeta_j \zeta_k) = \delta_{jk} \tag{6.17}$$

and

$$\rho_M = \sum_j a_j \zeta_j \tag{6.18}$$

For multispin Hamiltonians, the set of all operators ζ_j may be difficult to enumerate. Some general guiding principles exist. For any spin system and its Hamiltonian, H, the number of orthogonal operators which commute with H is one less than the number of different energy levels (the sum over all the populations being just the total number of spins and is fixed). As the Hamiltonians themselves consist of terms proportional to sums of spherical tensors, the ζ_j will also be proportional to sums of spherical tensors. The details of these operators ζ_j depend on the specifics of the spin system and the Hamiltonians. Two general cases can be specified:

1. The Hamiltonian is composed of two (or more) commuting operators. In high field the Zeeman Hamiltonian and the secular component of the dipole-dipole Hamiltonian comprise such a set. In zero field, the quadrupolar Hamiltonian is the sum of two terms: one proportional to the spin operator $(3I_z^2-I(I+1))$ and the second proportional to $\eta(I_x^2-I_y^2)$. For a spin-1 system, these terms commute. (For what should be obvious reasons I refer to the first term as "quadrupolar order" and the second as "eta order.") In either case, a set of operators which commute with H is given by either of these commuting operators and their powers and/or products. The set generated by this method will form a basis set of operators but will not generally be the orthonormal

basis set of the ζ_j. For example, quadrupolar order is a second rank tensor. Its square is a reducible fourth rank tensor which need not be orthogonal to it.

2. The Hamiltonian contains only non-commuting operators. An example is the zero field quadrupolar Hamiltonian of a half-integer spin nucleus. Then the only operators which commute with H are the powers of H. H^2, H^3,... are a basis set but, as in (1), not generally the orthonormal basis set of the ζ_j.

In either case, if the Hamiltonian contains only second rank tensor operators, the demagnetized operator ρ can only contain even rank operators. For isolated quadrupolar nuclei, the maximum rank spherical tensor operator in ρ is 2I, and for N coupled spin I nuclei no larger than 2NI.

Table 6.1: Operator Representations of Spin Density Matrices

Spin System	Dimension of ρ	Ranks of Operators in ρ
I = 1/2	2	1, 0
I = 1	3	2, 1, 0
2 × (I = 1/2)	4	2, 3×1, 2×0
I = 3/2	4	3, 2, 1, 0
I = 2	5	4, 3, 2, 1, 0
I = 5/2	6	5, 4, 3, 2, 1, 0
I = 3	7	6, 5, 4, 3, 2, 1, 0
I = 7/2	8	7, 6, 5, 4, 3, 2, 1, 0
3 × (I = 1/2)	8	3, 5×2, 9×1, 5×0

In the column "Rank of Operators", n×q means there are n orthogonal sets of qth rank tensors in an operator representation of ρ

Table 6.1 enumerates the number and rank of operators required to completely describe the density operator for various spin systems. Even though there are only three distinct energy levels in both I = 1

and I = 5/2 spin systems, the sets of operators ζ_j which describe these two systems are very different. For isolated spin-1 nuclei, the constants of the motion are precisely quadrupolar and eta order, two second rank tensors which are interconverted by rotations. For half-integer quadrupolar spins, only powers of H_Q itself commute with H_Q. For I = 5/2 the constants of the motion are not quadrupolar and eta order, but instead (in the limit of vanishing η) quadrupolar and hexadecapolar order, a fourth rank spherical tensor operator given by[126]

$$T_0^4 = \sqrt{\frac{1}{280}}\ \{35I_z^4 + 5[5-6I(I+1)]I_z^2 + 3[(I(I+1))^2-2I(I+1)]\} \qquad (6.19)$$

Figure 6.1 illustrates the difference between the two population operators which describe I = 1 and I = 5/2 spin systems in zero field.

What is the relevance of these rather arcane discussions? After demagnetization the norm of ρ is (ideally) not very different from its high field value and ρ contains only even rank tensor operators. It is, however, in eigenstates of H_{loc} and therefore time-independent; in the absence of any intercession by the experimentalist no useable signals emanate. If ρ can be perturbed so at to create coherence, transition frequencies might be observed which are determined by the selection rules corresponding to the matrix elements of the higher rank tensors created in ρ during the demagnetization. The next two sections deal with methods of creating and monitoring such coherence.

B. Zero Field NMR with Pulsed dc Fields

Two alternative zero field experiments are illustrated in Figure

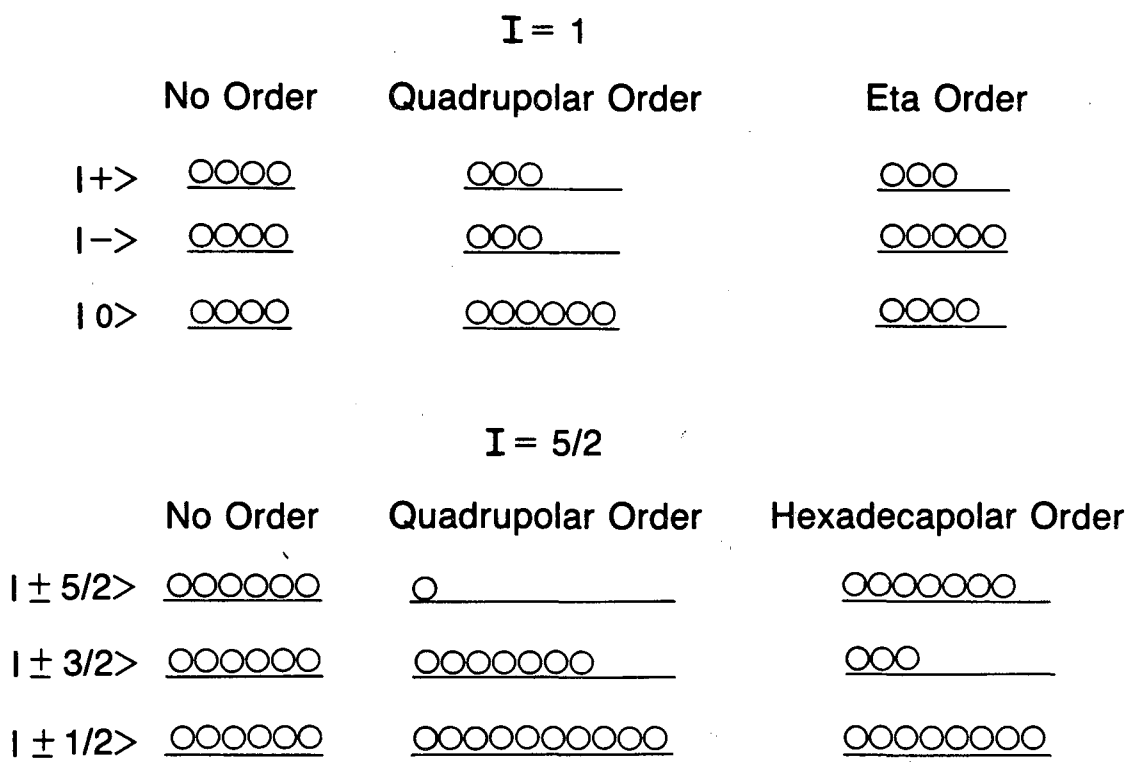

XBL 857-11255

Figure 6.1. Population operators for I = 1 and I = 5/2 (η = 0) in zero field. If all populations are equal, no order exists. I = 1 quadrupolar order corresponds to a difference in population between |0> and the average of the populations of |+> and |->; eta order, to the difference between |+> and |-> as shown at top. I = 5/2 quadrupolar order and hexadecapolar order correspond to the population ratios shown at bottom.

6.2. In these variants, the system is demagnetized not to some low field B_{int} but instead all the way to zero field. After demagnetization, a strong dc pulse ($\gamma B \gg H_{loc}$) is applied to the spin system. This transforms some of the nuclear spin order stored during demagnetization into coherences. (Similar narrowband behavior can be observed after application of a resonant rf pulse.[127]) At a time t_1, the intermediate field B_{int} may be suddenly turned on, trapping any coherence which has evolved into laboratory frame magnetization (as in Figure 6.2a); or, a second pulse may be applied which stores some of the evolved magnetization as population differences. Remagnetization to high field transforms these population differences into Zeeman order for observation (Figure 6.2b). The demagnetization process has been discussed in Chapter II. Some of the results of that discussion will be exploited below. For the moment, I concentrate instead on the zero field evolution period, t_1, instead.

Throughout this section, all operators are consistently expressed in the local (M) frame. The dc pulses, however, are inexorably tied to the laboratory (L) frame. A θ_z pulse applied in the laboratory frame will in fact correspond to a different pulse direction and effective nutation angle for each orientation of the local frame in the sample. Its effects are more simply described if the pulse is reformulated in the local frame. Assuming that laboratory frame pulses of only a single phase are applied, subsequent operations are marginally simplified if the pulse is applied along the laboratory z axis. Furthermore, it is convenient to express the transformation R which mediates between the two frames not in terms of rotations fixed in the laboratory frame but instead referenced to the local frame. In terms

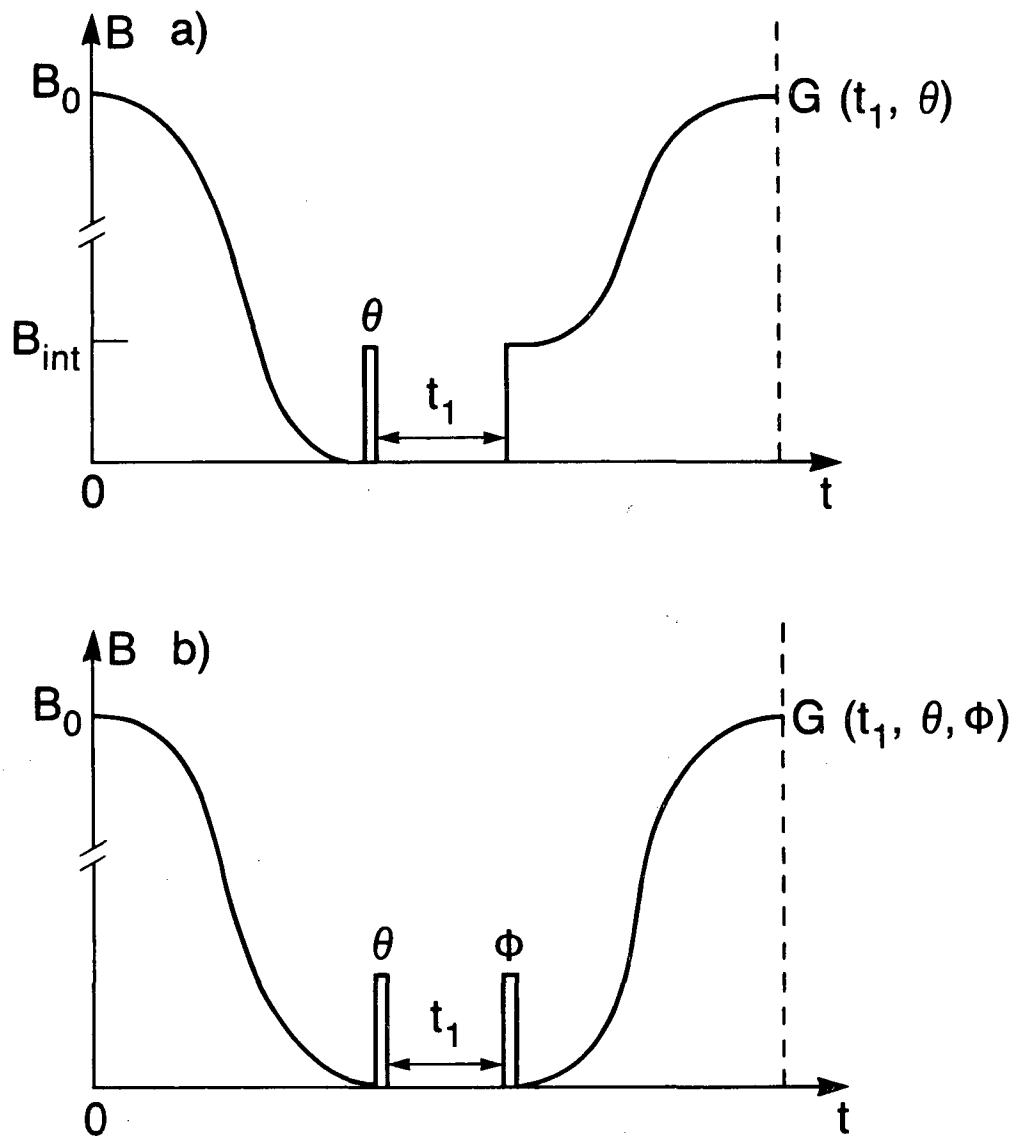

XBL 857-11249

Figure 6.2. Zero field NQR experiments using pulsed field to create and possibly store coherence. a). Sample is demagnetized to zero field. A dc pulse of length $\theta = \gamma_j B\tau$ applied to the sample creates coherence. A time t_1 later, the intermediate field is reapplied. This stores any magnetization which may have appeared along the axis defined by B_{int} for observation in high field as $G(t_1,\theta)$. b). A dc pulse of length θ creates coherence, and a time t_1 later a second dc pulse of length ϕ stores coherence as populations. The sample is remagnetized to high field where the signal $G(t_1,\theta,\phi)$ is observed.

of lab-based axes, I have defined

$$R^{-1}(\Omega)|L\rangle = \exp(-i\alpha I_{zL})\exp(-i\beta I_{yL})|L\rangle = |M\rangle \qquad (6.20)$$

The same rotations about fixed molecular frame axes effect the same transformation

$$R^{-1}(\Omega)|L\rangle = \exp(-i\alpha I_{zM})\exp(-i\beta I_{yM})|L\rangle = |M\rangle \qquad (6.21)$$

Wherever explicit forms for R are required in this chapter, the convenient if non-conventional representation of Equation (6.21) will be used. Transformed into the local frame,

$$\langle L|\exp(i\theta I_z)|L\rangle = \langle L|RR^{-1}\exp(i\theta I_z)RR^{-1}|L\rangle$$

$$= \langle M|\exp(-i\alpha I_z)\exp(-i\beta I_y)\exp(i\theta I_z)\exp(i\beta I_y)\exp(i\alpha I_z)|M\rangle \qquad (6.22)$$

where the pulse flip angle θ is defined for a field strength B_1, pulse length τ, and magnetogyric ratio γ by

$$\theta = 2\pi\gamma_j B_1 \tau \qquad (6.23)$$

The generalization to pulses applied along more than a single axis in the laboratory frame is tedious but straightforward.

The advantage of expressing ρ as a sum over spherical tensors should now be clear: under any number of frame transformations and/or strong dc pulses about whatever axis, order originally proportional to an nth rank tensor is transformed only into order associated with other nth rank tensors. Only time evolution transforms tensors of one rank into a second. Evolved order can be stored as a magnetization by a trapping field (as in Figure 6.2a) only if it corresponds to a first rank tensor; or, as a population difference by a second dc pulse (as in

Figure 6.2b) only if it corresponds to a tensor of the same rank as one of the ζ_j operators of Equation (6.18). Where the zero field NMR experiment described in Chapter III corresponds to autocorrelations of first rank tensors only, the one-pulse zero field experiment shown schematically in Figure 6.2a and described more fully below yields cross correlations between even rank ζ tensors and the first rank tensors (I_+, I_-, or I_0); the two-pulse zero field experiment of Figure 6.2b, auto- and cross-correlations of the ζ_j operators. The transition frequencies observed in this latter experiment are governed by the matrix elements of the even rank tensors ζ_j. The dipole selection rules of zero field NMR with sudden switching with $\rho(0)$ proportional to Zeeman order are overcome just as surely as they would be if high field initial conditions corresponding to higher forms of order could be created. One distinct advantage of zero field NMR or NQR with dc pulses is that there is less loss of signal intensity than might be achieved in any high field preparation schemes. Another possible advantage is discussed below in Section C.

The goal of the rest of this section is the calculation of the signal function $G(t_1)$ for the sequences of Figure 6.2. I specialize to the case $I = 1$ where these calculations are long and unwieldy but not undoable. Some experimental spectra derived by these two sequences are presented and briefly compared to theory. In either sequence the heart of the calculation is the transformation of the diagonal second-rank tensor operators U_0 and U_{2+}, corresponding to quadrupolar and eta order, under a dc pulse.

1. <u>Transformation and Evolution of Quadrupolar Order</u>

The first task is to find the form of the molecular frame

operator U_0 after the application of a θ pulse along the laboratory z-axis. A molecular frame form for the pulse is given in Equation (6.22). The transformed operator, $U_0(\theta)$, is

$$U_0(\theta) = R\exp(-i\theta I_z)R^{-1}U_0R\exp(i\theta I_z)R^{-1} \tag{6.24}$$

Explicit and lengthy calculations making liberal use of the relations in Table 3.2 give for a specific orientation Ω

$$U_0(\theta,\Omega) = a_0U_0 + a_{1+}U_{1+} + a_{1-}U_{1-} + a_{2+}U_{2+} + a_{2-}U_{2-} \tag{6.25}$$

with

$$\begin{aligned}
a_0 &= \frac{1}{4}\,[(3\cos^2\beta-1)^2 + 3\sin^2\beta\cos^2\beta\cos\theta + \frac{3}{2}\sin^4\beta\cos2\theta] \\
a_{1+} &= \sin\alpha\ c_1 + \cos\alpha\ c_2 \\
a_{1-} &= -\sin\alpha\ c_2 + \cos\alpha\ c_1 \\
a_{2+} &= -\sin2\alpha\ c_3 + \cos2\alpha\ c_4 \\
a_{2-} &= \sin2\alpha\ c_4 + \cos2\alpha\ c_3
\end{aligned} \tag{6.26}$$

where the coefficients c_1-c_4 are

$$\begin{aligned}
c_1 &= \frac{\sqrt{3}}{4}\sin\beta\cos\beta[(3\cos^2\beta-1)+2\cos\theta(\sin^2\beta-\cos^2\beta)-\sin^2\beta\cos2\theta] \\
c_2 &= \frac{\sqrt{3}}{4}\sin\beta\ [2\cos^2\beta\sin\theta + \sin^2\beta\sin2\theta] \\
c_3 &= \frac{\sqrt{3}}{8}\sin^2\beta\cos\beta\ \sin2\alpha(2\sin\theta-\sin2\theta)
\end{aligned} \tag{6.27}$$

$$c_4 = \frac{\sqrt{3}}{8} \sin^2\beta \cos 2\alpha[(1+\cos^2\beta)\cos 2\theta - 4\cos^2\beta\cos\theta + (3\cos^2\beta - 1)]$$

At a time t_1, the transformed operator $U_0(\theta,\Omega)$ evolves into

$$U_0(t_1,\theta,\Omega) = a_0U_0 + a_{2+}U_{2+} + a_{1+}(U_{1+}\cos\omega_{23}t_1 - I_x\sin\omega_{23}t_1) \tag{6.28}$$

$$+ a_{1-}(U_{1-}\cos\omega_{31}t_1 - I_y\sin\omega_{31}t_1) + a_{2-}(U_{2-}\cos\omega_{12}t_1 - I_z\sin\omega_{12}t_1)$$

2. <u>Transformation and Evolution of Eta Order</u>

In analogy to Equations (6.24) and (6.25),

$$U_{2+}(\theta) = R\exp(-i\theta I_z)R^{-1}U_{2+}R\exp(i\theta I_z)R^{-1} \tag{6.29}$$

and

$$U_{2+}(\theta,\Omega) = b_0U_0 + b_{1+}U_{1+} + b_{1-}U_{1-} + b_{2+}U_{2+} + b_{2-}U_{2-} \tag{6.30}$$

where

$$b_0 = \sqrt{3}\ \{\frac{\cos 2\alpha}{4} \sin^2\beta[(1+\cos^2\beta)\cos 2\theta - 4\cos^2\beta\cos\theta + (3\cos^2\beta - 1)]$$
$$+ \frac{\sin 2\alpha}{2} \sin^2\beta\cos\beta[\sin 2\theta - 2\sin\theta]\}$$

$$b_{1+} = \cos\alpha\cos 2\alpha\ c_5 + \cos\alpha\sin 2\alpha\ c_6 + \sin\alpha\cos 2\alpha\ c_7 + \sin\alpha\sin 2\alpha\ c_8$$

$$b_{1-} = \cos\alpha\cos 2\alpha\ c_7 + \cos\alpha\sin 2\alpha\ c_8 - \sin\alpha\cos 2\alpha\ c_5 - \sin\alpha\sin 2\alpha\ c_6$$

$$b_{2+} = \cos^2\beta\cos 2\theta + \sin^2\beta\cos\theta + \frac{1}{4}\cos^2 2\alpha\sin^4\beta(\cos 2\theta - 4\cos\theta + 3) \tag{6.31}$$

$$b_{2-} = \frac{\sin 4\alpha}{8} \sin^4\beta[\cos 2\theta - 4\cos\theta + 3] - \cos\beta[\sin^2\beta\sin\theta + \frac{1}{2}(1+\cos^2\beta)\sin 2\theta]$$

where

$$c_5 = \sin\beta[\tfrac{1}{2}(1+\cos^2\beta)\sin2\theta - \cos^2\beta\sin\theta]$$

$$c_6 = \sin\beta\cos\beta(\cos2\theta-\cos\theta) \tag{6.32}$$

$$c_7 = \frac{\sin\beta\cos\beta}{2}[3\sin^2\beta + (\cos^2\beta-\sin^2\beta)\cos\theta - (1+\cos^2\beta)\cos2\theta]$$

$$c_8 = \sin\beta[\cos^2\beta\sin2\theta + (\sin^2\beta-\cos^2\beta)\sin\theta]$$

As previously (Equation (6.28)) at a time t_1

$$U_{2+}(t_1,\theta,\Omega) = b_0U_0 + b_{2+}U_{2+} + b_{1+}(U_{1+}\cos\omega_{23}t_1-I_x\sin\omega_{23}t_1) \tag{6.33}$$

$$+ b_{1-}(U_{1-}\cos\omega_{31}t_1-I_y\sin\omega_{31}t_1) + b_{2-}(U_{2-}\cos\omega_{12}t_1-I_z\sin\omega_{12}t_1)$$

These compact forms (Equations (6.29) and (6.33)) show what operators are created after a pulse is applied to a demagnetized spin-1 nucleus. The signal observed in either of the experiments of Figure 6.2 depends on the distribution of initial conditions $\rho(0, \Omega)$. Most generally,

$$\rho(0,\Omega) = k_1(\Omega)U_0 + k_2(\Omega)U_{2+} \tag{6.34}$$

and the initially prepared operator is a function of Ω. In Chapter II I showed that, ignoring the singular points which exist for demagnetization along any of the molecular frame principal axes, after adiabatic demagnetization of an isolated spin-1 nucleus the initial condition is independent of Ω. This is a particularly fortuitous result and all subsequent calculations of signals $G(t_1)$ are based on this assumption. The demagnetized density operator is then

$$\rho(0) = \frac{1}{2}(\sqrt{3}\,U_0 + U_{2+}) \tag{6.35}$$

independent of Ω. (Depending upon the sign of the quadrupolar coupling constant, there may be an overall sign change in ρ.) Similarly,

$$\rho(t_1,\theta,\Omega) = \sqrt{3}\,U_0(t_1,\theta,\Omega) + U_{2+}(t_1,\theta,\Omega) \tag{6.36}$$

3. Calculation of Signals

Two cases need be treated, corresponding to the two experimental sequences of Figure 6.2.

a. Sudden switching of B

Evolution is terminated by the rapid reapplication of a large static magnetic field B_{int}. Just as in Chapters III-V, the observable is I_{zL}, or, in the molecular frame where the density operator is expressed

$$I_{zL} = \cos\beta I_{zM} - \cos\alpha\sin\beta\, I_{xM} + \sin\alpha\sin\beta I_{yM} \tag{6.37}$$

and the signal function for a particular orientation is

$$G(t_1,\theta,\Omega) = \mathrm{Tr}\,[\rho(t_1,\theta,\Omega)(\cos\beta I_{zM} - \cos\alpha\sin\beta I_{xM} + \sin\alpha\sin\beta I_{yM})] \tag{6.38}$$

As usual, the signal function is

$$G(t_1,\theta) = \int G(t_1,\theta,\Omega)\, P(\Omega)\, d\Omega \tag{6.39}$$

Useful angular averages of the trigonometric functions appear in Table 6.2. In combination with the orthogonality conditions of Equations (3.27) and (3.28) only a small number of terms contribute to the integral of Equation (6.39). The signal function integrated over a uniform powder distribution for that portion of ρ proportional to quadrupolar order is

$$G_Q(t_1,\theta) = \frac{\sqrt{3}}{15}\,[(2\sin 2\theta+\sin\theta)(\sin\omega_{23}t_1+\sin\omega_{31}t_1)] \tag{6.40}$$

and for that portion of ρ proportional to η order

$$G_\eta(t_1,\theta) = \frac{1}{15}\{[(2\sin 2\theta+\sin\theta)(\sin\omega_{23}t_1+2\sin\omega_{12}t_1)] + (\sin 2\theta + 2\sin\theta)\sin\omega_{31}t_1\} \tag{6.41}$$

Table 6.2: Averages of Trigonometric Functions

A. Functions of Polar Angle β

$\langle\cos^2\beta\rangle = \frac{1}{3}$	$\langle\sin^2\beta\rangle = \frac{2}{3}$	$\langle\cos^2\beta\sin^2\beta\rangle = \frac{2}{15}$	$\langle\cos^4\beta\sin^2\beta\rangle = \frac{2}{35}$
$\langle\cos^4\beta\rangle = \frac{1}{5}$	$\langle\sin^4\beta\rangle = \frac{8}{15}$	$\langle\cos^2\beta\sin^4\beta\rangle = \frac{8}{105}$	$\langle\cos^4\beta\sin^4\beta\rangle = \frac{8}{315}$
$\langle\cos^6\beta\rangle = \frac{1}{7}$	$\langle\sin^6\beta\rangle = \frac{16}{35}$	$\langle\cos^6\beta\sin^2\beta\rangle = \frac{2}{63}$	$\langle\cos^2\beta\sin^6\beta\rangle = \frac{16}{315}$
$\langle\cos^8\beta\rangle = \frac{1}{9}$	$\langle\sin^6\beta\rangle = \frac{128}{315}$	$\langle\cos^n\beta\rangle = \frac{1}{n+1}$	$\langle\sin^n\beta\rangle = \frac{n(n-2)\ldots 2}{(n+1)(n-1)\ldots 3}$ for n even

B. Functions of Azimuthal Angle α

$\langle\sin^2 n\alpha\rangle = \langle\cos^2 n\alpha\rangle = \frac{1}{2}$ $\quad\langle\sin^4 n\alpha\rangle = \langle\cos^4 n\alpha\rangle = \frac{3}{8}$ $\quad\langle\cos^2 n\alpha\sin^2 n\alpha\rangle = \frac{1}{8}$

$\langle\cos^2\alpha\cos 2\alpha\rangle = -\langle\sin^2\alpha\cos 2\alpha\rangle = \frac{1}{4}$ $\quad\langle\cos^6 n\alpha\rangle = \langle\sin^6 n\alpha\rangle = \frac{5}{16}$

Predictions as to the flip angle dependence of the signal intensities for each of these contributions separately are shown in Figure 6.3a and b. The total signal is the sum over these two terms weighted by the k_j coefficients. For the initial condition described in Equation (6.36), the predicted signal intensities are shown in Figure 6.3c. Some experimental results are shown in Figure 6.4. It is reasonable to compare theoretical calculations for isolated spins only to the

Figure 6.3. Coefficients from Equations (6.40) and (6.41) as a function of θ corresponding to the production and detection of signals proportional to sin ωt for initial conditions corresponding to uniformly prepared and detected a). quadrupolar order; b). eta order; and c). the density operator of Equation (6.35).

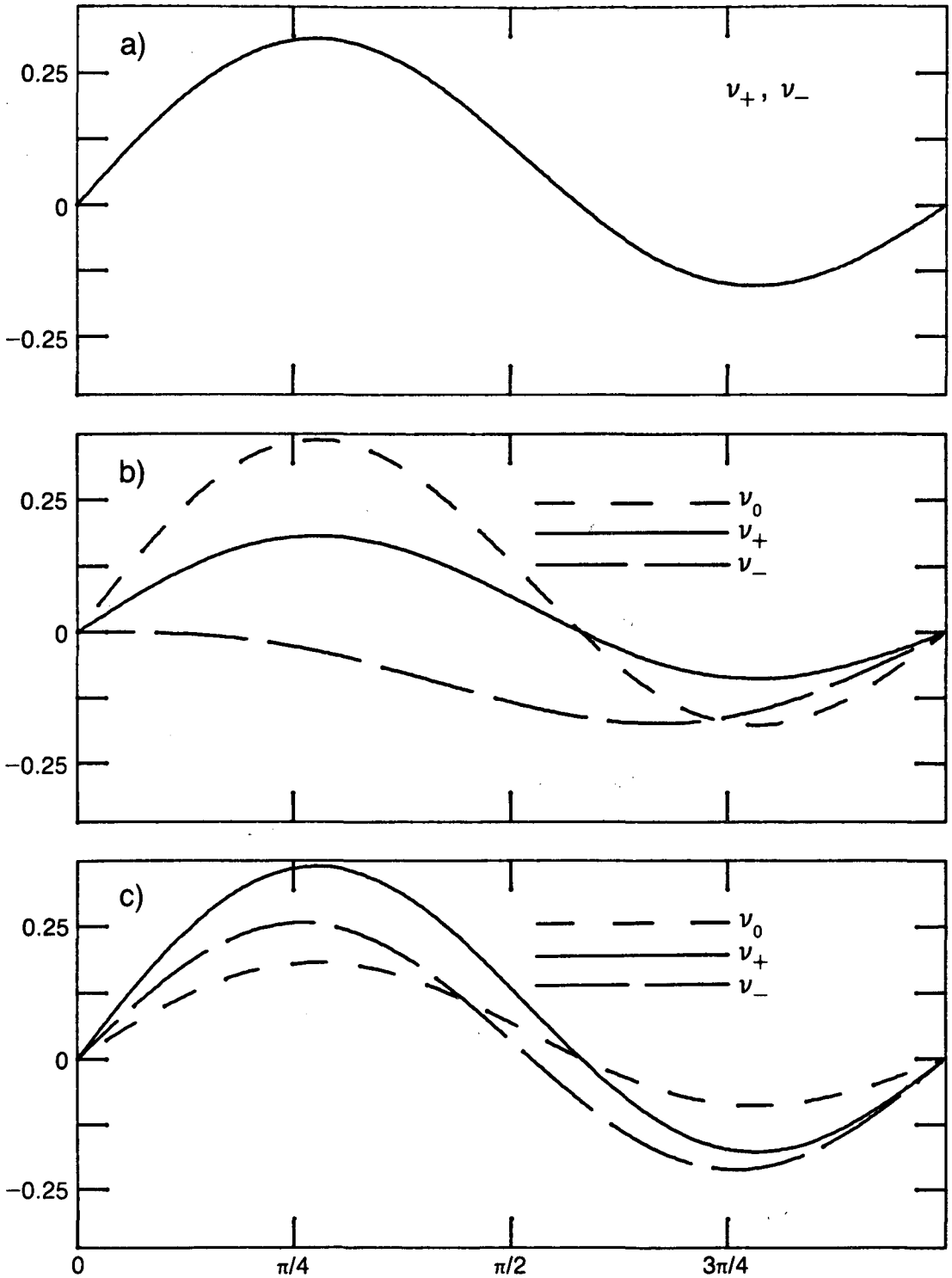

XBL 857-11242

Figure 6.4. Experimental one-pulse spectra (sine Fourier transforms) of DMB for a). $\theta = 40^{o}$; b). $\theta = 60^{o}$; c). $\theta = 90^{o}$; d). $\theta = 120^{o}$; e). $\theta = 135^{o}$; f). $\theta = 180^{o}$. For small flip angles, the spectra are relatively undistorted. As predicted, the ν_{+} lines grow in much more rapidly than ν_{-} or ν_{0}.

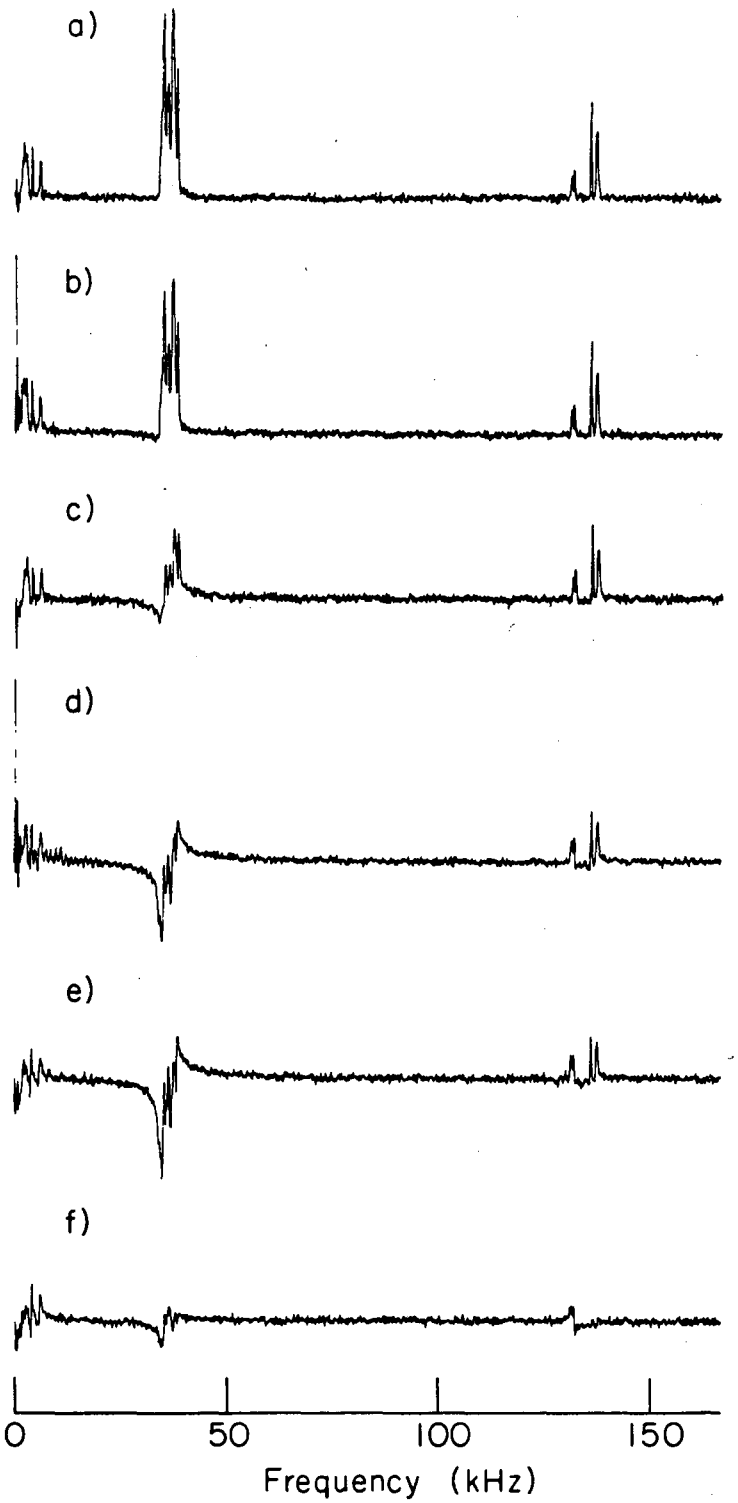

XBL 858-3507

intensities of the aromatic ring sites, which are much more isolated than are the the methyl group deuterons. The agreement between the theoretical predictions of Equations (6.40) and (6.41) and the observed spectra is not particularly striking. As predicted by theory, the ν_+ lines grow in somewhat more rapidly and are always stronger than either the ν_0 or ν_- lines, but the precise flip-angle dependence of Figure 6.3 is not reproduced. It is gratifying to observe that for flip angles $\approx \pi$, a minimum in the signal intensity is observed. This, at least, is consistent with theory.

Along axes other than that of the pulse, no signal should be observed in polycrystalline samples. The integration over α and β guarantees that magnetization can only appear along the axis of the applied field. This result is well-known in more traditional pulsed NQR[48] applications. Equivalent spectra are expected whether the the field cycle is executed as in Figure 6.1, or inverted (i.e. the intermediate field is suddenly turning off and a time t_1 later, order is stored with a short pulse).

b. Two-Pulse Experiments

Evolving coherence can also be stored for later observation by a second dc field pulse with flip angle ϕ and[62,128]

$$\rho(t_1,\theta,\phi,\Omega) = R\exp(-i\phi I_z)R^{-1}\exp(-iHt)R\exp(-i\theta I_z)R^{-1}\rho(0)$$
$$R\exp(i\theta I_z)R^{-1}\exp(iHt)R\exp(i\phi I_z)R^{-1} \qquad (6.42)$$

Remagnetization to high field restores that part of $\rho(t_1,\theta,\phi)$ which is proportional to $\rho(0)$ as Zeeman order suitable for detection. (The remainder of the diagonal elements of $\rho(t_1,\theta,\phi)$ remagnetize to quadrupolar order in high field. I will not concern myself with this

potential complication.) The detected operator is therefore identical to the initial operator, and the signal function is

$$G(t_1,\theta,\phi) = \int G(t_1,\theta,\phi,\Omega)\ P(\Omega)\ d\Omega = \int Tr[\rho(0)\rho(t_1,\theta,\phi,\Omega)]\ P(\Omega)\ d\Omega \quad (6.43)$$

Playing at old tricks (Equations (3.15)) again, the signal function is more readily calculated if the second pulse is treated as if it operated on the detected operator (with a negative flip angle) rather than on the evolved operator, and

$$\begin{aligned} G(t_1,\theta,\phi,\Omega) &= Tr\ \Big[R\exp(-i\phi I_z)R^{-1}\exp(-iHt)R\exp(-i\theta I_z)R^{-1}\rho(0) \\ &\qquad R\exp(i\theta I_z)R^{-1}\exp(iHt)R\exp(i\phi I_z)R^{-1}\ \rho(0)\Big] \\ &= Tr\Big[\{\exp(-iHt)R\exp(-i\theta I_z)R^{-1}\rho(0)R\exp(i\theta I_z)R^{-1}\exp(iHt)\} \\ &\qquad \{R\exp(i\phi I_z)R^{-1}\ \rho(0)R\exp(-i\phi I_z)R^{-1}\}\Big] \\ &= Tr\ [\rho(t_1,\theta,\Omega)\ \rho(0,-\phi,\Omega)] \end{aligned} \quad (6.44)$$

and

$$G(t_1,\theta,\phi) = \int Tr[\rho(t_1,\theta,\Omega)\rho(0,-\phi,\Omega)]\ P(\Omega)\ d\Omega \quad (6.45)$$

Substituting for ρ from Equation (6.34),

$$\begin{aligned} G(t_1,\theta,\phi) = \int Tr\ [&\{k_1U_0(t_1,\theta,\Omega)+k_2U_{2+}(t_1,\theta,\Omega)\} \\ &\{k_1U_0(0,-\phi,\Omega)+k_2U_{2+}(0,-\phi,\Omega)\}]\ P(\Omega)\ d\Omega \end{aligned} \quad (6.46)$$

The components of Equation (6.46) can be found elsewhere in this chapter (Equations (6.28),(6.33), (6.35), and Table 6.2). Three types of terms contribute to the signal. First, terms which originate as quadrupolar order in the initial condition and which are detected as

quadrupolar order in the detected operator. Second, terms which originate as eta order in the initial condition and which are detected as eta order in the detected operator. And last, terms which originate as quadrupolar order and are detected as eta order, or vice versa. Any pair of pulses will prepare and store some component of the total spin order, and no pair of pulses can force all of the initially prepared spin order to evolve. The signal amplitude is maximized for $\theta + \phi = 2n\pi$ (thus guaranteeing that for $t_1 = 0$, $G(t_1) = 1$; the first point in the free induction decay corresponds to the area under the spectrum). A general solution to Equation (6.43) is

$$G(t_1,\theta,\phi) = d_0 + d_{2+} + d_{1+}\cos\omega_{23}t_1 + d_{1-}\cos\omega_{31}t_1 + d_{2-}\cos\omega_{12}t_1 \quad (6.47)$$

where

$$d_j = \langle(a_j(\theta)+b_j(\theta))(a_j(-\phi)+b_j(-\phi))\rangle \quad (6.48)$$

and the angle brackets < > indicate an averaging over all orientations, Ω. For uniformly prepared initial conditions all autocorrelations ($\langle a_j a_j\rangle$ or $\langle b_j b_j\rangle$) contribute to the signal but the only non-zero cross-correlations are $\langle a_{1+}b_{1+}\rangle = -\langle a_{1-}b_{1-}\rangle$. All the correlation coefficients are given in Table 6.3. Figure 6.5 shows graphically the correlation coefficients for $\phi = -\theta$, where the total evolving signal intensity is maximized. As field pulses of only a single polarity are currently available, this sequence is mimicked by a (θ, $2\pi-\theta$) sequence of pulses. Figure 6.6 plots the predicted line intensities for the same two-pulse sequence assuming the initial condition of Equation (6.33). The entries in Table 6.3 predict that the spectrum is independent of which pulse comes first. Figure 6.7 compares the

Figure 6.5. Coefficients from Table 6.3 for $\phi = 2\pi - \theta$, corresponding to the production and detection of signals proportional to cos ωt for initial conditions corresponding to uniformly prepared and detected a). quadrupolar order; b). eta order; c). cross terms between quadrupolar and eta order. Heavy lines correspond to order stored as non-evolving U_{2+} or U_0 operators after the pulse. The amount of non-evolving order is independent of the relative amounts of quadrupolar and eta order. Only coefficients of ν_+ and ν_- terms are effected by the cross terms.

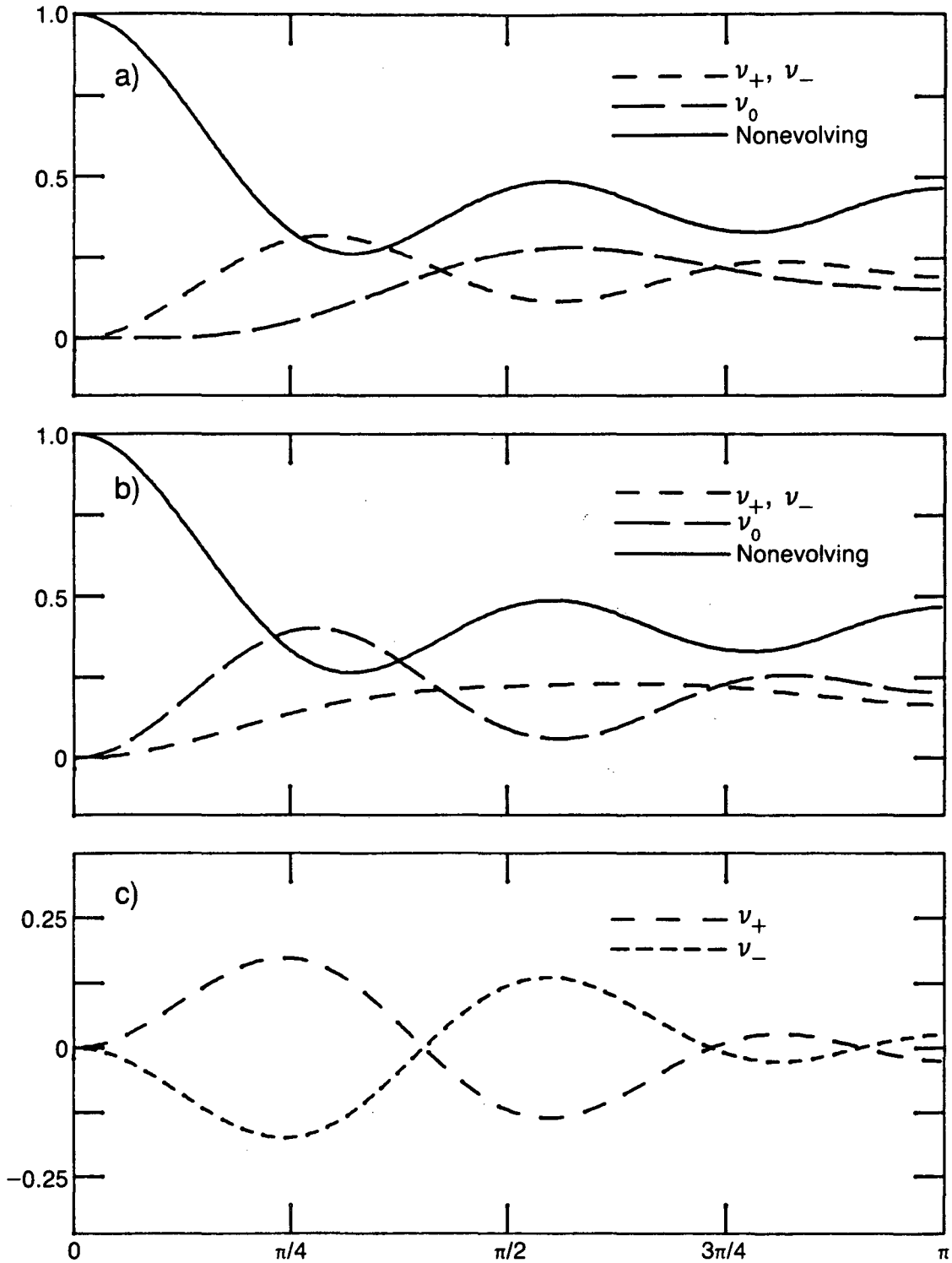

XBL 857-11244

Figure 6.6. Theoretical intensities observed in (θ, 2π - θ) two-pulse zero field experiment for the initial density operator and the detected operator proportional to ρ of Equation (6.35). The minimum in the nonevolving component of the stored order is observed for $\theta \sim 55^{\circ}$.

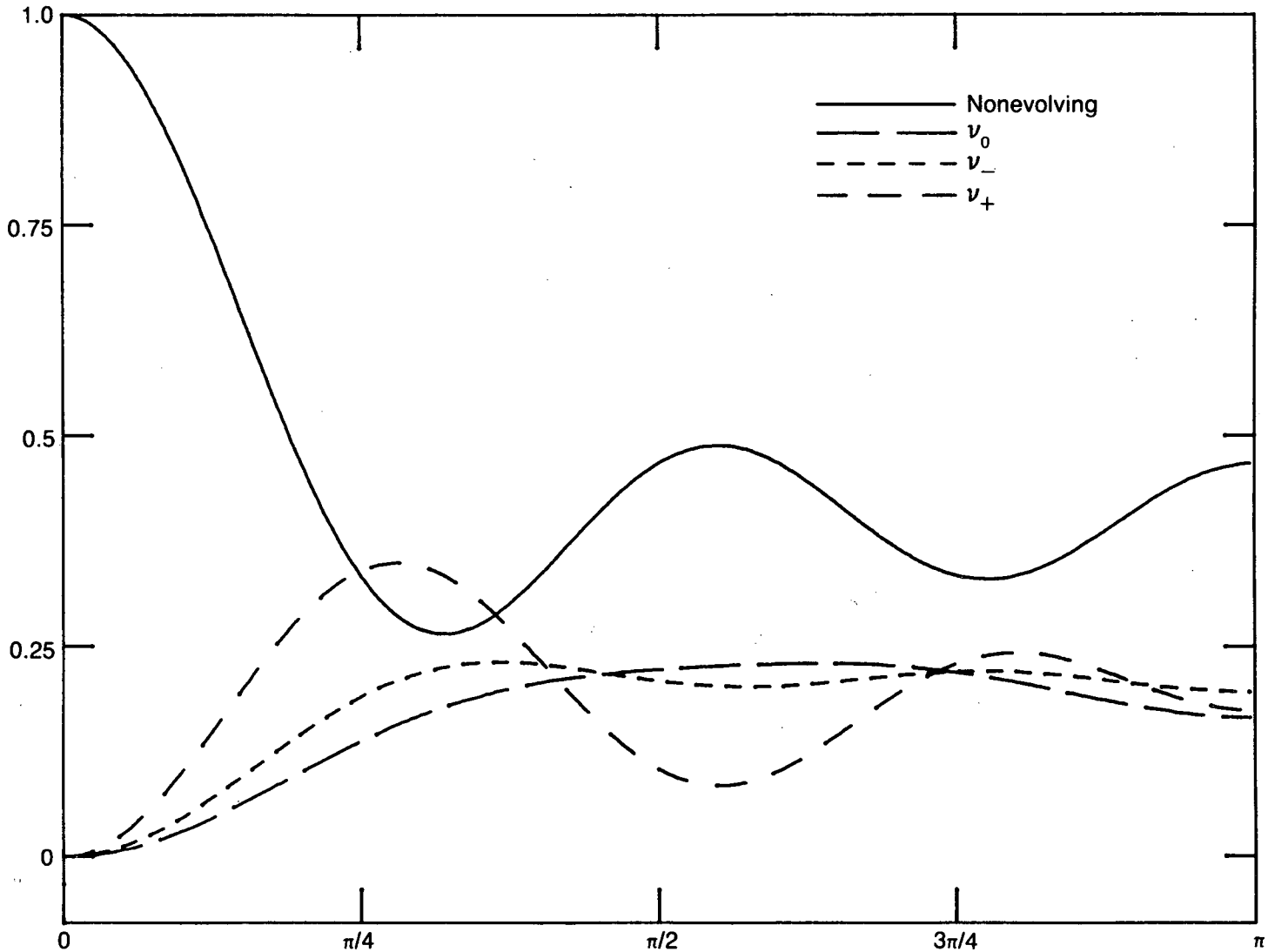

XBL 857-11243

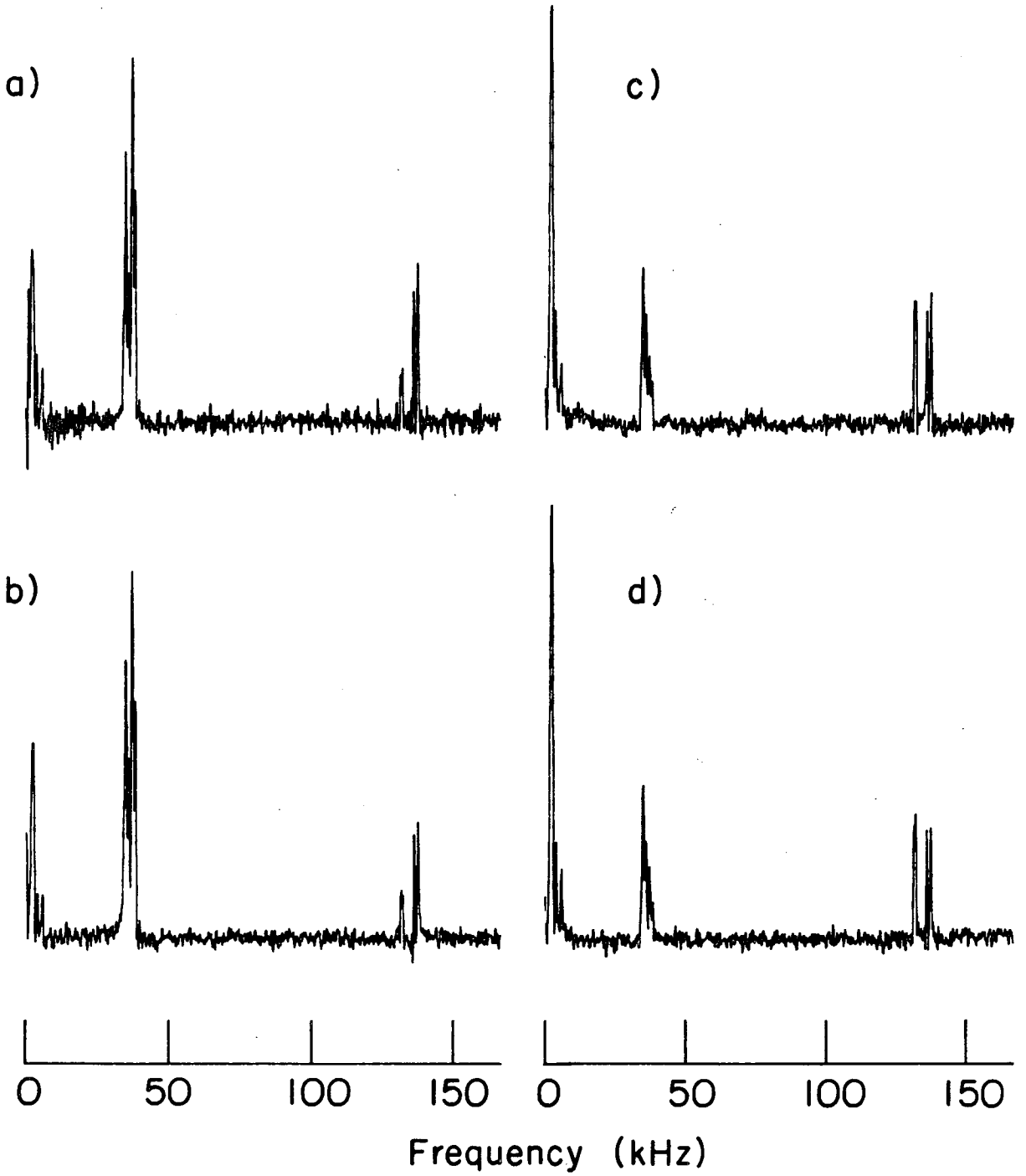

Figure 6.7. Experimental demonstration of the equivalence between (θ, 2π - θ) sequence and (2π-θ, θ) sequence for the two-pulse experiment on DMB. a). (45°, 315°) sequence. b). (315°, 45°) sequence. c). (90°, 270°) sequence. d). (270°, 90°) sequence.

experimentally observed spectra of perdeuterated DMB observed with a two-pulse (θ, $2\pi-\theta$) sequence and with a ($2\pi-\theta,\theta$) sequence. As predicted, the spectra are virtually identical.

The maximum evolving magnetization, integrated over the powder distribution, appears for $\theta \sim 55^{o}$, and approximately 70% of the prepared order is transformed into time-dependent eigenstates (as

Table 6.3: Correlation Coefficients for Two-Pulse Experiments

Term	n	m_1	m_2	m_3	m_4	m_5	m_6	m_7	m_8	m_9
$\langle a_0(\theta)a_0(-\phi)\rangle$	9	3	2	2	8	8	4	0	0	0
$\langle a_{1+}(\theta)a_{1+}(-\phi)\rangle$	3	3	-3	0	5	2	-2	-9	-18	6
$\langle a_{2+}(\theta)a_{2+}(-\phi)\rangle$	3	3	0	-3	4	7	-4	-12	-3	-6
$\langle b_0(\theta)b_0(-\phi)\rangle$	1	9	0	-9	12	21	-12	-36	-9	36
$\langle b_{1+}(\theta)b_{1+}(-\phi)\rangle$	1	9	-3	-6	13	16	-10	-33	-12	6
$\langle b_{2+}(\theta)b_{2+}(-\phi)\rangle$	9	3	2	2	8	8	4	0	0	0
$\langle b_{2-}(\theta)b_{2-}(-\phi)\rangle$	1	9	-12	3	16	1	-4	-24	-69	-30
$\langle b_{1+}(\theta)a_{1+}(-\phi)\rangle$	$\sqrt{3}/4$	0	-23	23	16	-80	32	-72	-120	-12

Expectation values of the coefficients are given by

$$\frac{n}{315}\Big[\, m_1 + m_2(\cos\theta+\cos\phi) + m_3(\cos2\theta+\cos2\phi) + m_4\cos\theta\cos\phi + m_5\cos2\theta\cos2\phi + m_6(\cos\theta\cos2\phi+\cos\phi\cos2\theta) + m_7\sin\theta\sin\phi \; m_8\sin2\theta\sin2\phi + m_9(\sin\theta\sin2\phi+\sin2\theta\sin\phi)\,\Big]$$

Correlation coefficients not listed are zero except

$\langle a_{1-}(\theta)a_{1-}(-\phi)\rangle = \langle a_{1+}(\theta)a_{1+}(-\phi)\rangle$; $\langle b_{1-}(\theta)b_{1-}(-\phi)\rangle = \langle b_{1+}(\theta)b_{1+}(-\phi)\rangle$

$\langle a_{1-}(\theta)b_{1-}(-\phi)\rangle = -\langle a_{1+}(\theta)b_{1+}(-\phi)\rangle$; $\langle a_{2-}(\theta)a_{2-}(-\phi)\rangle = \langle a_{2+}(\theta)a_{2+}(-\phi)\rangle$

compared to 60% starting from a high field quadrupolar ordered state and suddenly shutting off and on the external field). Figures 6.8-6.10

give some experimental data obtained by the (θ, 2π-θ) sequence described above. Figure 6.8 is a rather complete set of experiments on DMB as a function of θ. As predicted in Figure 6.6, the intensity of the ν_+ line approaches its maximum intensity very much more rapidly than the ν_- or ν_0 lines at the same site. For $\theta<\pi/2$, the agreement is qualitatively good. At larger flip angles, however, phase distortions appear in the spectrum which are not predicted by the theoretical treatment, and which are exacerbated as θ approaches π.

The spectra of the -CD_3 group are quite complex. In this very strongly coupled spin system, it is not surprising that a treatment based on the assumption of an isolated spin has little predictive quality. Overall, the signal-to-noise ratio in this two-pulse experiment appears not very different from the signal-to-noise ratio of the experiment described in Chapter III. It is surprising, and may provide some explanation for why the model calculations fail to reproduce the observed spectra, that the signal intensity at the ring sites is somewhat higher than in the direct, sudden-switching experiments of all previous chapters. This is almost certainly a signal that homonuclear level-crossings during the demagnetization transfer order back and forth between the rapidly-relaxing methyl group deuterons and their more sluggish ring-site neighbors. In the presence of such cross-relaxation during the demagnetization-remagnetization sequence, and because the extent of cross-relaxation is almost certainly orientation dependent, the calculations of Equations (6.28)-(6.43) cannot be expected to correspond too closely to experimental reality.

Figure 6.8. Sequence of two-pulse ^{2}D NQR spectra of DMB as a function of flip angle θ in (θ, 2π - θ) sequence. a). $\theta = 30^o$; b). $\theta = 45^o$; c). $\theta = 75^o$; d). $\theta = 90^o$; e). $\theta = 120^o$; f). $\theta = 135^o$; g). $\theta = 150^o$; h). $\theta = 180^o$. For small flip angles, the intensities of the ring sites lines follow roughly the predictions of Figure 6.6 but for larger flip angles the agreement is less good. Most spectra are a the sum over a pair of zero field FID's with each setting of the flip angle, repeated at 7.5 s intervals for a total of 512 points separated by 3 μs in t_1.

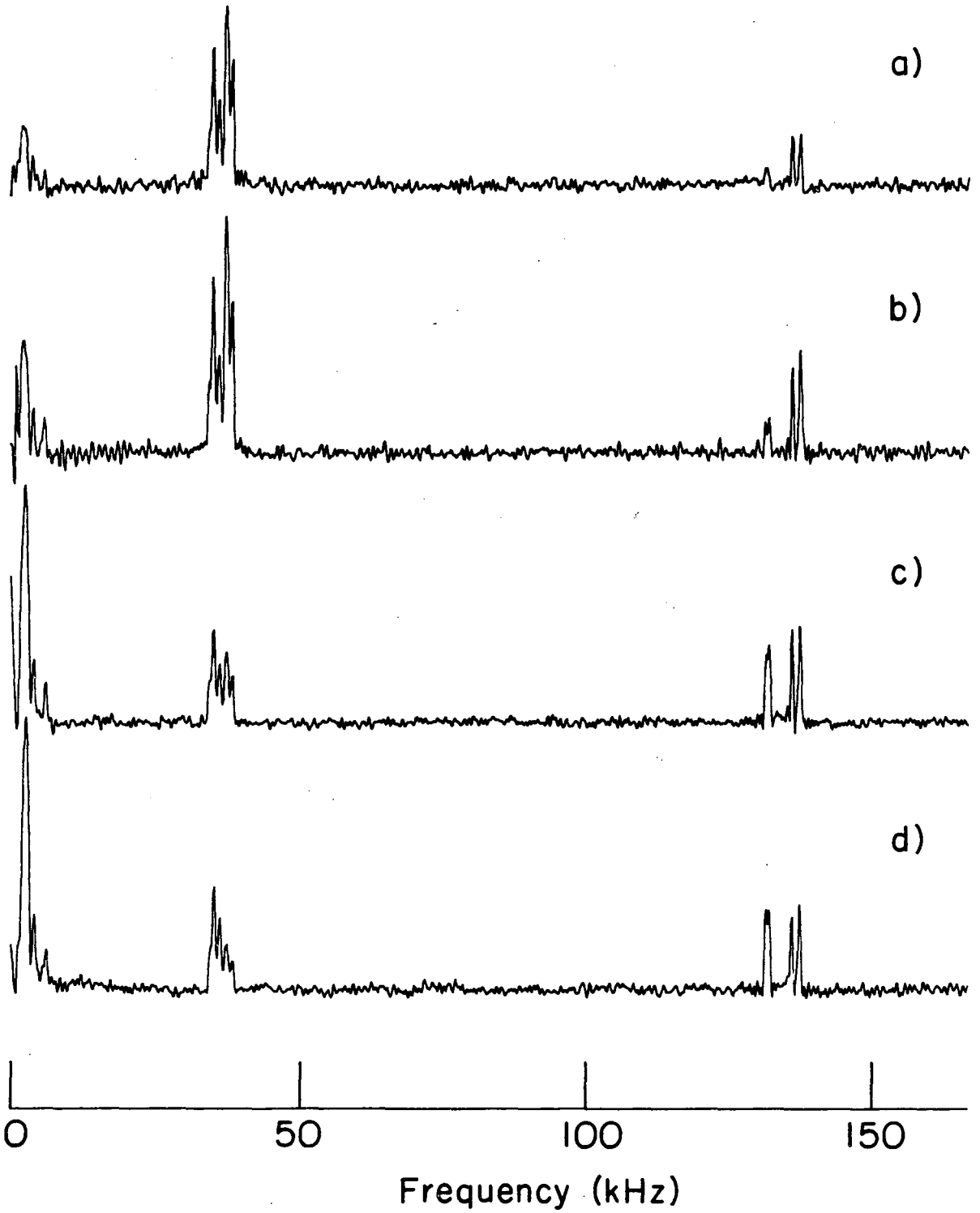

XBL 858-3503

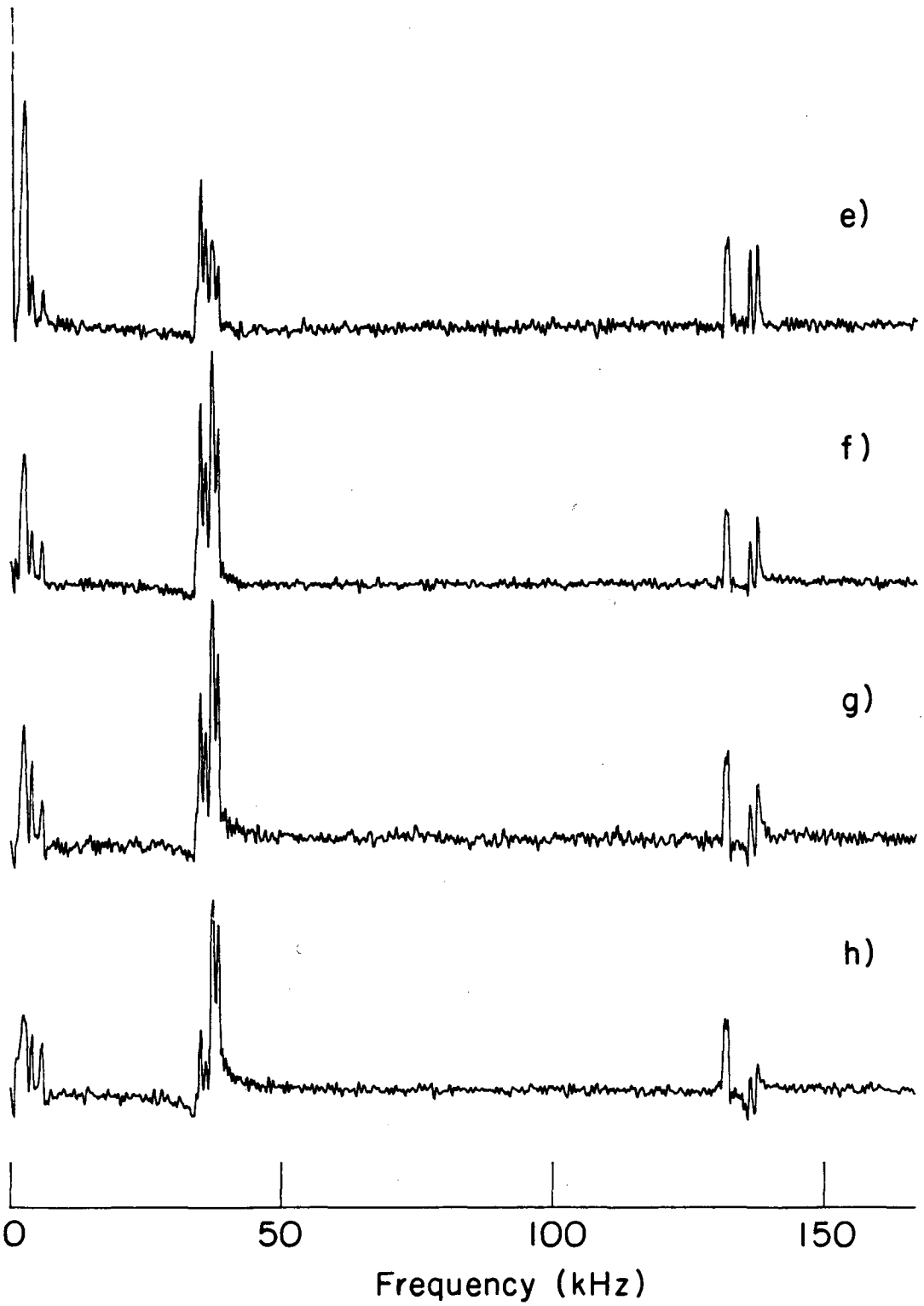

XBL 858-3544

Figure 6.9 shows two-pulse zero field NQR spectra of perdeuterated DMN. Compared to the spectrum of Figure 5.10, the signal intensity from the $-CD_3$ group is greatly depressed. This is almost certainly due to low field relaxation. In order to better satisfy the conditions for adiabaticity, the decay of the field from ~100 gauss to zero was purposely slowed form ~10ms to ~40ms. During this longer time in applied fields no larger than the local fields, magnetization (or whatever type of order it corresponds to at low field) stored in the $-CD_3$ group in high field largely disappears. The low field T_1 is ~25-40 ms. As in the spectra of DMB, the high frequency ν_+ lines grow in quite rapidly while the lower frequency ν_- and ν_0 lines reach the full intensity only for much longer pulses. For long pulses ($\theta \sim \pi$) some of the high frequency lines invert, while others seem unaffected in intensity over a broad range of flip angles. The large θ behavior is very different from that of either the theory or DMB.

Finally, in Figure 6.10 I show two two-pulse spectra of perdeuterated malonic acid ($CD_2(COOD)_2$). In malonic acid, there appears to be little of the distortion or line inversion observed in either DMB or DMN for large flip angles. Splittings are observed in nearly every high frequency line. As there are only four distinct deuterium quadrupolar coupling constants in malonic acid[129] these splittings are almost certainly due to dipole-dipole couplings between sites which have not been incorporated into the model for the intensities.

4. Summary

Summarizing the results of this discursion into the land of the spin-1: experiments using pulsed dc fields to coherently excite

Figure 6.9. Sequence of two-pulse ^{2}D NQR spectra of DMN as a function of flip angle θ in (θ, 2π - θ) sequence. To better satisfy the conditions for applicability of the adiabatic approximation, the transition from ~100 gauss to zero field was slowed to ~40 ms. The low field relaxation time of the -CD_3 group is apparently rather shorter than the 80 ms it takes to demagnetize from and remagnetize to 100 gauss as almost no -CD_3 signal is observed. a). $\theta = 45^o$; b). $\theta = 60^o$; c). $\theta = 80^o$; d). $\theta = 130^o$; e). $\theta = 150^o$; f). 180°. Some of the features of the qualitative pulse-length behavior of DMB are repeated in this spectrum but the response to the two-pulse sequence seems highly system-dependent.

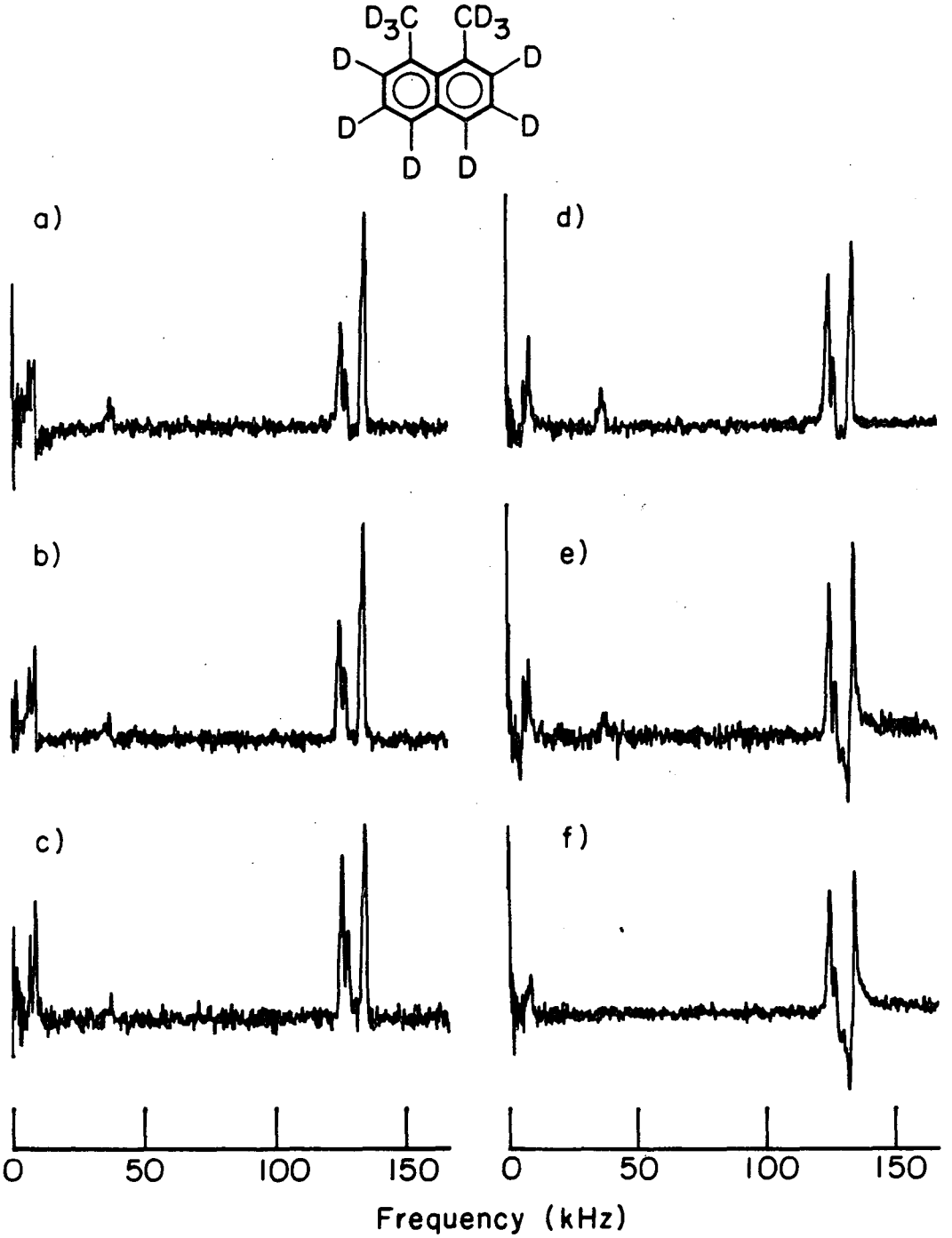

XBL 858-3506

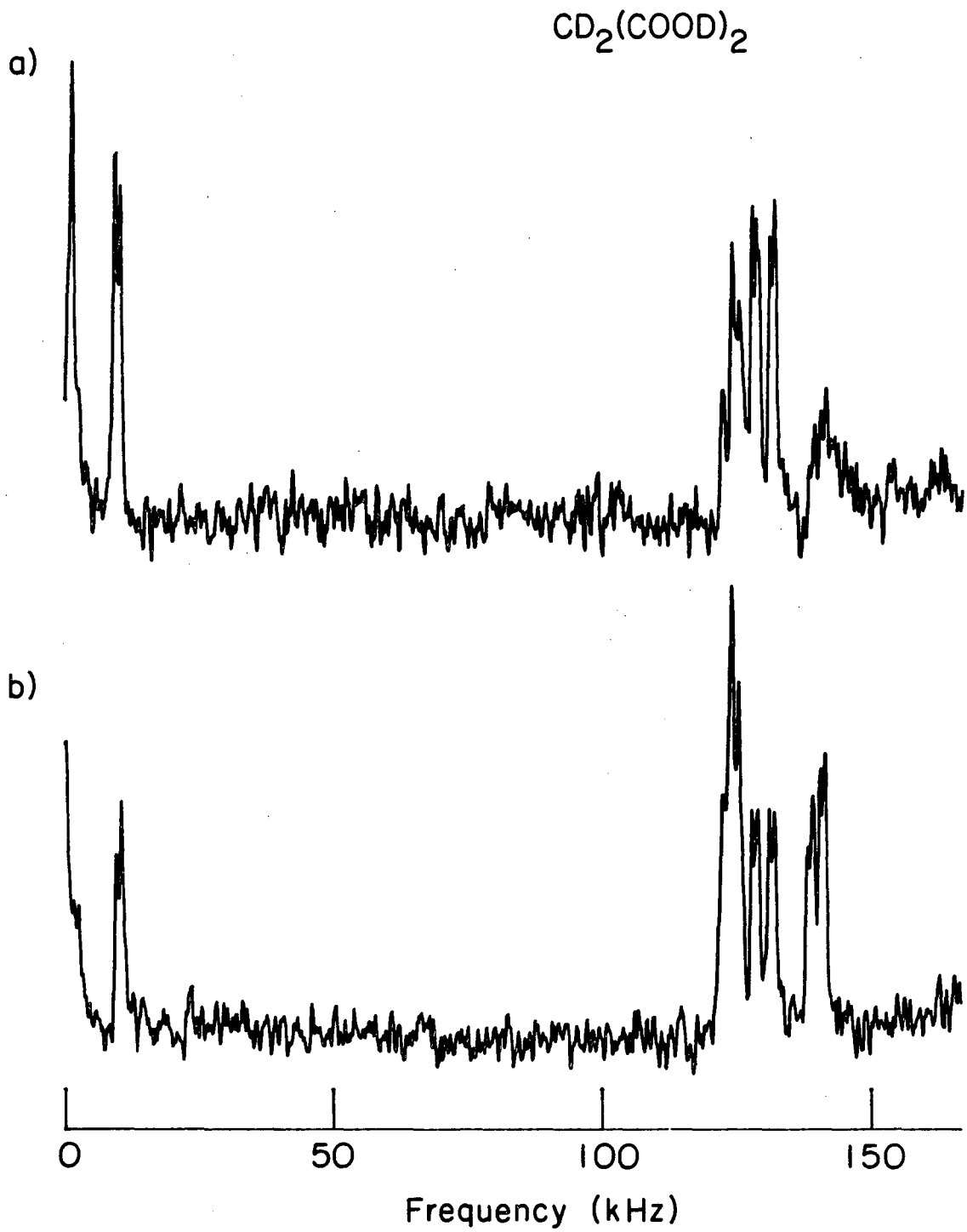

Figure 6.10. Zero field ^{2}D NQR of perdeuterated malonic acid ($CD_2(COOD)_2$) acquired by the two-pulse experiment for a). θ = 180°;

b). θ = 90°. Each of the lines is split by dipole-dipole couplings.

The flip angle dependence of the lines for θ = 180° is very different from either that of Figure 6.8 or 6.9.

demagnetized spin systems are feasible, and for deuterated systems these pulsed experiments result in signal-to-noise ratios not very different from those observed in the more traditional experiment. Exact modeling of intensities appears difficult, presumably because the dynamics of the demagnetization and remagnetization are quite complicated. Nevertheless, as long as only quadrupolar couplings are desired there is no strong objection to a technique capable of uncovering frequencies only. For systems characterized by very different T_1 spin-lattice relaxation times or where the high field detection sequence is more sensitive to some sites than others, the level-crossings which complicate the exact intensity calculation may result in higher sensitivity in the two-pulse experiment than would be observed in zero field NMR experiments which use suddenly switched fields to develop coherence. Finally, the two-pulse experiment (and variants thereof, some of which follow directly) may be technically simpler to execute. Whereas the experiment of Chapter III requires that a large rapidly switchable field B_{int} be applied to the sample for times ~ ms (see Chapter VIII), in the two-pulse experiment fields large compared to the local field need only be applied for times ~ μs. This may significantly simplify the design of the necessary hardware.[75]

For larger spin systems similar calculations are possible and may be most simply performed following the general outline of this section. For large I systems, or more complicated pulse sequences than the examples of this section, experience leads me to believe that paper and pencil calculations have only a small chance of fortuitously converging on correct answers in a finite amount of time. Brute force numerical integration over a powder distribution is an idea I find aesthetically

displeasing as well as expensive. These more complicated experiments will almost certainly benefit from the use of advanced artificial intelligence routines like Macsyma or SMP. But where the spin system is prepared by demagnetization to zero field, I believe it will be a rare case when calculations can accurately reproduce experimental intensities. In cyclic sequences, an analysis exploiting the machinery of average Hamiltonian theory[2,8,130] is highly to be recommended.

One might question the wisdom of worrying in great detail about an experiment whose interpretation is difficult and which seems to provide new information in only a limited number of experimental cases, particularly when zero field studies using the idea of suddenly switched fields prvovides much cleaner experimental results. In the next section, I will discuss some of the motivation for developing this new technique.

C. Indirect Detection

During the course of some studies of ^{1}H zero field NMR, we investigated the spectrum of lauric acid as a function of the ^{1}H-^{2}D ratio in randomly deuterated samples (see Figure 4.21). During one of these experiments a puzzling set of lines were observed (Figure 6.11). In addition to the normal broad spectrum centered about zero frequency, some relatively sharper lines at frequencies ~35 kHz and as high as ~120 kHz were observed. These line clearly fall outside the range of normal ^{1}H-^{1}H dipole-dipole couplings and were remarkably narrow by the standards of zero field NMR. Some time later, when the ^{2}D NQR spectrum of highly deuterated lauric acid was measured (Figure 5.11) the

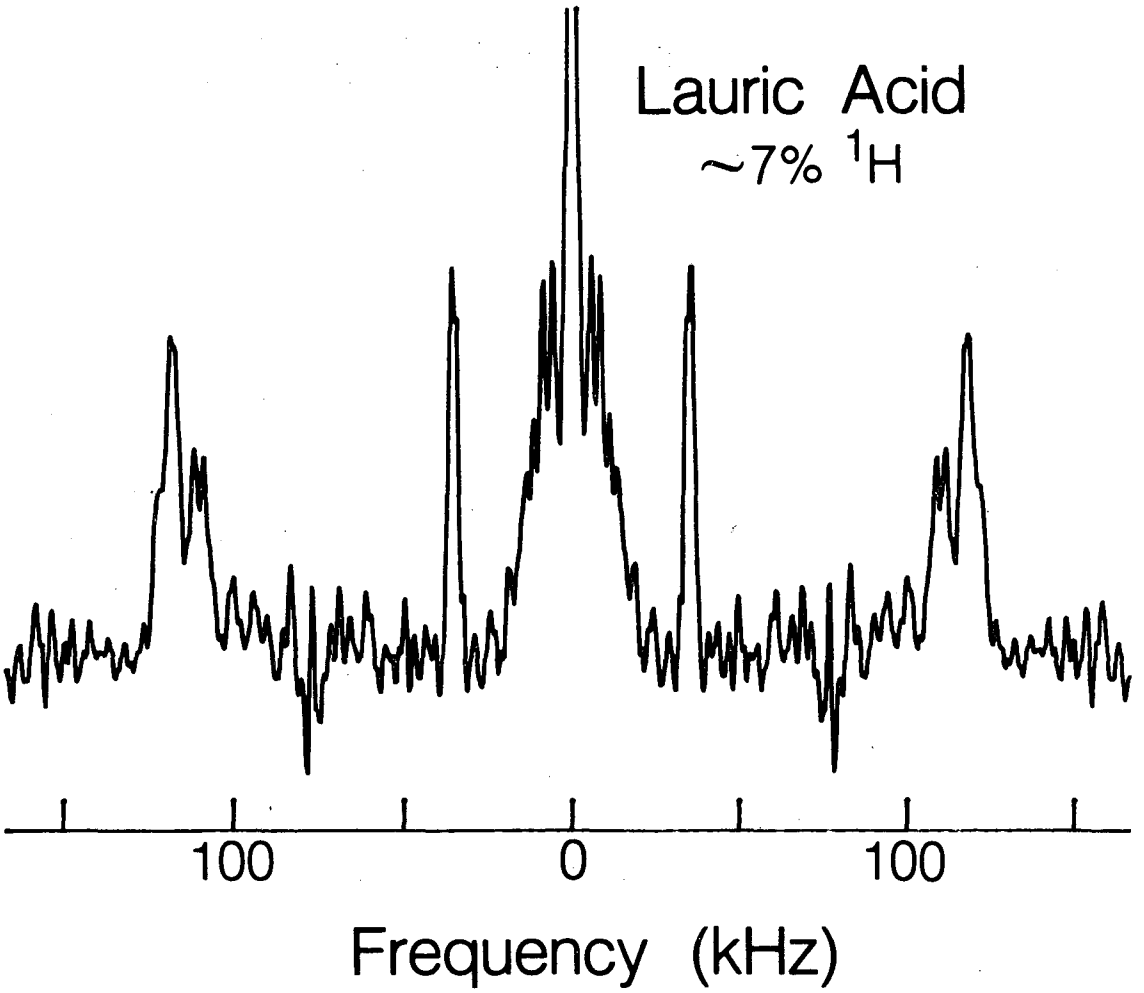

Figure 6.11. Indirectly detected ^{2}D NQR spectrum of lauric acid is randomly deuterated sample. This is the same sample whose spectrum was shown in Figure 4.21. It is unclear what experimental parameters differed so that the ^{2}D spectrum might be so clearly detected from the ^{1}H spectrum.

XBL 857-8936

identity of these lines became clear; the ^2D NQR spectral frequencies were indirectly observed through the residual ^1H spins. Level crossings between ^2D and ^1H are not expected to occur in fields as large as 100 gauss, the nominal intermediate field for ^1H zero field NMR experiments. Soon thereafter these lines disappeared and at the time no attempt was made to recover them.

As was outlined in Chapter II, extremely high sensitivity measurements of zero field NQR are possible when level crossings between spin-1/2 and quadrupolar spin systems can be used to transfer polarization to the quadrupolar nuclei during the demagnetization, and information imprinted in the zero field period can then be detected by observing the effect of the reverse process. One might wonder whether it is possible to exploit level crossings (where they exist) to enhance the sensitivity of time domain zero field experiments where direct detection experiments are insufficiently sensitive. Low sensitivity may be due to a low equilibrium value of the Curie constant, because the high field T_1 is inconveniently long, the low field T_1 is too short, or because the high field spectrum is difficult to observe with high sensitivity.

In the previous section examples of polarization transfer between inequivalent quadrupolar nuclei were presented. Level crossings in homonuclear systems probably occur only for specific orientations and values of the quadrupolar tensors involved, and there need be no field where the splittings between energy levels of neighboring nuclei are matched and polarization transfer is allowed. At high field, the difference in quadrupolar couplings slow cross relaxation between nuclei with different local quadrupolar couplings. In zero field, this

quenching effect is exacerbated because there are no diagonal elements of the dipole-dipole coupling between inequivalent ^2D nuclei.[66] Nonetheless, significant signal enhancement at sites with long T_1's due to the transfer of polarization between homonuclear ^2D spin sites in perdeuterated spin systems has been observed.

In mixed ^1H-^2D systems, level crossings certainly occur when the sample is demagnetized. But the simple argument of Chapter II probably does not apply to these systems. Where the splittings between quadrupolar energy levels are as small as in ^2D the level crossings do not occur in the simple sequence described in Chapter II. The ^1H dipolar bath is sufficiently broad so that all quadrupolar energy splittings may simultaneously be resonant with some energy-conserving spin-flip in the ^1H bath. One possible level-crossing scheme is shown in Figure 6.12. The levels connected by the ν_+ and ν_- lines are simultaneously matched to tha Zeeman-split spin-1/2 levels to within the energy spread of the dipolar bath. As long as $H_Z > H_D$, the dipolar and Zeeman baths may have very different spin temperatures and the demagnetized Zeeman reservoir is much colder. Both ν_+ and ν_- lines equilibrate to the ^1H Zeeman temperature. This establishes a state of pure quadrupolar order in the ^2D spins. If the ratio of ^2D to ^1H is low, then the amount of quadrupolar order is nearly independent of the size of the quadrupolar coupling constant. If significant warming of the ^1H bath occurs, successive level crossings transfer less order to sites with smaller couplings. At very low fields $H_Z \sim H_D$ the ν_0 splitting becomes resonant with the pure dipolar bath and may be further cooled. This establishes eta order consistent with the size of the ν_0 splitting and the extent to which polarization remains in the

Figure 6.12. Level crossing sequence for ^1H-^2D system of coupled spins. The ^1H energy levels are broadened by the homonuclear dipole-dipole couplings. The ^2D spins are nearly in their zero field energy levels. If η is small, then transitions which pump pure quadrupolar order ($|p\rangle \rightarrow |r\rangle$ and $|q\rangle \rightarrow |r\rangle$ are simultaneously allowed to within the dipolar linewidth of the Zeeman levels. Eta order may also be pumped by the $|p\rangle \rightarrow |q\rangle$ transition, but in moderately high fields the Zeeman spin temperature after demagnetiation is much colder than the dipolar spin temperature, so little eta order is prepared. Only at low fields where the ^1H dipolar and Zeeman levels merge can significant amounts of eta order be prepared via level crossings.

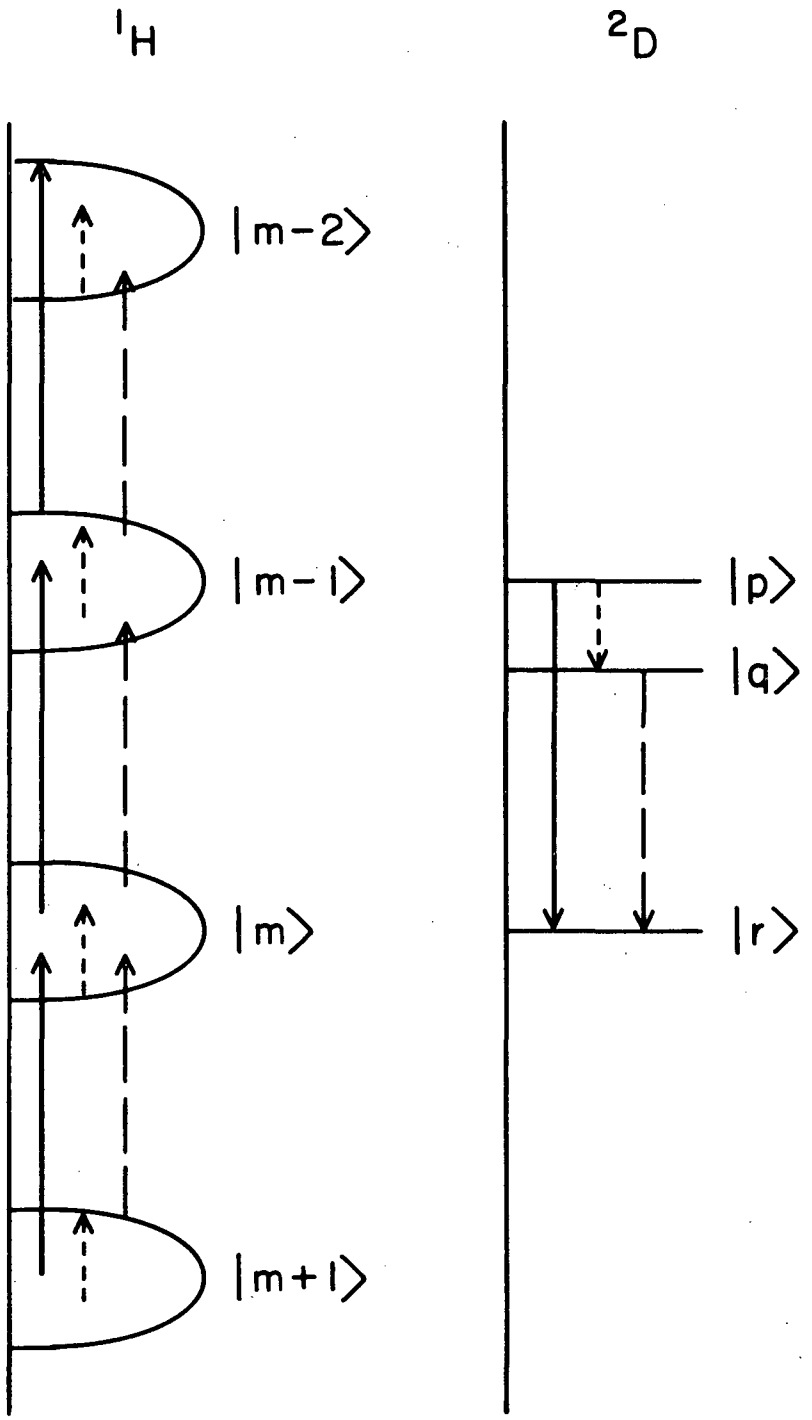

XBL 858-3624

dipolar bath. The relative amounts of quadrupolar and eta order depend on concentration and the size of η. In systems with relatively few ^2D nuclei and small asymmetry parameters this may well correspond very nearly to a state of spin temperature, where

$$\rho^D(0) = H_Q \tag{6.49}$$

Where η is small, this may not be very different from pure quadrupolar order.

The excitation of the spins proceeds as above. A θ pulse applied to the sample transforms some of the diagonal order in ρ into coherences. The density operator for the sample as a whole corresponds to separate contributions from ρ^D and ρ^H, which describes the ^1H bath. A θ pulse applied to the ^2D spins is a θ' pulse applied to the ^1H spins, where

$$\theta' = \theta\ (\gamma_H / \gamma_D) \tag{6.50}$$

Because the flip angles differ even for the same applied field and pulse length, the evolution of different types of nuclei can be separated out based on the selectivity of the applied dc pulses.[62] At the end of t_1, a second pulse stores evolved order. Remagnetization through the level crossing region encodes some of the information about the zero field evolution frequencies in the ^1H bath for detection through the amplitude of the high field ^1H free induction decay.

This selectivity is an important advantage in any experiment where the zero field frequencies of the "interesting" spins (^2D) are mapped out through its effect on the "uninteresting" spins (^1H). If the ^1H spins evolve during t_1, then the transfer of polarization back

from ^2D to ^1H during remagnetization will depend not only on the evolution of the ^2D spins in zero field but also on the evolution of the ^1H spins. More formally, this implies that the observable in any density matrix calculation is changing with t_1. This will certainly distort the signal function $G(t_1)$. If, however, $\theta' = 2n\pi$, then the ^1H evolution is suppressed and this distortion is minimized. (In some systems, it might prove more sensitive to initially destroy all ^1H order before t_1 by applying a sequence of $\theta = 2n\pi$ pulses. Then only order which is developed after polarization transfer back from the colder ^2D spins is observed in high field.)

Initial work exploiting time domain level-crossing spectroscopy confirms the basic principles discussed in this section.[62] Both transfers of order, during the demagnetization and remagnetization, are highly dependent on experimental parameters and no simple model for the intensities appear to have much predictive power. While some amplitude and/or phase distortions appear in the spectra, the theoretical difficulties associated with a complete and convincing analysis do not preclude the extraction of useful information from systems which are not amenable to techniques which rely on direct detection.

D. Zero Field-Zero Field Correlation Experiments

Among the most powerful of modern NMR techniques are the two-dimensional correlation experiments; i.e. experiments where the spectrum is observed as a function of two independent time variables (see Section I.B.1.a) in order to uncover the correlations between the evolution frequencies in the two time domains.[18] Many examples of

experiments applicable to weakly coupled liquids exist. These include COSY,[131] which maps out through-bond (J) coupling networks, and NOESY[132] which identifies through-space (dipole-dipole) couplings. Solid state analogs of these experiments are rare. My goal is to descibe such experiments for use in the structural analysis of complex systems of solid states spin systems in zero applied field. As usual, I focus on techniques applicable to the case of spin-1.

1. Correlation between Zero Field Lines

Figure 6.13a shows a two-dimensional zero field NMR experiment which correlates between lines arising from a single type of ^2D site. The spins are brought to an intermediate field which is suddenly turned off. Evolution continues for a time t_1. At $t = t_1$, a short pulse (for simplicity, aligned along the laboratory z-axis) is applied. Then the spins are allowed to evolve for a time t_2. At the end of this time period, the intermediate field is suddenly reapplied and the sample transported to high field for detection. The two time intervals are incremented independently, and a signal function $G(t_1,\theta,t_2)$ is measured in high field. The θ pulse transfers coherence between different lines in the three-level spin-1 system. Fourier transformation with respect to both t_1 and t_2 shows the correlations between, for example, the $\nu+$ and ν_- lines of a single ^2D site. (In the presence of couplings to other sites, correlations to other coupled spins may also be observed. I concentrate instead on cases where individual lines can be associated with individual sites and the couplings between sites are negligible.) As usual, the problem is to calculate

Figure 6.13. Two dimensional zero field-zero field correlation experiments. a). Sample is demagnetized to B_{int}, which is suddenly switched off. Evolution under the zero field quadrupolar Hamiltonian occurs for a time t_1. Then the intermediate field is pulsed on again. For short pulses, the field can be considered to be a rotation in spin space, and should reveal correlations between ν_+, ν_-, and ν_0 lines at the same site. For longer pulses, coherence which does not correspond to magnetization decays away. If the field pulse is long, spin diffusion between sites may occur. B_{int} is suddenly switched off and on again, and t_2 is encoded with new frequency information. b). Similar to a). except that the long field pulse is preceded by a short pulse to store coherence as population differences. Slow remagnetization to B_{int} and demagnetization back to zero field guarantees that if there is a field where spin diffusion between ^{2}D's is rapid, it can occur. A second pulse initiates t_2.

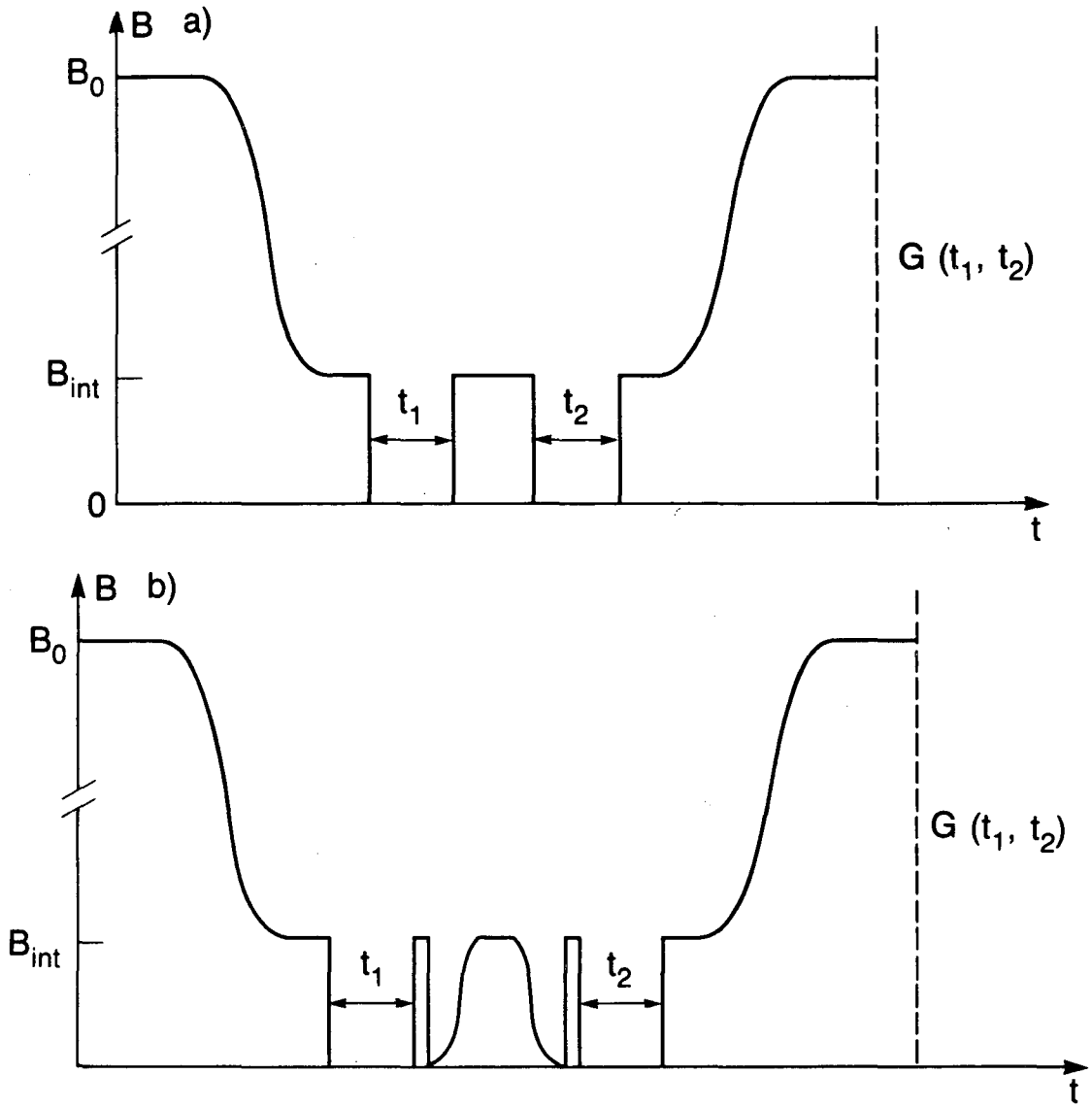

XBL 857-11257

$$G(t_1,\theta,t_2) = \mathrm{Tr}\,[I_{zL}\rho(t_1,\theta,t_2)] \tag{6.51}$$

with

$$\rho(t_1,\theta,t_2) = R\exp(-iHt_2)R^{-1}\exp(-i\theta I_z)R\exp(-iHt_1)R^{-1}\, I_{zL}$$
$$R\exp(iHt_1)R^{-1}\exp(i\theta I_z)R\exp(iHt_2)R^{-1} \tag{6.52}$$

By judicious rearrangement of Equation (6.51) and (6.52), G is rewritten in a form much simplified for calculation;

$$G(t_1,\theta,t_2) = \mathrm{Tr}\Big[\{R\exp(iHt_2)R^{-1}I_{zL}R\exp(-iHt_2)R^{-1}\} \tag{6.53}$$
$$\{\exp(-i\theta I_z)\exp(-iHt_1)R^{-1}I_{zL}R\exp(iHt_1)R^{-1}\exp(i\theta I_z)\}\Big]$$

$$= \mathrm{Tr}\,[I_{zL}(-t_2,\,0)\; I_{zL}(t_1,\,\theta)] \tag{6.54}$$

The advantage of rewriting Equation (6.51) in the form of Equation (6.53) is that $I_{zL}(t,0)$ is given in Equation (3.58). What remains is to apply a pulse to $I_{zL}(-t_2,0)$, take the trace, and integrate over the assumed powder distribution. In terms of the a_j coefficients defined in Equation (3.59), the rotated form $I_{zL}(t,\,\theta)$ is

$$\exp(i\theta I_z)I_{zL}(t)\exp(-i\theta I_z)=(a_1\cos\theta-a_2\sin\theta)I_x+(a_2\cos\theta+a_1\sin\theta)I_y \tag{6.55}$$
$$+\; a_3I_z+\; a_4U_0+\; (a_5\cos\theta-a_6\sin\theta)U_{1+}+\; (a_6\cos\theta+a_5\sin\theta)U_{1-}$$
$$+\; (a_7\cos2\theta+a_8\sin2\theta)U_{2+}+\; (a_8\cos2\theta-a_7\sin2\theta)U_{2-}$$

where all the coefficients are time dependent. Taking the trace as indicated in Equation (6.55) and integrating over $P(\Omega)$,

$$G(t_1,\theta,t_2)=\frac{1}{105}\{[\sum_{j\neq k}(21+14\cos\theta)\ K_{jk,jk} - (3+10\cos\theta+22\cos\theta)\ J_{jk,jk}\ ]$$

$$+[\sum_{j\neq k,l\neq m,j\neq l,k\neq m}(7-7\cos\theta)K_{jk,lm} + 3(1+\cos\theta-2\cos2\theta)\ J_{jk,lm}]\} \quad (6.56)$$

where

$$K_{jk,lm} = \cos\omega_{jk}t_1\cos\omega_{lm}t_2 \quad (6.57)$$

and

$$J_{jk,lm} = \sin\omega_{jk}t_1\sin\omega_{lm}t_2 \quad (6.58)$$

and the indices run from 1 to 3. Maximum intensity is transformed into correlations between peaks within a manifold (as opposed to the redundant diagonal peaks $\omega_1 = \omega_2$ which tell nothing about the correlations) for $\theta = \pi$. This experiment (or close relatives which develop polarization at many sites by starting from a demagnetized state) should assist in the interpretation of zero field spectra where the one-dimensional spectrum is too cluttered with overlapping lines to provide for an unambiguous assignment of the full quadrupolar tensor. A similar experimental sequence would be analogous to a zero field COSY experiment, where the quadrupolar couplings identify sites while the dipole-dipole couplings give the correlations between sites. The transfer of coherence between coupled spins occurs only on the time scale of spin diffusion which may be quite slow for inequivalent sites in zero field.[66,84] COSY-type experiments will probably show few cross-correlations other than those between equivalent sites.

2. Cross Relaxation Through Dipole-Dipole Couplings

Cross relaxation between dipole-dipole coupled deuterons occurs at a rate comparable to the inverse of the coupling constant ω_D only if

the quadrupolar plus Zeeman energies of neighboring deuterons are closely matched. Therefore, even in the best of circumstances roughly 500 μs must pass before magnetization originally localized on one spin might reasonably be expected to appear at a second, and perhaps much longer in zero field. As 500 μs is roughly equal to the inverse of the average zero field linewidth, coherence transfer experiments may never be capable of revealing the spin-spin correlations between ^{2}D in zero field. The time domain analog of the "double transition" ^{2}D NQR experiments[118] would be a "multiple quantum" experiment which, in analogy to high field experiments, would require both a preparation and mixing period again comparable to the inverse of the dipole couplings. Unless time-reversible pulse sequences[133] can be developed for spins in zero field, multiple quantum experiments suffer from the same problem; the multiple spin-correlations grow in at a rate comparable to the decay of the observable. In fact, they may be one and the same process.

A more generally applicable approach is indicated in the sequences of Figure 6.13. As the flip angle in Equations (6.51-57) becomes large ($\gg 2\pi$), transverse magnetization or other coherence (i.e. order in the density matrix ρ which does not commute with I_{jL}, where j is the axis along which the field pulse is applied) will decay in a time given roughly by the inverse of the quadrupole coupling constant. For pulses long compared to the inverse of the quadrupolar frequencies, the evolution under the truncated quadrupolar Hamiltonian cannot be ignored, and the frequency of evolution varies from orientation to orientation over the sample. (In fact, the sample is in high field with all the associated consequences.) For long pulses and where no

pulse sequences designed to elicit spin echoes[134] are applied the norm of ρ decreases with time. In return for this loss of signal power, some portion of ρ is diagonal in the high field basis set and disappears only with a time constant T_1, which is generally many milliseconds long and may be seconds long. If spin diffusion occurs during this rather longer period of time, and the field is again suddenly switched off and on again, the signal $G(t_1,t_2)$ will be imprinted with frequency information from both sites.

One serious objection to this experiment has already been discussed. Spin diffusion between inequivalent sites is fast only at specific values of the externally applied field which are almost certainly orientation dependent. Then unless by happenstance the intermediate field is one generally good value little transfer of magnetization will occur except within those spins systems which are strongly coupled, anyway.

The sequence of Figure 6.13b should prove vastly superior. It takes advantage of the fact that during an "adiabatic" change of the field one necessarily passes through whatever value of the field is optimal for spin diffusion between neighbors independent of orientation unless no good value exists. Order is stored in eigenstates of the zero field Hamiltonian (e.g. as second rank tensor operators proportional to U_0 or U_{2+} in a spin-1 system) by a short, strong dc pulse. This order is again characterized by a decay constant proportional to T_1. By slowly restoring the intermediate field, quadrupolar and eta order stored by the pulse is conserved and slowly transformed into Zeeman and quadrupolar order appropriate to high field. All values of the field where spin diffusion is likely to be

efficient are sampled. The evolution period t_2 can then be initiated either by demagnetization followed by a short pulse, or by sudden switching of the intermediate field. Finally, t_2 is ended and the system returned to high field for detection.

Numerous other variations on these simple correlation experiments which take advantage of incoherent, NOESY-like spin diffusion are possible.

VII. Considerations of Symmetry

In this chapter I address some rather obscure but interesting problems associated with the symmetry properties of the zero field Hamiltonian (H). An understanding of these properties is useful in explaining spectra of systems of coupled nuclear spins in zero applied field. Predictions of such gross spectral features as the numbers of allowed transitions (which was treated in a fairly general fashion in Chapter IV) become exact only if the symmetries of H are properly incorporated. Furthermore, this understanding of the limits nature has set may provide a basis for a reasoned evaluation of the usefulness of complicated pulse sequences designed to simplify the spectra of spin systems in zero field.

In Chapter I, the general approach to problems of high field NMR was presented. Formally:

1. An axis system is established fixed in the laboratory frame and defined by the direction of the applied magnetic field. Conventionally, the z-axis is chosen parallel to the applied field.
2. The elements of the spin Hamiltonian are organized. As the Zeeman interaction, H_Z, is much larger than the local Hamiltonians a basis of states is chosen which diagonalizes H_Z.
3. The internal Hamiltonians, H_{loc}, are expressed in the basis set defined in step 2 above. To first order in perturbation theory, only the truncated (diagonal) components of the local fields are observed. This is treated formally by entering a rotating reference frame where the orientation of the spin

reference frame is continuously changing with respect to the fixed spatial frame of reference. Only the value of the internal Hamiltonians averaged over the period of the rotation (i.e. at the windows where the spin and spatial reference frames coincide) is observed.

Selection rules are established based on the symmetry operations of the Hamiltonian $H = H_Z + H_{loc}$. Because the spin reference frame is rapidly rotating about its and the spatial frame's z-axis, all rotations about that axis commute with H and are symmetry operations of H. The projection of the angular momentum along the z-axis, $\langle I_z \rangle$, is quantized and transitions between states are allowed under dipole selection rules (i.e. the application of an oscillating rf field) only if

$$\langle I_z \rangle_f - \langle I_z \rangle_i = \Delta m = \pm 1 \tag{7.1}$$

where f labels the final state and i the initial state. Further averaging may take place in the spatial coordinates. In simple cases (e.g. MASS[35]) this can be treated by entering a second rotating frame which relates the axis of spatial rotation of the sample to the laboratory frame where measurements are made. A spatially rotating frame was also used in the analysis of the zero field NMR spectrum of the methyl group (Section IV.A.2).

Other symmetries of H (permutations of "identical" nuclei, i.e. nuclei with identical Larmor frequencies and the same set of couplings to other nuclei) may provide further selection rules. Where these additional selection rules exist they assist in the assignment of lines and the analysis of complex spectra.[135]

In this chapter, I present a related approach to an understanding

of the use of symmetry characteristics in the analysis of zero field NMR spectra. Formally:

1. An axis system is established fixed in a molecular coordinate system such that the Hamiltonian for all similar spin systems share an identical description independent of orientation.
2. The spin Hamiltonian is expanded in a basis set of spin operators referenced to this fixed spatial system and parameterized by the spatial variables. In the absence of motion, spin and spatial frames coincide.

In the absence of rapid rotation about a molecular axis (again as in $-CH_3$) there need be no axis along which any component of the angular momentum is quantized. If $\langle I_j \rangle$ is not a good quantum number then there exists no selection rule for Δm analogous to that of Equation (7.1). If there are selection rules they are imposed by other symmetry operations. These selection rules, where they exist, are determined by the set of operators which permute identical nuclei (again, spins which share the same set of coupling constants to all other spins).

In analogy to the analysis of symmetry constraints in high field (and because it is difficult to derive the effect of permutations on spinors), the set of permutations of identical spins will be assumed isomorphic to a set of symmetry operations comprised of rotations, inversions and reflections which act upon the spin degrees of freedom only. Symmetry operations of H are those which take the Hamiltonian (a contraction of spin and spatial degrees of freedom) and transform it into an identical Hamiltonian except for the possible permutation of spin labels between identical spins. The spin-space rotations which commute with H can be thought of (in homonuclear spins systems) as

corresponding to a set of dc pulses which (if applied in the molecular frame) would leave the Hamiltonian (and thus the density operator ρ) unchanged.

Application of a symmetry operation to an eigenstate ψ effects two distinct types of changes. First is a permutation of spin labels consistent with the interchange of symmetry-related spins where the spin reference frame is reoriented with respect to the spatial coordinate system. Second is the alteration of ψ because the spinors themselves (the single-spin bras or kets) are transformed under rotations and reflections. The first step is essentially the standard process of ordinary group theory.[136] The second is unique to problems of spins in zero applied field. Section A is entirely devoted to the clarification of this second effect.

It may seem strange that the symmetry operations are defined with respect to the transformation of the spin variables alone. Yet this must be the proper perspective. Simultaneous transformation of both spatial and spin variables through the same coordinate transformation yields an equivalent Hamiltonian with identical eigenvalues independent of the transformation as H is merely reexpressed in a different reference system. While the invariance of zero field Hamiltonians to coordinate transformations is the raison d'être of zero field NMR, the simultaneous transformation of spin and spatial frames in the sense of Equation (1.14) is uninteresting.

The goal of this chapter is to identify and characterize the symmetry operations characteristic of the zero field Hamiltonian and to describe their influence on the observable, the zero field spectrum. In the presence of molecular motion, the spatial degrees of freedom

become time-dependent and the Hamiltonian again separates into two reference frames which only intermittently coincide. Then the arguments and conclusions of this chapter require significant modification.

In the first section which follows, the types of symmetry operations are summarized and rules are established to describe their effect on eigenstates. In the second section, I present several illustrative examples which demonstrate the use of these rules in the classification of zero field Hamiltonians and the prediction of zero field spectra.

A. Formal Aspects

1. Symmetry Operations

An operator ξ is a symmetry operator for the Hamiltonian H if

$$\xi^{-1} H \xi = H \tag{7.2}$$

If ξ is a symmetry operation, then for $|\psi_j\rangle$ an eigenstate of H

$$\xi |\psi_j\rangle = a\, |\psi_k\rangle \tag{7.3}$$

where $|a|^2 = 1$ and if $j \neq k$ then $|\psi_j\rangle$ and $|\psi_k\rangle$ are degenerate.

2. Operations in Spin Space

The set of possible symmetry operations for isolated spin systems are described in standard texts on the theory of point groups.[136,137] These are: rotations about a fixed axis, reflections in a plane, simultaneous inversion of all coordinates through the origin of the reference frame, and the improper rotations. Following standard

notation, the symmetry operations are represented by the symbols C_n, σ, i, and S_n. Due to an unavoidable overlap of notation, σ is used in other chapters to represent the chemical shift. In this chapter the chemical shift will not appear and some confusion is avoided. The symbol i, however, will be used to represent both the inversion operation and to represent $(-1)^{1/2}$. Caveat emptor!

Products of only two operations generate both others. I choose to treat C_n and σ as the fundamental operations. The form of these symmetry operations can be derived from the requirement that all observables (e.g. angular momenta) are unaffected by the spinor behavior of the eigenstates, and therefore spin and spatial angular momenta (which as operators correspond to observables) must transform identically under any of the operations of the group.

a. Rotations about a Fixed Axis

Rotations about a fixed axis are described by the Euler angles of Chapter I and the various relations summarized in Equation (1.25). A C_{nj} symmetry operation is equivalent to a rotation of $2\pi/n$ about the j axis, and

$$\begin{aligned} C_{2j}^{-1} I_k C_{2j} &= -I_k \qquad \text{if } j \neq k \\ &= I_k \qquad \text{if } j = k \end{aligned} \tag{7.4}$$

and any representation of the C_{2j} operation must be consistent with understanding. For j = x, y, or z the rotation operators for spins-1/2 are

$$R_j(\phi) = \exp(i\phi I_j) = \cos\frac{\phi}{2} + i s_j \sin\frac{\phi}{2} \tag{7.5}$$

where the s_j are the Pauli spin matrices. Therefore, for j = x, y, or

z, $C_{2j} = is_j$.

More generally the spinor transformation associated with a C_{nj} operation is the product of rotations about the y and z axes and is described by a sequence of transformations of the form of Equation (7.5). This net transformation is precisely equivalent to a Wigner rotation matrix. Rotations about the z-axis through ϕ append a phase factor $\exp(i\phi/2)$ for each $|\alpha\rangle$ spinor and $\exp(-i\phi/2)$ for each $|\beta\rangle$ spinor. The net effect on a typical wavefunction $|\psi\rangle = |\alpha_1\rangle|\beta_2\rangle\ldots|\alpha_n\rangle$ is to multiply it by the product of the phase factors for each of the individual spinors.

Rotations about the x- or y-axes additionally may change the projection of the spin angular momentum along the z-axis. Under a C_{2y} rotation all spinors in a spin-1/2 system are transformed from $|\alpha\rangle \rightarrow -|\beta\rangle$ and $|\beta\rangle \rightarrow |\alpha\rangle$. Applied to a system of n identical spins in a plane, the C_{nj} operation interchanges the spin labels referenced to the fixed spatial axes of all spins not on the axis of rotation (e.g. takes the spin initially labeled 1 into 2, 2 into 3, ..., and n into 1). Therefore, the net effect of a C_{2z} operation on four identical spins in the arrangement of a square is

$$C_{2z}|\alpha\beta\alpha\alpha\rangle = -|\alpha\alpha\alpha\beta\rangle \tag{7.6}$$

In particular a 2π rotation about any axis transforms a spin-1/2 spinor into its negative. The eigenstates of H are products of the spinors describing each individual spin. In systems of odd numbers of spins-1/2 a 2π rotation and the identity operation, E, are not equivalent. A 2π rotation corresponds instead to the symmetry operation denoted $\bar{E}$ where $\bar{E}^2 = E$ and, for all ξ, $\bar{E}\xi = -\xi\bar{E}$. A 4π

rotation transforms a spinor into itself and is equivalent to E. Because 2π and 4π rotations are distinct symmetry operations, odd numbers of half-integer spin nuclei can only be treated using the formalism of the double groups.[138,139] In the double group representations, the order of all classes of rotations is doubled (i.e. only after 2n applications of a C_n operation does the system return to its original state).

b. Reflections Through a Plane

The spin-space reflection operators are required to be similar in effect to to the operators which generate the improper rotations on spatial angular momenta. Where σ_j is a symmetry plane perpendicular to the j axis,

$$\begin{aligned} \sigma_j^{-1} I_k \sigma_j &= -I_k \qquad \text{if } j = k \\ &= I_k \qquad \text{if } j \neq k \end{aligned} \tag{7.7}$$

By comparison to Equation (7.4) the spin-space component of σ_j is

$$\sigma_j = \bar{E}\, C_{2j} = C_{2j}^{-1} = -is_j \tag{7.8}$$

(The equivalence is Equation (7.8) is not meant to suggest that C_{2j}^{-1} and σ_j are identical operations. These two operations act similarly on the spinors themselves; this is, however, only the second of the consequences of the symmetry operation. They differ with respect to the relationship between the transformed spin and spatial frames.) The operation of spin reflection interchanges spin labels for spins which do not lie in the plane of reflection, turn $|\alpha\rangle$ into $|\beta\rangle$ and vice versa if $j \neq z$, and appends phase factors as derived from Equation (7.8). Applied to the same four-spin wavefunction as before, and where z lies

in the plane of the square,

$$\sigma_z|\alpha\beta\alpha\alpha\rangle = -|\alpha\beta\alpha\alpha\rangle \tag{7.9}$$

c. Inversion

The inversion operator, represented by i, is constructed by a succession of improper rotations

$$\begin{aligned} i &= \sigma_x\sigma_y\sigma_z = -i^3 s_x s_y s_z \\ &= -i^4 s_z^2 = \bar{E} \end{aligned} \tag{7.10}$$

Under inversion, all coordinate are interchanged with their negative and all spinors are multiplied by -1. For even numbers of spins, the inversion operation merely interchanges labels on spins related by the inversion; for odd numbers, also multiplies all wavefunctions by 2π. Applied to the same four-spin eigenstate

$$i\,|\alpha\beta\alpha\alpha\rangle = |\alpha\alpha\alpha\beta\rangle \tag{7.11}$$

d. Improper Rotation Axis

The composite operations S_n are derived by applying sequentially the component symmetry operations, and

$$S_{2z}|\alpha\beta\alpha\alpha\rangle = \sigma_z C_{2z}|\alpha\beta\alpha\alpha\rangle = -\sigma_z|\alpha\alpha\alpha\beta\rangle = |\alpha\alpha\alpha\beta\rangle \tag{7.12}$$

The S_2 operation is identical to the inversion operation. More generally $S_{nj} = \sigma_j C_{nj}$.

3. Operations in Time

In the absence of an external field the zero field Hamiltonians of Chapter I exhibit time reversal symmetry. Because each element of the Hamiltonian contains only products of pairs of angular momentum operators, time reversal (which corresponds to taking all velocities

and angular momenta into their negative) is an explicit symmetry operation of H. While the fundamental properties of the time reversal operator T are explained in detail elsewhere,[104,105] I provide a brief review here.

The relation which serves to define T is

$$T|\psi\rangle = \exp(iHt)T\exp(iHt)|\psi\rangle \tag{7.13}$$

In words, applying the operator T to an eigenstate $|\psi\rangle$ leaves it in the same state as if the eigenstate evolved under the Hamiltonian H for a time t, the time reversal operator is applied, and evolution continues for a time t. An equivalent formulation is given in the operator equations

$$\exp(-iHt) = T^{-1}\exp(iHt)T \tag{7.14}$$

or

$$-iHt = T^{-1}(iHt)T \tag{7.15}$$

The solutions to Equation (7.15) are constrained by the requirements that

$$[T, H] = 0 \tag{7.16}$$

because T is a symmetry operation of H and

$$[T, t] = 0 \tag{7.17}$$

because the time (t) enters the problem only parametrically. Then

$$iT = -Ti \tag{7.18}$$

and

$$T|a\psi\rangle = a^{*}T|\psi\rangle \tag{7.19}$$

In analogy to spatial angular momenta (which are the vector cross product of direction vector and a velocity, and therefore reverse sign under time reversal), it is further required that all spin angular momenta anticommute with T; that is,

$$T\, I_j T^{-1} = -\, I_j \tag{7.20}$$

Traditionally, T is factored into two components;

$$T = \Theta\, K \tag{7.21}$$

where K is the operation of complex conjugation, and Θ is chosen so that T satisfies Equation (7.17). Then

$$\Theta\, K\, I_j K^{-1} \Theta^{-1} = \Theta\, I_j^{*}\, \Theta^{-1} = -\, I_j \tag{7.22}$$

Choosing the Pauli representation for the spin-1/2 particle, Equation (7.18) suggests

$$\Theta = a\, s_y = a \begin{bmatrix} 0 & -i \\ i & 0 \end{bmatrix} \tag{7.23}$$

and the proportionality constant a is conventionally chosen to equal 1. For a spin-1/2 particle,

$$\begin{aligned} T^2 &= \Theta\, K\, \Theta\, K = \begin{bmatrix} 0 & -i \\ i & 0 \end{bmatrix} K \begin{bmatrix} 0 & -i \\ i & 0 \end{bmatrix} K \\ &= \begin{bmatrix} 0 & -i \\ i & 0 \end{bmatrix} \begin{bmatrix} 0 & i \\ -i & 0 \end{bmatrix} = \begin{bmatrix} -1 & 0 \\ 0 & -1 \end{bmatrix} = \bar{E} \end{aligned} \tag{7.24}$$

and for N coupled spins-1/2

$$T = \prod_{j=1}^{N} T_j \tag{7.25}$$

Since T is a symmetry operation of the Hamiltonian H, for each $|\psi\rangle$ an

eigenstate of H, $T|\psi\rangle$ is also an eigenstate. But

$$\begin{aligned} \langle\psi|T\psi\rangle &= \langle T\psi|T^2\psi\rangle^* \\ &= \langle T^2\psi|T\psi\rangle \end{aligned} \tag{7.26}$$

Two cases need be considered:

1. $T^2 = -1$ (i.e. an odd number of half-integer spin nuclei). Then

$$\langle\psi|T\psi\rangle = -\langle\psi|T\psi\rangle = 0. \tag{7.27}$$

$|\psi\rangle$ and $|T\psi\rangle$ are different, and necessarily degenerate, eigenstates of H. This is known as Kramer's degeneracy. For spin systems which exhibit Kramer's degeneracy, the standard point groups covered in most texts on group theory are inadequate. The less familiar double group representations, which incorporate the double-valued nature of the half-integral spins, are required.[139]

2. $T^2 = 1$ (i.e. an even number of half-integral spins, or only integer spins). Then T introduces no necessary degeneracy. Its existence, however, does lead to other conclusions; to wit,

$$\begin{aligned} \langle\psi|I_j|\psi\rangle &= -\langle\psi|T^{-1}I_jT|\psi\rangle = -\langle T\psi|I_j|T\psi\rangle \\ &= -\langle\psi|I_j|\psi\rangle = 0 \end{aligned} \tag{7.28}$$

and the expectation values of all angular momentum operators are quenched for nondegenerate eigenstates of the zero field Hamiltonian. In the presence of degeneracies mandated by other symmetries, the expectation values of I_j summed over all degenerate states must vanish.

B. Examples

1. Two Coupled Spin-1/2 Nuclei

a. Identical Pair

A convenient choice of reference system is to align the internuclear vector with the molecular z axis. Independent of the identity of the two spins, the zero field Hamiltonian has the symmetry of the point group $D_{\infty h}$. As the number of spins is even, there is no need to resort to the double group representations. Based on the discussion in the previous section of the point group operations, the transformation table for representative operations in each class of the point group $D_{\infty h}$ is given in Table 7.1, below.

Table 7.1

Operations of the group $D_{\infty h}$

$D_{\infty h}$	E	$2C_{\infty}^{\phi}$	...	$\infty\sigma_v$	i	$2S_{\infty}^{\phi}$	...	∞C_2
$\alpha\alpha$	$\alpha\alpha$	$\exp(i\phi)\alpha\alpha$	...	$-\beta\beta$	$\alpha\alpha$	$-\exp(i\phi)\alpha\alpha$	...	$-\beta\beta$
$\alpha\beta$	$\alpha\beta$	$\alpha\beta$	...	$\alpha\beta$	$\beta\alpha$	$\beta\alpha$	...	$\beta\alpha$
$\beta\alpha$	$\beta\alpha$	$\beta\alpha$	...	$\beta\alpha$	$\alpha\beta$	$\alpha\beta$	...	$\alpha\beta$
$\beta\beta$	$\beta\beta$	$\exp(-i\phi)\beta\beta$	...	$-\alpha\alpha$	$\beta\beta$	$-\exp(-i\phi)\beta\beta$	...	$-\alpha\alpha$
$\Sigma\,\chi$	4	$2+2\cos\phi$	...	2	2	$-2\cos\phi$	...	0

Using the grand orthogonality theorem, the eigenstates of H transform as the Σ_g^+, Σ_u^+, and Π_g representations of the group $D_{\infty h}$. Where Γ is the representation, selection rules are governed by the requirement that for initial state ψ_i, final state ψ_f, and transition operator T the product

$$\Gamma_{\psi_i} \times \Gamma_T \times \Gamma_{\psi_f} \tag{7.29}$$

contains the totally symmetric representation (generally labeled A_1 but in this group Σ_g^+). For the sudden switching experiment of Chapter III, the transition operators whose selection rules are required are proportional to the angular momentum operators. I_x and I_y transform as Π_g and connect the Σ_g^+ representation to the degenerate Π_g representation (that is, the m = 0 state of the triplet manifold to the pair of triplet states with $|m| = 1$). I_z, which transforms according to the representation Π_g^-, connects the degenerate pair of eigenstates one to another. None of these operators connects the ungerade (antisymmetric) representations to the gerade (symmetric) representations. Therefore the observed spectrum is a single line at zero frequency and a pair symmetrically placed about zero.

b. Heteronuclear Pair

The same group classification applies, because for two dipole-coupled spins H is the same (as usual, to within a scaling constant) independent of whether the spins are identical. The four eigenstates of the heteronuclear pair transform as the same set of irreducible representations as the eigenstates of the homonuclear pair. The transition moment operators, T, differ because the initial condition does. As was previously discussed in Chapter III, the initial condition is the sum of a symmetric first rank tensor (the high field operator $I_z + S_z$) and an antisymmetric first rank tensor ($I_z - S_z$). The molecular frame tensors derived from the symmetric combination transform as the normal angular momenta described above. Molecular frame tensors derived from the second term are of opposite symmetry with respect to all the symmetry operations which exchange spin labels. They belong only to the ungerade representations of the group, and

transform as Σ_u^- and Π_u. These operators connect the ungerade to gerade states (i.e. the singlet to the triplet). Spectra of the two spin system in β-$Ca(H^{13}COO)_2$ which demonstrate these selection rules are shown in Figure 7.1. The full complement of six allowed pairs of lines predicted by Equation (4.22) might only be observed if the cylindrical symmetry of H were broken, e.g. by an asymmetric dipolar tensor, in addition to both the symmetric and antisymmetric components in the initially prepared density operator.

2. Four Spin Systems

a. The Square

The simplest arrangement of four identical spins is in the spatial arrangement of a square. The group of symmetry operations is D_{4h}. As the number of spin-1/2 nuclei is even, the double group is not needed. Furthermore, only classification according to the group D_4 is necessary, as D_{4h} is a product group. The effect of the additional operation σ_h (where the local reference frame is chosen so that the square lies flat in the x-y plane) is to transform a state into itself (if there are an even number of spins up) or its negative (if there are an odd number of spins up). To save space, only transformation rules for the combined spin and space symmetry operations are given rather than the complete correlation table. Furthermore, only a single specific operation from each class is treated. Operations are represented in the shorthand notation

$$\xi(1234) = (WXYZ) \tag{7.30}$$

to indicate that after the operation, spin W is in the position in the spatial reference frame that 1 previously occupied, X where 2 was, and

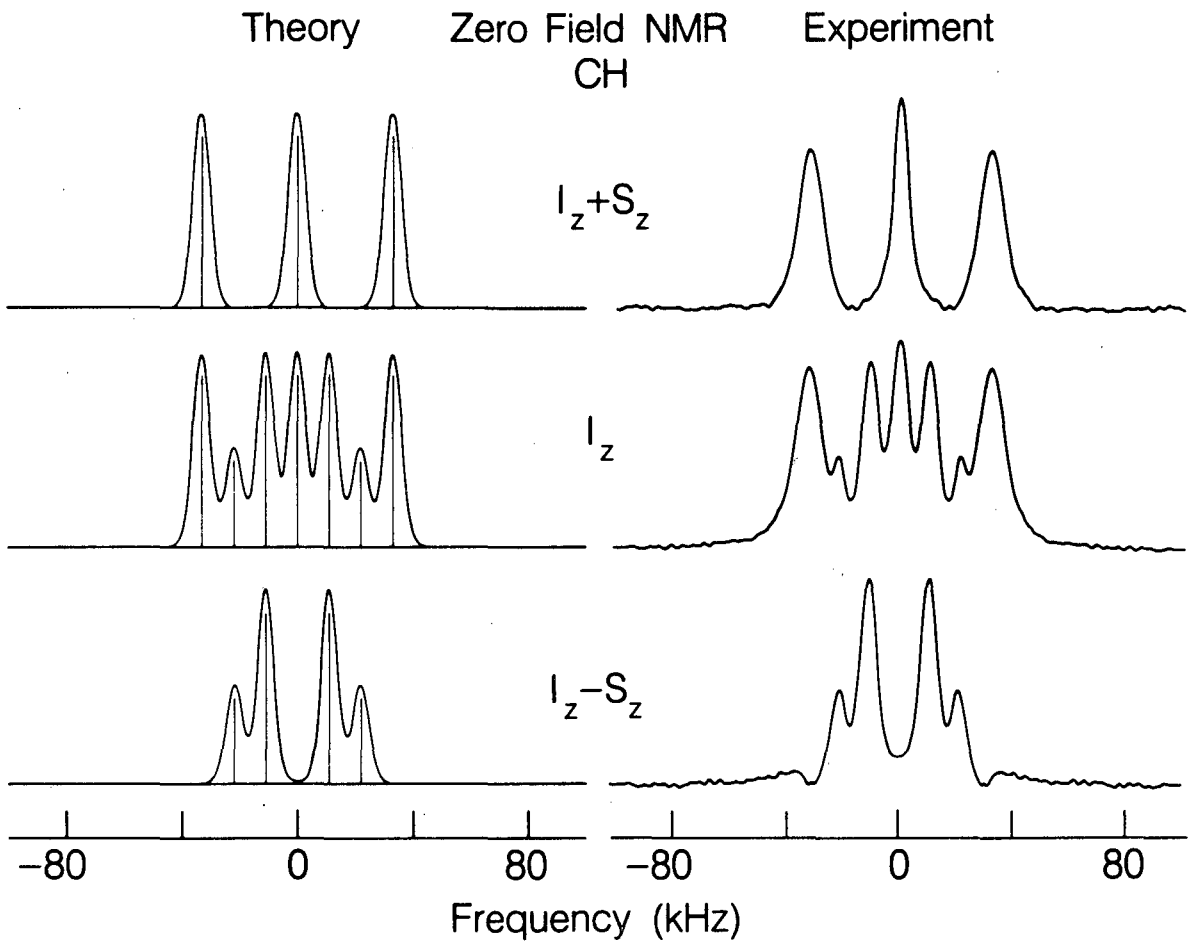

XBL 852-1111

Figure 7.1 Zero field NMR spectra of two-coupled spin-1/2 nuclei. At the top, initial condition corresponding to equal magnetization at two sites (the pure symmetric operator); in the middle, at one site only (equal amounts of symmetric and antisymmetric transition moment operators); at the bottom, equal and opposite amounts of magnetization at the two sites (only the antisymmetric operator). At left, theoretial stick spectra and broadened spectra; at right, experimental spectra. The number of observed lines follows the argument in the text.

so on. Furthermore, $W = \bar{2}$ implies that, as a result of the operation, the spinor originally located at 2 has flipped from $|\alpha\rangle$ to $|\beta\rangle$ or vice versa. Finally, phase factors are given as multiplicative constants preceding the resultant. In this form, and with $m = \Sigma\, I_{zj}$ in the initial state, Table 7.2 gives the transformations of $|\psi\rangle$ for a typical element in each class of D_4. D_{4h} is the product of D_4 and the reflection through the plane containing these spins. The latter takes states with m odd into their negative and has no effect on states with m even. Odd m states belong only to the ungerade representations of the group and even m states only to the gerade representations. (Beware! This is an unconventional definition of the product group, D_{4h}. In most applications D_{4h} is given as the product of D_4 and the inversion operator, i. The product groups are identical but the notation is not. One-dimensional representations are identical, but two dimensional representations gerade referenced to the σ_h are ungerade referenced to i, and vice versa.) Using these rules and the

Table 7.2

Operations of the Group D_{4h}

Operation:	E	C_{4z}	C_{4z}^2	C_2'	C_2''
Resultant:	(1234)	$(i)^m(4123)$	$(-1)^m(3412)$	$(-1)^m(\bar{2}\bar{1}\bar{4}\bar{3})$	$e^{(5m\pi i/4)}(\bar{3}\bar{2}\bar{1}\bar{4})$

results of Table 7.2, the sum of the characters, χ, for the gerade (even m) and ungerade (odd m) representations separately is

	E	$2C_{4z}$	C_{4z}^2	$2C_2'$	$2C_2''$
$\Sigma\ \chi_g$	8	-2	4	4	0
$\Sigma\ \chi_u$	8	0	0	0	0

(7.31)

The eigenstates partition into the representations

$$2A_{1g} + 3B_{1g} + B_{2g} + E_g + A_{1u} + A_{2u} + B_{1u} + B_{2u} + 2E_u \qquad (7.32)$$

I_z belongs to the irreducible representation A_{2g}, and (I_x, I_y) to E_u (again, referenced to the σ_h operation and not i). Summarizing the allowed transitions, (I_x, I_y) couple the degenerate E representations to all one-dimensional states with the opposite u-g symmetry for a total of 16 pairs of lines. I_z connects $E \rightarrow E$, $A_1 \rightarrow A_2$, and $B_1 \rightarrow B_2$ if both initial and final states have the same u-g symmetry. In the gerade manifold, I_z is responsible for 3 pairs of lines and a singlet at zero frequency; in the ungerade manifold, for an additional 3 pairs and a singlet at zero frequency. The spectrum is predicted to consist of 22 pairs of lines and a singlet at zero frequency. Computer simulation reveals 21 pairs and a singlet, and is illustrated in the simulation in Figure 7.2a. In small systems of spins, it is not unusual for some transition frequencies to be accidentally degenerate and coincide.

b. <u>The Rectangle</u>

Starting from the analysis of the symmetry properties of four spins arranged in a square makes other four spins systems easier. In the rectangular array of four spins the appropriate point group (D_{2h}) is a subgroup of D_{4h} and contains only eight one-dimensional representations. Correlations between the representations of D_{4h} and

Figure 7.2 Theoretical stick spectra simulations for identical four spins in the configuration corresponding to a). a square; b). a rectangle; c). a general, asymmetric grouping. Although some allowed lines have very low intensity, the number of allowed pairs follows closely the predictions of the argument in the text (respectively 22 pairs, 46 pairs, and 120 pairs).

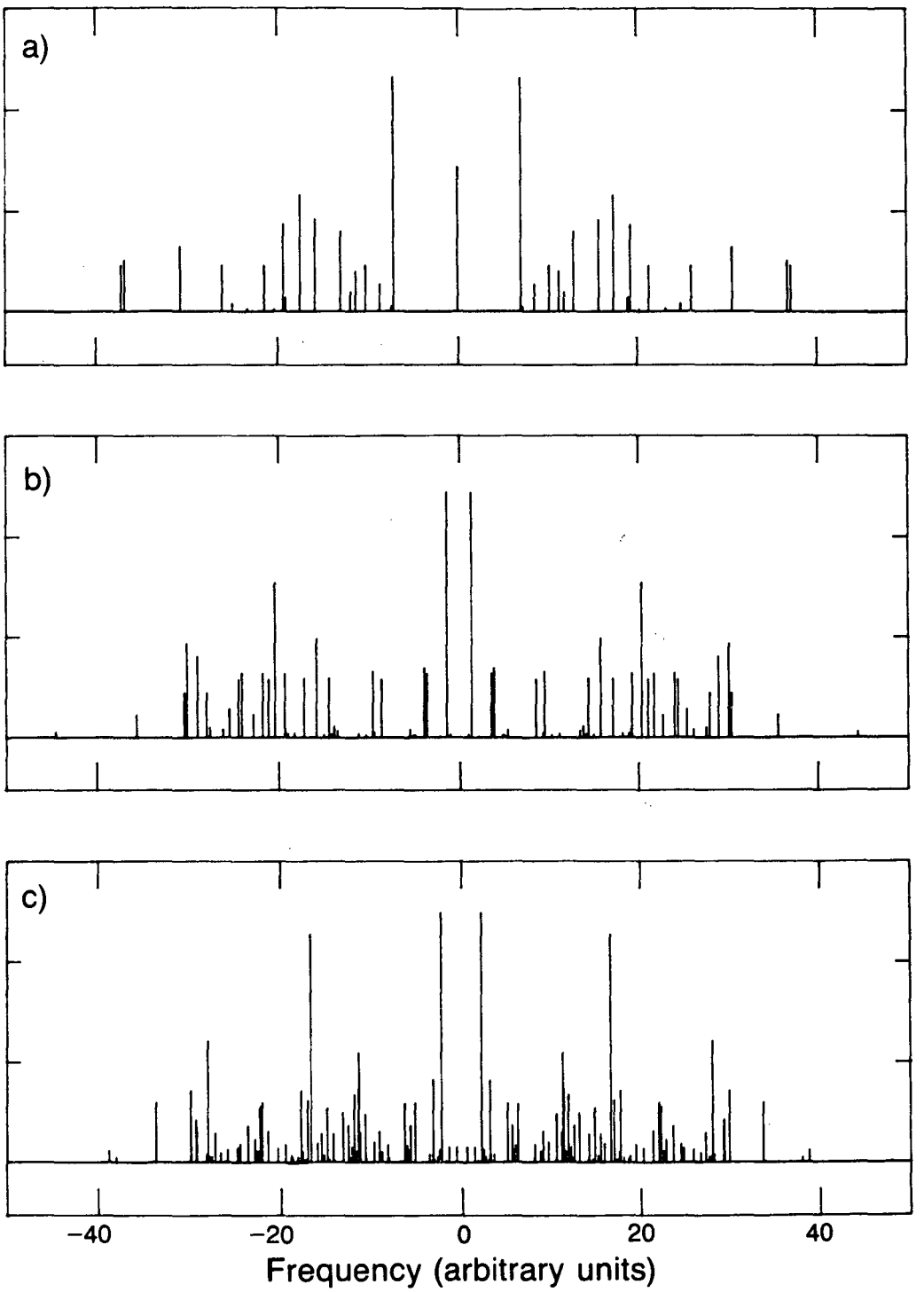

XBL 857-11246

its subgroup D_{2h} are given in Table 7.3. (where gerade states correlate only to gerade and ungerade to ungerade) [137]

Table 7.3

Correlations Between D_{4h} and D_{2h}

Class in D_{4h}	B_1, A_1	B_2, A_2	E
Class in D_{2h}	A	B_1	B_2, B_3

and the states partition into the classes

$$5A_g + B_{1g} + B_{2g} + B_{3g} + 2A_u + 2B_{1u} + 2B_{2u} + 2B_{3u} \tag{7.33}$$

Selection rules can be summarized as:

Operator	I_z	I_y	I_x
Correlations	$(A \to B_1), (B_2 \to B_3)$	$(A \to B_2), (B_1 \to B_3)$	$(A \to B_3), (B_1 \to B_2)$

(7.34)

where, in my unconventional group notation, (again, g and u are defined with respect to the σ_z operation and not the inversion center) I_x and I_y belong to the ungerade representations and connect u→g and g→u, and I_z is gerade and connects u→u and g→g. Each ungerade operator transition operator is responsible for 16 pairs of lines, and I_z contributes 14 more. Computer simulations agree with these predictions. The spectrum of a rectangular array of four spins is shown in Figure 7.2b. Most of the predicted lines are observed. Some lines have very low intensities, and others overlap (within the resolution of the plot) or coincide so the full complement of lines is not observed in the simulation.

c. General Four-Spin Systems

Finally, Figure 7.2c shows the spectrum of a four spin system

with no symmetry. Equation (4.22) predicts 120 pairs of lines. The number of lines which appear in the computer simulation is exactly 120 pairs. The experimental spectra of Figures 4.11 and 4.15 with experimentally achievable linewidths show little structure due to isolated lines.

3. Three Spins 1/2

The highest symmetry in three spin systems is the arrangement corresponding to the spatial arrangement of an equilateral triangle. where all internuclear distance (and therefore coupling constants) are alike in homonuclear spin systems. Naively we would classify this group this set as belonging to the symmetry group D_{3h}. Because $T^2 = -1$ for odd numbers of spins-1/2, a 2π rotation does not correspond to the identity operation and the number of operations in the point group is twice as large as are in D_{3h} (consisting of $\bar{E}$ times all of the normal point group operations). The double group is not, however, a product group in that the new classes and representations are not direct products of the new operation $\bar{E}$ with all of the previous operations. For D'_{3h} the character table for the double group representations is given in Table 7.4.[139] In the notation introduced above, the effect of

Table 7.4

Extra Characters of the Double Group Representations for D'_{3h}

	E	$\bar{E}$	$2C_3$	$2\bar{C}_3$	$3C'_2, 3\bar{C}'_2$	$\sigma_h, \bar{\sigma}_h$	$2S_3$	$2\bar{S}_3$	$3\sigma_v, 3\bar{\sigma}_v$
Γ^1	2	-2	1	-1	0	0	$\sqrt{3}$	$-\sqrt{3}$	0
Γ^2	2	-2	1	-1	0	0	$-\sqrt{3}$	$\sqrt{3}$	0
Γ^3	2	-2	-2	2	0	0	0	0	0

the symmetry operations (only for one member in each class and only for

unbarred operations, as the barred operations are identical except for a factor of -1) is given in Table 7.5. Summing over the characters, the grand orthogonality theorem predicts that the eigenstates partition into the classes

$$2\Gamma^3 + \Gamma^1 + \Gamma^2 \tag{7.35}$$

The angular momentum operators, like all observables, must belong to the single valued representations (otherwise, observables would exhibit spinor behavior directly). I_z belongs to A_2' and (I_x, I_y) to E''. Given these transition operators, eigenstates are coupled if they belong to representations for $\Gamma^j \rightarrow \Gamma^j$, and Γ^1, $\Gamma^2 \rightarrow \Gamma^3$. Transitions between Γ^1 and Γ^2 are forbidden. This corresponds to a total of five pairs of lines and a singlet at zero frequency. An example is shown in Figure 7.3a which is a computer simulation of the spectrum of three ^1H spins in the configuration of an equilateral triangle.

Table 7.5

Operations of the Double Group D_{3h}'

E	C_{3z}	C_2	σ_h	S_3	σ_v
(123)	$e^{2i\pi m/3}(312)$	$(-1)(\bar{1}\bar{3}\bar{2})$	$(-1)^{-m}(\bar{1}\bar{2}\bar{3})$	$e^{(-m\pi i/3)}(312)$	$(i)^{2m-1}(\bar{1}\bar{3}\bar{2})$

In three-spin systems of lower symmetry, it is simple to derive the appropriate representations by working with the appropriate subgroups of D_{3h}' in the same manner used in the comparison of the three four-spin systems in the previous subsection. First the equilateral triangle is transformed into an isosceles triangle by moving spin 3

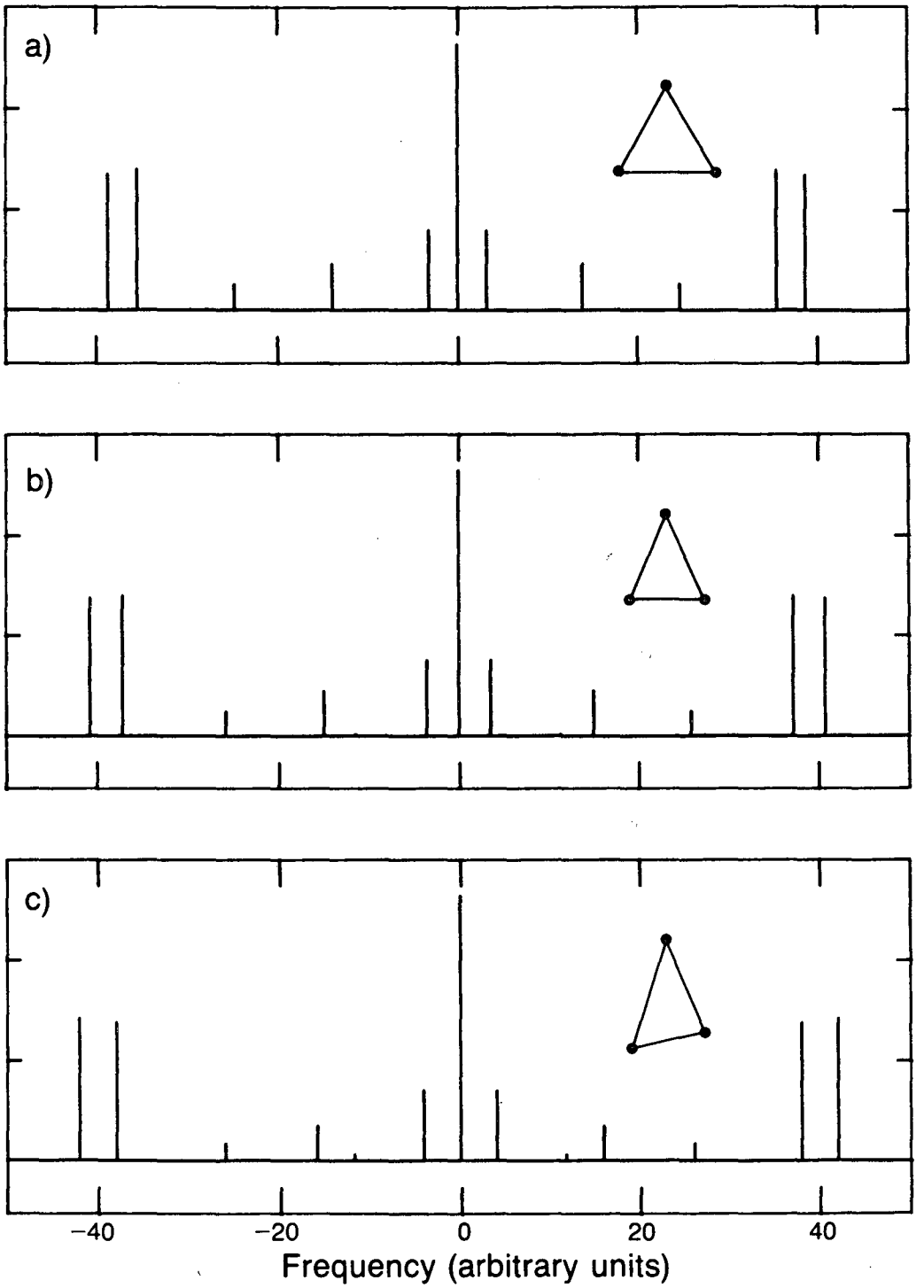

Figure 7.3 Simulated stick spectra for 3 identical spins in the configuration corresponding to a). an equilateral triangle; b). an isosceles triangle; c). a scalene triangle. In a). only 5 pairs are observed; in b). a sixth pair appears but with very low intensity. In c). the intensity of the new pair is somewhat larger.

along the perpendicular bisector of r_{12}. The C_3 and S_3 symmetry axes are lost, as well as 2 each of the C_2 and σ_h operations. The remaining classes of double group operations are E, $\bar{E}$, $\{C_2, \bar{C}_2\}$, $\{\sigma_v, \bar{\sigma}_v\}$, and $\{\sigma_v', \bar{\sigma}_v'\}$ and the group is C_{2v}' (after a slight redefinition of axes; previously, the z axis was chosen along the C_3 axis; here, it lies along the perpendicular bisector of r_{12}. Only one spinor representation of the double group exists and all eigenstates fall into this one class. Transitions are allowed between all four degenerate pairs and also between pairs of degenerate states. Thus, six pairs of lines and a singlet are predicted, and are shown in the simulation of Figure 7.3b.

This is, in fact, the maximum number of lines allowed for a three spin system and the number predicted in Equation (4.22). The scalene triangle (no symmetry elements except for the necessary inversion plane corresponding to the plane defined by the three nuclear sites) belongs to the double group C_s' with operations E,$\bar{E}$, σ, and $\bar{\sigma}$. There are two spinor representations. Each is one-dimensional but the two representations are degenerate according to the conditions of the Frobenius-Schur test.[105] All transitions are allowed and the maximum of six pairs and a singlet at zero frequency are again observed (Figure 7.3c).

4. Heteronuclear Spins

As I mentioned near the beginning of this chapter identical spins are those which share identical sets of coupling constants to all other spins. In a two-spin system, spins are identical independent of their precise nature as the system supports only one coupling constant. In larger spin systems, this need not be so. Figure 7.4 compares the

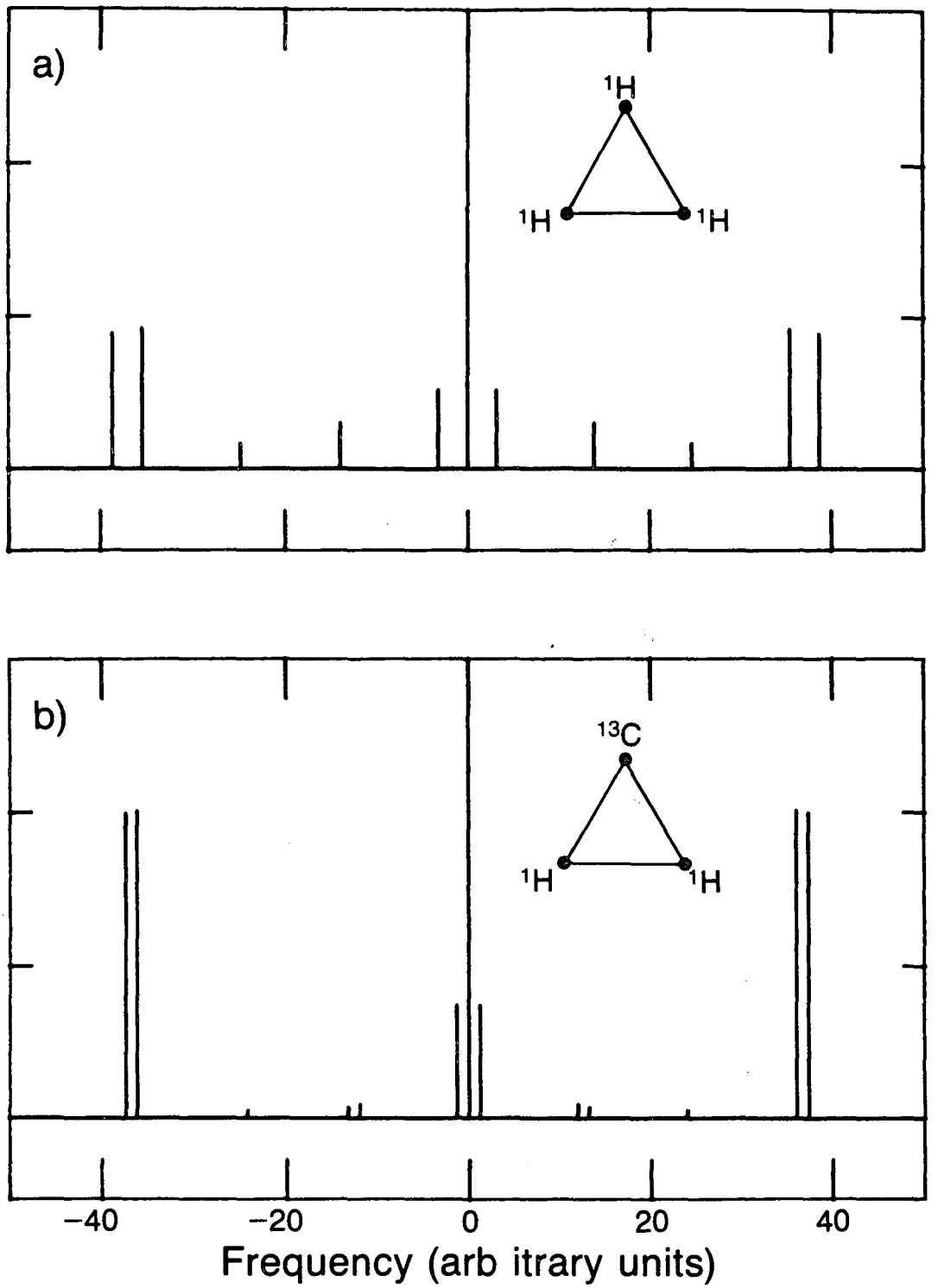

Figure 7.4 Simulations for three spin groupings in equilateral triangle. a). Identical spins; and b). One heteronuclear spin (i.e. different γ) and two identical spins. b). shows the number of lines predicted for the asymmetric systems.

computer-simulated spectra for the array of three identical spins in the configuration corresponding to an equilateral triangle as discussed above to the spectrum of a heteronuclear I_2S triplet with the same geometric configuration. Figure 7.4b clearly shows all six pairs of allowed lines. The symmetry is determined not by the spatial orientation, but by the coupling constants. In homonuclear spin systems only these parameters are proportional to one another. This correspondance between the coupling constants and the geometrical form is convenient as it affords a simple treatment of the symmetry operations based on the isomorphism between the permutations of spins and the exchange of spatial positions. Where this isomorphism no longer holds, it is not obvious how best to proceed.

C. Conclusions

The techniques of this chapter can be extended to cover systems of coupled quadrupolar spins ($I \geq 1$). Because the quadrupolar interaction dominates the spectrum and the dipole-dipole coupling is usually only a small perturbations, these methods will rarely be necessary or even particularly useful. But for coupled spins-1/2 in zero field, the symmetry properties are the only source of selection rules and may have a marked simplifying effect on the zero field spectrum. It is straightforward to extend the principles discussed in this chapter to higher rank operator initial conditions.

VIII. Experimental Details

This chapter summarizes the design criteria and the experimental apparatus used in field cycling Fourier transform zero field NMR and NQR experiments. A more complete technical description is given elsewhere.[75] First, I describe the general experimental approach to the creation of the zero field region. Second, I provide a brief overview of the solid state high field NMR spectrometer used in the polarization and detection periods. Zero field NMR experiments have been performed on two very similar machines in the Pines laboratory. Most of the work presented in this thesis was executed on the β spectrometer, and some machine-specific characteristics are mentioned. Finally, I conclude with some thoughts on alternative solutions to the problem of high sensitivity zero field magnetic resonance.

A. Zero Field Region

The distinctive aspect of the field cycling scheme described in Chapter III is that the evolution of coherence is initiated and terminated by the sudden removal and reapplication, respectively, of a large static field. Chapter VI introduced the possibility of zero field nuclear resonance with demagnetization to zero field and where short, strong DC field pulses initiate evolution. Instrumentation requirements are similar for these two experiments. For concreteness, I specialize the discussion to systems of dipole-dipole coupled spins where an intermediate field of 100 gauss is sufficient, and to experiments where the field is suddenly switched off and on. Identical

hardware with only modest modifications serves to provide the larger intermediate field required in NQR or where pulsed fields are useful.

1. Timing Considerations

There are two practical criteria for the measurement of zero field NMR signals by the general scheme of Figure 3.1. First, the field cycle must be sufficiently rapid that magnetization created in the high field polarization phase survives to be observed in the detection phase; therefore, the total cycle time (τ_c) can be no longer than the high field T_1. In many samples, low field T_1's are significantly shorter than high field T_1's and zero field signal may not be observed even if τ_c is much shorter than the high field T_1. Second, the actual switching period between the high field condition ($H_Z \gg H_{loc}$) to the low field condition ($H_Z \ll H_{loc}$) must occur sufficiently rapidly so that coherence does not decay. This coherence is precisely those terms in ρ which become time-dependent as a consequence of the switching itself. The switching time, τ_s, should be much shorter than T_2, the coherence lifetime. If the spectrum contains no resolved lines then its spectral width is characterized by the square root of its second moment, and $M_2^{-1/2} < T_2$. A stringent criterion is therefore that $\tau_s \ll M_2^{-1/2}$. Then negligible evolution occurs under H_{loc} during the switching off and on of the fields. Instantaneous switching in the sense of the sudden approximation[64] would require that $\tau_s \ll 1/\omega_0$, where ω_0 is the Larmor frequency in the intermediate field. Larmor precession during the field transient does not destroy coherence and should be of little consequence.

2. Field Cycling

As zero field frequencies range from 1 Hz to 1 GHz, no single

technique is universally applicable. For nuclear spin systems where the zero field frequencies are much larger than ~1 MHz, pure NQR is sufficiently sensitive. As described in Chapter II, field cycling techniques are normally required only at lower frequencies or where the concentration of the interesting spins is low. In our work, we have concentrated on spin systems where the natural frequencies are < 1 MHz, and $\tau_s \simeq 1\ \mu s$ is adequate. While switching of small electromagnets on this time-scale is feasible[53a,74], it is difficult to turn off and on the large fields (> 1 Tesla) routinely used to prepare and detect magnetization in NMR spectrometers in such short times. Neither is it necessary to do so. Just as two separate timing criteria govern the successful execution of the experiment, the field can be brought from a large value to zero in two separate stages.

The field cycle is illustrated in Figure 8.1 and will be described using the notation of that figure. In the first stage, the sample is removed from the polarizing magnet (B_0) by mechanical means and the applied field is lowered from the large value appropriate for polarizing the spins to an intermediate value (100 gauss) which can be easily switched. In the second stage, this intermediate field is quenched. The first stage need only be completed in a time ~T_1 which may be as long as minutes. It is conveniently accomplished by mechanical shuttling of the sample from the bore of the main magnet B_0 to a point ~75 cm below the center of B_0 and where the fringe field due to B_0 is ~100 gauss. Because of the stresses involved in repeated acceleration and decelaration, the sample must be contained in a shatter-resistant container. Kel-f and nylon cylinders have the appropriate tensile qualities. The second stage must be completed in

Figure 8.1 Diagram of the field cycling apparatus and the timing sequence of the pulsed fields. B_0 is the superconducting solenoid where the polarization and detection periods occur; B_1 and B_2 are switchable electromagnets positioned ~75 cm beneath the bore of B_0. A glass tube encloses the sample and guides it between the high and low field regions. As the sample is removed from B_0 it travels in the fringe field of B_0 to a field of 100 gauss. Both electromagnets are switched on; B_2 rapidly causes the field to nearly double, and B_1 slowly compensates for the fringe field due to B_0. Then B_2 is rapidly switched off and the evolution period t_1 is initiated. When B_2 is turned back on t_1 is ended. B_1 is turned off, then B_2 and the sample returned to high field.

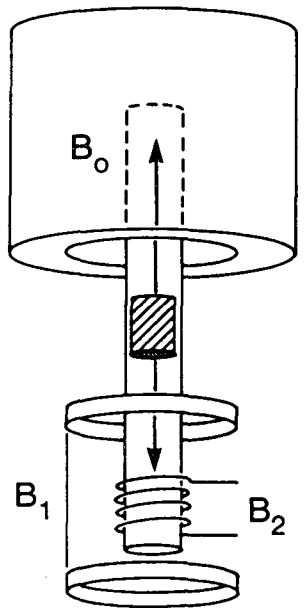

$B = B_o + B_1 + B_2$

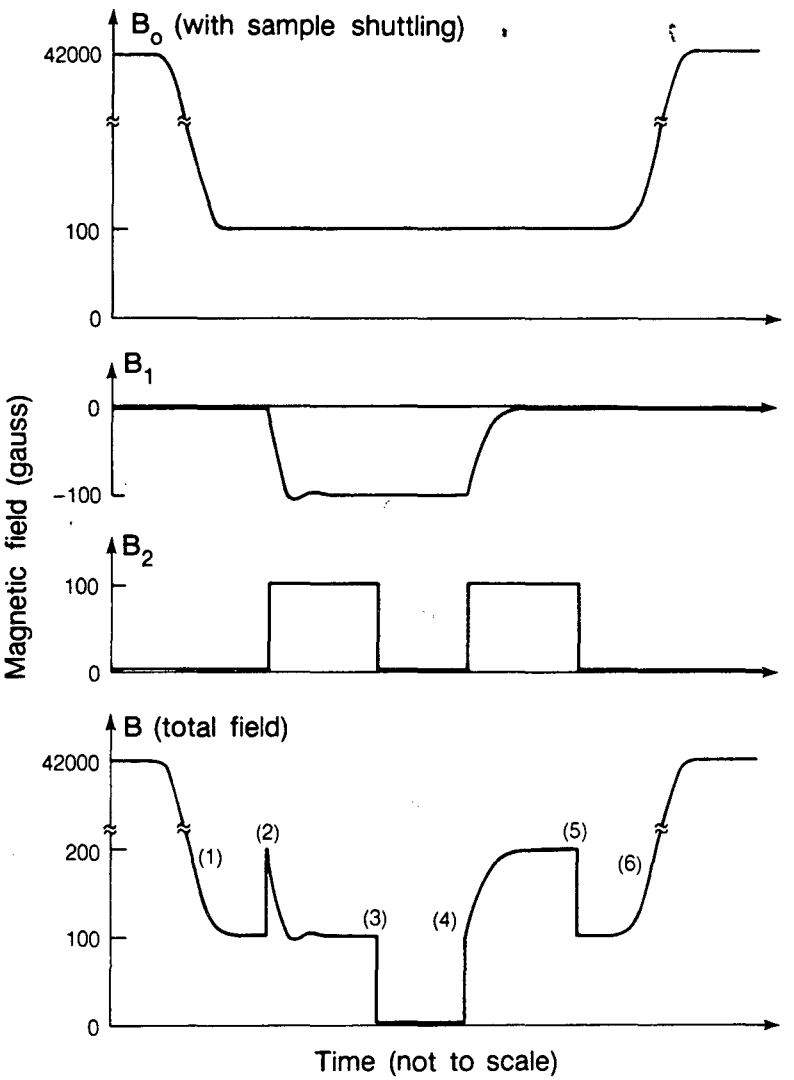

XBL 854-10155

the shorter period, τ_s.

3. Area of Zero Field

Below the main solenoid B_0 lies the zero field region. A pair of electromagnets (B_1 and B_2) are wound which provide a means for applying time-varying fields to the sample. The overall goal is to provide a mechanism for suddenly switching off the residual field at the sample which still arises primarily from the fringe field due to B_0. In principle, a single precisely-wound magnet coil might be designed to simultaneously compensate for the residual magnetic field over the volume of the sample and afford rapid switchability. In practice, such a unified approach imposes intolerable design requirements and we have chosen to separate out the two functions. B_1 (in conjunction with a number of unswitched shim coils) is designed to accurately negate the fringe fields and produce a sizeable volume of zero or near-zero field. This coil is referred to as the bucking coil. B_2 is a small, low-homogeneity coil which just barely encloses the sample volume and is called the switching coil. It is designed to be rapidly switched on and off, and is the source of the "suddenness" in the experiment. This two-coil arrangement poses one complication. B_1 nulls the fringe fields over a large volume of space. Were it energized continuously, the sample would pass through a field-free region during transit and before feeling the effects of the switching coil. Therefore B_1 as well as B_2 must be switched. This insures that the sample always remains in a large applied field until B_2 is shut off. The complete field cycle is shown in Figure 8.1.

Adiabatic field cycles can be executed by merely reversing the sequence of low field pulsed fields. After mechanical translation of

the sample, B_1 is turned on and the field slowly (~ ms) is reduced from 100 gauss to zero. Then a short pulse can be applied through B_2 to initiate coherence or store evolved order. In pulsed experiments, B_2 may be replaced with a more homogeneous small solenoid.

If the intermediate field does not satisfy the high field condition, then order in the intermediate field will be some linear combination of Zeeman (high field) order and dipolar or quadrupolar (zero field) order. When the applied field is switched off, only the Zeeman order evolves. No new frequencies can be observed because the Hamiltonian supports no others. The overall intensity of the spectrum, and therefore signal-to-noise ratio, will be diminished and relative intensities may be distorted. But no frequency distortion will be observed.

4. Details of the Field Cycle

The complete field cycle is composed of the following steps:

1. The sample is polarized for a time $\sim T_1$ in the high field B_0.

2. A three-way gas valve is switched. Negative pressure applied to the bottom of the glass tube which contains the sample holder causes the sample to move from the bore of the magnet into position in the zero field region. Throughout the transit period (~150 ms), the sample resides in the fringe field due to B_0 which is always greater than 100 gauss. Marginally faster transport is possible (at the expense of significantly more broken glass and frayed graduate student nerves).

3. Both coils (switching and bucking) are simultaneously energized. The switching coil B_2 adds a field equal and parallel to the fringe field of B_0 and the applied field rapidly (~300 ns)

approaches ~200 gauss. B_1 energizes more slowly (~10 ms) and the applied field slowly falls back to the field of B_2 alone. If at all times the applied fields are large compared to the local fields, these additional transients have no effect on the stored nuclear magnetization.

4. The switching coil B_2 is quenched. Zero field evolution is initiated. At a time t_1, the switching coil is reenergized. The evolved magnetization is stored.

5. The bucking coil is switched off. The field gradually increases.

6. The three-way gas valve is switched. Pressure applied at the sample returns it to high field.

7. The amplitude of the evolved magnetization is sampled.

Each time steps (1-7) are executed, a single value of the zero field free induction decay is measured. The entire evolution and decay is mapped out by incrementing the time interval t_1 from zero to some value where no further evolution is observed. Nyquist's theorem states that any waveform must be sampled at least twice per cycle if aliasing of frequencies is to be avoided. The highest frequencies which appear in the zero field spectrum are no smaller than the highest frequencies observed in the high field spectrum. This determines the proper value of the t_1 increment. In many dipolar coupled systems, sampling increments of 4-10 μs are adequate (giving bandwidths from ±50 to ±125 kHz). NQR studies frequently require larger bandwidths and t_1 increments of 3 μs or less are common. Figure 8.2 shows a typical zero field NQR ^{2}D free induction decay $G(t_1)$ for perdeuterated 1,4-dimethoxybenzene detected by the point-by-point experimental procedure

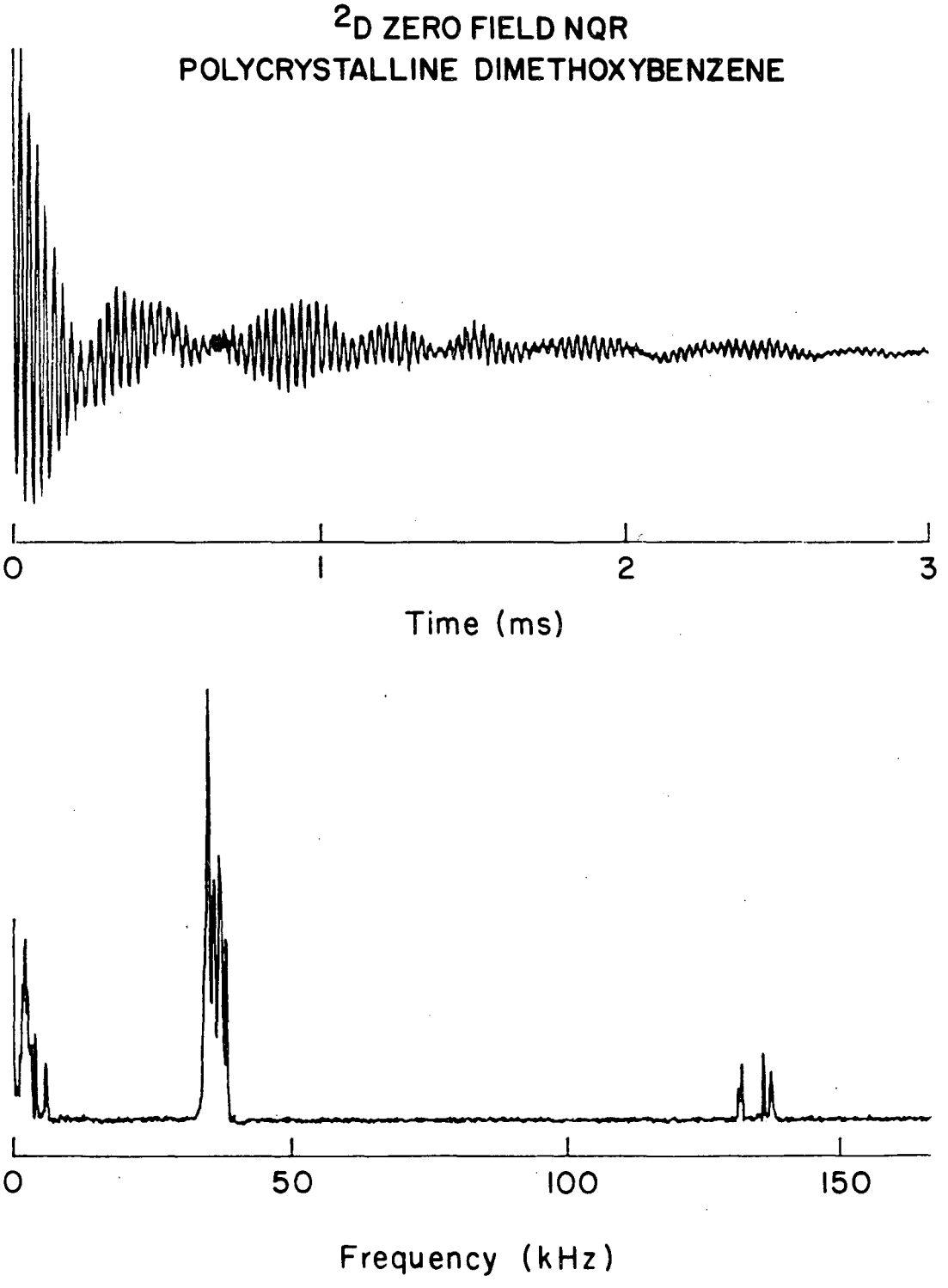

Figure 8.2 ^{2}D NQR free induction decay (the signal function $G(t_1)$ from polycrystalline perdeuterated dimethoxybenzene and the associated spectrum, $f(\omega)$.

described above. Below is its Fourier transform, the zero field spectrum $f(\omega)$.

5. Zero Field Homogeneity

The homogeneity of the zero field region is determined by the care with which the bucking coil is wound and the shim coil currents are adjusted. Residual fields no larger than .1 gauss can be measured using only a commercial gaussmeter as probe. Because small fields are truncated by the larger local fields (see Section III.D) it is rare that much finer adjustment is necessary. Where necessary, further improvements can be made by iteratively shimming on the zero field NMR signal in liquid samples.

B. High Field NMR Spectrometer

The high field portions of our experiments take place in a homebuilt solid state NMR spectrometer documented more fully elsewhere.[140] The nominal field strength of the superconducting solenoid is 42 kgauss (4.2 Tesla) corresponding to a ^1H resonance frequency of 185.03 MHz. Without room temperature shims, the homogeneity of the field is ~1 ppm over 1 cm^3. The field is extremely stable and no lock is necessary. A homebuilt microprocessor-based programmable pulser[141] controls all aspects of spectrometer operation and executes all timing-critical operations. It is based on a 10 MHz clock and the shortest time increments available are 100 ns. A total of 20 logic outputs are available to control the output of rf pulses (two sets of six gates each), trigger auxiliary devices (e.g. the three-way air valve and current pulsers), and initiate digitization of

the data.

1. Transmitter Section

The transmitter section is designed to provide spectrally pure rf pulses at high power levels and over a broad range of frequencies. Its heterodyne design affords maximum convenience in changing the frequency of the rf pulses delivered to the probe. The local oscillator (lo) frequency is 30 MHz. Four phases of 30 MHz rf set 90° apart are available. The Larmor frequency is produced by mixing the lo with the intermediate frequency (if) derived from a highly stable frequency synthesizer. In high field experiments on ^{2}D, the Larmor frequency (28.4 MHz) is uncomfortably close to the lo frequency and no heterodyning is performed. Instead, four phases of 28.4 MHz rf are produced directly. Finally, the filtered Larmor frequency is delivered to final stage amplifiers which are capable of delivering more than 100 watts of rf power at the ^{1}H, ^{7}Li, and ^{31}P Larmor frequencies, and more than 1000 watts at the ^{13}C, ^{2}D, and ^{27}Al Larmor frequencies.

All probes used in the experiments described in Chapters III-VI are home-built and employ a gapped-solenoid resonator in series with high power capacitors. The gapped-solenoid design suffers from a relatively poor filling factor and lowered sensitivity, but was deemed necessary to afford access to the probe from below. When air pressure is applied from below, the sample is held snugly in place within the rf coil by a Kel-f plastic stop. With the rf pulse powers provided by the final stage amplifiers, rf fields larger than 50 kHz ($\pi/2$ pulse $\leq$ 5 μs) can be applied at the Larmor frequency of any of the nuclei listed above.

2. Receiver Section

After the application of a strong (≥ 100 watt) rf pulse, the receiver and tank circuit appear to recover fully in ~20 μs. The receiver section has an overall noise figure of 3 dB or better at all frequencies of interest. Over most of the Larmor frequencies of interest, the receiver is based on a phase-sensitive superheterodyne detector which mixes the rf down successively to 30 MHz and finally to audio frequencies. The audio frequency signal is equivalent to the rotating frame signal. Under control of the pulse programmer, the spectrometer data acquisition system is instructed to sample each phase of the audio-frequency signal. As it is acquired, two 10-bit data words are delivered to the spectrometer's minicomputer (a Data General NOVA model). Data acquisition rates are limited by the rate of direct memory transfer. Typical maximum transfer rates are ~200 kilosamples/second, and as many as 2048 complex data points may be sampled in a single pass.

3. High Field Detection Sequences

The importance of efficient high field detection sequences cannot be overemphasized! Because the zero field signal is observed with no better signal-to-noise ratio than that of the high field signal, improvements in overall experimental performance come most quickly with improvements in the high field detection sequence. Because the experiments can be rather lengthy and demanding of the spectrometer, it is also essential that the detection sequence be phase-cycled. The output from some of the very high-power amplifiers seem temperature-sensitive. Zero field free induction decays in deuterated samples which require overnight runs inevitably exhibited very low-frequency drift which could be largely suppressed by adding together only a pair

of decays with properly cycled detection sequences.

In the discussions of Chapters III-VI the details of the high field detection sequence were ignored. Tacitly, I assumed that the amplitude of the evolved magnetization could be sampled directly. In practice, any detection sequence must transfer longitudinal magnetization into transverse magnetization which can be measured. If the entire high field signal is sampled and digitized, then the resulting signal function is a two-dimensional data set $G(t_1,t_2)$ where t_1 is the zero field interval and t_2 is the high field interval.

This general class of experiment is shown in Figure 8.3. The simplest detection sequence is to apply a single rf pulse to the sample and immediately begin sampling the transverse magnetization. Because the high field signal may decay significantly during the recovery time of the receiver it is preferable to record the amplitude of the signal after a solid echo sequence.[142] In rigid quadrupolar I = 1 systems the solid echo accurately reproduces the free induction decay. In dipole-dipole coupled systems, the solid echo is not equivalent to the free induction signal following a pulse and the spectrum is distorted. Two-dimensional Fourier transformation results in a two-dimensional spectrum $f(\omega_1, \omega_2)$ where the projections along the ω_1 and ω_2 axes correspond to each of the one-dimensional spectra and the cross-peaks in the two-dimensional plane indicate the correlations between the two frequency domains. Figure 8.4 is such a two-dimensional zero field-high field correlation spectrum. It shows the zero field NMR spectrum of $Ba(ClO_3)_2 \cdot H_2O$. In the zero field domain the triplet of lines introduced in Figure 3.3 reappears. In the high field domain, the classic Pake powder pattern is observed. Lines which appear at zero

Figure 8.3 Two dimensional zero field-high field correlation experiment. After the sample is returned to B_0, its high field free induction decay is measured after a resonant rf pulse. Fourier transformation of $G(t_1, t_2)$ with respect to both t_1 and t_2 produces the two dimensional spectrum $f(\omega_1, \omega_2)$.

Figure 8.4 Two dimensional zero field-high field correlation spectrum of polycrystalline $Ba(ClO_3)_2 \cdot H_2O$. For each of 64 values of t_1, the zero field interval, the high field signal after a solid echo is accumulated and stored. A double real Fourier transformation is applied to the signal function $G(t_1,t_2)$. At the left and at top are the projections of the zero and high field spectra. In the center, the correlations between the two frequency domains. Signals which appear at zero frequency in the ω_1 domain correlate most strongly with signals from orientations of the two-spin system which are nearly at the edges of the high field powder pattern. Zero field signals which appear at ±42 kHz correlate to orientations which appear near the peaks of the high field powder pattern.

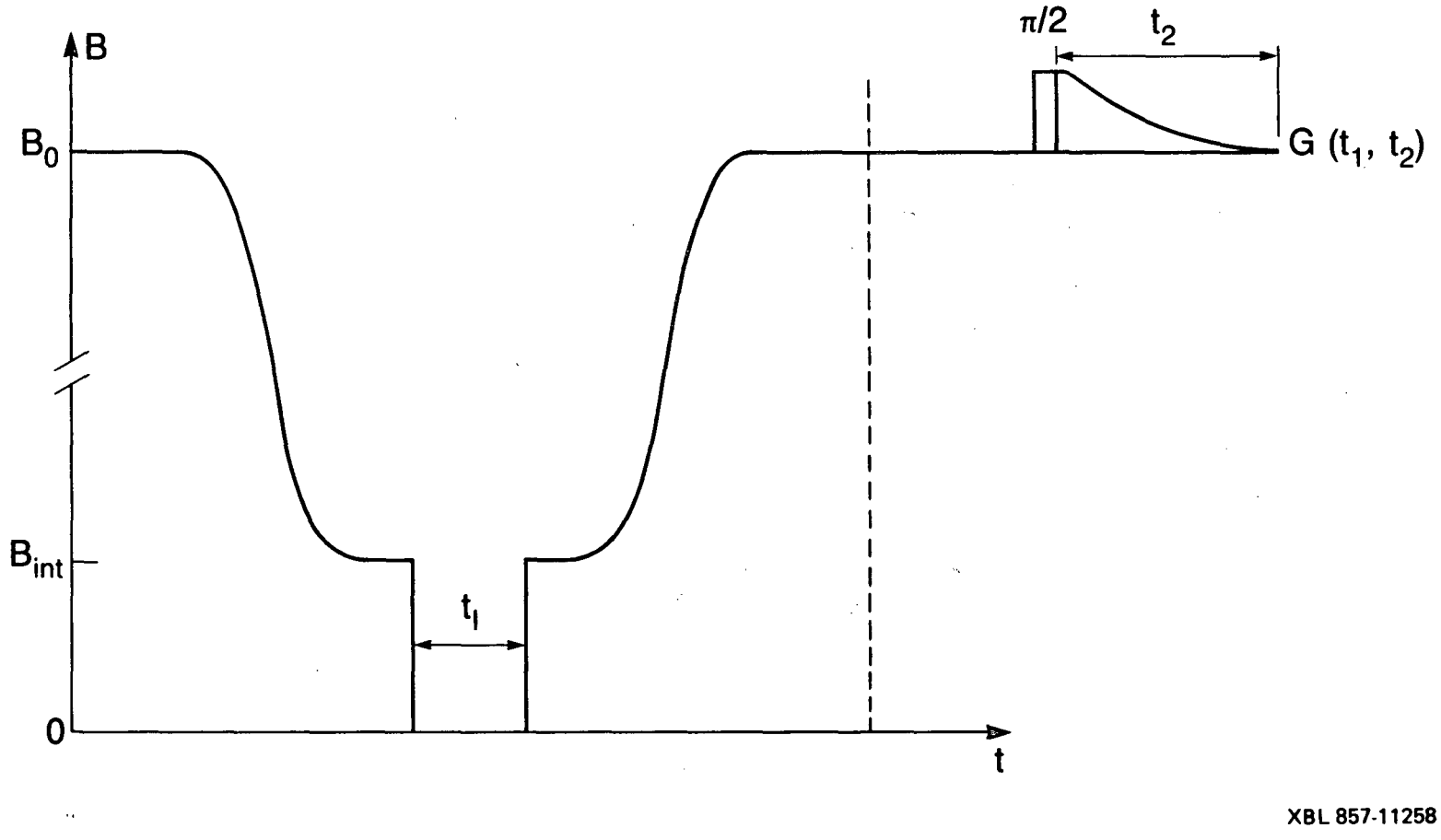

Figure 8.3

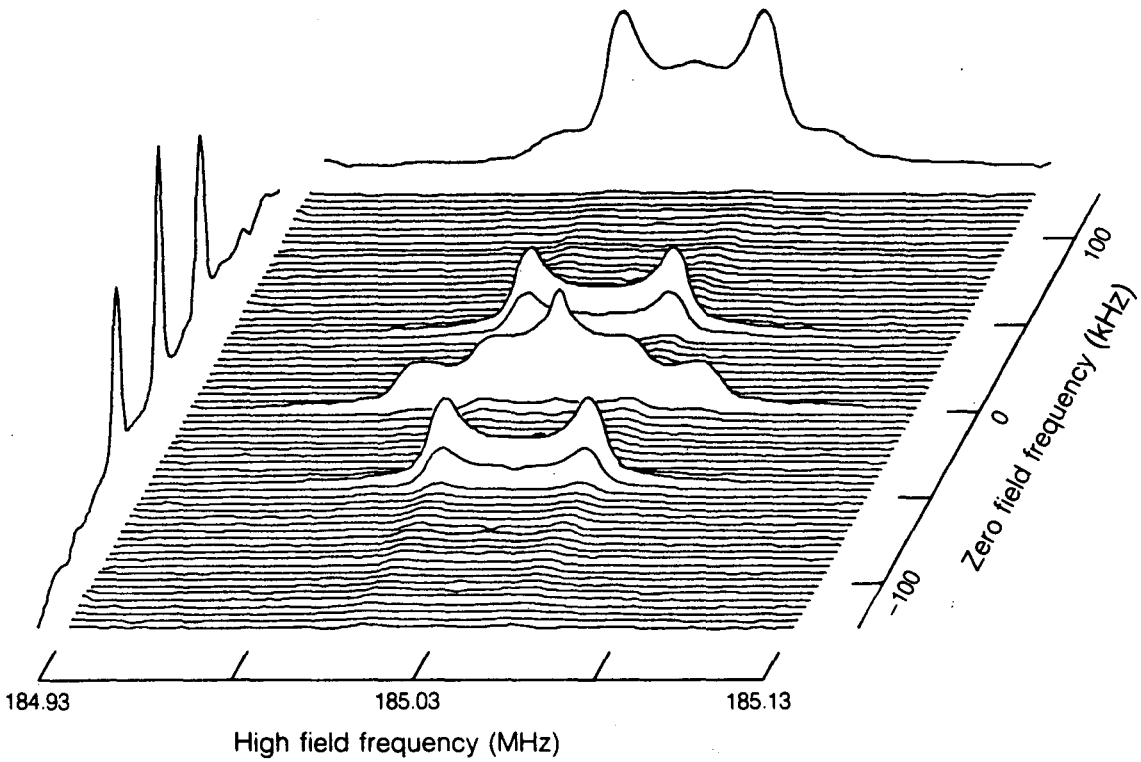

XBL 852-1105

Figure 8.4

frequency in the ω_1 (zero field) dimension correlate most strongly to the highest frequency components of the ω_2 (high field) dimension (i.e. those portions of the powder which are least truncated by the Zeeman field), and vice versa. This agrees with the treatment of the zero field intensities given in Chapter III and contains essentially the same information as the single-crystal high field-zero field experiments in Figure 3.2.

As the motivation for performing the zero field experiment is that the high field dipolar and quadrupolar powder patterns are broad, often featureless, and largely devoid of useful information it will rarely prove interesting to accumulate a normal high field free induction decay in t_2. As long as the same Hamiltonians govern the dynamics of both t_1 and t_2, ω_2 contains the same information as ω_1 except at significantly lower resolution. Two options, then, are available: first, the high field evolution can be made more interesting by selectively averaging away the second-rank tensor interactions,[2,8] or second, information about the high field evolution can be sacrificed in order to maximize the sensitivity with which the zero field signals are mapped out. Almost without exception, we have chosen this latter alternative. By applying a simple sequence of a large number of closely-spaced pulses, evolution under the high-field Hamiltonians can be eliminated and the transverse magnetization observed to decay with a time constant more nearly that characteristic of high field T_1's than of high field T_2's. Using pulsed spin-lock[143] detection sequences in t_2, the signal can be sampled repeatedly at very nearly its initial value. Integrating over the signal sampled in the windows of the detection sequence results in large gains (anywhere from 5-50) in the

signal-to-noise ratio of the zero field experiment. Detection sequences used in the high-field observation of zero field NMR are summarized in Figure 8.5.

In many systems, spin-lock detection sequences may not be possible to execute. Transverse magnetization cannot be preserved longer than the time constant known as $T_{1\rho}$.[21] $T_{1\rho}$ is short for systems where the local Hamiltonian is time-dependent (i.e. motionally averaged). Heteronuclear dipole-dipole couplings (e.g. in organic solids where the ^{1}H nuclei are dilute in ^{2}D) seem not to be efficiently averaged away by the spin-lcoking sequence. No sequences seem available which significantly extend the decay time of half-integer quadrupolar nuclei where only the central transition is observed. In these systems, the inefficiency of the high field detection sequence may severely limit the sensitivity of the zero field method, and argues strongly for the continued development of the time domain indirect detection methods briefly explored in Chapter VI.[62] Zero field NQR studies are particularly hampered by the difficulty of designing efficient high field detection sequences.

Ideally, one would like to incorporate high resolution chemical shift measurements in the high field time-interval t_2 to provide correlations between the geometric factors derived from the dipolar spectra in ω_1 with site identification via chemical shifts in ω_2 by magic angle spinning. Practical considerations make such an experiment difficult. Rotation about a laboratory-fixed axis during the zero field interval reintroduces powder broadening even in zero field (see Appendix B). High speed spinning inserts ($\geq$ 3 kHz) are not readily started and stopped. In homonuclear spin systems, one can compensate

Figure 8.5 Pulse sequences for use in zero field NMR experiments.
a). 90° pulse initiates evolution. The high field free induction decay is sampled as soon as possible after the pulse.
b). Solid echo sequence. The second pulse causes the magnetization to refocus and form an echo. This allows for the magnetization to be sampled many μs after the pulse and alleviates experimental difficulties associated with the dead time of the receiver.
c). Multiple pulse sequence (WAHUHA). Sampling in the windows after every fourth pulse yields the high field chemical shift spectrum.
d). Pulsed spin locking (or multiple echoes). After each pulse, the magnetization can be sampled. For dipole-dipole coupled spin systems, $\theta = 45^{o}$ minimizes the decay. For quadrupolar systems θ is chosen empirically; in ^{2}D NQR, $\theta \sim 80^{o}$ often appears optimal.

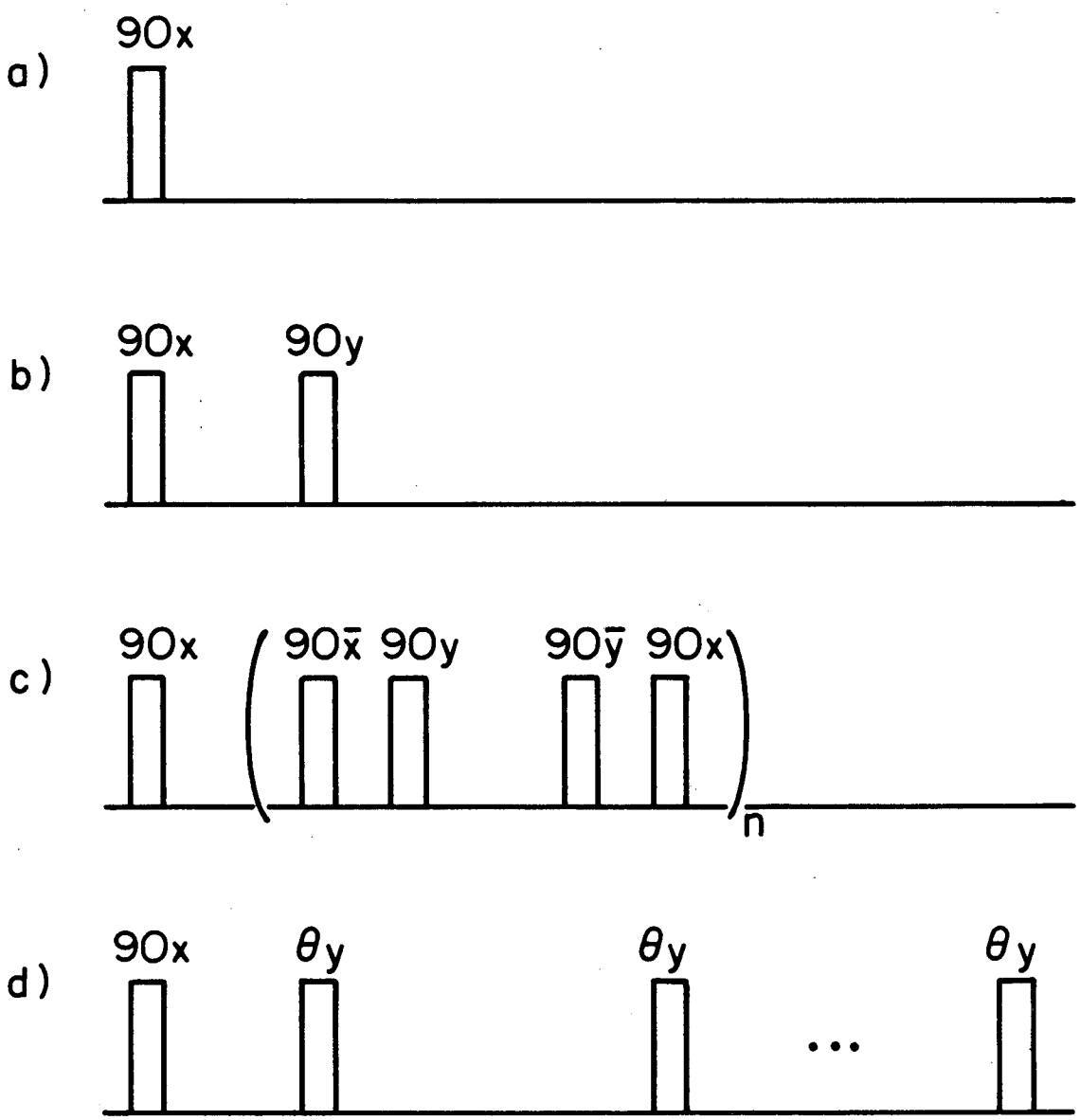

XBL 847-3138

for the spinning by cycling not to zero field but to some small field whose amplitude and direction are precisely adjusted to null the effects of the spatial rotation. No such adjustment can be made in heteronuclear spin systems where magic angle spinning in combination with high power heteronuclear decoupling proves most powerful. Magic angle hopping in t_2[144] may prove more feasible.

C. Extensions and Improvements

1. Electronically Switched Main Coil

For systems whose T_1's are so short that all prepared magnetization disappears during the mechanical shuttling between high and intermediate fields, the entire field cycle may be executed in a sequence of two electronic steps. Variable field T_1 spectrometers[145] are designed to allow for rapid (~ms) variations of large fields (~1 Tesla). In other applications, the feasibility of rapid switching of extremely large fields (~40 T in ~5 ms) has been demonstrated.[146] While the initial polarization amplitude and the detection sensitivity may suffer due to the lower values of B_0, for samples with short T_1's the decrease in cycle time should more than compensate for the smaller signals predicted if T_1 were sufficiently long.

2. Direct Detection in Zero Field

One of the most exciting and promising of new technological advances in the sensitive detection of low frequency rf signals is the dc SQUID (Superconducting QUantum Interference Device). It is an ultra-low noise rf flux detector (where normal Faraday-law detectors are sensitive to the derivative of the flux). As such, it is equally

sensitive over a broad range of rf frequencies. Recent experiments have demonstrated its sensitivity in the detection of fluctuations in the macroscopic polarization of an ensemble of nuclear spins[147] and other experiments have demonstrated its sensitivity in the direct observation of oscillating magnetizations in zero field[148] and even to the very lowest frequencies.[49] SQUID detectors in a zero field spectrometer would make realistic the direct observation of signals at the low frequencies characteristic of the local fields themselves. Their high sensitivity may even alleviate the need for a large polarizing field. Use of SQUIDs to sample the evolving signal directly in zero field-zero field correlation experiments (see Section VI.C) will turn three-dimensional (and therefore often intolerably long) investigations into more routine two-dimensional work.

Appendix A

In this appendix I treat the case where the high field spectrum is sufficiently broad that pulsed NMR techniques are incapable of exciting and detecting the signal from the entire high field powder pattern, but where some portion of the high field spectrum is uniformly observed. These conditions are fulfilled if

$$\frac{3e^2qQ}{2I(2I-1)} \gg \omega_1 > \frac{3}{4\omega_0}\left(\frac{e^2qQ}{2I(2I-1)}\right)^2 \qquad (A.1)$$

that is, the first order quadrupolar shifts are larger than the rf field which is larger than the second order shifts. This is commonly the case for half-integral quadrupolar nuclei, where the central transition between the high field eigenstates $|1/2\rangle$ and $|-1/2\rangle$ is unshifted to first order by the quadrupolar coupling, and the only significant signal after a resonant rf pulse of realistic strength arises from the coherence between these two levels.

The approach in this appendix is to repeat the calculation of Section III.B but to use as the observable not I_{zL} but instead the actual observable

$$\ell \equiv I_{xL}^{(-1/2 \rightarrow 1/2)} \qquad (A.2)$$

i.e. transverse magnetization corresponding only to coherence between these two levels. For small flip angles, it has been shown that the excitation of this coherence is independent of the orientation of the particular crystallite in any lab-based frame.[149] Then

$$G(t_1) = \mathrm{Tr}\ [\ \ell \exp(-i\theta I_y)\rho(t_1)\exp(i\theta I_y)] \tag{A.3}$$

where the evolved longitudinal order stored in $\rho(t_1)$ is transformed into an observable by an rf pulse of θ radians about the y-axis. For the initial density operator $\rho(0) = I_{zL}$,

$$G(t_1) = \mathrm{Tr}\ [\ \ell \exp(-i\theta I_y) I_{zL} \exp(i\theta I_y)] \tag{A.4}$$

It will be convenient to express all operators in a spherical tensor basis set. In the lab frame,

$$\ell = \sum_{n=1}^{I+1/2} a_n\ (\ T^j_{-1L} - T^j_{1L}\ ) \tag{A.5}$$

where $j = 2n-1$, and

$$I_{zL} = T^1_{0L} \tag{A.6}$$

and

$$I_{zL}(t_1) = T^1_{0L}(t_1) \equiv \exp(-iHt)\ T^1_{0L}\ \exp(iHt) \tag{A.7}$$

It will also prove convenient to permute the operators in Equation (A.3) so that the rf excitation is formally applied to the observed operator, which is orientation independent, rather than the evolved operator, where its effects are strongly orientation-dependent[42] and

$$G(t_1) = \mathrm{Tr}\ [\ \exp(i\theta I_{yL})\ell\exp(-i\theta I_{yL})\ T^1_{0L}(t_1)] \tag{A.8}$$

Focusing on the transformed operator

$$\exp(i\theta I_{yL})\ell\exp(-i\theta I_{yL}) = \sum_{n=1}^{I+1/2} a_n \sum_{m=-j}^{j} [d^j_{m-1}(\theta) - d^j_{m1}(\theta)]\ T^j_{mL}$$

$$= \sum_{n=1}^{I+1/2} a_n \sum_{m=-j}^{j} d^j_{m-1}(\theta)\, T^j_{mL} \qquad (A.9)$$

Because the evolved operator $I_{zL}(t_1)$ corresponds to longitudinal order, only terms in the sum of Equation (A.9) where m = 0 can contribute to the trace of Equation (A.8). Defining

$$b_n = 2a_n\, d^j_{0-1}(\theta) \qquad (A.10)$$

and

$$G(t_1) = \mathrm{Tr}\,[\,\{T^1_{0L}(t_1)\}\{\sum_{n=1}^{I+1/2} b_n\, T^j_{0L}\}] \qquad (A.11)$$

Equation (A.11) is most readily evaluated in the molecular frame where the Hamiltonian is homogeneous. The laboratory and molecular frames are related by a coordinated transformation $R(\Omega)$. The signal function is calculated for a single orientation Ω and integrated over a powder distribution function (all Ω equally probable), and

$$G(t_1) = \int G^{\Omega}(t_1)\, d\Omega$$

$$= \int \mathrm{Tr}\,[R\{\sum_{n=1}^{I+1/2} b_n\, T^j_{0L}\}R^{-1}\exp(-iH_M t_1)R\; T^1_{0L}R^{-1}\exp(-iH_M t_1)]$$

$$= \int \mathrm{Tr}\,[\sum_{n=1}^{I+1/2} b_n \sum_{\kappa=-j}^{j} D^j_{\kappa 0}(\Omega)T^j_{\kappa M}\exp(-iH_m t_1)(\sum_{k=-1}^{1} D^1_{k0}(\Omega)T^1_{kM})\exp(iH_M t_1)]\,d\Omega$$

$$= \sum_{n=1}^{I+1/2} b_n \int \sum_{\kappa=-j}^{j} \sum_{k=-j}^{j} D^j_{\kappa 0}(\Omega)\, D^j_{k0}(\Omega)\; \mathrm{Tr}\,[\,T^j_{\kappa M}\, T^1_{kM}(t_1)]\; d\Omega \qquad (A.12)$$

The only angular dependence in Equation (A.12) lies in the rotation matrices (because it has been assumed that the detected operator can be uniformly excited). Using the well-known rotation matrix properties exploited in Chapter VI, [7]

$$D^{j*}_{kq} = (-1)^{k-q} D^{j}_{-k-q} \tag{A.13}$$

and

$$\frac{\int D^{j'*}_{k'q'}(\Omega)\, D^{j}_{kq}(\Omega)\, d\Omega}{\int d\Omega} = \frac{1}{2j+1}\, \delta_{jj'}\delta_{kk'}\delta_{qq'} \tag{A.14}$$

the normalized, integrated signal intensity is

$$G(t_1) = \sum_{n=1}^{I+1/2} b_n \left\{ \sum_{\kappa=-j}^{j} \sum_{k=-1}^{1} \frac{\int D^{j*}_{\kappa 0}(\Omega)\, D^{1}_{k0}(\Omega)\, d\Omega}{\int d\Omega} \mathrm{Tr}\, [T^{j}_{\kappa M}\, T^{1}_{kM}(t_1)] \right\}$$

$$= b_1 \sum_{\kappa=-1}^{1} \frac{(-1)^{\kappa}}{3} \mathrm{Tr}\, [T^{1}_{-kM} T^{1}_{kM}(t_1)]$$

$$= \frac{1}{3} b_1 \; [I_{xM} I_{xM}(t_1) + I_{yM} I_{yM}(t_1) + I_{zM} I_{zM}(t_1)] \tag{A.15}$$

All other terms have zero integrated intensity due to the orthogonality condition Equation (A.14). The signal detected in high field is identical to that observed if the entire powder pattern were observed to within a scaling constant

$$b_1 = \frac{3}{4I(I+1)} \sin\theta \tag{A.16}$$

For large flip angles θ, the details of the excitation and detection period t_2 become important because the amount of the operator $I_{zL}(t_1)$ transformed into an observable transverse magnetization becomes

orientation dependent. In this case the integration in Equation (A.15) includes an additional Ω dependence in the detected operator. Both the effective nutation frequency under the influence of an applied rf field and the subsequent signal amplitude of the central transition depend on the magnitude of the high field value of the quadrupolar coupling and therefore on Ω.[42] Only for small flip angle excitation is uniform excitation of the central transition possible. Quantifying this last statement, field cycling zero field spectra of half-integral quadrupolar nuclei can be observed without intensity distortion if the high field signal is measured immediately after a θ pulse for

$$\gamma B_{rf}\tau = \theta < \frac{\pi}{2(2I+1)} \tag{A.17}$$

where τ is the length of the applied pulse and B_{rf} the strength of the rf field.[149]

Appendix B

Where molecules or portions of molecules are non-rigid, the spin Hamiltonians described in Chapter I are insufficient to provide a complete description of the spectral features observed in NMR experiments. In the presence of motion, the spatial terms in these Hamiltonians become time-dependent and only a motionally averaged tensor is observed. This fact is well known from high field studies, and is the basis for lineshape studies of chemical exchange in solution[150] and studies of restricted motion in solids[151]. For motions which are either fast or slow (as compared to the strength of the interaction being observed) it is easy to predict the result: fast motions yield zero field spectra with sharp lines at the time-averaged value of the tensor, while very slow motions show up as discrete zero field lines at each possible value of the tensor. The intermediate case (motion or exchange at rates comparable to the magnitude of the NMR Hamiltonian) affects the lineshapes, and a detailed analysis is required to solve the problem completely. Methods applicable to high field NMR are well known, and are presented by others in detail elsewhere. Some consideration has been given to the intermediate regime in pure NQR[152]. In this appendix, I present an approach to the analysis of a few representative cases in the fast motion limit where a simple solution is available and which are relevant to the experimental results of the main portion of this thesis. The treatment in this section closely follows the results of Bayer,[95] Abragam,[11] and Barnes.[122] In the intermediate motion limit, the prediction of spectral features is considerably more complicated.[153,154]

Where rapid motion occurs about a single axis its effects can be simply incorporated into the expressions for the NMR and NQR Hamiltonians. As a model for these concepts I consider an axially symmetric quadrupolar Hamiltonian where the magnitude of the quadrupolar tensor $\tilde{V}$ is unchanged during the motion. A formally equivalent example is the dipolar coupling between two spin-1/2 nuclei.

Four categories of motion are treated. Three occur in a molecular frame: rapid, isotropic rotation about an axis; two-fold jumps: and small librational modes. The last takes place in a lab frame: physical rotation of the sample. I start with a common approach to these types of motion. First, the static Hamiltonian is transformed from its principal axis system (xyz) to a frame where the motion is described more simply (XYZ). For clarity, I assume this transformation can be accomplished by a single rotation by a θ degrees about the Y axis. In this new frame, the expanded form of the quadrupolar Hamiltonian (Equation (1.54) (where $\eta = 0$) is

$$H_Q = -A[\{3I_z^2-I(I+1)\}(\frac{3\cos^2\theta-1}{2})+\frac{3}{4}\sin^2\theta(I_+^2+I_-^2)-3\sin\theta\cos\theta(I_XI_Z+I_ZI_X)] \quad (B.1)$$

For rapid motion, the time average of this Hamiltonian is responsible for the observed features. It will be analyzed for each of the four motional models.

A. Rotations about a Molecular Axis

Allowing the molecule or molecular unit to undergo rapid rotation about the new Z axis introduces a time dependence into H_Q (or H_D). As the rotation frequency is assumed large compared to our Hamiltonian,

what is actually observed is H_Q averaged over a rotational cycle. Entering an interaction frame which follows the motion of the spatial angular momentum, J_Z, at a frequency ω

$$\tilde{H}_Q(t) = \langle \exp(-i\omega J_z t) H_Q \exp(i\omega J_z t) \rangle \qquad (B.2)$$

Only the first term in Equation (B.1) is time independent. All other terms have zero time average over a rotational cycle. The averaged Hamiltonian which gives rise to the observed spectrum is then

$$\overline{H}_Q = - A \left(\frac{3\cos^2\theta - 1}{2}\right) (3I_Z^2 - I(I+1)) \qquad (B.3)$$

and the averaged Hamiltonian retains the axial symmetry of the static Hamiltonian with an effective quadrupolar tensor scaled by $(3\cos^2\theta-1)/2$. If the local environment of the quadrupole varies during a rotational period, and therefore the instantaneous value of the quadrupolar tensor takes on different values during that period, the averaged tensor need not be axially symmetric.[45]

Similar effects of motional averaging are required in zero field NMR studies of dipolar systems undergoing rapid reorientation. For many coupled spins computer simulations are required. DBZINT.FOR is designed to simulate systems with a single axis of rotation. Two common examples of rapidly reorienting systems in the solid state are methyl groups and benzene, which spins rapidly about its hexad axis. Figure B.1 compares simulated zero field and high field spectra of isolated groupings of these two spin systems. Averaging any rigid structure over a classical rotation about a molecule-fixed axis results in a zero field Hamiltonian isomorphic with a high field Hamiltonian with all the molecular rotation axes aligned along the field. The fast

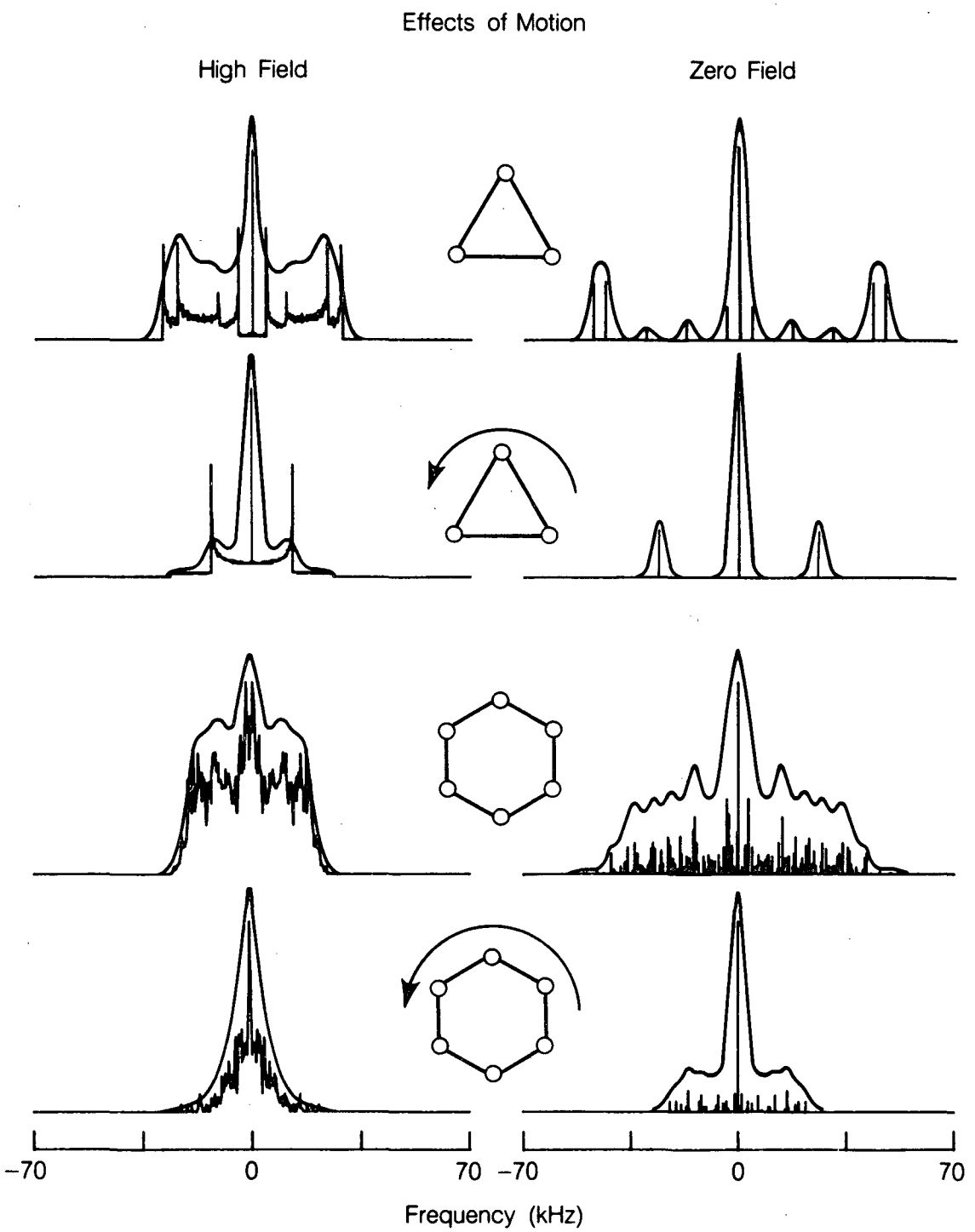

Figure B.1 High field and zero field NMR simulations for static and rapidly spinning $-CH_3$ groups and benzene rings, showing the effects of motional averaging on pure dipolar spectra.

molecular rotation performs the same truncation of terms as a large Zeeman energy.

B. Discrete Jumps

For jumps about the Z axis through discrete angles, the instantaneous electric field gradient tensor is calculated for each discrete orientation and a time-weighted average derived by summing over all allowed orientations.[91,93] For a two site jump (as executed by D_2O in many inorganic crystals at high temperature[91]) I assume the individual sites have identical tensors related by a symmetry plane. The (XYZ) reference frame is chosen so that the Z-axis is along a vector which bisects the D-O-D bond angle, 2θ, and lies in the plane defined by the three nuclei. The first site is related to this frame via a rotation about the Y-axis of θ degrees ($R_Y(\theta)$); the second, via $R_Y(-\theta)$. Time averaging Equation (B.1) is equivalent to taking the average value of these two tensors;

$$\overline{H}_Q = \frac{1}{2}(H_{Q1} + H_{Q2}) = -A[(3I_{ZM}^2 - I(I+1))(\frac{3\cos^2\theta - 1}{2}) + \frac{3}{4}\sin^2\theta(I_{+M}^2 + I_{-M}^2)] \quad (B.4)$$

Even if the tensors of the static sites are equivalent and axially symmetric, the coefficient of the term $(I_{+M}^2 + I_{-M}^2)$ in the averaged tensor need not vanish and the motion appears to shrink the norm of H_Q. Depending on θ, and the number of sites. the jumping motion also may introduce a marked departure from axial symmetry. (For specific values of θ, the axis system in the new frame may need to be relabeled to conform with the conventional notation of Equation (1.57).) In a two site jump where $2\theta \sim 109.5^o$ (the tetrahedral angle), $\eta \sim 1$.

C. Torsion and Small Librations

As a final simple example of molecular motion in zero field, we consider the effect of small amplitude torsional or librational modes.[95] These are modeled by allowing Z to represent the equilibrium or average orientation of the tensor, and introducing small rotations about the y axis of θ radians. For small θ and to lowest non-vanishing order in θ we can expand Equation (B.1) in powers of θ as

$$\tilde{H}_Q(t) = - A[(1 - \frac{3\theta^2}{2})(3I_Z^2 - I(I+1)) + \frac{3}{4}\theta^2(I_+^2 + I_-^2) - 3\theta(I_X I_Z + I_Z I_X)] \quad (B.5)$$

Averaging over θ to get the time-averaged Hamiltonian, $\bar{H}_Q$, for harmonic modes this last term disappears and $\bar{H}_Q$ can be rewritten as

$$\overline{H}_Q = - A[(1 - \frac{3\overline{\theta^2}}{2})(3I_Z^2 - I(I+1)) + \frac{3}{4}\overline{\theta^2}\ (I_+^2 + I_-^2)] \quad (B.6)$$

where

$$\overline{\theta^2} = \langle\theta^2(t)\rangle \quad (B.7)$$

This corresponds to a scaled quadrupolar coupling constant and an asymmetry parameter of $\eta = 3\langle\theta^2\rangle/2$. By a similar treatment, dipolar tensors can develop an asymmetry.[92] In two-spin heteronuclear spin-1/2 systems with such an asymmetric dipolar tensor (and therefore no degenerate energy levels) all 12 lines predicted by Equation (4.22) should be observed.

For each of these molecular frame motions, the averaged tensor may have different value and symmetry than the static tensor. Under any of these types of motion the Hamiltonian remains homogeneous, if

all sites or crystallites undergo the same type of motion independent of their orientation in the lab frame. As long as the motion is rapid, spectra of the motionally averaged systems retain the sharp features of zero field NMR of static samples; no broadening is introduced unless the motional behavior is itself inhomogeneous over the sample. This is similar to the case of high field single crystal NMR. The Hamiltonian at equivalent orientations is truncated by the field but the spectrum remains sharp because all sites are truncated identically.

D. Sample Rotation

As a final example of the effects of motion on zero field spectra, we consider the effects of bulk sample rotation on zero field spectra. This type of motion differs from those described above in that the axis of rotation differs for each crystallite orientation in a fixed lab-based frame of reference. Proceeding as above, H is transformed into a lab based frame (XYZ) as in Equation (B.1), where the angle θ is now orientation dependent. For fast rotation and only homonuclear couplings, the averaging in Equation (B.2) is formally equivalent to entering the rotating frame of high field NMR studies; this is a consequence of Larmor's theorem, and

$$\overline{H}_Q = - A\left(\frac{3\cos^2\theta - 1}{2}\right)(3I_Z^2 - I(I+1)) \qquad \text{(B.8)}$$

where θ is now referenced to a laboratory frame. With sufficiently fast sample rotation the zero field spectrum of an isolated deuteron or two spin-1/2 system will broaden into a Pake pattern exactly as if it were in a large externally applied field. For most systems, practical

sample rotation rates will be too slow for this simple treatment to apply. The primary effect of the rotation will be to cause some broadening in the observed line features. A combination of sample spinning at frequency ω_r and a magnetic field B such that $\omega_r = \gamma_j B$ will produce an untruncated Hamiltonian H_D or H_Q, and thus a normal zero field spectrum, in rough analogy to the cancellation of nutation and sample rotation in high field.

Appendix C

Source Listings of Zero, Low, and High Field Dipole-dipole simulation programs DBZINT.FOR, HETZF.FOR, LOFIELD.FOR, and PAT6.FOR

```
      program dbzint
c
c     computes intensities for the dz/tb field-cycling experiment on
c     coupled proton systems
c     this one is set up to generate spectra to dbz's specifications

      dimension numb(2,64),lst(2,64),isp(6),coors(6,3),dd(15),theta(15)
      dimension phi(15),vv(4096),pp(4096),e(64),ss(1024),vr(1024),iflip(2)
      complex h(4096),u(4096),xx(4096),yy(4096),zz(4096),wvec(64)
      character*64 title
      common/et/ title,e
      common n,nst,lst
      equivalence (h(1),xx(1))
c
      indx(i,j)= (j-1) * nst  +  i
c
      kfunk(i1,i2)=(2*n - i1)*(i1 - 1)/2  -  i1  +  i2
c
c
      dconst=120.067
      pi=4.0 * atan(1.0)
      rad57=180. / pi
c
      np=1024
c
10    type 501
501   format('1',//,' enter the type of system :',/,5x,'0 = general',
     1  /,5x,'1 = two flipping water molecules',/,5x,
     2  '2 = a planar polygon of spins          ',$)
      accept *,isys
c
      if(isys .eq. 1) go to 30
c
c
c     questions for the general and planar-polygon cases .....
c
c
      type 502
502   format(//,' how many spins ? (.lt. 7) ',$)
      accept *,n
c
      if(isys .eq. 2) go to 15
c
      type 503
503   format(///,' enter the x, y, and z coordinates of each nucleus ',
     1  '(in Angstroms) :',/)
c
      do 12 i=1,n
      type 504,i
504   format(5x,'nucleus ',i1,' :  ',$)
      accept *,(coors(i,j), j=1,3)
12    continue
c
      go to 18
c
c
15    type 505
505   format(//,' enter the nearest-neighbor separation in Angs. : ',$)
      accept *,side
c
      rr=side / (2 * sin(pi/n))
```

```
      angle=0.0
      dangle=2*pi/n
c
      do 16 i=1,n
      coors(i,1)=rr * cos(angle)
      coors(i,2)=rr * sin(angle)
      coors(i,3)=0.0
16    angle=angle + dangle
c
c
18    k=0
      do 20 i=1,n-1
      do 20 j=i+1,n
      k=k+1
      xxx=coors(j,1) - coors(i,1)
      yyy=coors(j,2) - coors(i,2)
      zzz=coors(j,3) - coors(i,3)
      rrr=sqrt(xxx*xxx + yyy*yyy + zzz*zzz)
      dd(k)=dconst / rrr**3
      costh=zzz / rrr
      sinth=sqrt(xxx*xxx + yyy*yyy) / rrr
      theta(k)=sign(pi/2,sinth)
      if(costh .ne. 0.0) theta(k)=atan2(sinth,costh)
      phi(k)=sign(pi/2,xxx)
      if(xxx .ne. 0.0) phi(k)=atan2(yyy,xxx)
20    continue
c
      print 501
      print 602, isys
      print 702, n
702   format(//,i4,' SPINS .....')
      if(isys .eq. 0) go to 22
      print 705, side
705   format(//,' enter the nearest-neighbor separation in Angs. : ',
     1  f9.3)
22    print 503
      do 25 i=1,n
      print 708, i,(coors(i,j), j=1,3)
708   format(/,5x,'nucleus ',i1,' :  ',3f10.3)
25    continue
c
      go to 35
c
c
c     questions for two flipping waters .....
c
c
30    type 511
511   format(///,' NOTE : water-1 is located at the origin with its',
     1  /,' H-H vector along the z-axis.')
c
      type 512
512   format(//,' enter the intramolecular H-H distance in Angs. : ',$)
      accept *,rhh
c
      type 513
513   format(/,' enter the inter-water separation in Angs. : ',$)
      accept *,rww
c
      type 514
514   format(/,' enter polar angles theta and phi (in degs.) describing',
     1  /,' the position of water-2 relative to water-1 : ',$)
      accept *,thetaw,phiw
```

```
c
      type 515
515   format(/,' enter polar angles theta and phi (in degs.) describing',
     1 /,' the orientation of the H-H vector in water-2 : ',$)
      accept *, theta2,phi2
c
      n=4
c
      dd(1)=dconst / rhh**3
      dd(2)=dconst / rww**3
      dd(3)=dd(2)
      dd(4)=dd(2)
      dd(5)=dd(2)
      dd(6)=dd(1)
c
      theta(1)=0.0
      theta(2)=thetaw / rad57
      theta(3)=theta(2)
      theta(4)=theta(2)
      theta(5)=theta(2)
      theta(6)=theta2 / rad57
c
      phi(1)=0.0
      phi(2)=phiw / rad57
      phi(3)=phi(2)
      phi(4)=phi(2)
      phi(5)=phi(2)
      phi(6)=phi2 / rad57
c
      print 501
      print 602, isys
      print 511
      print 512
      print 518, rhh
518   format(f10.3)
      print 513
      print 518, rww
      print 514
     hetaw,phiw
519   format(2f10.3)
      print 515
      print 519, theta2,phi2
c
c
c
35    type 555
555   format(//,' is there rapid motion around the z axis ?',/,
     1 ' (0=no,1=yes) ',$)
      accept *,imot

      type 573
573   format(' for no visual output of matrices, enter -1 here ')
      accept *,mview


c
      type 520
520   format(//,' in which "spec" file should data be stashed ?',
     1 /,' (for no spectrum storage, enter -1)  ',$)
      accept *,ifl
c
      if(imot .ne. 0) print 556
556   format(//,' THERE BE RAPID MOTION AROUND THE Z AXIS, MATEY')
```

```
      print 520
      print 602, ifl
c
      nst=2**n
      nm1=n-1
      np1=n+1
      ncp=n * nm1 / 2
      do 38 k=1,ncp
38    dd(k)=dd(k) / 4
c
c
c     generate and arrange the spin-product states .....
c
      call numsort(numb,n,nst)
c
      k=0
      do 45 js=1,np1
      is=np1 - js
      do 40 j=1,nst
      if(numb(2,j) .ne. is) go to 40
      k=k+1
      lst(1,k)=numb(1,j)
      lst(2,k)=is
40    continue
45    continue
c
c
c     set up the untruncated dipolar Hamiltonian .....
c
      do 100 m=1,nst
      do 100 l=1,m
      lm=indx(l,m)
      h(lm)=0.0
c
      if(l .ne. m) go to 60
c
c     diagonal "A" terms ....
c
      msk=1
      do 50 k=1,n
      isp(k)=-1
      if((lst(1,l) .and. msk) .ne. 0) isp(k)=1
50    msk=msk + msk
c
      kk=0
      do 55 i=1,nm1
      do 55 j=i+1,n
      kk=kk+1
      costh=cos(theta(kk))
      p2=3*costh*costh - 1
      h(lm)=h(lm)  -  dd(kk) * p2 * isp(j) * isp(i)
55    continue
      go to 100
c
c
c     off-diagonal terms ....
c
60    jw=1
      jsp=0
      msk=1
      do 75 k=1,n
      if((lst(1,l) .and. msk) - (lst(1,m) .and. msk)) 70,75,70
70    jsp=jsp + 1
```

```
      iflip(jw)=k
      jw=2
75    msk=msk + msk
c
      if(jsp .gt. 2) go to 95
      if(jsp .eq. 1) go
      kd=kfunk(iflip(1),iflip(2))
      if(lst(2,1) .ne. lst(2,m)) go to 78
c
c     "B" flip-flop terms ....
c
      costh=cos(theta(kd))
      h(lm)=dd(kd) * (3*costh*costh - 1)
      go to 95
c
c     "E" terms ....
c
78    if(imot .ne. 0) go to 95
      sinth2=sin(theta(kd)) ** 2
      h(lm)= -dd(kd) * 3 * sinth2 * cexp(cmplx(0.0,-2*phi(kd)))
      go to 95
c
c     "C" terms ....
c
80    if(imot .ne. 0) go to 95
      kfl=iflip(1)
      msk=1
      do 85 k=1,n
      if(k-kfl) 81,85,82
81    kd=kfunk(k,kfl)
      go to 84
82    kd=kfunk(kfl,k)
84    sincos=3 * sin(theta(kd)) * cos(theta(kd))
      kspin=-1
      if((lst(1,1) .and. msk) .ne. 0) kspin=1
      h(lm)=h(lm) - dd(kd) * kspin * sincos * cexp(cmplx(0.0,-phi(kd)))
85    msk=msk + msk
c
c
95    ml=indx(m,l)
      h(ml)=conjg(h(lm))
c
100   continue
c
c
      if(n .gt. 4 .or. mview .lt. 0) go to 105
      title=' THE HAMILTONIAN .....'
      call hardball(h,0)
c
c
c     now diagonalize the sucker .....
c
105   call heigen(h,u,nst)
c
      do 110 i=1,nst
      ii=indx(i,i)
110   e(i)=real(h(ii))
c
      print 521
521   format('1',//,' ENERGIES IN KHZ .....',//)
      print 522, (e(i), i=1,nst)
522   format(f15.4)
```

```
c
      if(n .gt. 4 .or. mview .lt. 0) go to 120
      title='EIGENVECTORS .....'
      call hardball(u,-1)
c
c
c     generate Ix, Iy, and Iz in the spin-product basis .....
c
120   do 150 i=1,nst
      do 150 j=1,nst
      ij=indx(i,j)
      xx(ij)=0.0
      yy(ij)=0.0
      zz(ij)=0.0
      if(i .ne. j) go to 130
c
      zz(ij)=lst(2,i) - n/2.0
      go to 150
c
130   if(iabs(lst(2,i) - lst(2,j)) .ne. 1) go to 150
      ksp=0
      msk=1
      do 140 k=1,n
      if((lst(1,i) .and. msk) .eq. (lst(1,j) .and. msk)) go to 140
      ksp=ksp + 1
140   msk=msk + msk
c
      if(ksp .ne. 1)       xx(ij)=0.5
      if(j .gt. i) yy(ij)=cmplx(0.0,-0.5)
      if(i .gt. j) yy(ij)=cmplx(0.0,0.5)
c
150   continue
c
c
c     convert Ix, Iy, and Iz to the basis set of the full dipolar Hamiltonian
c
      call uamu(u,xx,nst,wvec)
      call uamu(u,yy,nst,wvec)
      call uamu(u,zz,nst,wvec)
c
      if(n .gt. 4 .or. mview .lt. 0) go to 160
      title='Ix in the dipolar basis .....'
      call hardball(xx,1)
      title='Iy in the dipolar basis .....'
      call hardball(yy,1)
      title='Iz in the dipolar basis .....'
      call hardball(zz,1)
c
c
c     calculate frequencies and intensities .....
c
160   dink=0.0001
      p0=n * 2.**(n-2)
c
      k=0
      do 180 i=1,nst
      do 180 j=1,nst
      ij=indx(i,j)
      ji=indx(j,i)
      vvv=e(j) - e(i)
      ppp=real( xx(ij)*xx(ji) + yy(ij)*yy(ji) + zz(ij)*zz(ji) ) / 3
      if(ppp .lt. dink) go to 180
```

```
      k=k+1
      if(k .eq. 4097) go to 190
      vv(k)=vvv
      pp(k)=ppp/p0
180   continue
c
c
c     sort frequencies and intensities .....
c
190   iover=0
      if(k .gt. 4096) iover=1
      kmax=min0(k,4096)
      do 200 i=1,kmax-1
      do 200 j=i+1,kmax
      if(vv(j) .ge. vv(i)) go to 200
      call switch(vv(i),vv(j))
      call switch(pp(i),pp(j))
200   continue

      vwide = 2.0*(abs(vv(1)))
      type 534, vwide
534   format(' Full scale width of spectrum is  ',f10.4,' kHz')
      type 532
532   format(' How big should the spectrum we dump into be ?')
      accept *, v2max
      if (vwide .ge. v2max) v2max = 1.2*vwide

c
c
c     generate a spectrum .....
c
      dv=1024. / v2max
      hzppt=1000./dv
      vmax=v2max/2.0
c
      do 210 i=1,np
210   ss(i)=0.0
c
      do 220 k=1,kmax
      iv=513 + nint(vv(k)*dv)
      if (iv .eq. 1025) go to 220
      ss(iv)=ss(iv) + p vr(iv)=vv(k)
220   continue
c
c
c     output results .....
c
      print 530
530   format('1',//,10x,'frequency (kHz)',6x,'intensity',6x,
     1  'point #',/,10x,15('-'),6x,9('-'),6x,7('-'),/)
c
      k=0
      do 230 iv=1,np
      if(ss(iv) .lt. dink) go to 230
      k=k+1
      print 531, k,vr(iv),ss(iv),iv
531   format(i4,f18.4,f18.6,i11)
230   continue
c
      if(iover .eq. 1) print 533
533   format(///,' NOTE : there are over 4096 allowed transitions -- ',
     1  'lines missing in the table and in the plot')
```

```
c
c
      subroutine switch(a,b)
      c=a
      a=b
      b=c
      return
      end
c
c
c
c
c
      subroutine hardball(p,ibasis)
c
c     displays complex matrices (up to 16x16) on one page
c
c             ibasis=0  :  spin-product basis
c             ibasis=1  :  other
c             ibasis=-1 :  half and half
c
      complex p(256)
      dimension mag(16),iph(16),lst(2,16),idp(4,16),e(16)
      character*64 title
      common/et/ title,e
      common n,nst,lst
c
      indx(i,j)=(j-1)*nst + i
c
      pi=4.0*atan(1.0)



      rad57=180 / pi
c
      do 10 k=1,4
      do 10 j=1,16
10    idp(k,j)=' '
c
      print 101, title
101   format('1',//,5x,64a)
      print 102
102   format(///)
c
 sis .eq. 1) go to 20
c
c
c     set up +'s and -'s to describe direct product states.....
c
      msk=nst / 2
      do 15 k=1,n
      do 14 j=1,nst
      if(lst(1,j) .and. msk) 12,13,12
12    idp(k,j)=1h+
```

```
      go to 14
13    idp(k,j)=1h-
14    continue
      msk=msk / 2
15    continue
      if(ibasis .eq. 0) print 105, ((idp(k,j), k=1,4), j=1,nst)
105   format(11x,16(' :',4a1,'>'))
c
20    if(ibasis .ne. 0) print 106, (e(j), j=1,nst)
106   format(11x,16f7.2)
c
c
c
c     calculate phase and magnitude for each matrix element, then print....
c
30    print 112
112   format(1x,130(1h-))
c
      do 50 i=1,nst
      do 40 j=1,nst
      ij=indx(i,j)
      xx=real(p(ij))
      yy=aimag(p(ij))
      zz=cabs(p(ij))
      if(zz .lt. 0.0001) go to 35
      if(xx) 34,31,34
31    if(yy) 33,32,32
32    iph(j)=90
      go to 40
33    iph(j)=-90
      go to 40
34    ph=atan2(yy,xx) * rad57
      iph(j)=ph + sign(0.5,ph)
      go to 40
35    iph(j)=0
40    mag(j)=1000. * zz  +  sign(0.5,zz)
      if(ibasis .le. 0) print 114, (idp(k,i), k=1,4),(mag(j), j=1,nst)
114   format(1h0,'   <',4a1,':',16i7)
      if(ibasis .eq. 1) print 115, e(i),(mag(j), j=1,nst)
115   format(1h0,f7.2,' :',16i7)
      print 116, (iph(j), j=1,nst)
116   format(10x,16i7)


50    continue
c
      return
      end
```

```
      program HETZF
c
c     computes intensities for the dz/tb field-cycling experiment on
c     coupled proton systems with one spin allowed to be a heteronucleus
c
      dimension numb(2,64),lst(2,64),isp(6),coors(6,3),dd(15),theta(15)
      dimension phi(15),vv(600),pp(600),e(64),ss(1001),vr(1001),iflip(2)
      complex h(4096),u(4096),xx(4096),yy(4096),zz(4096),wvec(64)
      complex xx1,yy1,zz1, xd(4096), yd(4096), zd(4096)
      equivalence (h(1),xx(1))
c
      indx(i,j)= (j-1) * nst  +  i
c
      kfunk(i1,i2)=(2*n - i1)*(i1 - 1)/2  -  i1  +  i2
c
c
      dconst=120.067
      pi=4.0 * atan(1.0)
      rad57=180. / pi
c
      np=1001
c
10    type 501
501   format('1',//,' enter the type of system :',/,5x,'0 = general',
     1  /,5x,   '2 = a planar polygon of spins          ',$)
      accept *,isys
c
      if(isys .eq. 1) go to 10
c
c
c     questions for the general and planar-polygon cases .....
c
c
      type 502
502   format(//,' how many spins ? (.lt. 7) ',$)
      accept *,n
c
      type 514
514   format(//,' enter the gamma of the heteronuke (spin 1) : ',$)
      accept *, grat
c
      if(isys .eq. 2) go to 15
c
      type 503
503   format(///,' enter the x, y, and z coordinates of each nucleus ',
     1  '(in Angstroms) :',/)
c
      do 12 i=1,n
      type 504,i
504   format(5x,'nucleus ',i1,' :  ',$)
      accept *,(coors(i,j), j=1,3)
12    continue
c
      go to 18
c
c
15    type 505
505   format(//,' enter the nearest-neighbor separation in Angs. : ',$)
      accept *,side
c
      rr=side / (2 * sin(pi/n))
      angle=0.0
      dangle=2*pi/n
```

```
c
      do 16 i=1,n
      coors(i,1)=rr * cos(angle)
      coors(i,2)=rr * sin(angle)
      coors(i,3)=0.0
16    angle=angle + dangle
c
c
18    k=0
      do 20 i=1,n-1
      do 20 j=i+1,n
      k=k+1
      xxx=coors(j,1) - coors(i,1)
      yyy=coors(j,2) - coors(i,2)
      zzz=coors(j,3) - coors(i,3)
      rrr=sqrt(xxx*xxx + yyy*yyy + zzz*zzz)
      dd(k)=dconst / rrr**3
      if (i .eq. 1) dd(k) = dd(k)*grat
      costh=zzz / rrr
      sinth=sqrt(xxx*xxx + yyy*yyy) / rrr
      theta(k)=sign(pi/2,sinth)
      if(costh .ne. 0.0) theta(k)=atan2(sinth,costh)
      phi(k)=sign(pi/2,xxx)
      if(xxx .ne. 0.0) phi(k)=atan2(yyy,xxx)
20    continue
c
      print 501
      print 602, isys
      print 502
      print 602, n
      if(isys .eq. 0) go to 22
      print 505
      print 518, side
22    print 503
      do 25 i=1,n
      print 504, i
      print 508, (coors(i,j), j=1,3)
508   format(3f9.3)
25    continue
c
      go to 35
518   format(f10.3)
c
c
c
c
c
35    type 513
513   format(//,' is there rapid motion around the z axis ?',
     1  /,' (0=no,1=yes) ',$)
      accept *, imot
      type 520
520   format(//,' in which "spec" file should data be stashed ?',
     1  /,' (for no spectrum storage, enter -1)  ',$)
      accept *,ifl
c
      print 520
      print 602, ifl
c
      nst=2**n
      nm1=n-1
      np1=n+1
      ncp=n * nm1 / 2
```

```
      do 38 k=1,ncp
38    dd(k)=dd(k) / 4
c
c
c     generate and arrange the spin-product states .....
c
      call numsort(numb,n,nst)
c
      k=0
      do 45 js=1,np1
      is=np1 - js
      do 40 j=1,nst
      if(numb(2,j) .ne. is) go to 40
      k=k+1
      lst(1,k)=numb(1,j)
      lst(2,k)=is
40    continue
45    continue
c
c
c     set up the untruncated dipolar Hamiltonian .....
c
      do 100 m=1,nst
      do 100 l=1,m
      lm=indx(l,m)
      h(lm)=0.0
c
      if(l .ne. m) go to 60
c
c     diagonal "A" terms ....
c
      msk=1
      do 50 k=1,n
      isp(k)=-1
      if((lst(1,l) .and. msk) .ne. 0) isp(k)=1
50    msk=msk + msk
c
      kk=0
      do 55 i=1,n-1
      do 55 j=i+1,n
      kk=kk+1
      costh=cos(theta(kk))
      p2=3*costh*costh - 1
      h(lm)=h(lm)  -  dd(kk) * p2 * isp(j) * isp(i)
55    continue
      go to 100
c
c
c     off-diagonal terms ....
c
60    jw=1
      jsp=0
      msko 75 k=1,n
      if((lst(1,l) .and. msk) - (lst(1,m) .and. msk)) 70,75,70
70    jsp=jsp + 1
      iflip(jw)=k
      jw=2
75    msk=msk + msk
c
      if(jsp .gt. 2) go to 95
      if(jsp .eq. 1) go to 80
c
```

```
      kd=kfunk(iflip(1),iflip(2))
      if(lst(2,l) .ne. lst(2,m)) go to 78
c
c     "B" flip-flop terms ....
c
      costh=cos(theta(kd))
      h(lm)=dd(kd) * (3*costh*costh - 1)
      go to 95
c
c     "E" terms ....
c
78    if (imot .eq. 1) go to 95
      sinth2=sin(theta(kd)) ** 2
      h(lm)= -dd(kd) * 3 * sinth2 * cexp(cmplx(0.0,-2*phi(kd)))
      go to 95
c
c     "C" terms ....
c
80    if (imot .eq. 1) go to 95
      kfl=iflip(1)
      msk=1
      do 85 k=1,n
      if(k-kfl) 81,85,82
81    kd=kfunk(k,kfl)
      go to 84
82    kd=kfunk(kfl,k)
84    sincos=3 * sin(theta(kd)) * cos(theta(kd))
      kspin=-1
      if((lst(1,l) .and. msk) .ne. 0) kspin=1
      h(lm)=h(lm) - dd(kd) * kspin * sincos * cexp(cmplx(0.0,-phi(kd)))
85    msk=msk + msk
c
c
95    ml=indx(m,l)
      h(ml)=conjg(h(lm))
c
100   continue
c
c
c     now diagonalize the sucker .....
c
      call heigen(h,u,nst)
c
      do 110 i=1,nst
      ii=indx(i,i)
110   e(i)=real(h(ii))
c
      print 521
521   format(/////,' ENERGIES IN KHZ .....',//)
      print 522, (e(i), i=1,nst)
522   format(f15.4)
c
c
c     generate Ix, Iy, and Iz in the spin-product basis .....
c
      do 150 i=1,nst
      do 150 j=1,nst
      ij=indx(i,j)
      xx(ij)=0.0
      yy(ij)=0.0
      zz(ij)=0.0
      xd(ij)=0.0
      yd(ij)=0.0
```

```
      zd(ij)=0.0
      kk=0
      if(i .ne. j) go to 130
c     now calculate Sz matrix(zd) and Iz + grat*Sz (zz)
c
      izax=mod(lst(1,i),2)
      jzax=lst(2,i) - izax
      zd(ij)=0.5 * grat*(2*izax - 1)
      zz(ij)=jzax-(n-1)/2.0 + zd(ij)
      go to 150
c
130   if(iabs(lst(2,i) - lst(2,j)) .ne. 1) go to 1sp=0
      msk=1
      do 140 k=1,n
      if((lst(1,i) .and. msk) .eq. (lst(1,j) .and. msk)) go to 140
      kk=k
      ksp=ksp + 1
140   msk=msk + msk
c
      if(ksp .ne. 1) go to 150
      zax=0.5
      if (kk .eq. 1) zax=grat/2
      xx(ij)=zax
      if(j .gt. i) yy(ij)=cmplx(0.0,-zax)
      if(i .gt. j) yy(ij)=cmplx(0.0,zax)
      if (kk .ne. 1) go to 150
      xd(ij)=zax
      if (j. gt. i) yd(ij)=cmplx(0.0,-zax)
      if (j. lt. i) yd(ij)=cmplx(0.0,zax)
c
150   continue
c
c
c     convert Ix, Iy, and Iz to the basis set of the full dipolar Hamiltonian
c
      call uamu(u,xx,nst,wvec)
      call uamu(u,yy,nst,wvec)
      call uamu(u,zz,nst,wvec)
      call uamu(u,xd,nst,wvec)
      call uamu(u,yd,nst,wvec)
      call uamu(u,zd,nst,wvec)
c
c
c     calculate frequencies and intensities .....
c
      dink=0.0001
c
      if (if1 .gt. 0) call defile('spec',if1,0)

      do 235 irep=1,2
c
c     loop over detection by the heteronucleus and the abundant spin
c
      if(irep .eq. 1) p0=3 * grat * grat * 2.**(n-2)
      if(irep .eq. 2) p0=3 * (n-1) * 2.**(n-2)
c
      k=0
      do 180 i=1,nst
      do 180 j=1,nst
      ij=indx(i,j)
      ji=indx(j,i)
      vvv=e(j) - e(i)
```

```
c       xx1,yy1,zz1 contain the detection matrices.  first time thru, we
c       assume the detection is via grat*(Sx,Sy,Sz); next time around,
c       via (Ix,Iy,Iz)
c
        xx1=xd(ji)
        yy1=yd(ji)
        zz1=zd(ji)
        if (irep .eq. 1) go to 175
        xx1=xx(ji)-xd(ji)
        yy1=yy(ji)-yd(ji)
        zz1=zz(ji)-zd(ji)
175     ppp=real( xx(ij)*xx1 + yy(ij)*yy1 + zz(ij)*zz1 ) / p0
        if(abs(ppp) .lt. dink) go to 180
        k=k+1
        if(k .eq. 601) go to 190
        vv(k)=vvv
        pp(k)=ppp
180     continue
c
c
c       sort frequencies and intensit
190     iover=0
        if(k .gt. 600) iover=1
        kmax=min0(k,600)
        do 200 i=1,kmax-1
        do 200 j=i+1,kmax
        if(vv(j) .ge. vv(i)) go to 200
        call switch(vv(i),vv(j))
        call switch(pp(i),pp(j))
200     continue
c
c
c       generate a spectrum .....
c
        vmax=amax1(1.2 * abs(vv(1)),dink)
        dv=500 / vmax
        hzppt=2 * vmax
c
        do 210 i=1,np
210     ss(i)=0.0
c
        do 220 k=1,kmax
        iv=501 + nint(vv(k) * dv)
        ss(iv)=ss(iv) + pp(k)
        vr(iv)=vv(k)
220     continue
        if (irep .eq. 2) go to 223
        print 550, grat
550     format(//, ' the heteronucleus has a gamma = ', f6.4)
        if (imot .eq. 1) print 555
555     format(//, ' spectrum calculated assuming rapid rotation about z ')
c
c       output results .....
c
        print 528
528     format('1',//,10x, frequency (khz)',6x, intensity ,6x,
     1    point #',6x,'in S spin spectrum',/,10x,15('-'),6x,
     2   9('-'),6x,7('-'),/)
        go to 225
223     print 530
530     format(//,10x,'frequency (kHz) ,6x,'intensity',6x,
     1   'point #',/,10x,15('-'),6x,9('-'),6x,7('-'),/)
```

```
c
225     k=0
        do 230 iv=1,np
        if(abs(ss(iv)) .lt. dink) go to 230
        k=k+1
        print 531, k,vr(iv),ss(iv),iv
531     format(i4,f18.4,f18.6,i11)
230     continue
c
        if(iover .eq. 1) print 533
533     format(///,' NOTE : there are over 600 allowed transitions -- ',
     1   'lines missing in the table and in the plot')
c
c
        if(ifl .lt. 0) go to 235
c
c
        vmin=-vmax
        print 535, vmin,vmax,hzppt
535     format(///,3x,'spectral range : ',f10.4,' kHz to ',f10.4,' kHz',
     1   5x,'(',f9.4,' Hz per point)')
c
        write(1,602) np
        write(1,603) hzppt
        write(1,603) (ss(i), i=1,np)
235     continue

        close(unit=01)
c
c
240     type 539
539     format(///,' another system ?? (0=no,1=yes) ',$)
        accept *,ian
  .ne. 0) go to 10
c
        print 540
540     format('1',//)
c
c
602     format(i6)
603     format(e14.6)
c
        end
c
c
c
c
c
        subroutine switch(a,b)
        c=a
        a=b
        b=c
        return
        end
```

```
      program lofield
c
c     computes intensities for a general powder pattern of
c     coupled protons (up to 4)
c     in a small applied dc field in non-rotating frame
c     otherwise, this one is exactly like pat4
c     this one is set up to generate spectra to dbz's specifications
c

      dimension numb(2,16),lst(2,16),isp(4), coors(4,3)
      dimension dd(6),theta(6),iflip(2)
      dimension phi(6),e(16),ss(1024)
      complex h0(256),h(256),u(256),xx(256),yy0(256)
      complex xx0(256),yy(256),zz(256),wvec(16), zz0(256)
      character*15 gname
      character*64 title
      common/et/ title,e
      common n,nst,lst

c
      indx(i,j)= (j-1) * nst  +  i
c
      kfunk(i1,i2)=(2*n - i1)*(i1 - 1)/2  -  i1  +  i2
c
c
      dconst=120.067
      pi=4.0 * atan(1.0)
      rad57=180. / pi
      bad = 0.
      np=1024
c     initialize the spectrum matrix ss
      do 1553 j=1,np
1553  ss(j) = 0.0
c
c     set up the spectral width as 250 kHz full width centered about
c     point 513

      v2max = 250.
      hzppt = 125./511.
      vmax = 125.

c     bad holds all the intensity that fall outside of the chosen band
c     width for our spectrum

      bad = 0.

10    type 501
501   format('1',//,' enter the type of system :',/,5x,'0 = general',
     1  /,5x, '1 = a planar polygon of spins          ',$)
      accept *,isys
c
c     questions for the general and planar-polygon cases .....
c
c
4477  type 502
502   format(//,' how many spins ? (.le. 6) ',$)
      accept *,n
c
      if ((n .lt. 2) .or. (n .gt. 6)) go to 4477
      type 598
598   format(' how many steps along beta in interval 0-90 ?' )
      accept *, m2
      type 596
```

```
596     format(' and how many along the equator ? ')
        accept *, n2
c
        type 554
554     format(' enter the value of the static field in kHz ')
        accept *, fld

        type 556
556     format(' enter the angle omega between lab z-axis and residual
     1 field : ')
        accept *, omega
        ome2 = omega/rad57
        com = cos(ome2)
        som = sin(ome2)

c
        if(isys .eq. 1) go to 15
c
        type 503
503     format(///,' enter the x, y, and z coordinates of each nucleus ',
     1   '(in Angstroms) :',/)
c
        do 12 i=1,n
        type 504,i
504     format(5x,'nucleus ',i1,' :  ',$)
        accept *,(coors(i,j), j=1,3)
12      continue
c
        go to 18
c
c
15      type 505
505     format(//,' enter the nearest-neighbor separation in Angs. : ',$)
        accept *,side
c
        rr=side / (2 * sin(pi/n))
        angle=0.0
        dangle=2*pi/n
c
        do 16 i=1,n
        coors(i,1)=rr * cos(angle)
        coors(i,2)=rr * sin(angle)
        coors(i,3)=0.0
16      angle=angle + dangle
c
c
18      k=0
        do 20 i=1,n-1
        do 20 j=i+1,n
        k=k+1
        xxx=coors(j,1) - coors(i,1)
        yyy=coors(j,2) - coors(i,2)
        zzz=coors(j,3) - coors(i,3)
        rrr=sqrt(xxx*xxx + yyy*yyy + zzz*zzz)
        dd(k)=dconst / rrr**3
        costh=zzz / rrr
        sinth=sqrt(xxx*xxx + yyy*yyy) / rrr
        theta(k)=sign(pi/2,sinth)
        if(costh .ne. 0.0) theta(k)=atan2(sinth,costh)
        phi(k)=sign(pi/2,xxx)
        if(xxx .ne. 0.0) phi(k)=atan2(yyy,xxx)
20      continue
c
```

```
      print 501
      print 602, isys
      print 702, n
702   format(//,i4,' SPINS .....')
      if(isys .eq. 0) go to 22
      print 705, side
705   format(//,' enter the nearest-neighbor separation in Angs. : ',
     1  f9.3)
22    print 503
      do 25 i=1,n
      print 708, i,(coors(i,j), j=1,3)
708   format(/,5x,'nucleus ',i1,' :  ',3f10.3)
25    continue
c

      type 520
520   format(' enter file name for spectrum dump' /,
     1 ' for no spec spectrum storage, enter -1 ')
      accept 5202, jnp, gname(1:jnp)
5202  format(q,a)
      if (gname(1:2) .eq. '-1' ) ifl = -1

      if (ifl .ne. -1) then
c
      print 520
      print 5202, jnp, gname(1:jnp)
c
      else
      end if
      nst=2**n
      nm1=n-1
      np1=n+1
      ncp=n * nm1 / 2

38    dd(k)=dd(k) / 4
c
c
c     generate and arrange the spin-product states .....
c
      call numsort(numb,n,nst)
c
      k=0
      do 45 js=1,np1
      is=np1 - js
      do 40 j=1,nst
      if(numb(2,j) .ne. is) go to 40
      k=k+1
      lst(1,k)=numb(1,j)
      lst(2,k)=is
40    continue
45    continue

c
c     set up the untruncated dipolar Hamiltonian .....
c     store it in matrix h0
c     matrix h will represent the combined dipolar + Zeeman Hamiltonians
c

      do 100 m=1,nst
      do 100 l=1,m
      lm=indx(l,m)
      h0(lm)=0.0
c
```

```
      if(l .ne. m) go to 60
c
c     diagonal "A" terms ....
c
      msk=1
      do 50 k=1,n
      isp(k)=-1
      if((lst(1,l) .and. msk) .ne. 0) isp(k)=1
50    msk=msk + msk
c
      kk=0
      do 55 i=1,nm1
      do 55 j=i+1,n
      kk=kk+1
      costh=cos(theta(kk))
      p2=3*costh*costh - 1
      h0(lm)=h0(lm)  -  dd(kk) * p2 * isp(j) * isp(i)
55    continue
      go to 100
c
c
c     off-diagonal terms ....
c
60    jw=1
      jsp=0
      msk=1
      do 75 k=1,n
      if((lst(1,l) .and. msk) - (lst(1,m) .and. msk)) 70,75,70
70    jsp=jsp + 1
      iflip(jw)=k
      jw=2
75    msk=msk + msk
c
      if(jsp .gt. 2) go to 95
      if(jsp .eq. 1) go to 80
c
      kd=kfunk(iflip(1),iflip(2))
      if(lst(2,l) .ne. lst(2,m)) go to 78
c
c     "B" flip-flop terms ....
c
      costh=cos(theta(kd))
      h0(lm)=dd(kd) * (3*costh*costh - 1)
      go to 95
c
c     "E" terms ....
c
78    sinth2=sin(theta(kd)) ** 2
      h0(lm)= -dd(kd) * 3 * sinth2 * cexp(cmplx(0.0,-2*phi(kd)))
      go to 95
c
c     "C" terms ....
c
80    kfl=iflip(1)
      msk=1
      do 85 k=1,n
      if(k-kfl) 81,85,82
81    kd=kfunk(k,kfl)
      go to 84
82    kd=kfunk(kfl,k)
84    sincos=3 * sin(thetaheta(kd))
      kspin=-1
      if((lst(1,l) .and. msk) .ne. 0) kspin=1
```

```
      h0(la)=h0(la) - dd(kd)*kspin*sincos*cexp(cmplx(0.0,-phi(kd)))
85    msk=msk + msk
c
c
95    ml=indx(m,l)
      h0(ml)=conjg(h0(la))
c
100   continue
c
c
c     generate Ix, Iy, or Iz in the spin-product basis .....
c     calculate the value of the zeeman field when rotated into the
c     molecular frame of reference

      do 1500 i=1,nst
      do 1500 j=1,nst
      ij=indx(i,j)
      xx(ij)=0.0
      yy(ij)=0.0
      zz(ij)=0.0
      if(i .ne. j) go to 130
c
      zz(ij)=lst(2,i) - n/2.0
      go to 150
c
130   if(iabs(lst(2,i) - lst(2,j)) .ne. 1) go to 150
      ksp=0
      msk=1
      do 140 k=1,n
      if((lst(1,i) .and. msk) .eq. (lst(1,j) .and. msk)) go to 140
      ksp=ksp + 1
140   msk=msk + msk
c
      if(ksp .ne. 1) go to 150
      xx(ij)=0.5
      if(j .gt. i) yy(ij)=cmplx(0.0,-0.5)
      if(i .gt. j) yy(ij)=cmplx(0.0,0.5)

150   continue
c

1500  continue
c

c     now add in a zeeman term for the rotated field, that is,
c     the field vector now expressed in the molecular frame
c     the truncation is now done numerically, because the coefficient
c     applied to the field is much larger than the unit of the dipolar
c     couplings

c     the coefficients on each part of the field represent the effect
c     of having rotated it through (gamma, beta) in the 2 angles

c     now loop over orientations of the values of gamma and cos(beta)
c     for each field orientation, calculate states and energies

      finc = 2./float(m2-1)
      ginc = pi/float(n2-1)
      do 2700 m1 = 1,m2

c     loop over values of cos(beta) from -1 to 1

      c1 = -1. + finc*float(m1-1)
```

```
      beta = acos(c1)

c     loop over values of gamma from 0 to pi

32    do 2600 ll = 1,n2
  float(ll-1)*ginc
      s1 = sin(beta)
      c2 = cos(gamma)
      s2 = sin(gamma)
      s1s2 = s1*s2
      s1c2 = s1*c2
      c1c2 = c1*c2
      c1s2 = c1*s2

      do 444 i = 1,nst
      do 444 j = 1,nst
      ij = indx(i,j)
      zz0(ij) = (-1.*s1c2*xx(ij) + s1s2*yy(ij) + c1*zz(ij))

c     while we're looping, set up Ix, Iy (lab-based) in the molecular frame

      yy0(ij) = s2*xx(ij) + c2*yy(ij)
      xx0(ij) = c1c2*xx(ij) + s1*zz(ij) - c1s2*yy(ij)

      h(ij) = h0(ij) + f1d*(zz0(ij)*com+xx0(ij)*som)


444   continue
c
c
c     now diagonalize the sucker .....

      call heigen(h,u,nst)
c

      do 110 i=1,nst
      ii=indx(i,i)
      e(i) = real(h(ii))
110   continue
c
c     convert lab based Iz to the basis set of the complete Hamiltonian

c
      call uamu(u,zz0,nst,wvec)
c
c     calculate frequencies and intensities .....
c
      p0=n * 2.**(n-2)
c
      do 180 i=1,nst
      do 180 j=1,nst
      vvv = 0.
      ij=indx(i,j)
      ji=indx(j,i)
      vvv=e(j) - e(i)
      ppp=real(zz0(ji)*zz0(ij))
      slot = vvv/hzppt
      jkl = nint(slot) + 513
      if ((jkl .ge. 1) .and. (jkl .le. 1024)) go to 1705
      bad = bad + ppp/p0
      go to 180
1705  ss(jkl) = ss(jkl) + ppp/p0
180   continue
```

```
c
2600    continue
c
2700    continue

c       output results .....
c
c
        vmin=-vmax
        print 535, vmin,vmax,hzppt
535     format(///,3x,'spectral range : ',f10.4,' kHz to ',f10.4,' kHz',
     1   5x,'(',f9.4,' Hz per point)')
c
        if (ifl .ne. -1) then
        open(unit=1, name=gname(1:jnp), status = 'new')
        write(1,602) np
        write(1,603) hzppt
        write(1,603) (ss(i), i=1,np)
        close(unit=01)

        else
        end if
c
c
240     type 539
539     format(///,' another system ?? (0=no,1=yes) ',$)
        accept *,ian
        if(ian .ne. 0) go to         print 540
540     format('1',//)
c
c
602     format(i6)
603     format(e14.6)
c
        end
c
c
c
c
c
        subroutine switch(a,b)
        c=a
        a=b
        b=c
        return
        end
c
```

```
      program pat6
c
c     computes intensities for a general powder pattern of
c     coupled protons (up to 6)
c     this one is set up to generate spectra to dbz's specifications
c     third attempt at calculating powders; 10/12/84
c     designed to be compiled with imsl routines eigch et al

      dimension numb(2,64),lst(2,64),isp(6), coors(6,3)
      dimension dd(15),theta(15),iflip(2)
      dimension phi(15),e(64),ss(1024)
      complex h0(4096),h(4096),u(4096),xx(4096)
      complex xx0(4096),yy(4096),zz(4096),wvec(64)
      real work(192)
      character*64 title
      common/et/ title,e
      common n,nst,lst

c
      indx(i,j)= (j-1) * nst  +  i
c
      kfunk(i1,i2)=(2*n - i1)*(i1 - 1)/2  -  i1  +  i2
c
c
      dconst=120.067
      pi=4.0 * atan(1.0)
      rad57=180. / pi
      bad = 0.
      np=1024
c     initialize the spectrum matrix ss
      do 1553 j=1,np
1553  ss(j) = 0.0
c
c     set up the spectral width as 250 kHz full width centered about
c     point 513

      v2max = 250.
      hzppt = 125./511.
      vmax = 125.

c     bad holds all the intensity that fall outside of the chosen band
c     width for our spectrum

      bad = 0.

10    type 501
501   format('1',//,' enter the type of system :',/,5x,'0 = general',
     1  /,5x, '1 = a planar polygon of spins          ',$)
      accept *,isys
c
c     questions for the general and planar-polygon cases .....
c
c
4477  type 502
502   format(//,' how many spins ? (.le. 6) ',$)
      accept *,n
c
      if ((n .lt. 2) .or. (n .gt. 6)) go to 4477
      type 598
598   format(' how many steps along beta in interval 0-90 ?' )
      accept *, m2
      type 596
```

```
596     format(' and how many along the equator ? ')
        accept *, n2
c
        if(isys .eq. 1) go to 15
c
        type 503
503     format(///,' enter the x, y, and z coordinates of each nucleus ',
     1   '(in Angstroms) :',/)
c
        do 12 i=1,n
        type 504,i
504     format(5x,'nucleus ',i1,' :  ',$)
        accept *,(coors(i,j), j=1,3)
12      continue
c
        go to 18
c
c
15      type 505
505     format(//,' enter the nearest-neighbor separation in Angs. : ',$)
        accept *,side
c
        rr=side / (2 * sin(pi/n))
        angle=0.0
        dangle=2*pi/n
c
        do 16 i=1,n
        coors(i,1)=rr * cos(angle)
        coors(i,2)=rr * sin(angle)
        coors(i,3)=0.0
16      angle=angle + dangle
c
c
18      k=0
        do 20 i=1,n-1
        do 20 j=i+1,n
        k=k+1
        xxx=coors(j,1) - coors(i,1)
        yyy=coors(j,2) - coors(i,2)
        zzz=coors(j,3) - coors(i,3)
        rrr=sqrt(xxx*xxx + yyy*yyy + zzz*zzz)
        dd(k)=dconst / rrr**3
        costh=zzz / rrr
        sinth=sqrt(xxx*xxx + yyy*yyy) / rrr
        theta(k)=sign(pi/2,sinth)
        if(costh .ne. 0.0) theta(k)=atan2(sinth,costh)
        phi(k)=sign(pi/2,xxx)
        if(xxx .ne. 0.0) phi(k)=atan2(yyy,xxx)
20      continue
c
        print 501
        print 602, isys
        print 702, n
702     format(//,i4,' SPINS .....')
        if(isys .eq. 0) go to 22
        print 705, side
705     format(//,' enter the nearest-neighbor separation in Angs. : ',
     1   f9.3)
22      print 503
        do 25 i=1,n
        print 708, i,(coors(i,j), j=1,3)
708     format(/,5x,'nucleus ',i1,' :  ',3f10.3)
25      continue
```

```
c
      type 520
520   format(//,' in which "spec" file should data be stashed ?',
     1  /,' (for no spectrum storage, enter -1)  ',$)
      accept *,ifl
c
      print 520
      print 602, ifl
c
      nst=2**n
      nm1=n-1
      np1=n+1
      ncp=n * nm1 / 2
      do 38 k=1,ncp
38    dd(k)=dd(k) / 4
c
c
c     generate and arrange the spin-product states .....
c
      call numsort(numb,n,nst)
c
      k=0
      do 45 js=1,np1
      is=np1 - js
      do 40 j=1,nst
      if(numb(2,j) .ne. is) go to 40
      k=k+1
      lst(1,k)=numb(1,j)
      lst(2,k)=is
40    continue
45    continue

c
c     set up the untruncated dipolar Hamiltonian .....
c     store it in matrix h0
c     matrix h wille combined dipolar + Zeeman Hamiltonians
c


      do 100 m=1,nst
      do 100 l=1,m
      lm=indx(l,m)
      h0(lm)=0.0
c
      if(l .ne. m) go to 60
c
c     diagonal "A" terms ....
c
      msk=1
      do 50 k=1,n
      isp(k)=-1
      if((lst(1,l) .and. msk) .ne. 0) isp(k)=1
50    msk=msk + msk
c
      kk=0
      do 55 i=1,nm1
      do 55 j=i+1,n
      kk=kk+1
      costh=cos(theta(kk))
      p2=3*costh*costh - 1
      h0(lm)=h0(lm)  -  dd(kk) * p2 * isp(j) * isp(i)
55    continue
```

```
      go to 100
c
c
c     off-diagonal terms ....
c
60    jw=1
      jsp=0
      msk=1
      do 75 k=1,n
      if((lst(1,l) .and. msk) - (lst(1,m) .and. msk)) 70,75,70
70    jsp=jsp + 1
      iflip(jw)=k
      jw=2
75    msk=msk + msk
c
      if(jsp .gt. 2) go to 95
      if(jsp .eq. 1) go to 80
c
      kd=kfunk(iflip(1),iflip(2))
      if(lst(2,l) .ne. lst(2,m)) go to 78
c
c     "B" flip-flop terms ....
c
      costh=cos(theta(kd))
      h0(lm)=dd(kd) * (3*costh*costh - 1)
      go to 95
c
c     "E" terms ....
c
78    sinth2=sin(theta(kd)) ** 2
      h0(lm)= -dd(kd) * 3 * sinth2 * cexp(cmplx(0.0,-2*phi(kd)))
      go to 95
c
c     "C" terms ....
c
80    kfl=iflip(1)
      msk=1
      do 85 k=1,n
      if(k-kfl) 81,85,82
81    kd=kfunk(k,kfl)
      go to 84
82    kd=kfunk(kfl,k)
84    sincos=3 * sin(theta(kd)) * cos(theta(kd))
      kspin=-1
      if((lst(1,l) .and. msk) .ne. 0) kspin=1
      h0(lm)=h0(lm) - dd(kd)*kspin*sincos*cexp(cmplx(0.0,-phi(kd)))
85    msk=msk + msk
c
c
95    ml = indx(m,l)
      h0(ml) = conjg(h0(lm))

100   continue
c
c
c
c     generate Ix, Iy, or Iz in the spin-product basis .....
c     calculate the value of the zeeman field when rotated into the
c     molecular frame of reference

      do 1500 i=1,nst
      do 1500 j=1,nst
  i,j)
```

```
      xx(ij)=0.0
      yy(ij)=0.0
      zz(ij)=0.0
      if(i .ne. j) go to 130
c
      zz(ij)=lst(2,i) - n/2.0
      go to 150
c
130   if(iabs(lst(2,i) - lst(2,j)) .ne. 1) go to 150
      ksp=0
      msk=1
      do 140 k=1,n
      if((lst(1,i) .and. msk) .eq. (lst(1,j) .and. msk)) go to 140
      ksp=ksp + 1
140   msk=msk + msk
c
      if(ksp .ne. 1) go to 150
      xx(ij)=0.5
      if (j .gt. i) yy(ij)=cmplx(0.0,-0.5)
      if (i .gt. j) yy(ij)=cmplx(0.0,0.5)
150   continue
c

1500  continue
c
c     now add in a zeeman term for the rotated field, that is,
c     the field vector now expressed in the molecular frame
c     the truncation is now done numerically, because the coefficient
c     applied to the field is much larger than the unit of the dipolar
c     couplings

c     the coefficients on each part of the field represent the effect
c     of having rotated it through (gamma, beta) in the 2 angles

c     now loop over orientations of the values of gamma and cos(beta)
c     for each field orientation, calculate states and energies

      finc = 2./float(m2-1)
      ginc = pi/float(n2-1)
      do 2700 m1 = 1,m2

c     loop over values of cos(beta) from -1 to 1

      c1 = -1. + finc*float(m1-1)
      beta = acos(c1)

c     loop over values of gamma from 0 to pi

32    do 2600 l1 = 1,n2
      gamma = float(l1-1)*ginc
      s1 = sin(beta)
      c2 = cos(gamma)
      s2 = sin(gamma)
      s1s2 = s1*s2
      s1c2 = s1*c2
      c1c2 = c1*c2
      c1s2 = c1*s2

      do 444 i = 1,nst
      do 444 j = 1,nst
      ij = indx(i,j)
      h(ij) = h0(ij) + 10000.*(-1.*s1c2*xx(ij) + s1s2*yy(ij) + c1*zz(ij))
```

```
c       while we're looping, set up Ix (lab-based) in the molecular frame

        xx0(ij) = c1c2*xx(ij) + s1*zz(ij) - c1s2*yy(ij)

444     continue
c
c       now diagonalize the sucker .....

        cst,11,e,u,nst,work,ier)
        if (ier .ne. 0) type 577, ier
577     format(' eigch error code = ', i6)
c

c       convert Ix to the basis set of the complete Hamiltonian

        call matraml(u,xx0,nst,wvec)

        call matml(xx0,u,nst,wvec)
c
c       calculate frequencies and intensities .....
c
        p0=n * 2.**(n-2)
c
        do 180 i=1,nst
        do 180 j=1,nst
        vvv = 0.
        ij = indx(i,j)
        ji = indx(j,i)
        ppp= xx0(ij)*xx0(ji)
        if (abs(ppp) .le. 1.e-4) go to 180
        vvvi=e(j) - e(i)
        if (vvvi .gt. 0.0) vvv = vvvi - 10000.
        if (vvvi .lt. 0.0) vvv = vvvi + 10000.
        slot = vvv/hzppt
        jkl = nint(slot) + 511
        if ((jkl .ge. 1) .and. (jkl .le. 1024)) go to 1705
        bad = bad + ppp/p0
        go to 180
1705    ss(jkl) = ss(jkl) + ppp/p0
180     continue
c
2600    continue
c
2700    continue

c       output results .....
c
c
        vmin=-vmax
        print 535, vmin,vmax,hzppt
535     format(///,3x,'spectral range : ',f10.4,' kHz to ',f10.4,' kHz',
     1   5x,'(',f9.4,' Hz per point)')
c
        call defile('spec',if1,0)
        write(1,602) np
        write(1,603) hzppt
        write(1,603) (ss(i), i=1,np)
        close(unit=01)
c
c
240     type 539
539     format(///,' another system ?? (0=no,1=yes) ',$)
        accept *,ian
```

```
      if(ian .ne. 0) go to 10
c
      print 540
540   format('1',//)
c
c
602   format(i6)
603   format(e14.6)
c
      end
```

References

1. D. A. Shirley, S. S. Rosenblum, and E. Matthias, Phys. Rev. 170, 363 (1968); H. Haas and D. A. Shirley, J. Chem. Phys. 58, 3339 (1973); H. Barfuss, G. Böhnlein, H. Hohenstein, W. Kreiche, M. Meinhold, H. Niedrig, and K. Reuter, J. Mol. Struct. 58, 503 (1980).

2. M. Mehring, High Resolution NMR in Solids, (Springer-Verlag, Berlin, 1983).

3. A. R. Edmonds, Angular Momentum in Quantum Mechanics, (Princeton University, Princeton, 1974).

4. B. L. Silver, Irreducible Tensor Methods: An Introduction for Chemists, (Academic, New York, 1976).

5. H. J. Lipkin, Lie Groups for Pedestrians, (North-Holland, Amsterdam, 1966).

6. G. Racah, Phys. Rev. 61, 186 (1942); 62, 438 (1942); 63, 367 (1943).

7. M. E. Rose, Elementary Theory of Angular Momentum, (J. Wiley, New York, 1967).

8. U. Haeberlen, Adv. Magn. Reson. Suppl. 1 (1976).

9. J. H. Van Vleck, Phys. Rev. 74, 1168 (1948).

10. C. P. Slichter, Principles of Magnetic Resonance, (Springer-Verlag, Berlin, 1978).

11. A. Abragam, Principles of Nuclear Magnetism, (Clarendon, Oxford, 1982).

12. P.-K. Wang, C. P. Slichter, and J. H. Sinfelt, Phys. Rev. Lett. 53, 82 (1984).

13. M. H. Cohen and F. Reif, Sol. State Phys. 5, 321 (1957).

14. T. P. Das and E. L. Hahn, Sol. State Phys. Suppl. 1 (1958).

15. R. Bersohn, J. Chem. Phys. 20, 1505 (1952).

16. G. Volkoff, Can. J. Phys. 30, 820 (1953).

17. U. Fano, Rev. Mod. Phys. 29, 74 (1957).

18. W. P. Aue, E. Bartholdi, and R. R. Ernst, J. Chem. Phys. 64, 2229 (1976).

19. A. E. Taylor and W. R. Mann, Advanced Calculus, (Wiley, New York, 1972).

20. R. V. Pound, Phys. Rev. 81, 156 (1951).

21. A. G. Redfield, Phys. Rev. 98, 1787 (1955).

22. C. P. Slichter and W. C. Holton, Phys. Rev. 122, 1701 (1961).

23. A. G. Anderson and S. R. Hartmann, Phys. Rev. 128, 2023 (1962).

24. A. Abragam and W. G. Proctor, Phys. Rev. 109, 1441 (1958).

25. M. Goldman, Spin Temperature and Nuclear Magnetic Resonance in Solids, (Clarendon, Oxford, 1970).

26. N. Bloembergen and J. A. Rowland, Acta. Met. 1, 731 (1953).

27. R. V. Pound, Phys. Rev. 79, 685 (1950).

28. E. R. Andrew and R. Bersohn, J. Chem. Phys. 18, 159 (1950).

29. H. S. Gutowsky and G. E. Pake, J. Chem. Phys. 18, 162 (1950).

30. S. K. Garg, J. A. Ripmeester, and D. W. Davidson, J. Magn. Reson. 35, 145 (1979).

31. F. Bloch, Phys. Rev. 102, 104 (1956).

32. J. S. Waugh, L. M. Huber, and U. Haeberlen, Phys. Rev. Lett. 20, 180 (1968).

33. W.-K. Rhim, D. D. Elleman, and R. W. Vaughan, J. Chem. Phys. 59, 3740 (1973).

34. D. P. Burum and W.-K. Rhim, J. Chem. Phys. 71, 944 (1979).

35. E. R. Andrew, Int. Rev. Phys. Chem. 1, 195 (1981).

36. M. M. Maricq and J. S. Waugh, J. Chem. Phys. 70, 3300 (1979).

37. J. S. Waugh, Proc. Nat. Acad. Sci. 73, 1394 (1976); R. K. Hester, J. L. Ackerman, B. L. Neff, and J. S. Waugh, Phys. Rev. Lett. 36, 1081 (1976).

38. M. E. Stoll, A. J. Vega, and R. W. Vaughan, J. Chem. Phys. 65, 4093 (1976).

39. M. Linder, A. Höhener, and R. R. Ernst, J. Chem. Phys. 73, 4959 (1980).

40. M. Munowitz and R. G. Griffin, J. Chem. Phys. 76, 2948 (1982); 77, 2217 (1982).

41. S. Ganapathy, S. Schramm, and E. Oldfield, J. Chem. Phys. 77, 4360 (1982).

42. A. Samoson and E. Lippmaa, Chem. Phys. Lett. 100, 205 (1983); Phys. Rev. B28, 6567 (1983).

43. M. Bloom, J. H. Davis, and A. L. MacKay, Chem. Phys. Lett. 80, 198 (1981); E. Sternin, M. Bloom, and A. L. MacKay, J. Magn. Reson. 55, 274 (1983).

44. J. H. Davis, Biochimica et Biophysica Acta 737, 117 (1983).

45. H. L. Casal, D. G. Cameron, and E. C. Kelusky, J. Chem. Phys. 80, 1407 (1980).

46. T. K. Pratum and M. P. Klein, J. Magn. Reson. 53, 473 (1983); 55, 421 (1983).

47. F. Reif and E. M. Purcell, Phys. Rev. 91, 631 (1953).

48. M. Bloom, E. L. Hahn, and B. Herzog, Phys. Rev. 97, 1699 (1955).

49. G. J. Enholm et al, Cryogenics 19, 673 (1979); Phys. Rev. Lett. 42, 1702 (1979); J. Low Temp. Phys. 39, 417 (1980).

50. N. F. Ramsey and R. V. Pound, Phys. Rev. 81, 278 (1951).

51. A. G. Anderson, Phys. Rev. 115, 863 (1959); 125, 1517 (1962).

52. A. G. Redfield, Phys. Rev. 130, 589 (1963).

53. a. R. L. Strombotne and E. L. Hahn, Phys. Rev. A133, 1616 (1964);
b. R. E. Slusher and E. L. Hahn, Phys. Rev. 166, 332 (1968);
c. J. Koo and Y.-N. Hsieh, Chem. Phys. Lett. 9, 238 (1971);
d. Y. Hsieh, J. C. Koo, and E. L. Hahn, Chem. Phys. Lett. 13, 563 (1972).

54. R. Blinc et al, J. Chem. Phys. 57, 5087 (1972).

55. D. T. Edmonds, M. J. Hunt, and A. L. MacKay, J. Magn. Reson. 11, 77 (1973); C. R. Brett and D. T. Edmonds, J. Magn. Reson. 49, 304 (1982).

56. Y. N. Hsieh, P. S. Ireland, and T. L. Brown, J. Magn. Reson. 21, 445 (1976); T. L. Brown et al, J. Am. Chem. Soc. 104, 1172 (1982).

57. a. J. L. Ragle, M. Mokarram, D. Presz, and G. Minott, J. Magn. Reson. 20, 195 (1975).
b. G. L. Minott III and J. L. Ragle, Adv. Nuc. Quad. Reson. 3, 205 (1978).

58. D. P. Weitekamp, A. Bielecki, D. Żax, K. Zilm and A. Pines, Phys. Rev. Lett. 50, 1807 (1983).

59. A. Bielecki, J. B. Murdoch, D. P. Weitekamp, D. B. Zax, K. W. Zilm, H. Zimmerman, and A. Pines, J. Chem. Phys. 80, 2232 (1984).

60. D. B. Zax, A. Bielecki, K. W. Zilm, and A. Pines, Chem. Phys. Lett. 106, 550 (1984).

61. D. B. Zax, A. Bielecki, A. Pines, and S. W. Sinton, Nature 312, 351 (1984).

62. J. M. Millar, A. M. Thayer, A. Bielecki, D. B. Zax, and A. Pines, J. Chem. Phys. 83, 934 (1985).

63. D, B. Zax, A. Bielecki, K. W. Zilm, A. Pines, and D. P. Weitekamp, J. Chem. Phys. 83, xxxx (1985).

64. A. Messiah, Quantum Mechanics (North-Holland, Amsterdam, 1961) Vol. II.

65. G. M. Muha, J. Magn. Reson. 49, 431 (1982); 53, 85 (1983).

66. S. Vega, Adv. Magn. Reson. 6, 259 (1973).

67. M. Goldman, Compt. Rend. 246, 1058 (1958).

68. R. Blinc, Adv. Nuc. Quad. Reson. 2, 71 (1975).

69. a. D. T. Edmonds, Phys. Rep. C29, 235 (1977);
b. D. T. Edmonds, Int. Rev. Phys. Chem. 2, 103 (1982).

70. D. T. Edmonds and J. P. G. Mailer, J. Magn. Reson. 26, 93 (1977).

71. A. Wright, Phys. Rev. 76, 1826 (1949).

72. M. Packard and R. Varian, Phys. Rev. 93, 941 (1954).

73. D. F. Elliott and R. T. Schumacher, J. Chem. Phys. 26, 1350 (1957).

74. E. M. Purcell and R. V. Pound, Phys. Rev. 81, 279 (1951).

75. A. Bielecki, D. B. Zax, K. W. Zilm, and A. Pines, submitted to Rev. Sci. Instr.

76. J. W. Emsley, J. Feeney, and L. H. Sutcliffe, High Resolution Nuclear Magnetic Resonance Spectroscopy (Pergamon, Oxford, 1966) Volume II.

77. S. Vega and A. Pines, J. Chem. Phys. 66, 5624 (1977).

78. A. Wokaun and R. R. Ernst, J. Chem. Phys. 67, 1753 (1977).

79. S. Vega, J. Chem. Phys. 68, 5518 (1978).

80. O. W. Sorenson, G. W. Eich, M. H. Levitt, G. Bodenhausen, and R. R. Ernst, Prog. Nucl. Magn. Reson. Spectrosc., 16, 163 (1983).

81. S. Vega, J. Chem. Phys. 63, 3769 (1975).

82. M. H. Cohen, Phys. Rev. 96, 1278 (1954).

83. E. Brun and B. Derighetti, Helv. Phys. Acta 34, 383 (1961).

84. G. W. Leppelmeier and E. L. Hahn, Phys. Rev. 141, 724 (1966).

85. R. A. Marino and S. M. Klainer, J. Chem. Phys. 67, 3388 (1977).

86. R. S. Cantor and J. S. Waugh, J. Chem. Phys. 73, 1054 (1980).

87. A. R. Kessel and O. S. Zueva, Phys. Lett 68A, 347 (1978); A. E. Mefed, Sov. Phys. Solid State 21, 485 (1979).

88. K. Müller, P. Meier, and G. Kothe, Prog. Nucl. Magn. Reson. Spectrosc. 17, xxxx, (1985).

89. A. Abragam and K. Kambe, Phys. Rev. 91, 894 (1953).

90. S. K. Sikka, S. N. Momin, H. Rajagopal, and R. Chidambaram, J. Chem. Phys. 48, 1883 (1969).

91. T. Chiba, J. Chem. Phys., 39, 947 (1963).

92. J. Schaefer, R. A. McKay, E. O. Stejskal, and W. T. Dixon, J. Magn. Reson. 52, 123 (1983); J. Schaefer, E. O. Stejskal, R. A. McKay, and W. T. Dixon, J. Magn. Reson. 57, 85 (1984).

93. B. H. Meier, F. Graf, and R. R. Ernst, J. Chem. Phys. 76, 767 (1982).

94. J. Tritt-Goc, N. Pislewski, and U. Haeberlen, private communication.

95. H. Bayer, Z. Phys. 130, 227 (1951).

96. R. Kubo and T. Toyabe, in Magnetic Resonance and Relaxation, ed. R. Blinc (North-Holland, Amsterdam, 1967) p. 810.

97. H. Eisendrath, W. Stone, and J. Jeener, Phys. Rev. B17, 47 (1978); H. Eisendrath and J. Jeener, Phys. Rev. B17, 54 (1978).

98. S. Hartmann and E. L. Hahn, Phys. Rev. 128, 2042 (1962).

99. A. Pines, M. G. Gibby, and J. S. Waugh, J. Chem. Phys. 59, 569 (1973).

100. G. Bodenhausen, Prog. Nucl. Magn. Reson. Spectrosc. 14, 137 (1981).

101. D. P. Weitekamp, Adv. Magn. Reson. 11, 111 (1983).

102. A. Wokaun and R. R. Ernst, Mol. Phys. 36, 317 (1978).

103. S. W. Sinton, D. B. Zax, J. B. Murdoch, and A. Pines, Mol. Phys., 53, 333 (1984).

104. A. Abragam and B. Bleaney, Electron Paramagnetic Resonance of Transition Ions, (Clarendon, Oxford, 1970) Ch. XV.

105. L. Falicov, Group Theory and its Physical Applications, (University of Chicago, Chicago, 1966) Ch. VII.

106. M. R. Churchill, F. J. Hollander and J. P. Hutchinson, Inorg. Chem. 16, 2697 (1977); A. G. Orpen et al, J. C. S. Chem. Commun. 723, (1978); R. W. Broach and J. M. Williams, Inorg. Chem. 18, 314 (1979).

107. A. T. Nicol and R. W. Vaughan, "Transition Metal Hydrides", Adv. Chem. Ser. 167, 248 (1978).

108. M. Celio and P. F. Meier, Phys. Rev. B27, 1908 (1983); E. Holzschuh and P. F. Meier, Phys. Rev. B29, 1129 (1984).

109. R. S. Hayano et al, Phys. Rev. B20, 850 (1979).

110. Y. Wang, G. D. Stucky, and J. M. Williams, J. C. S. Perkins II 35 (1973); J. D. Becker, D. Suwelack, and M. Mehring, Sol. State Comm. 25, 1145 (1978); M. Mehring and J. D. Becker, Phys. Rev. Lett. 47, 366 (1981).

111. J. Klinowski, M. W. Anderson, and J. M. Thomas, J. C. S. Chem. Commun. 523 (1983).

112. D. Muller, W. Gessner, H. J. Behrens, and G. Scheler, Chem. Phys. Lett. 79, 59 (1983); C. A. Fyfe, G. C. Gobbi, J. Klinowski, J. M. Thomas, and S. Ramdas, Nature 296, 530 (1982).

113. M. H. Levitt, D. Suter, and R. R. Ernst, J. Chem. Phys. 80, 3064 (1984).

114. H. W. Spiess and H. Sillescu, J. Magn. Reson. 42, 381 (1981).

115. R. Eckman, "Hydrogen and Deuterium NMR of Solids by Magic Angle Spinning," Ph.D. Dissertation, University of California, Berkeley, 1982 (published as Lawrence Berkeley Laboratory Report LBL-14200).

116. M. Bloom, J. H. Davis, and M. I. Valic, Can. J. Phys. 58, 1510 (1980).

117. H. W. Spiess, Advances in Polymer Science, eds. H. H. Kausch and H. G. Zachmann (Springer-Verlag, Berlin, 1985).

118. D. T. Edmonds, M. J. Hunt, and A. L. MacKay, J. Magn. Reson. 11, 77 (1973); 20, 505 (1975); D. T. Edmonds and A. A. L. White, J. Magn. Reson. 31, 149 (1978).

119. I. J. F. Poplett and J. A. S. Smith, J. C. S. Faraday Trans. 1, 74, 1077 (1978); I. J. F. Poplett, Adv. Nuc. Quad. Reson. 4, 115 (1980).

120. J. W. Emsley, J. C. Lindon, and J. Tabony, Mol. Phys. 26, 1499 (1973); P. Diehl, M. Reinhold, and A. S. Tracey, J. Magn. Reson. 19, 405 (1975); S. Hsi, H. Zimmerman, and Z. Luz, J. Chem. Phys. 69, 4126 (1978).

121. E. T. Lippmaa, M. A. Alla, T. J. Pehk, and G. Engelhardt, J. Am. Chem. Soc. 100, 1929 (1978); R. Eckman, M. Alla, and A. Pines, J. Magn. Reson. 41, 440 (1980).

122. R. G. Barnes, Adv. Nuc. Quad. Reson. 1, 335 (1974).

123. M. Rinne and J. Depireux, Adv. Nuc. Quad. Reson. 1, 357 (1974).

124. J. Jeener and P. Broekaert, Phys. Rev. 157, 232 (1967).

125. T. M. Barbara, R. Tycko, and D. P. Weitekamp, J. Magn. Reson. 62, 54 (1985).

126. H. A. Buckmaster, R. Chatterjee, and Y. H. Shing, Phys. Status Solidi A13, 9 (1972).

127. V. S. Grechishkin, V. P. Anferov, and N. Ja. Sinjavsky, Adv. Nucl. Quad. Reson. 5, 1 (1984).

128. R. Kreis, D. Suter, and R. R. Ernst, Chem. Phys. Lett. 118, 120 (1985).

129. C. Muller, S. Idziak, N. Pislewski, and U. Haeberlen, J. Magn. Reson. 47, 227 (1982).

130. U. Haeberlen and J. S. Waugh, Phys. Rev. 175, 453 (1968); 185, 420 (1969).

131. K. Nagayama, K. Wuthrich, and R. R. Ernst, Biochem. Biophys. Res. Commun. 90, 305 (1979); A. Bax and R. Freeman, J. Magn. Reson. 44, 542 (1981).

132. J. Jeener, B. H. Meier, P. Bachmann, and R. R. Ernst, J. Chem. Phys. 71, 4546 (1979); S. Macura and R. R. Ernst, Mol. Phys. 41, 95 (1980); G. Wider, S. Macura, A. Kumar, R. R. Ernst, and K. Wuthrich, J. Magn. Reson. 56, 207 (1984).

133. J. Baum, M. Munowitz, A. N. Garroway, and A. Pines, J. Chem. Phys. 83, 2015 (1985).

134. E. L. Hahn, Phys. Rev. 80, 580 (1950); I. Solomon, Phys. Rev. 110, 61 (1958); W.-K. Rhim, A. Pines, and J. S. Waugh, Phys. Rev. B3, 684 (1971).

135. R. G. Jones, NMR: Basic Principles and Progress, 1, 97 (1969).

136. E. B. Wilson, Jr., J. C. Decius, and P. C. Cross, Molecular Vibrations, (Dover, New York, 1980).

137. M. Hammermesh, Group Theory and its Application to Physical Problems, (Addison-Wesley, Reading, 1962).

138. E. P. Wigner, Group Theory and its Application to the Quantum Mechanics of Atomic Spectra, (Academic, New York, 1959).

139. G. F. Koster, Sol. State Phys. 5, 174 (1957).

140. S. W. Sinton, "NMR Studies of Oriented Molecules," Ph.D. Dissertation, University of California, Berkeley, 1981 (published as Lawrence Berkeley Laboratory Report LBL-13736).

141. G. Drobny, "NMR Studies of Liquid Crystals and Molecules Dissolved in Liquid Crystal Solvents," Ph.D. Dissertation, University of California, Berkeley, 1982 (published as Lawrence Berkeley Laboratory Report LBL-15254).

142. J. G. Powles and J. H. Strange, Proc. Phys. Soc. 82, 6 (1963); P. Mansfield, Phys. Rev. A137, 961 (1965).

143. E. D. Ostroff and J. S. Waugh, Phys. Rev. Lett. 16, 1097 (1966); W.-K. Rhim, D. P. Burum, and D. D. Elleman, Phys. Rev. Lett. 37, 1764 (1976); D. Suwelack and J. S. Waugh, Phys. Rev. B22, 5110 (1984); M. M. Maricq, Phys. Rev. B25, 6622 (1982).

144. A. Bax, N. M. Szeverenyi, and G. E. Maciel, J. Magn. Reson. 52, 147 (1983); N. Szeverenyi, A. Bax, and G. E. Maciel, J. Magn. Reson. 61, 440 (1985).

145. K. Hallenga and S. H. Koenig, Biochemistry 15, 4255 (1975); R. D. Brown III, C. F. Brewer, and S. H. Koenig, Biochemistry 16, 3883 (1977); M. Stohrer and F. Noack, J. Chem. Phys. 67, 3729 (1977); C. F. Polnaszek and R. G. Bryant, J. Chem. Phys. 81, 4308 (1984).

146. A. P. J. van Deursen and A. R. de Vroomen, J. Phys. E. 17, 155 (1984).

147. T. Sleator, E. L. Hahn, C. Hilbert, and J. C. Clarke, submitted to Phys. Rev. Lett.

148. C. Hilbert, J. C. Clarke, T. Sleator, and E. L. Hahn, Appl. Phys. Lett. 47, xxxx (1985).

149. D. Fenzke, D. Freude, T. Fröhlich, and J. Haase, Chem. Phys. Lett. 111, 171 (1984).

150. R. Kubo, Nuovo Cimento, Suppl. 6, 1063 (1957); R. A. Sack, Mol. Phys. 1, 163 (1958).

151. R. P. Mason, C. F. Polnaszek, and J. H. Freed, J. Phys. Chem. 78, 1324 (1974); S. Alexander, A. Baram, and Z. Luz, Mol. Phys. 27, 441 (1974); H. W. Spiess, Chem. Phys. 6, 217 (1974); A. Baram, Z. Luz, and S. Alexander, J. Chem. Phys. 64, 2231 (1976).

152. S. Alexander and A. Tzalmona, Phys. Rev. A138, 845 (1965).

153. M. Mehring, private communication.

154. J. W. Hennel, A. Birczynski, S. F. Sagnowski, and M. Stachurowa, Z. Phys. B. 60, 49 (1985).

This report was done with support from the Department of Energy. Any conclusions or opinions expressed in this report represent solely those of the author(s) and not necessarily those of The Regents of the University of California, the Lawrence Berkeley Laboratory or the Department of Energy.

Reference to a company or product name does not imply approval or recommendation of the product by the University of California or the U.S. Department of Energy to the exclusion of others that may be suitable.

LAWRENCE BERKELEY LABORATORY
TECHNICAL INFORMATION DEPARTMENT
UNIVERSITY OF CALIFORNIA
BERKELEY, CALIFORNIA 94720